Investigations into the Integrated Metabolism of Glucocorticoids and Glucose in Skeletal Muscle

By

Agnieszka Ewa Zielinska

A thesis submitted to the University of Birmingham

for the degree of

DOCTOR OF PHILOSOPHY

School of Clinical and Experimental Medicine

College of Medical and Dental Sciences

University of Birmingham

June 2015

Abstract

Skeletal muscle plays a central role in maintaining metabolic homeostasis in health and disease. An important metabolic component of muscle is the integrated metabolism of glucose and glucocorticoids (GCs) in the lumen of the sarcoplasmic reticulum (SR). Glucose-6-phosphate (G6P) transported into the SR by the G6P transporter (G6PT) is metabolised by hexose-6-phosphate dehydrogenase (H6PDH) to produce nicotinamide adenine dinucleotide phosphate reduced (NADPH) cofactor that is utilised by 11β-hydroxysteroid dehydrogenase type 1 (11β-HSD1) to reduce inactive GCs to their active forms. This thesis evaluated the SR unit as a site of integrated metabolism using a range of genetic models and screening methods. We demonstrate that perturbation of redox and metabolic balance through the distribution of H6PDH enzyme resulted in novel stress responses leading to shifts in redox and energy metabolism. Particularly, we show how the SR can elicit transcriptional changes that appear to adapt NADPH redox perturbation and also increase energy metabolism through augmented mitochondrial function. These data presented a novel sensing pathway within the SR unit that could have important relevance to metabolic and energetic control of skeletal muscle.

For Savio and Olivier

Acknowledgments

Firstly, I would like to show my appreciation to my supervisor, Prof Gareth Lavery, for all his help, encouragement and support throughout this research project. I am also grateful to Prof Paul Stewart and Prof Jeremy Tomlinson for their valuable advice and Prof Jerzy Adamski and Dr Cornelia Prehn for sharing their expertise in metabolomics technology and analysis.

Additionally, I express my gratitude to Dr Khalid Saqib for introducing me to the main techniques in the lab and to Dr Iwona Bujalska for her helpful discussion, guidance with writing this thesis and friendship.

I would like to thank the past and present colleagues and friends on the 2nd floor IBR, in particular the Lavery group, for making my PhD such a memorable experience.

Massive thank you to my ‘new sister’, Maryam Nasiri, for being my best friend and sharing last five years together. I will never forget our USA adventures, shopping and coffee times.

Last, but not least, I would like to thank my mum for all her support over the years and hours spent on the phone. I am most grateful to my husband Savio and son Olivier for giving me strength, happiness and love. They always know how to put a smile on my face and keep me going.

This work was supported by the Biotechnology and Biological Sciences Research Council.

Table of Contents

List of Figures

List of Tables

Abbreviations

β-geo	β-galactosidase/neomycin phosphotransferase fusion gene
3β-HSD	3β-hydroxysteroid dehydrogenase type II
^{3}H-11-DHC	Tritiated [1,2,6,7-^{3}H(N)]-11-DHC
6PGL	6-phosphogluconate
11β-HSD1	11β-hydroxysteroid dehydrogenase type 1
11β-HSD2	11β-hydroxysteroid dehydrogenase type 2
11-DHC	11-dehydrocorticosterone
A	11-dehydrocorticosterone
AC	Acylcarnitines
ACC	Acetyl-CoA carboxylase
ACTH	Adrenocorticotropic hormone
ACRD	Apparent cortisone reductase deficiency
ADP	Adenosine diphosphate
AFMID	Arylformamidase
AHA/NHLBI	American Heart Association/ National Heart, Lung, and Blood Institute
AMD1	Adenosylmethionine decarboxylase 1
AME	Apparent mineralocorticoid excess
AMPD1	Adenosine monophosphate deaminase 1 (isoform M)
ATF6	Activating transcription factor-6
ATP	Adenosine triphosphate
ATPIII	Third Report for the National Cholesterol Education Program's Adult Treatment Panel
B	Corticosterone
BECN	Beclin
bHLH	Muscle-specific basic helix-loop-helix
BiP	Binding immunoglobulin protein
BMI	Body mass index
BSA	Bovine serum albumin
CAT	Carnitine translocase
cDNA	Complementary deoxyribonucleic acid
COX	Cyclooxygenase
CPT	Carnitine palmitoyltransferase
CPT-II	Carnitine palmitoyltransferase II deficiency
CRD	Cortisone reductase deficiency
CRH	Cortocotropin-releasing hormone
CS	Citrate synthase
Ct	Cycle threshold
CVD	Cardiovascular disease
CYTC	Cytochrome C
DAG	Diacylglycerol
DGC	Dystrophin-associated glycoprotein complex
DEX	Dexamethasone
DDIT3	DNA damage-inducible transcript 3
DHEA	Dehydroepiandrosterone
DMD	Duchenne muscular dystrophy

DMEM	Dulbecco's modified eagle medium
DMSO	Dimethyl sulfoxide
DNA	Deoxyribonucleic acid
E	Cortisone
ECL	Enhanced chemilumiscence
EEF2	Eukaryotic translation elongation factor 2
eIF1α	Eukaryotic initiation factors 1α
EMMA	European Mouse Mutant Archive
ENO3	Enolase 3, beta muscle
EUCOMM	European conditional mouse mutagenesis project
ER	Endoplasmic reticulum
F	Cortisol
$FADH_2$	Flavin adenine dinucleotide
FCS	Fetal calf serum
FFA	Free fatty acid
FGF	Fibroblast growth factor
FOXO	Forkhead family of transcription factors
FRT	Flippase recognition target sequence
FRZB	Frizzled-related protein
G6P	Glucose-6-phosphate
G6Pase	Glucose-6-phosphatase
G6PDH	Glucose-6-phosphate dehydrogenase
G6PT	Glucose-6-phosphate transporter
GAPDH	Glyceraldehyde 3-phosphate dehydrogenase
GC	Glucocorticoid
GFP	Green fluorescence protein
Gluc	Glucose
GLUT-4	Glucose transporter type 4
GM	Complete growth medium
GR	Glucocorticoid receptor
GRE	Glucocorticoid response element
GSD	Glycogen storage disease
H6KO	H6PDH knockout mice (generated during this PhD)
H6PDH	Hexose-6-phosphate dehydrogenase
H6PDHKO	H6PDH knockout mice (previously generated)
HDL	High-density lipoprotein
HGF	Hepatocyte growth factor
HK	Hexokinase
HPA	Hypothalamic-pituitary-adrenal axis
HRP	Horseradish peroxidase
HSP70	Heat shock protein-70
HSP90	Heat shock protein-90
HSPa5	Heat shock 70 kDa protein 5
IFG	Impaired fasting glycaemia
IFU	Infectious units of virus
IGF1	Insulin-like growth factor 1
IGF-IR	Insulin-like growth factor receptor
IGT	Impaired glucose tolerance

INDO	Indoleamine 2,3-dioxygenase 1
InsR	Insulin receptor
IMGU	Insulin-mediated glucose uptake
InsR	Insulin receptor
IRE1	Inositol requiring enzyme 1
ITG1BP3	Integrin binding protein 1 beta 3
JNK	Jun NH2-terminal kinase
KO	Knockout
LDL	Low-density lipoprotein
LysoPC	LysoPhosphatidylcholine
MAFbx	Muscle atrophy F-box
Mef-2	Myocyte enhancer factor 2
Mef2c-Cre	Myocyte enhancer factor 2c promoter driven Cre
MFN	Myocyte nuclear factor
MHC	Myosin heavy chain
MIBP	Muscle integrin binding protein
MR	Mineralocorticoid receptor
MRF	Myogenic regulatory transcription factor
Mrf-4	Muscle-specific regulatory factor 4
mtDNA	Mitochondrial DNA
mTOR	Mammalian target of rapamycin
mTORC1	Mammalian target of rapamycin complex 1
Myf-5	Myogenic factor 5
MyoD	Myogenic differentiation 1
mRNA	Messenger RNA
MTHFD2	Methylenetetrahydrofolate dehydrogenase (NAD^+ dependent)
MuRF1	Muscle ring finger 1
MYH2	Myosin, heavy polypeptide 2, skeletal muscle, adult
Na	Nicotinic acid
NaAD	Nicotinic acid adenine dinucleotide
NAD	Nicotinamide adenine dinucleotide
NADSYN1	NAD synthetase 1
NAM	Nicotinamide
NaMN	Nicotinic acid mononucleotide
NADP	Nicotinamide adenine dinucleotide phosphate
NADPH	Nicotinamide adenine dinucleotide phosphate reduced
NADH	Nicotinamide adenine dinucleotide reduced
NAMPT	Nicotinamide phoshoribosyltransferase
NaPRT	Nicotinate phosphoribosyltransferase
NAPRT1	Nicotinate phosphoribosyltransferase domain containing 1
ND	NADH dehydrogenase
NEB	Nebulin
NF-κB	Nuclear factor-kappa B
NMN	Nicotinamide mononucleotide
NMNAT	Nicotinamide mononucleotide adenylyltransferase
NMRK2	Nicotinamide riboside kinase
NMP	Nucleoside monophosphate
NR	Nicotinamide riboside

QPRT	Quinolinate phosphoribosyltransferase
Orn	Ornithine
P450scc	P450 cholesterol side chain cleavage enzyme
pA	Povine growth hormone polyadenylation sequence
PBS	Phosphate-buffered saline
Pax	Paired-box protein
PC	Phosphatidylcholine
PCOS	Polycystic ovary syndrome
PCR	Polymerase chain reaction
PCr	Phosphocreatine
PDHC	The pyruvate dehydrogenase complex
PDK4	Pyruvate dehydrogenase kinase, isozyme 4
PERK	PKR-like ER protein kinase
Pi	Inorganic phosphate
PI3K	Phosphatidylinositol 3-kinase
PGC-1α	Peroxisome proliferator activated receptor-γ co-activator 1α
PKR	Protein kinase R
PRRX1	Paired related homeobox 1
PVDF	Polyvinylidene difluoride membrane
PYCR1	Pyrroline-5-carboxylate reductase 1
RC	Mitochondrial respiratory chain
RNA	Ribonucleic acid
rRNA	Ribosomal ribonucleic acid
RT	Reverse transcription
SA	Splice acceptor
SCAD	Short-chain acyl-CoA dehydrogenase
SIRT	Sirtuins
SMOX	Spermine oxidase
SR	Sarcoplasmic reticulum
SRD	Short-chain alcohol dehydrogenase
SULT2A1	DHEA sulfotransferase
TAG	Triglyceride
T2DM	Type 2 diabetes mellitus
TC	Tissue culture
TCA	Tricarboxylic acid
TG	Triglyceride
TGF-β	Transforming growth factor β
THE	Tetrahydrocortisone
THF	5β-tetrahydrocortisol
TLC	Thin layer chromatography
TRP	Tryptophan
VLDL	Very low density lipoprotein
WHO	World health organisation
WT	Wild type
XBP1	X-box-binding protein 1
xLeu	xLeucine

Chapter 1- General Introduction

1.1 Skeletal muscle as a metabolic tissue

Skeletal muscle is a form of striated muscle along with cardiac and smooth muscle and is under the control of the somatic nervous system. It is the most abundant peripheral tissue type in the human body constituting approximately 40% of the total body mass (42% for an average adult male and 36% for an average adult female) (Smith and Muscat 2005). The major function of skeletal muscle is to generate motile force through contraction in order to provide the stability and power for all body movements (Schuler et al. 2005).

Skeletal muscle as a metabolic tissue plays a major function in whole body metabolic energy regulation under different physiological conditions such as reduced blood flow and oxygen supply or increased energy demand during exercise (Dash et al. 2008). Muscle accounts for ~30% of total energy metabolism at rest whilst 90% of the 20-fold increase at peak physical activity (Zurlo et al. 1990).

Two metabolic patterns for skeletal muscle energy metabolism have been characterised (detailed in Section 1.1.3). The fast muscle fibres (type II fibres) use mainly glycolytic metabolism to generate short bursts of power mainly from phosphocreatine and glycogen. Conversely, type I fibres are classified as slow fibres use oxygen to produce adenosine triphosphate (ATP) in order to maintain long-term contractions (Ventura-Clapier et al. 2007).

In addition, skeletal muscle provides the most significant store of essential amino acids in the body (Bronk 1999) and controls metabolism via modulation of both circulating and stored lipid flux. Lipid catabolism accounts for up to 70% of the energy requirements for resting muscle. After prolonged exercise, muscle oxidises

carbohydrates and lipids as the dominating ATP-producing systems through aerobic metabolism. Glucose as a major carbohydrate substrate is stored as muscle glycogen; however, the extracellular glucose contribution increases with exercise duration (Westerblad et al. 2010). Endurance exercise depends on fatty acids and lipid mobilisation from other tissue (Figure 1-1). This underlines the importance of glucose and fatty acids for supplying energy in muscle (Smith and Muscat 2005).

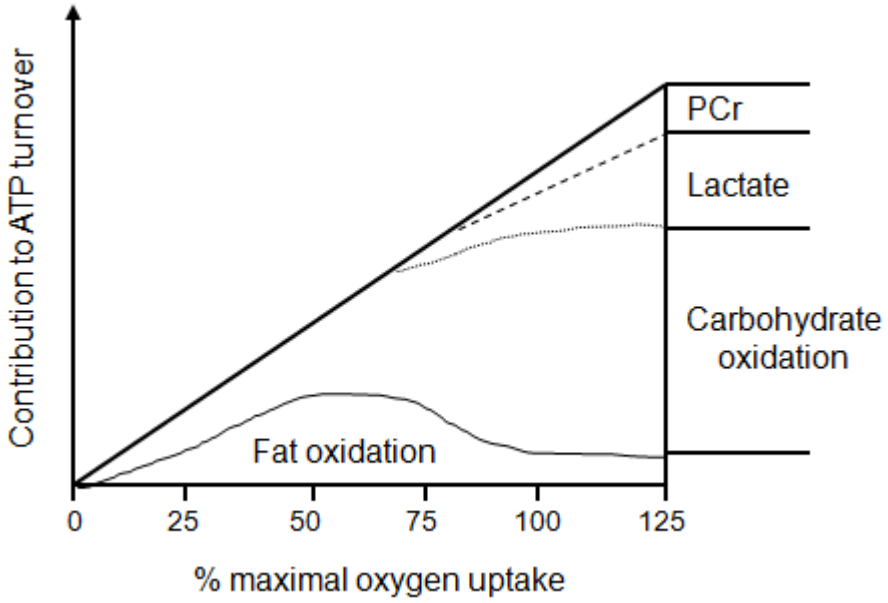

Figure 1-1 Schematic representation of the relationship between different energy substrates as a function of exercise intensity

The rate of ATP turnover was estimated in human leg muscles during upright cycling. Phosphocreatine (PCr) and lactate significantly contribute to ATP production only at high exercise intensities whereas the role of protein metabolism is considered to equal zero (Westerblad et al. 2010).

An additional substrate for aerobic metabolism is amino acids derived from muscle protein degradation; however, this contributes very little to the overall energy metabolism during prolonged exercise (~5% with sufficient carbohydrate metabolism and ~10% in the almost complete lack of carbohydrate availability) (Westerblad et al. 2010).

Importantly, skeletal muscle plays a significant role in determining whole body insulin sensitivity and lipid profile as the regulator of metabolism. Muscle metabolism is a potentially important therapeutic target used in the battle against a number of diseases caused by caloric excess, physical inactivity or ageing that lead to skeletal muscle insulin resistance, a risk factor for the development of type II diabetes and cardiovascular disease or sarcopenia, consequently increasing mortality risk. Thus, fully defining the physiology of skeletal muscle is critical to design interventions to optimise an individual's capacity to resist these diseases.

Skeletal muscle could be regarded as being as important as the liver and adipose tissue when considering the metabolic development of obesity and insulin resistance. Glucocorticoids, a group of hormones, play an important role in the incidence and progression of muscle insulin resistance (Section 1.6.3.2). Therefore, the mechanisms by which glucocorticoid metabolism can influence muscle phenotype requires a full investigation. This thesis will examine the role of skeletal muscle in local and systemic glucocorticoid production impacting whole body metabolism.

1.1.1 Myogenesis

Skeletal muscle myogenesis is a multistep process of muscle cell formation that begins with the commitment of an embryonic precursor to the myogenic lineage, then the proliferation of these myoblasts followed by their differentiation into postmitotic myocytes and finally fusion of myocytes to form multinucleated fibres called myotubes (Figure 1-2). This process is regulated by the basic helix-loop-helix myogenic regulatory transcription factors (MRFs) including myogenic differentiation 1 (MyoD), myogenic factor 5 (Myf-5), myogenin and muscle-specific regulatory factor 4

(Mrf-4) which are engaged in complex signaling cascades (Jin et al. 2007). During embryo development, the paired-box protein-3 (Pax-3) and Pax-7 maintain population of quiescent satellite cells and, together with Myf-5, play a role in the expansion of activated myoblasts. Additionally, MyoD determines the differentiation potential of an activated myoblast and acts together with myogenin and myocyte enhancer factor 2 (Mef-2) to drive differentiation. Finally, Mrf-4 is required for terminal differentiation and muscle hypertrophy (Jin et al. 2007).

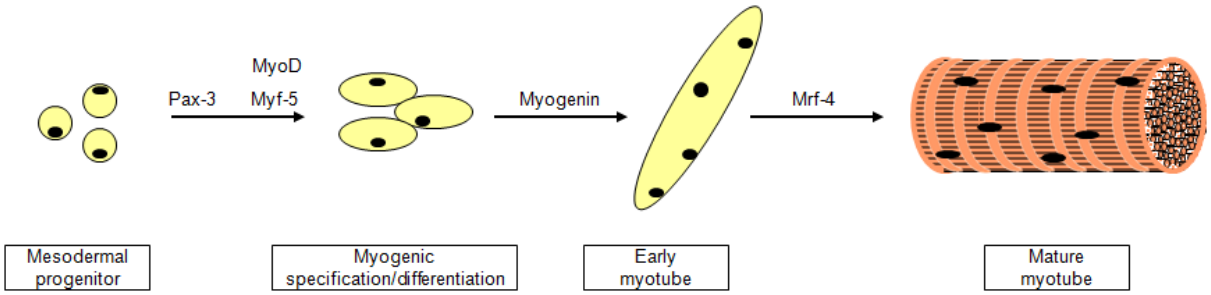

Figure 1-2 Schematic development of mature myotubes

Muscle precursor cells fuse together forming multinucleated myotubes that express characteristic contractile proteins.

Each mature muscle cell contains multiple nuclei and arises from separate myoblasts fused together. Single, elongated and cylindrical myotubes do not have a proliferative capacity (Rando and Blau 1994).

The main source of cells for muscle formation during regeneration in response to injury, disease or training is muscle precursors called satellite cells (Figure 1-3). These cells are located between the basal lamina and the myofibre plasma membrane and are responsible for muscle postnatal growth (Morgan and Partridge 2003;Yin et al. 2013). Satellite cells are predominantly quiescent in adult muscle, and they appear in the limbs at about 17.5 days postcoitum after primary muscle fibres

have formed. They express a range of proteins including M-cadherin, a calcium-dependent cell adhesion molecule, c-met, the receptor for HGF, myocyte nuclear factor (MNF) and Pax7. During postnatal growth, satellite cells proliferate and either fuse with each other to form myotubes and then myofibres or fuse with damaged muscle fibres. Some of them also form new satellite cells (Seale and Rudnicki 2000).

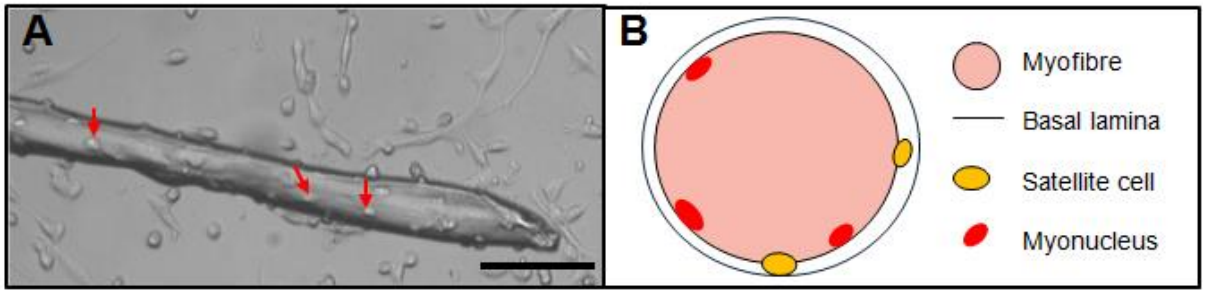

Figure 1-3 Localisation of a satellite cell on skeletal muscle fibre

Red arrows show satellite cells (A); schematic representation of a muscle fibre cross-section with satellite cells attached to its surface (B).

Interestingly, satellite cells isolated from old mice produce fewer colonies with lower reserve cells when compared to young mice. Therefore, ageing may impair the ability of some progenitors to produce reserve cells. Depletion of satellite cells could potentially contribute to the age-related decline in skeletal muscle quality and performance (Day et al. 2010).

1.1.2 Skeletal muscle structure

Skeletal muscle is composed of individual, elongated, multinucleated cells called myotubes or myofibres which lie in parallel linked by connective tissue. These components are organised into regular arrays of thin actin and thick myosin proteins that act as the integrated contractile and functional unit of muscle termed

the sarcomere, organised as repeated units in long filaments (Figure 1-4). Sarcomeres in series form myofibrils that determine the striated appearance of skeletal muscle (Brooks 2003).

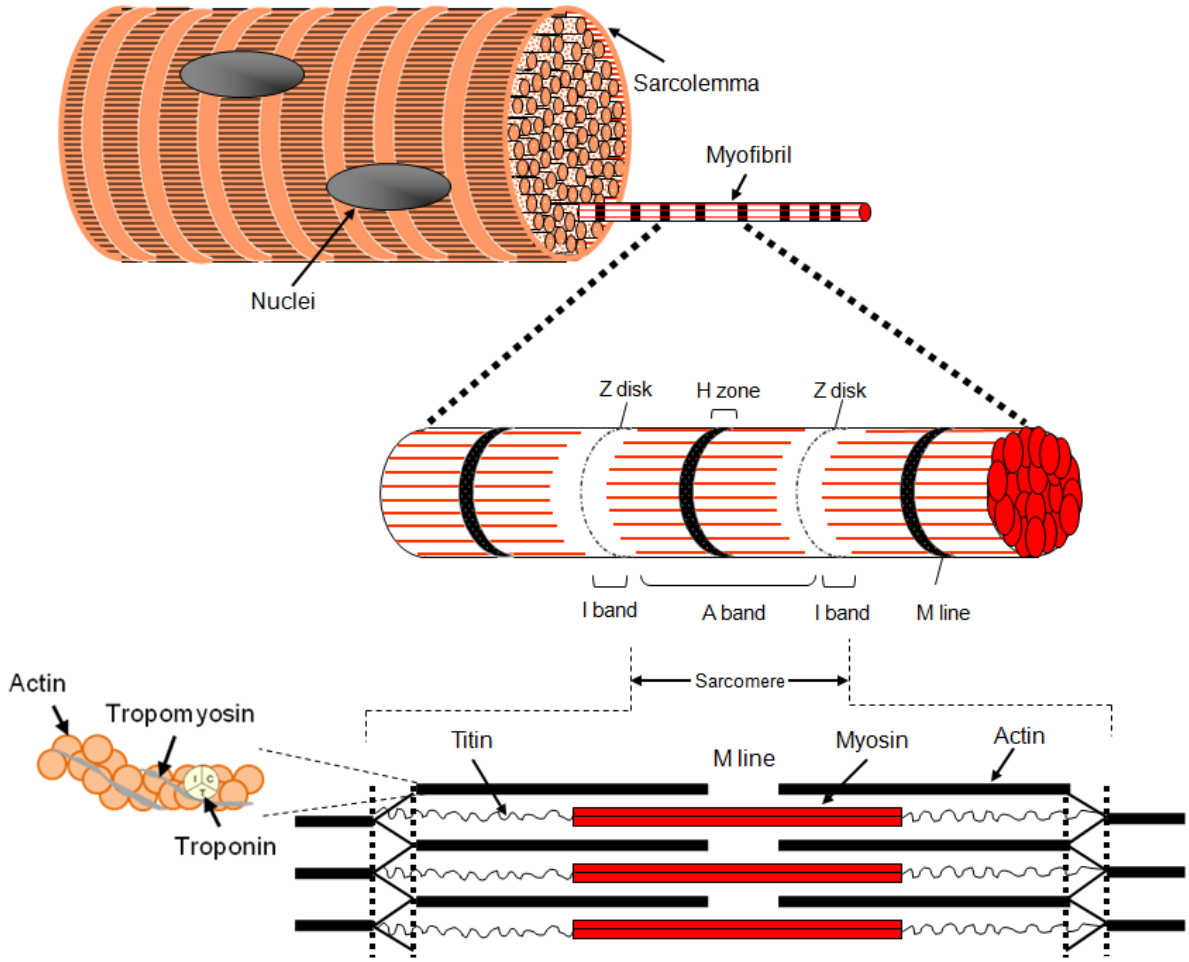

Figure 1-4 Structure of skeletal muscle

Skeletal muscle is composed of muscle fibres formed from many cylindrical subcellular structures called myofibrils which display a repeat banding pattern of overlapping thin and thick filaments organised in sarcomeres. The thin filaments are composed of three proteins: actin, tropomyosin, and troponin whereas the thick filaments comprise a large molecular weight protein called myosin. Titin is a large molecular weight protein that extends from the M lines to the Z disks and is associated with thick filaments (Farah and Reinach 1995;Tajsharghi 2008).

The thin filaments of skeletal muscle are composed of three proteins: actin, tropomyosin and troponin. Actin has myosin-binding sites and when the muscle

is at rest, tropmyosin blocks the myosin-binding sites, so that actin and myosin cannot interact. When contraction occurs, tropomyosin is displaced allowing actin and myosin to interact. This is caused by the Ca^{2+} sensitive conformational changes in the troponin complex (Farah and Reinach 1995). Troponin consists of three globular proteins located at regular intervals along the tropomyosin filaments. When the intracellular calcium ions concentration increases, calcium binds to troponin C resulting in a conformational change within troponin complex (Farah and Reinach 1995;Tajsharghi 2008). During excitation-contraction coupling in skeletal muscle, calcium ions increase in the cytosol in response to depolarisation of the fibre's exterior membranes. Excitation begins with the arrival of a neurotransmitter at the sarcolemma followed by the release of calcium ions from the sarcoplasmic reticulum resulting in muscle contraction (Wingertzahn and Ochs 1998).

Skeletal muscle is intrinsically elastic and can stretch and return to its original length; however, actin and myosin filaments do not display long-range elasticity. Another integral part of the myofibril called titin, connecting myosin filaments, forms a third filament system of the sarcomere. This filament system spans from the Z disk to the M line (Wang et al. 1991) and is important for the structural integrity of the myofibril and the passive tension response of a stretched muscle fibre. Titin's force repositions the thick filaments in the center of the sarcomere after contraction or stretches maintaining sarcomere length (Labeit et al. 1997).

1.1.3 Skeletal muscle fibre types

Skeletal muscle fibres are very heterogeneous in their structural and functional properties (Table 1-1).

Table 1-1 Similarities and differences between the fibre types of skeletal muscle

Fibre type	Type I fibres	Type IIa fibres	Type IIx fibres	Type IIb fibres
Contraction time	Slow	Moderately fast	Fast	Very fast
Size of motor	Small	Medium	Large	Very large
Resistance to fatigue	High	Fairly high	Intermediate	Low
Activity used for	Aerobic	Long-term anaerobic	Short-term anaerobic	Short-term anaerobic
Max. duration of use	Hours	<30 minutes	<5 minutes	<1 minute
Power produced	Low	Medium	High	Very high
Mitochondrial density	High	High	Medium	Low
Capillary density	High	Intermediate	Low	Low
Oxidative capacity	High	High	Intermediate	Low
Glycolic capacity	Low	High	High	High
Major storage fuel	Triglycerides	Creatine phosphate, glycogen	Creatine phosphate, glycogen	Creatine phosphate, glycogen
Myosin heavy chain	MYH7	MYH2	MYH1	MYH4

In general, adult mammalian muscle can contain four major myosin heavy chain (MHC) isoforms which are functionally distinct. They present different actin-activated ATPase actions and produce different rates of thin filament motility (Wells et al. 1996). Therefore, muscle fibres have been classified into two main types: type I (slow-twitch, oxidative) and type II (fast-twitch, glycolytic) and also into IIa / IIb / IIx subtypes. Type I fibres express slow MHC isoforms. These fibres are resistant to fatigue generating energy by oxidising fatty acids as a fuel source whereas type II fibres expressing fast MHC isoforms can achieve much higher shortening velocities, but fatigue relatively quickly when compared to type I fibres because they utilise anaerobic glycolytic metabolism for energy production (Bottinelli and Reggiani 2000;Brooks 2003). Type IIa and IIx fibres produce energy from fatty acid oxidation and glycolysis whilst type IIb fibres are solely glycolytic

(Bottinelli and Reggiani 2000). The majority of muscle beds are composed of both type I and type II fibres; however, the muscle composition varies according to its action. Exercise can influence MHC expression which consequently triggers switching from type IIb to type IIa and type I fibres (Jarvis et al. 1996).

There is also type IId fibre types identified in mouse, rat and rabbit (Hamalainen and Pette 1993) as well as type IIc included within the type IIa fibre class and found in rat (about 4%) (Tasic Dimov and Dimov 2007), but they are very rare in human (less than 1-2%) (Billeter et al. 1980). In addition, muscle can also consist of “hybrid" fibres containing two MHC isoforms such as type I/IIa, IIax or IIxb found in both human and mouse (Bloemberg and Quadrilatero 2012; Smerdu et al. 1994).

1.1.4 Regulators of skeletal muscle development

Numerous environmental and hormonal factors are sensed by skeletal muscle to regulate proliferation and differentiation of satellite cells leading to muscle growth and development or atrophy. The positive signals (anabolic factors) include exercise, insulin-like growth factors (IGFs) and nutrients whereas negative inputs (catabolic factors) are derived from cytokines, glucocorticoids and myostatin (Figure 1-5).

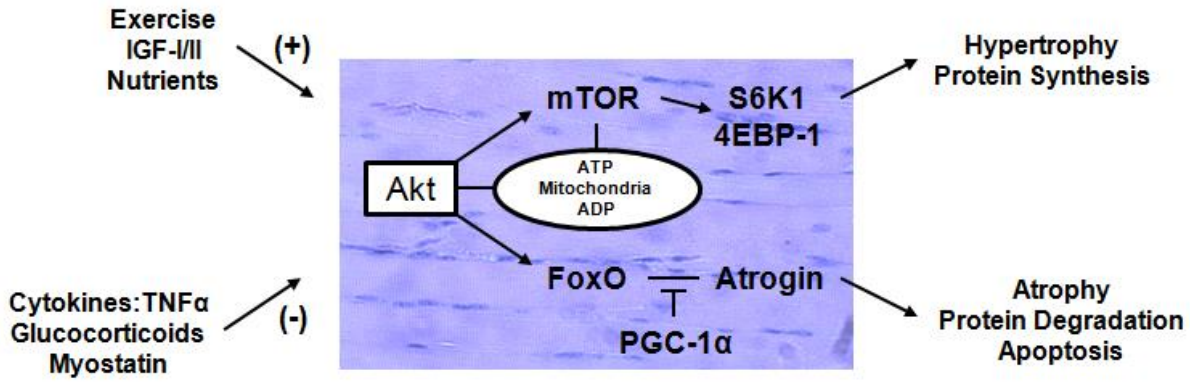

Figure 1-5 A representation of genetic and environmental factors determining skeletal muscle size

As a response to diverse stimuli, the protein kinase Akt plays a central role in integrating the anabolic and catabolic triggers by transducing growth factor and cytokine signals via changes in the phosphorylation of other metabolically important enzymes [mammalian target of rapamycin (mTOR)] and transcription factors (FoxO). The mTOR activates protein translation and synthesis via S6 kinase 1 (S6K1) and 4E binding protein 1 (4EBP-1) phosphorylation to stimulate hypertrophy. In contrast, a decrease in Akt signalling stimulates the expression of FoxO-dependent atrophy related genes such as atrogin-1 and other components of the proteasome to degrade muscle protein and initiate muscle wasting. However, the peroxisome proliferator activated receptor-γ co-activator 1α (PGC-1α) protects muscle from atrophy by inhibiting FoxO (Frost and Lang 2007).

The IGF-I, synthesised by skeletal myocytes and the liver, acts via an autocrine, paracrine and also endocrine mechanism through the IGF-insulin receptor (IGF-IR) which is expressed on the cell surface of skeletal muscle (Goldspink 1999). Initially, IGF-I inhibits differentiation and promotes myogenesis, subsequently stimulating differentiation of skeletal myoblasts (Adi et al. 2002;Engert et al. 1996).

Myostatin, a member of the transforming growth factor β (TGF-β) superfamily, is an important regulator of muscle growth. Myostatin acts *in vivo* by regulating the balance between proliferation and differentiation of embryonic muscle progenitors. It promotes satellite cells terminal differentiation through the activation of p21 and MyoD (McCroskery et al. 2003). Loss of function of myostatin in mice and cattle

displays induced hyperplasia and, to a lesser extent, hypertrophy of muscle suggesting that myostatin negatively regulates muscle growth by inhibiting myoblast proliferation (Kambadur et al. 1997;Thomas et al. 2000;Zhu et al. 2000).

There are also other factors associated with regulating myocyte development such as hepatocyte growth factor (HGF) and fibroblast growth factor-1 and -2 (FGF1, -2); they enhance muscle cells proliferation in response to muscle damage and regulate satellite cell activation in response to muscle injury, respectively (Flanagan-Steet et al. 2000;Maina et al. 1996).

Additionally, certain endogenous steroids, including androgens such as testosterone in males and oestrogens in post-menopausal women on estrogen replacement therapy, impact upon myocyte development increasing skeletal muscle mass (Fink et al. 2006;Sipila and Poutamo 2003).

1.1.5 Energy-supplying pathways during contraction in the skeletal muscle

Skeletal muscle is vital to life by providing the mechanical power for locomotion, posture and breathing. Force in muscle is generated by the myosin “cross-bridges” formed by the myosin motor head interacting with specific sites on a thin actin filament. During this process, ATP binds to the ATPase site on the myosin motor head, upon which it is hydrolysed to adenosine diphosphate (ADP) and inorganic phosphate leading to a conformational change with actin release from the actin-myosin complex and the myosin filament movement along the actin filament (Geeves and Holmes 1999).

There are three sources of high-energy phosphate to keep the ATP pool in the range required for muscle contraction (Figure 1-6). Of greater quantitative importance for the ATP generation is the utilisation of creatine phosphate, also called phosphocreatine, stored in the muscle. Creatine phosphate contains a high-energy phosphate bond that can be hydrolysed to re-synthesize ATP. Skeletal muscle stores of creatine phosphate provide quantitatively the greatest contribution to energy provision in the first few seconds of high intensity exercise such as sprinting (Greenhaff 2001).

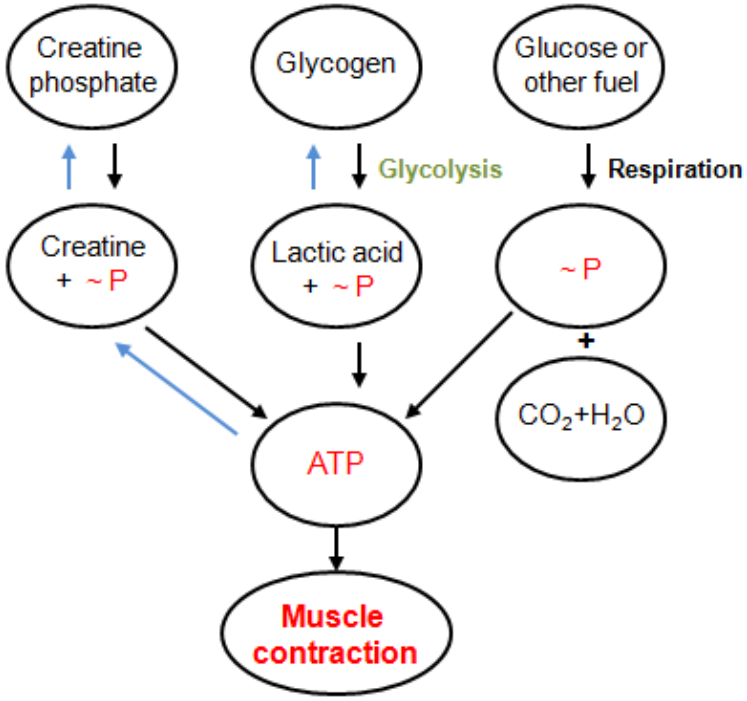

Figure 1-6 Sources of energy for muscle contraction

Three sources of high-energy phosphate to keep the ATP pool filled include creatine phosphate, glycogen and cellular respiration in the mitochondria of the fibres.

In addition, ATP can be also generated through glycolysis by which glycogen and glucose are converted to two pyruvate molecules. During anaerobic glycolysis, pyruvate forms lactic acid via lactate dehydrogenase yielding only 3 ATP per

molecule of glycogen, but the maximum rate of glycolysis can be reached within a few seconds of the onset of exercise. In the presence of oxygen, pyruvate enters the Krebs cycle as acetyl-CoA via the pyruvate dehydrogenase complex (PDHC). In contrast, complete breakdown of glycogen via glycolysis, the Krebs cycle and the electron transfer chain yields 39 ATP per molecule of glycogen (Burton et al. 2003).

Another energy source in the form of ATP for muscle contraction is provided by oxidation of blood glucose and β-oxidation of fatty acids (detailed in Section 1.1.7).

1.1.6 Glucose metabolism in the skeletal muscle

Of great importance is the role of skeletal muscle in metabolic regulation as the major site of glucose disposal after a meal either for storage as glycogen or its utilisation in energy generating pathways (Angione et al. 2011;Larsen et al. 2008).

Glucose is an obligatory metabolic fuel used by all cells of the body, with some tissue such as the brain greatly dependent upon it. It is derived from three sources: intestinal absorption during the fed state, glycogenolysis and gluconeogenesis during fasting. In muscle, glucose is transported through the insulin-dependent glucose transporter type 4 (GLUT-4) on the cell membrane where it is irreversibly phosphorylated by the enzyme hexokinase to glucose-6-phosphate (G6P) (Whitesell et al. 2003), and then depending on requirements and hormonal signals, stored as glycogen or metabolised in a number of metabolic pathways (Figure 1-7).

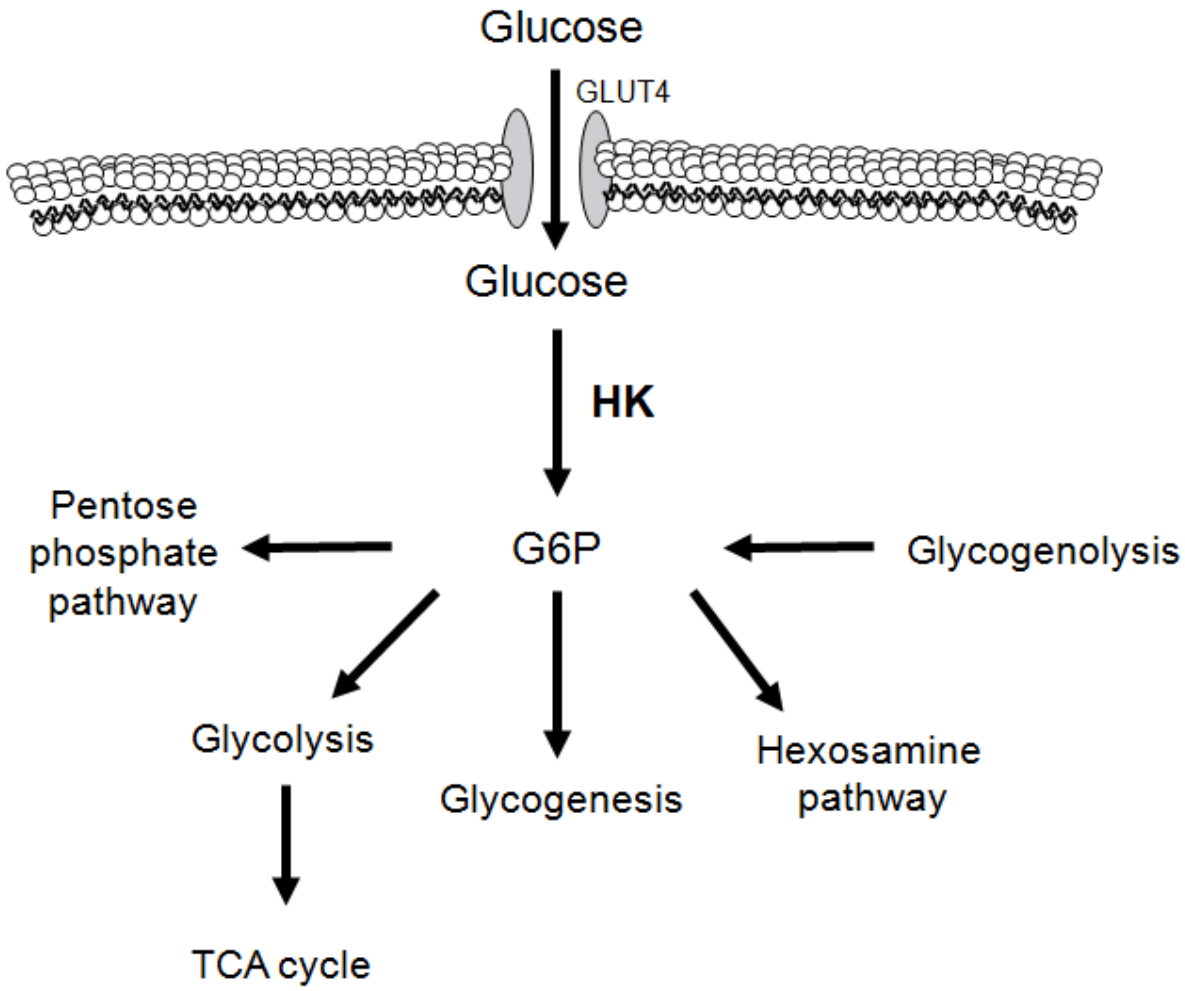

Figure 1-7 Glucose sensing in the skeletal muscle

In muscle, glucose is phosphorylated to G6P by hexokinase (HK), and then G6P is utilised in a variety of metabolic pathways. Abbreviations: GLUT4 (glucose transporter type 4), G6P (glucose-6-phosphate), TCA (tricarboxylic acid) cycle.

Glycolysis is the metabolic pathway that converts glucose to the monocarboxylates such as pyruvate or L-lactate and is highly regulated by a number of factors including phosphofructokinase and glyceraldehyde 3-phosphate dehydrogenase (GAPDH). The free energy released in this process is used to form the high-energy compounds ATP and reduced nicotinamide adenine dinucleotide (NADH) (Kockskamper et al. 2005). Lactate and pyruvate can be transported from muscle to

liver where they can be utilised as gluconeogenic precursors to form glycogen as required. Glycogenolysis involves the breakdown of glycogen to G6P, and subsequently G6P is hydrolysed by glucose-6-phosphatase to free glucose (Gerich et al. 2001). Interestingly, during fasting, muscle can decrease its glucose uptake using oxidised fatty acids as the main energy source and releasing alanine, glutamine and other amino acids that can be metabolised in gluconeogenesis for net glucose production by the liver (Larsen et al. 2008). Also, G6P can be converted to fructose-6-phosphate and then metabolised through the hexosamine pathway. The hexosamine pathway is a relatively minor branch of glycolysis encompassing ~3% of total glucose utilised. In the first step of this pathway, fructose-6-phosphate is converted to glucosamine-6-phosphate by the rate-limiting enzyme glutamine:fructose-6-phosphate amidotransferase. The end product of the hexosamine pathway, uridine diphosphate N-acetylglucosamine, serves as a common precursor for all amino sugars used for synthesis of glycoproteins, lipids and proteoglycans (Schleicher and Weigert 2000).

In addition, the pentose phosphate pathway is an alternative metabolic pathway for glucose breakdown that synthesises precursors for nucleotide biosynthesis and generates nicotinamide adenine dinucleotide phosphate reduced (NADPH). Depending on the cell requirements, NADPH can be utilised for anabolic reactions as well as maintaining cellular redox homeostasis. The pentose phosphate pathway is comprised of two phases: the oxidative and non-oxidative phases. The rate-limiting enzyme of this pathway is glucose-6-phosphate dehydrogenase (G6PDH) which converts G6P to 6-phosphoglucono-δ-lactone and consequently generates NADPH (Tsouko et al. 2014).

The citric acid cycle, also known as the tricarboxylic acid (TCA) cycle, or the Krebs cycle, is a key metabolic pathway that unifies carbohydrate, lipids and protein metabolism. Glycolysis supplies pyruvate that is oxidised by the mitochondrial TCA cycle, and the reducing equivalents are transferred through the electron transport chain for ATP production (Fernie et al. 2004).

1.1.7 Fatty acids β-oxidation in the skeletal muscle

Fatty acids provide highly efficient energy storage as they are stored as triglycerides in adipose tissue forming anhydrous fatty droplets. In the fasted state when glucose levels are low, lipid oxidation is the predominant metabolic activity of resting skeletal muscle (Kim et al. 2000). Free fatty acids are oxidised to provide energy in the form of ATP through the mitochondrial β-oxidation pathway. Fatty acids are transported in the form of acyl-CoAs across the outer mitochondrial membrane. This is a rate limiting step of β-oxidation dependent upon carnitine palmitoyltransferase-1 (CPT-1) which controls a long-chain fatty acid entry into the mitochondria forming acylcarnitine (Bruce et al. 2006;Dagher et al. 2001). Chemical inhibition of CPT1 by etomoxir promotes lipid deposition and insulin resistance in rats placed on a high-fat diet (Dobbins et al. 2001) whereas overexpression of CPT1 in skeletal muscle ameliorates high fat diet-induced insulin resistance by enhancing fatty acid oxidation (Bruce et al. 2009).

Subsequently, acylcarnitine is transported across the inner mitochondrial membrane via carnitine translocase (CAT), and then is converted back to acyl-CoA by an enzyme located in the inner mitochondrial membrane, CPT2, leaving the free carnitine to cycle back to the cytosol. Once in the mitochondrial matrix, acyl-CoA is

broken down in four reactions that occur in repeating cycles involving the following enzymes: acyl-CoA dehydrogenase, enoyl-CoA hydratase, L-3-hydroxyacyl-CoA dehydrogenase and 3-ketoacyl-CoA thiolase. In each round, acyl-CoA is progressively shortened by two carbons producing acetyl-CoA and one molecule of NADH and flavin adenine dinucleotide ($FADH_2$) respectively (Lopaschuk et al. 2010). Next, this acetyl-CoA enters the mitochondrial TCA cycle whereas both NADH and $FADH_2$ are used by the electron transport chain to generate ATP molecules.

1.1.7.1 Mitochondria in the skeletal muscle

In metabolically active skeletal muscle, mitochondria accounts for ~5% of the fibre volume and are rigidly located between bundles of myofilaments (Liu et al. 2014).

Mitochondria, called the ‘’biochemical powerhouse’’ of the cell, are highly dynamic organelles that undergo constant migration and morphological changes. Mitochondria are involved in a number of homeostatic and signaling processes such as the TCA cycle and β-oxidation of fatty acids (Liu et al. 2014;Patergnani et al. 2011). These organelles are the major site of oxidative metabolism playing critical role in ATP production. Mitochondria generate 36-38 of ATP molecules in the breakdown of a single glucose molecule by the reactions of the citrate cycle and the oxidation of the resulting NADH and $FADH_2$ by the respiratory chain (Tarasov et al. 2012).

Most mitochondria contain between one and ten copies of mitochondrial DNA (mtDNA) which is highly susceptible to oxidative damage mainly caused by the high concentration of reactive oxygen species within the mitochondrial matrix and the lack of DNA-protective histones. This results in strand breaks, abasic sites, base changes and deletions and consequently leads to malfunction of proteins synthesis and

altered mtDNA replication and/or transcription efficiency. The ratio of mtDNA to nuclear DNA is an indicator of mitochondrial biogenesis as the mitochondrial genome encodes most of the enzymatic subunits of the oxidative phosphorylation system (Phillips et al. 2014).

1.2 Hormonal regulation of skeletal muscle

Skeletal muscle is an endocrine organ producing systemic and local glucocorticoids (GCs). Muscle is also a target tissue for growth factors and hormones; amongst them are GCs and insulin. GC excess, seen in Cushing's syndrome, leads to muscle atrophy and metabolic changes.

1.2.1 Insulin

The primary role of insulin is to lower blood glucose and maintain its levels within an optimal range for normal physiological function. Insulin is a peptide hormone synthesised as a preprohormone in the β-cells of islets of Langerhans in the pancreas and is produced and stored in the body as an inactive hexamer. Circulating and biologically active insulin is a monomer composed of two polypeptide chains of 21 and 20 amino acids connected by two disulfide bridges (Sanger 1959).

Insulin secretion is mainly regulated by plasma glucose levels; however, other stimuli such as amino acids can also enhance its secretion. Circulating glucose enters pancreatic β-cells via the glucose transporter 2. Glucose is then phosphorylated by the enzyme glucokinase and further metabolised in the mitochondria generating ATP. Elevated ATP/ADP ratio closes the ATP-dependent K+ channels on the β-cell membrane. Decreased efflux of potassium ions and their increased levels at the

inner leaflet of the membrane lead to the cell membrane depolarisation and consequently open the voltage-dependent calcium channels increasing calcium concentration in the cytosol and subsequently leading to insulin secretion. Elevated blood glucose levels induce insulin release from the β-cells whilst a drop in blood glucose levels results in reduced rate of glycolysis and insulin secretion (Larsen et al 2008).

The action of insulin is mediated through the activation of cell surface receptors, mainly the insulin receptor (InsR) responsible for metabolic regulation but also insulin-like growth factor receptor (IGF-IR) involved in normal growth and development. The insulin signalling pathway is initiated by insulin binding to its receptors and their autophosphorylation on multiple tyrosine residues which lead to the activation of multiple signalling molecules. Insulin signalling induces glucose uptake and metabolism and also changes in lipid and protein metabolism (Larsen et al. 2008;Morgan et al. 2009).

1.2.2 Glucocorticoid structure, synthesis and action

Glucocorticoids (cortisol in humans and corticosterone in rodents) are endogenous steroid hormones released naturally from the adrenal cortex via stress-mediated or circadian activation of the hypothalamic-pituitary-adrenal axis (Section 1.2.2.3). They play an important role in energy homeostasis, immune response, skeletal muscle growth, cell proliferation and survival (Patel et al. 2014). GCs also exert critically important roles in muscle permissive and adaptive metabolism. They promote skeletal muscle atrophy by enhancing protein degradation and reducing protein synthesis pathways. These steroid hormones are widely used clinically for the

suppression of inflammation in chronic inflammatory diseases such as asthma, rheumatoid arthritis and autoimmune diseases.

The predominant actions of GCs are through the glucocorticoid receptor (GR), which forms a heterocomplex with 2 molecules of heat shock protein-90 (HSP90), stoichiometric amounts of heat shock protein-70 (HSP70), p23 and immunophilin (Pratt and Toft 1997). The GR is transferred between the cytoplasm and nucleus upon ligand binding. Steroid binds to GR leading to hsp-immunophilin complex dissociation. Subsequently, the liganded GRs rapidly dimerise and translocate into the nucleus where they bind to glucocorticoid response elements (GRE) on glucocorticoid-responsive genes resulting in modified transcription (Figure 1-8) (Barnes 1998).

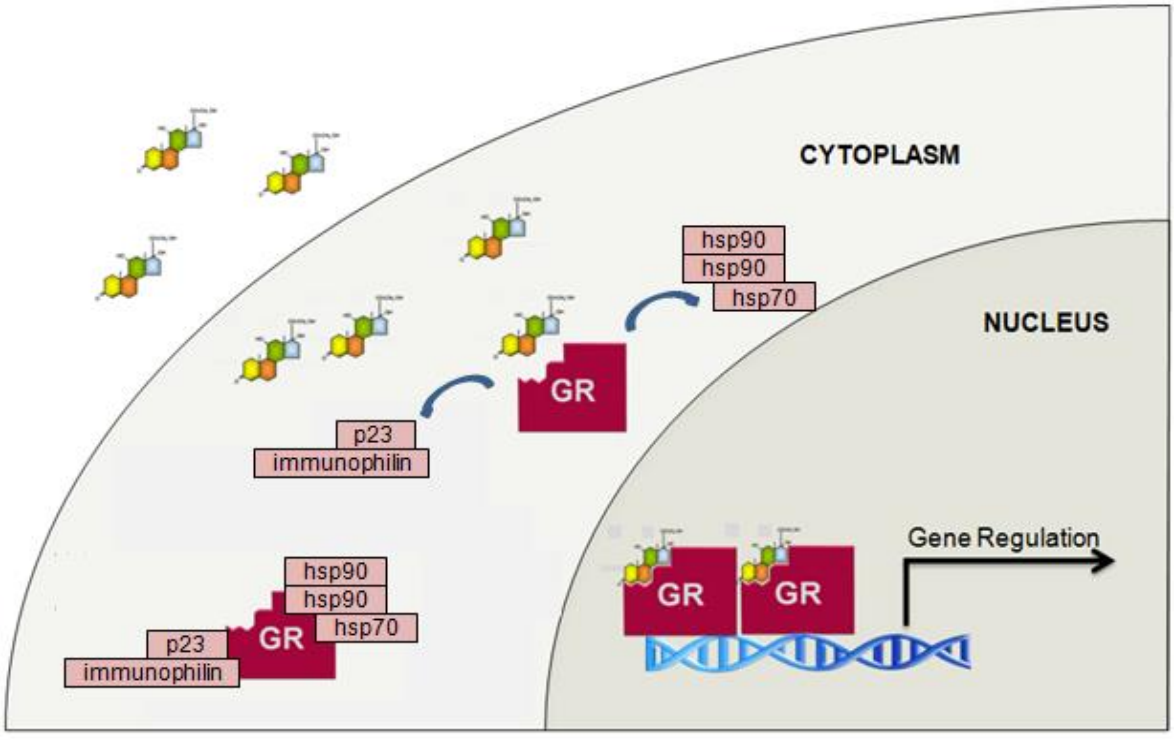

Figure 1-8 Genomic actions of glucocorticoids

Upon steroid binding to GR in the cytoplasm, the GR dimer translocates into the nucleus and regulates gene transcription.

However, not all responses to GCs are dependent upon GR dimers binding directly with DNA. Other pro-inflammatory signalling pathways involve GR monomers tethering with DNA-bound pro-inflammatory transcription factors such as nuclear factor-kappa B (NF-κB) (Nixon et al. 2011).

In addition to the genomic actions of GCs, some effects can occur within minutes of drug administration and are insensitive to transcriptional inhibition. These non-genomic GC effects are mediated by membrane-bound receptors or by physiochemical interactions with cellular membranes (Liu et al. 2005), and their example is the activation of the insulin signalling factors phosphatidylinositol 3-kinase (PI3K) and protein kinase B/akt demonstrated in human vascular endothetial cells (Hafezi-Moghadam et al. 2002). Recent findings suggest that non-genomic activity might be important in mediating the therapeutic effects when used in high dose to reduce side effects (Liu et al. 2005).

Physiologically, GCs increase blood glucose and fatty acids stimulating hepatic gluconeogenesis and adipose tissue lipolysis in the fasting state. Though, in the fed state they work with insulin to promote carbohydrate and lipid storage. GCs also inhibit the translocation of the GLUT-4 to the cell membrane consequently leading to reduced level of intracellular glucose (Morgan et al. 2004). They inhibit the activity of lipoprotein lipase in skeletal muscle and the uptake of circulating triglyceride leading to dislipidemia (Whorwood et al. 2002). Overall, the action of glucocorticoids mainly depends on the levels of circulating GC and GR expression (Abdallah et al. 2005a).

1.2.2.1 Adrenal glands

Glucocorticoids such as cortisol can be synthesised by the adrenal glands in response to stress (van Raalte et al. 2009). These organs are positioned above the kidneys and surrounded by a capsule of adipose and fibrous tissue. Each gland is composed of two distinct structures called the medulla and the cortex. The adrenal cortex constitutes 90% of the weight of the adrenal gland and is divided into three distinct zones: the outer zone called zona glomerulosa located beneath the capsule; the thickest zone, zona fasciculata, (>70% of the cortex) and the zona reticularis located next to the medulla (Figure 1-9). The adrenal glands have one of the highest blood supplies per gram of tissue, delivered to this gland by the inferior phrenic artery, the renal arteries and the aorta (Arlt and Stewart 2005;Rosol et al. 2001).

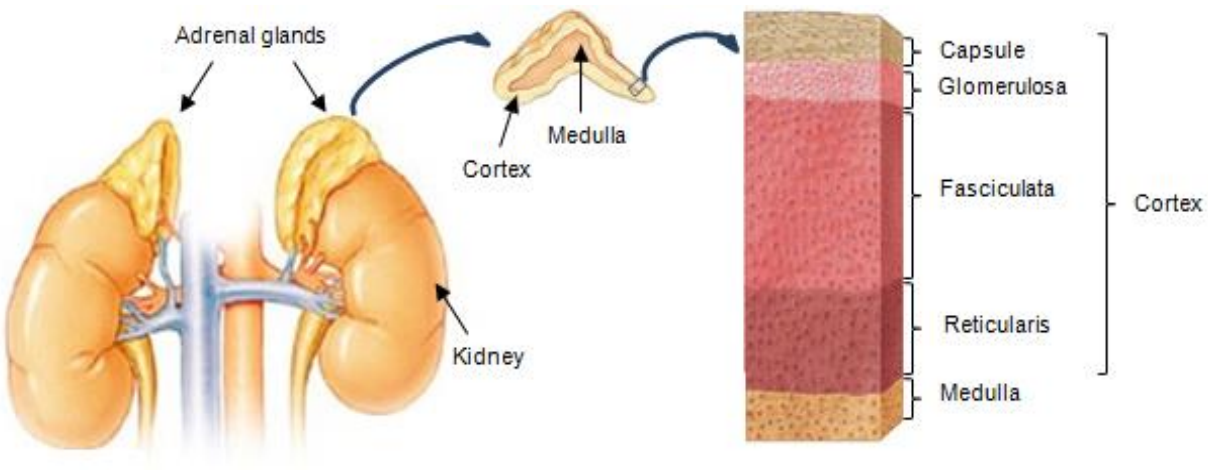

Figure 1-9 The structure of adrenal glands

The adrenal glands are located above the kidneys and are divided into two distinct structures: the outer adrenal cortex and the inner adrenal medulla. The cortex comprises three distinct zones: the glomerulosa, fasciculata and reticularis.

1.2.2.2 Steroidogenesis

There are three main types of hormones produced by the adrenal cortex: glucocorticoids (cortisol, corticosterone), mineralocorticoids (aldosterone, deoxycorticosterone) and sex steroids [dehydroepiandrosterone (DHEA), androstenedione]. All steroid hormones are derived from the cyclopentanoperhydrophenanthrene structure which contains three cyclohexane rings and a single cyclopentane ring (Figure 1-10). Cholesterol is the precursor for all adrenal hormones, and it can be either generated *de novo* from acetyl-CoA within the adrenal cortex or provided from the circulation in the form of low-density lipoprotein (LDL) cholesterol (Arlt and Stewart 2005;Larsen et al. 2008).

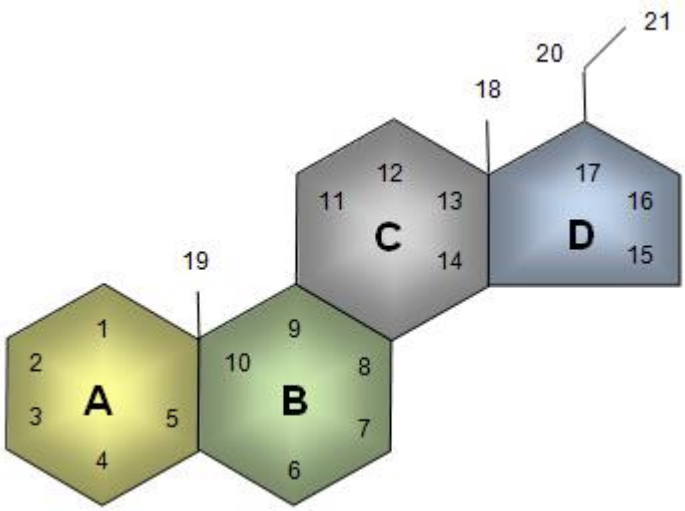

Figure 1-10 The cyclopentanoperhydrophenanthrene structure of adrenal steroids

The letters designate the rings whereas the numbers designate the carbon atoms.

There are a number of enzymes driven by biochemical pathways and involved in the synthesis of steroids which takes place in three different zones of the adrenal cortex (Figure 1-11). The initial step of steroidogenesis is the transport of intracellular cholesterol from the outer to inner mitochondrial membrane where it is converted to

pregnenolone by the P450 cholesterol side chain cleavage enzyme (P450scc). In the cytoplasm, 3β-hydroxysteroid dehydrogenase type II (3β-HSD) converts pregnenolone to progesterone which is hydroxylated to 17-OH-progesterone by P450c17. 17-Hydroxylation is important for glucocorticoid synthesis secreted in high amounts from the zona fasciculata under the control of adrenocorticotropic hormone (Arlt and Stewart 2005). By contrast, the zona glomerulosa is specialised for mineralocorticoid synthesis because of the zonal-specific expression of aldosterone synthase (CYP11B2, P450c18). Both zona fasciculata and zona reticularis express P450c17 which beside 17α-hydroxylase also possesses 17,20 lyase activity resulting in the production of DHEA and androstenedione in zona reticularis. DHEA is coverted to DHEAS, the major product of adrenal steroidogenesis, by DHEA sulfotransferase (SULT2A1) (Arlt & Stewart 2005;Larsen et al. 2009).

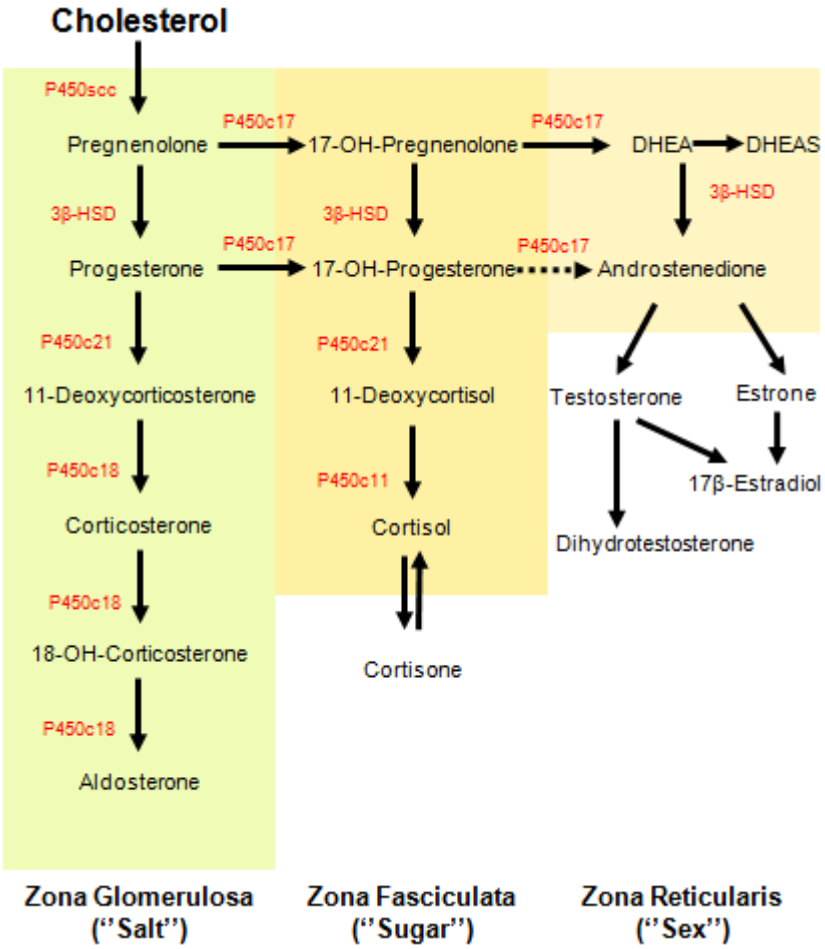

Figure 1-11 Adrenal steroidogenesis

Each zona of the adrenal cortex has distinct enzyme profile and is responsible for synthesis of specific steroids.

In contrast to humans, rodents do not express P450c17 in the adrenal glands consequently lacking 17α-hydroxylase activity to produce cortisol. Therefore, the most abundant naturally occurring GC they generate is corticosterone (Košir et al. 2011).

1.2.2.3 The hypothalamus-pituitary-adrenal axis

Glucocorticoid hormones are secreted by the cortex of the adrenal gland under the control of the hypothalamic-pituitary-adrenal (HPA) axis (Figure 1-12)

(van Raalte et al. 2009). In response to stress, the hypothalamus releases cortocotropin-releasing hormone (CRH) into the hypophyseal portal vein. CRH stimulates the anterior pituitary to secrete adrenocorticotropic hormone (ACTH) into the circulation. Subsequently, ACTH drives the adrenal gland to secrete cortisol which can inhibit its own release through a classical feedback process involiving the negative regulation of CRH and ACTH release (Gathercole et al. 2013).

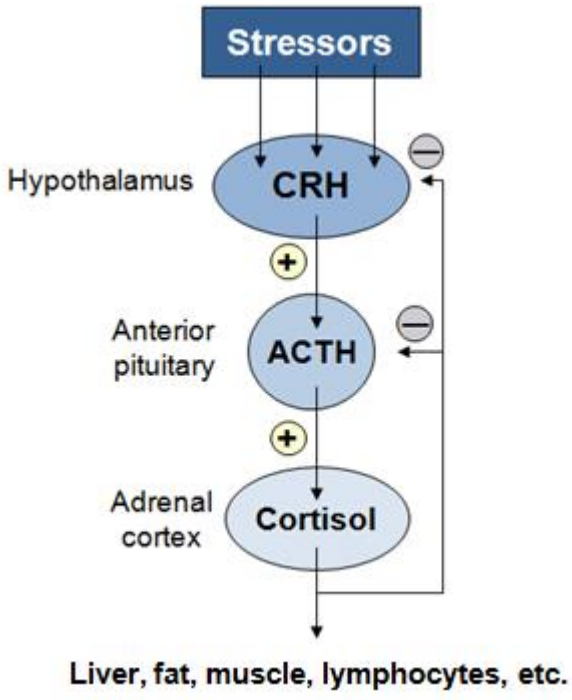

Figure 1-12 Regulation of adrenal glucocorticoid secretion by HPA axis

ACTH is secreted from the anterior pituitary under the influence of CRH which is released by the hypothalamus in response to stressors (hypoglycaemia, hypotension, surgery, injury etc.). Negative feedback of cortisol inhibits both CRH and ACTH secretion. Abbreviations: CRH (cortocotropin-releasing hormone), ACTH (adrenocorticotropic hormone).

Corisol is secreted at a rate of 10-15 mg/dL in a pulsatile fashion with a circadian rhythm with different levels throughout a 24 hour cycle (highest levels on wakening followed by a slow decline through the day). Circulating GC levels are greater during

the activity period [day for diurnal species (humans) and night for nocturnal species (rodents)] reaching their peak levels at the beginning of the activity period (Gathercole et al. 2013;Larsen et al. 2008).

1.2.2.4 Metabolic actions of glucocorticoids

Physiologically, GCs are released as a part of the response to stress, inflammation, pain or infection. They are among the most effective medications for the treatment of inflammatory disease (rheumatoid arthritis), autoimmune and allergic diseases (Song et al. 2011). However, long exposure to GCs leads to muscle myopathy, osteoporosis, accumulation of visceral fat depot or metabolic disease such as insulin resistance and type 2 diabetes (Figure 1-13) (Gathercole et al. 2013).

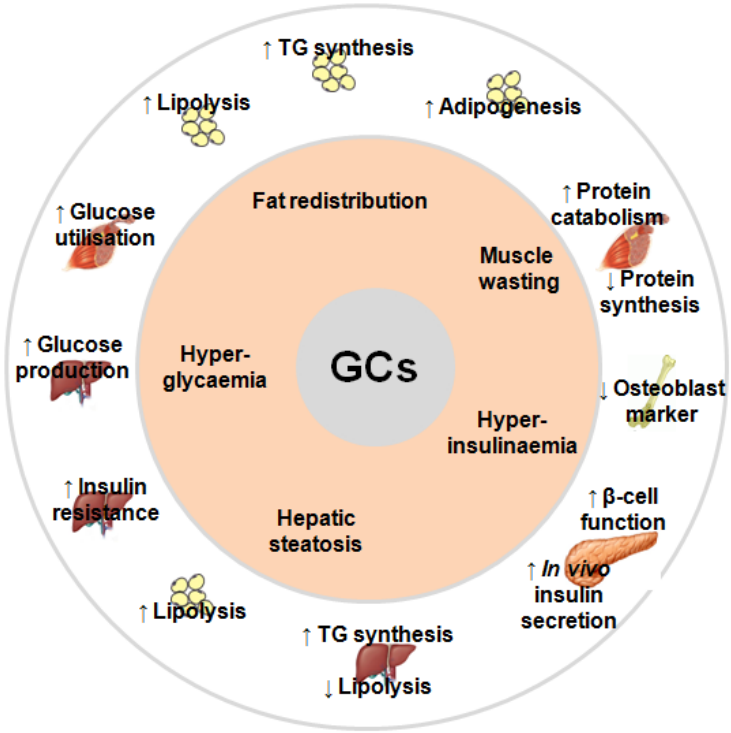

Figure 1-13 A summary of selected GC-induced pathways and GC-responsive tissues

GCs have diverse actions that affect a number of tissues including liver, skeletal muscle and adipose tissue. Abbreviations: GC (glucocorticoid), TG (triglyceride).

GCs regulate numerous tissue-specific physiological processes. In liver, they enhance gluconeogenesis and glucose release stimulating the activity of gluconeogenic enzymes. GCs also control carbohydrate metabolism by increasing hepatic glucose output during fasting contributing to the hyperglycaemic state (Gathercole et al. 2013;Kraus-Friedmann 1984). In addition, GCs inhibit hepatic lipolysis by stimulating the production of the LDL particles and decreasing intrahepatic triglyceride turnover (Dolinsky et al. 2004).

In adipose tissue, GCs regulate both adipogenesis and hypertrophy enhancing pre-adipocyte differentiation and triglyceride (TAG) accumulation resulting in central obesity seen in the Cushing's syndrome. However, GCs increase lipolysis leading to elevated circulating free fatty acid levels (Peckett et al. 2011). Thus, the effect of GCs in adipose tissue differs depending on the depot; hence, their impact on insulin sensitivity in adipose tissue still remains unclear.

In skeletal muscle, GCs directly interfere with the insulin signaling cascade resulting in decreased insulin-mediated glucose uptake (IMGU) and glycogen synthesis (Peppa et al. 2010). GCs inhibit glucose uptake mainly through inhibition of GLUT4 translocation to the membrane and glucose utilisation in skeletal muscle (Patel et al. 2014). Furthermore, GCs reduce skeletal muscle mass both by inhibiting protein synthesis and by inducing protein degradation known as steroid myopathy (Long et al. 2001). They decrease protein synthesis by reducing transport of amino acids into muscle and by inhibiting the anabolic effects of insulin and IGF1 (Biedasek et al. 2011;Itoh et al. 2004;van Raalte et al. 2009). GC excess induces muscle atrophy by stimulating catabolic pathways (protein breakdown) through

increased expression of the two E3 ubiquitin ligases atrogin-1 and muscle ring finger 1 (MuRF-1) and inhibiting anabolic pathways (protein synthesis) (Biedasek et al. 2011;Bodine et al. 2001). Glucocorticoid-induced activation of the ubiquitin-proteasome-system and increased expression of the MuRF-1 and Antrogin-1 lead to muscle atrophy. Pharmacological use of GCs induces skeletal muscle catabolism which in rats, can be prevented with growth hormone or IGF-1 treatment (Itoh et al. 2004).

1.2.2.5 GC metabolism

Once in circulation, approximately 90% of cortisol is bound to a specific glucocorticoid α2-globulin leaving only 10% circulating in a free form. Endogenous and exogenous glucocorticoids act on intracellular receptors to regulate the transcription of specific target genes. The GR or type 2 corticosteroid receptor is ubiquitously expressed throughout the body whereas the mineralocorticoid receptor (MR or type 1 corticosteroid receptor) is mainly localised in specific anatomical sites, including the kidney, distal nephron, colon and sweat glands. Pre-receptor metabolism of glucocorticoids determines tissue-specific sensitivity. The MR is protected from glucocorticoid activation by the enzyme 11β-hydroxysteroid dehydrogenase type 2 (11β-HSD2) that converts active cortisol to inactive cortisone in humans whereas GR activation can be amplified by the enzyme 11β-hydroxysteroid dehydrogenase type 1 (11β-HSD1) catalysing the reverse reaction (Tomlinson et al. 2004).

1.2.2.6 11β-HSD and pre-receptor metabolism

Two isoforms of the enzyme 11β-hydroxysteroid dehydrogenase (11β-HSD) have been characterised and cloned: 11β-HSD1 and 11β-HSD2. Their N-terminal anchor sequences determine both dehydrogenases orientation exclusively to the endoplasmic reticulum (ER) membrane (Odermatt et al. 1999). The catalytic domain of 11β-HSD1 is located within the lumen of the ER (Ozols 1995) whereas the catalytic domain of 11β-HSD2 is orientated towards the cytosol (Odermatt et al. 1999).

The 11β-HSDs catalyse the convertion of hormonally active cortisol and inactive cortisone (Figure 1-14). 11β-HSDs belong to the short-chain dehydrogenases/reductases (SRDs) superfamily, also known as short-chain alcohol dehydrogenases. 11β-HSD1 is a predominantly NADPH-dependent isozyme acting mainly as a nicotinamide adenine dinucleotide phosphate ($NADP^+$)-dependent dehydrogenase in the cell-free system and a NADPH-dependent oxo-reductase in intact cells and tissues. 11β-HSD2 is a nicotinamide adenine dinucleotide (NAD^+)-dependent dehydrogenase (Tomlinson et al. 2004).

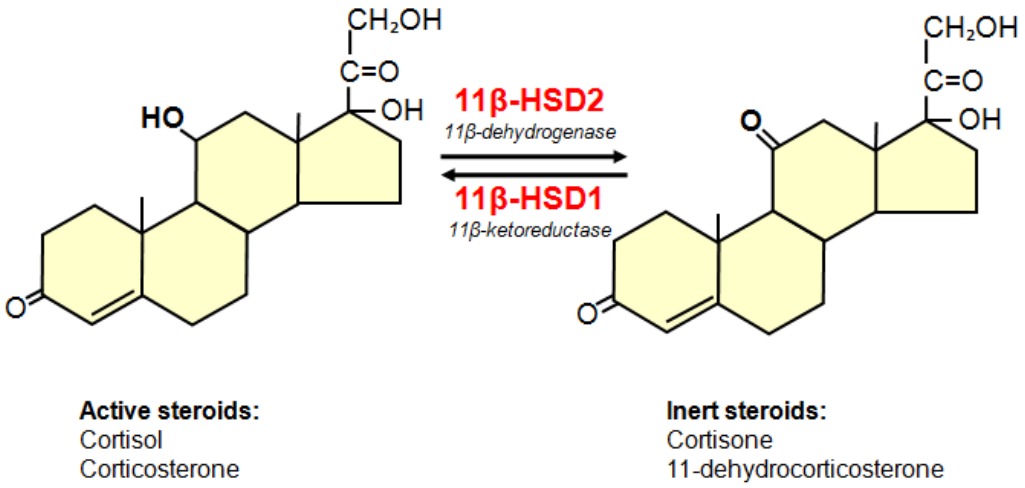

Figure 1-14 Cortisol-cortisone interconversion by the 11β-HSD enzymes

11β-HSD1 converts hormonally active cortisol in humans and corticosterone in rodents to inactive cortisone and 11-dehydrocorticosterone respectively whereas 11β-HSD2 catalyses the reverse reaction.

1.2.2.6.1 11β-hydroxysteroid dehydrogenase type 2

11β-HSD2 is a high-affinity NAD^+-dependent dehydrogenase that irreversibly converts active cortisol to cortisone. 11β-HSD2 is expressed mainly in kidneys and colon. The main function of this enzyme in the kidney is to exclude cortisol from binding to and activating the mineralocorticoid receptor (Edwards et al. 2007). Inactivating mutations in the *HSD11B2* gene lead to a syndrome named apparent mineralocorticoid excess (AME), in which GCs activate renal MR resulting in sodium retention, hypertension and hypokalemia. In addition, pharmacological inhibition or mutation of 11β-HSD2 in placenta reduces fetal growth and alters tissue maturation (Cottrell et al. 2013;Seckl 2004).

1.2.2.6.2 11β-hydroxysteroid dehydrogenase type 1

The *HSD11B1* gene is located on chromosome 1q32.2. It was first purified from rat liver by Carl Monder's group in 1988 (Lakshmi and Monder 1988). The human

enzyme was purified in 2002. The *HSD11B1* gene is over 30 kb in length consisting of 6 exons and 5 introns; it encodes a 34 kDa glycosylated enzyme (Tomlinson et al. 2004).

11β-HSD1 is highly expressed throughout the body in many metabolically active tissues such as liver, adipose tissue, skeletal muscle and brain. 11β-HSD1 is a bidirectional enzyme which predominantly acts as an oxo-reductase converting hormonally inactive cortisone in humans and 11-dehydrocorticosterone (11-DHC) in rodents to active cortisol and corticosterone, respectively, thereby increasing intracellular GCs and regulating metabolic processes including hepatic glucose output, cellular differentiation and energy metabolism (Hewitt et al. 2005; Jang et al. 2007;Lavery et al. 2007;Zielinska et al. 2011).

1.3 The SR as a metabolic unit to support GC metabolsim

The sarcoplasmic reticulum (SR) as a skeletal muscle metabolic unit compromises several metabolic pathways related to carbohydrate metabolism, biotransformation, steroid metabolism and protein processing.

The ER/SR is a specialised three-dimensional network of endomembranes, comprising a complex grid of microtubules and cisternae, responsible for protein folding, processing and trafficking to the cell surface (Deldicque 2013). The ER lumen is considered to be the largest intracellular organelle constituting about 10% of the total cell volume (Csala et al. 2006;Patergnani et al. 2011). There are three types of ER including smooth ER, rough ER and the nuclear envelope. Structural diversity of the ER is related to the variety of its cellular functions. Additionally to the protein

synthesis and maturation, the ER acts as proteins transport route and a dynamic reservoir of calcium ions (Patergnani et al. 2011).

The SR of skeletal muscle resembles the smooth ER found in other cell types. Importantly, the SR is the primary site of intracellular calcium storage, release and uptake in skeletal muscle (Rossi and Dirksen 2006). It controls the contraction-relaxation cycle of muscle by regulation of calcium ions in the cytosol (Section 1.1.2) (Xia et al. 2003).

Skeletal muscle can generate glucose from G6P through the SR luminal glucose-6-phosphatase-β (G6Pase-β) at the terminal step of glycogenolysis. This step requires transfer of G6P by the G6P transporter (G6PT) from cytosol to the lumen of the SR where G6Pase-β hydrolyses G6P to glucose and inorganic phosphate (Chen et al. 2010). G6P can be also metabolised by an enzyme, hexose-6-phosphate dehydrogenase (H6PDH), to produce 6-phosphogluconate (6PGL) and NADPH used by 11β-HSD1 for glucocorticoid activation (Section 1.2.2.6.2) (Figure 1-15) (Lavery et al. 2008b).

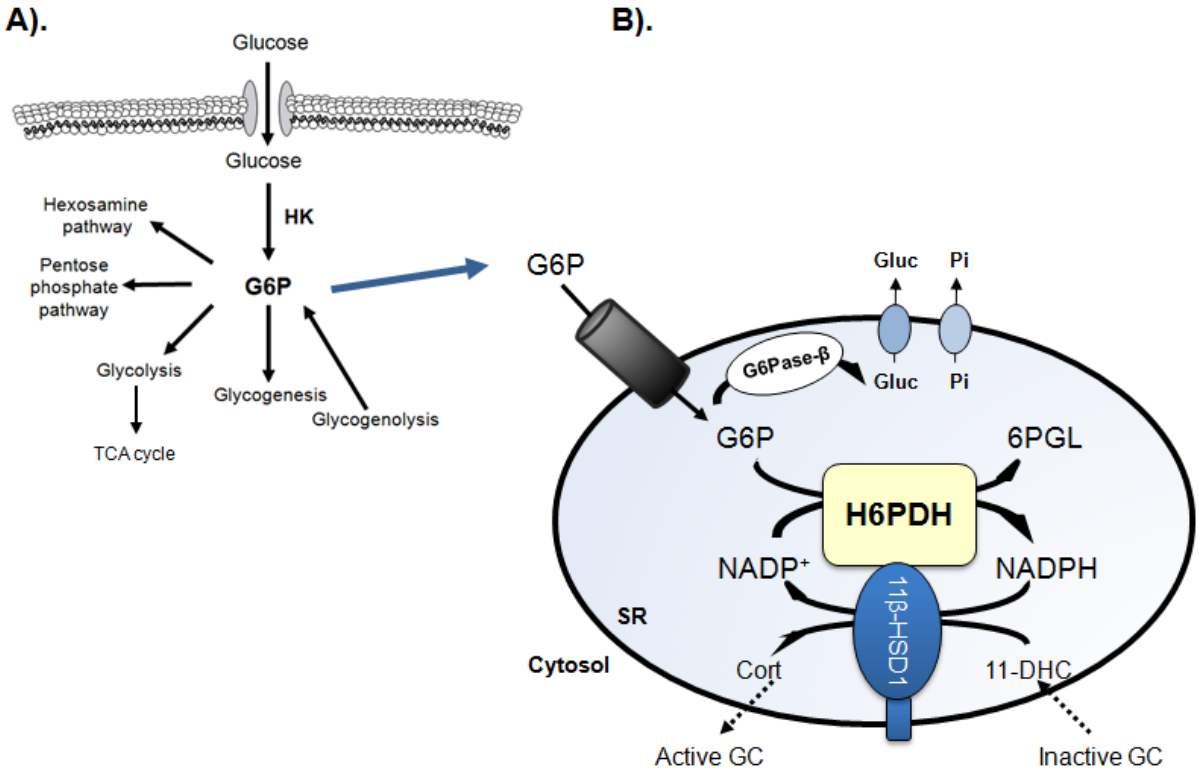

Figure 1-15 G6P metabolism in the SR lumen

G6P can be utilised in a number of pathways (A; detailed in Section 1.1.6); however, G6P can be also transported by G6PT from cytosol to the ER/SR lumen where is metabolised by H6PDH to produce NADPH utilised by 11β-HSD1 for GC activation (B).

1.3.1 Glucose-6-phosphate transporter (G6PT, Slc37a4)

G6P concentration in ER lumen is essential for determining 11β-HSD1 oxo-reductase activity (Walker et al. 2007). The primary function of G6PT is translocation of G6P from the cytoplasm to the lumen of the ER (Agrawal et al. 2012). G6P is then hydrolysed to glucose and inorganic phosphate by either G6Pase-α (restricted to liver, kidney and intestine) or G6Pase-β which is expressed ubiquitously (Shieh et al. 2003). A previous study showed that the concerted action of both G6PT and G6Pase-α is required to maintain glucose homeostasis between meals whereas the synchronised action of G6PT and G6Pase-β is important for normal neutrophil function (Pan et al. 2009). Furthermore, G6P transported by G6PT to the ER/SR can

also be utilised by enzyme H6PDH to produce 6PGL with the concomitant generation of NADPH, thereby maintaining adequate levels of reductive cofactors in the oxidising environment for 11β-HSD1 mediated glucocorticoid activation (Lavery et al. 2008b).

Human G6PT is a single copy gene consisting of 9 exons of approximately 5.3 kb of DNA located on chromosome 11q23. Human G6PT is a 10-transmembrane domain protein located in the ER lumen (Chen et al. 2003a).

Importantly, glycogen storage disease type I (GSD-I) is a group of autosomal recessive disorders caused by a deficiency in the enzyme G6Pase (GSD-Ia) or G6PT (GSD-Ib) (Chen et al. 2002). Together, G6PT and G6Pase maintain glucose homeostasis. Because their activities are co-dependent, both GSD-Ia and GSD-Ib patients manifest the symptoms of failed G6P hydrolysis such as growth retardation, hypoglycaemia, hepatomegaly, nephromegaly, hyperlipidemia and lactic academia (Chen et al. 2003b;Shieh et al. 2003). In addition, GSD-Ib patients present the symptoms of neutropenia and myeloid dysfunctions (Chen et al. 2003b). Mutations in *G6PC* (GSD-Ia) cause approximately 80% of GSD-I whereas mutations in *Slc37a4* (GSD-Ib) lead to 20% of GSD-I (Bali et al. 1993).

1.3.2 H6PDH and muscle function

H6PDH is a bifunctional enzyme that catalyses the first two steps of an ER-specific pentose phosphate pathway generating the cofactor, NADPH, for 11β-HSD1 promoting its oxo-reductase activity. H6PDH is a free-floating enzyme within the ER lumen whereas 11β-HSD1 is bound to the inner ER membrane

(Odermatt et al. 2001). H6PDH regulates the direction of endogenous 11β-HSD1 enzyme activity within the ER/SR lumen (Lavery et al. 2008b).

H6PDH was initially purified from rabbit liver microsomes and subsequently the human H6PDH cDNA and gene were cloned and identified (Mason et al. 1999). Sequence analyses indicate that H6PDH is biochemically distinct from its cytosolic homolog, G6PDH (Hewitt et al. 2005; White et al. 2007). Similarities and differences between both enzymes are summarised in the Table 1-2 (Senesi et al. 2010).

Table 1-2 Comparison of G6PDH to H6PDH

Characterisation	G6PDH	H6PDH
Chromosome location	Xq28	1p36
Sequence length	515 AA	791 AA
Catalysed reaction	D-G6P + $NADP^+$= D-glucono-1,5-lactone-6-phosphate + NADPH	D-G6P + $NAD(P)^+$ + H_2O= 6-phospho-D-gluconate + NAD(P)H
Cofactors	$NADP^+$	$NAD(P)^+$, deoxy $NADP^+$
Substrates	G6P	G6P, hexose-6-phosphates, glucose-6-sulfate, glucose
Intracellular location	Cytosol, soluble	ER, soluble
Interactions	Homodimer or homotetramer	Homodimer, association to 11β-HSD1
Involvement in pathology	Chronic non-spherocytic hemolytic anemia	Apparent cortisone reductase deficiency, skeletal myopathy

To investigate the role of H6PDH in regulating 11β-HSD1 activity and GC metabolism, H6PDH global knockout (H6PDHKO) mice were previously generated. Inactivation of murine *H6PD* gene changes the direction of 11β-HSD1, only dehydrogenase activity was detectable in a variety of H6PDHKO tissues.

Additionally, urine analysis from H6PDHKO mice revealed the presence of mostly metabolites of 11-DHC. These findings confirm that H6PDH plays an essential role in the regulation of NADPH-dependent oxo-reductase activity of 11β-HSD1 (Lavery et al. 2006).

1.3.2.1 NADPH/$NADP^+$ redox status in the SR

H6PDH is a housekeeping enzyme, and within the SR utilises G6P and $NADP^+$ to generate reducing NADPH for several ER reductases including 11β-HSD1. H6PDH may act as a metabolic sensor by connecting intermediary metabolism to hormonal signalling (Banhegyi et al. 2009). Changes in an NADPH/$NADP^+$ ratio in the SR might cause disruption in the thiol-disulfide redox leading to incorrect protein folding and activation of the unfolded protein response (UPR) pathway as a compensatory mechanism and consequently resulting in myopathy development (Rogoff et al. 2010). Previous findings show that cortisone reduction by 11β-HSD1 is driven by the luminal generation of NADPH by H6PDH and is independent of cytosolic NADPH resources (Csala et al. 2006). Therefore, H6PDH activity relies on the G6P transport across the ER membrane by G6PT (Zielinska et al. 2011).

1.3.2.2 NADH/NAD^+ redox status in the cytosol

Interestingly, the cytosolic NADH/NAD^+ redox is essential for initiation of muscle contraction as it triggers release of intracellular calcium ions from the SR by the calcium release channels or ryanodine receptors (RyR). Cytosolic NADH/NAD^+ levels are regulated by GAPDH which is associated with the SR membrane. Therefore, changes in activity of this enzyme might lead to more significant changes of local

NADH/NAD^+ levels in close proximity to SR bound proteins (such as the RyR and SERCA) (Zima et al. 2003). The ratio of NADH/NAD^+ varies as a response to changes in metabolism and indicates the metabolic state of a cell or tissue, for instance, during ischemia cytosolic NADH/NAD^+ ratio increases up to 30 times (Park et al. 1998).

1.3.2.3 NAD^+ metabolism

The role NAD^+ fulfils in muscle energy signalling and homeostasis, and its ability to stimulate mitochondrial function, has recently risen to prominence. NAD^+ is an enzyme co-factor central to metabolism and essential for life in all organisms and importantly, fundamental to skeletal muscle metabolism. It functions both as a co-enzyme for oxidoreductases and as a source of ADP-ribosyl groups for the sirtuins (SIRT) family of protein deactylases which can signal to increase mitochondrial metabolism and insulin sensitivity in skeletal muscle playing an important role in life span extension (Bieganowski and Brenner 2004; Tempel et al. 2007). Among seven members of the sirtuin family, SIRT1 and SIRT3 are of particular interest with regard to skeletal muscle metabolism following the discovery that they positively regulate the PGC-1α, a potent transcriptional co-activator of mitochondrial biogenesis. SIRT1 is involved in the process of glucose metabolism and insulin secretion. Down-regulation of SIRT1 protein levels under insulin-resistant conditions in C2C12 myotubes leads to insulin resistance (Sun et al. 2007) whereas SIRT3 is localised primarily in mitochondria and is associated with ageing by regulating mitochondrial function (Jing et al. 2011). As a substrate for SIRT1/3, NAD^+ is rapidly consumed; thus, there is a necessity to

generate new NAD^+ or re-synthesise NAD^+ from by-products of the NAD^+-degradation reaction.

NAD^+ can be *de novo* synthesised from tryptophan taken up from the diet or in the Preiss-Handler pathway by utilising the vitamin precursor of NAD^+, nicotinic acid (Na) (Houtkooper et al. 2010). Na is generally acquired from the diet or from the hydrolysis of nicotinamide (NAM), whereas NAM is the breakdown product of NAD^+. Both Na and NAM are first converted to their mononucleotide forms: nicotinic acid mononucleotide (NaMN) or nicotinamide mononucleotide (NMN), and then the enzyme nicotinamide mononucleotide adenylyltransferase (NMNAT) produces the nicotinic acid adenine dinucleotide ($NaAD^+$) or NAD^+ respectively. Finally, $NaAD^+$ is converted to NAD^+ by the enzyme NAD^+ synthetase (Khan et al. 2007). In cytosol, NAD^+ can be phosphorylated by NAD^+ kinase to $NADP^+$ which then can be further reduced to NADH or NADPH in the pentose phosphate pathway (Figure 1-16) (Outten and Culotta 2003).

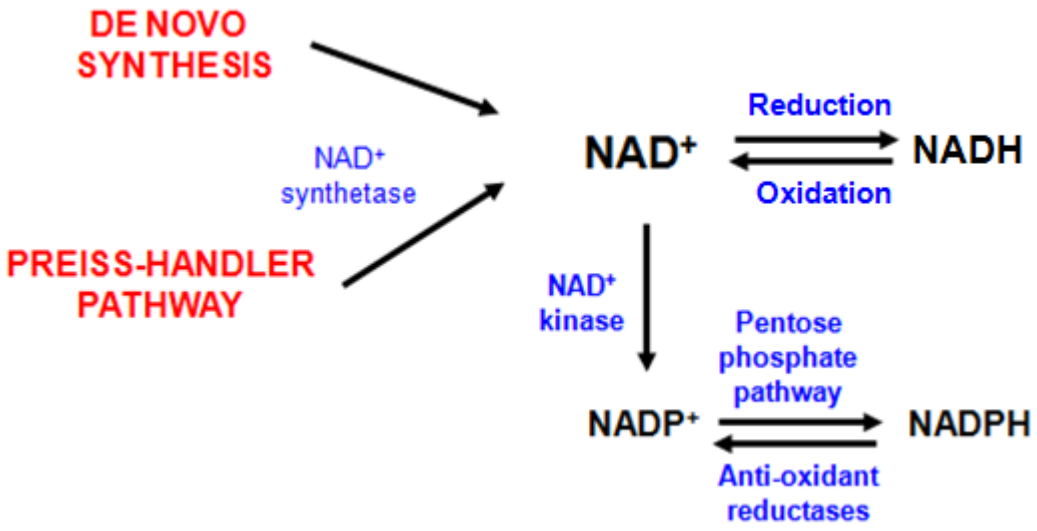

Figure 1-16 Schematic representation of NAD^+ and $NADP^+$ conversion

Because cellular NAD^+ is consumed in numerous pathways, its replenishment is critical to preserving signalling competency and supporting NAD(P)(H)-dependent reactions.

1.4 *In vivo* genetic manipulations of ER/SR genes

1.4.1 11β-HSD1 mouse models

11β-HSD1 animal models have highlighted the critical role of 11β-HSD1 in the regulation of metabolic phenotype in different tissues as well as its impact on global metabolic phenotype.

Global knockout of 11β-HSD1 in mice has a beneficial metabolic (cardioprotective) phenotype. 11β-HSD1 mice are protected from the metabolic consequences of obesity having improved glucose tolerance, increased insulin sensitivity, “cardioprotective” high density lipoprotein (HDL)-cholesterol level and lower plasma triglyceride (Kotelevtsev et al. 1997a). 11β-HSD1 KO mice are also protected from type 2 diabetes while on a high fat diet (Morton et al. 2004).

Most recent research has examined the insulin sensitivity in 11β-HSD1KO mice focussing on the liver and adipose tissue considering 11β-HSD1 inhibitors (Section 1.4.1.1) as attractive targets for a number of disorders including type 2 diabetes, insulin resistance and associated cardiovascular disease.

Interestingly, mice overexpressing 11β-HSD1 in adipose tissue develop visceral obesity, insulin resistance, hypertension and dyslipidemia (Masuzaki et al. 2001;Masuzaki et al. 2003). In addition, liver-specific overexpression of 11β-HSD1 leads to insulin resistance and hypertension, but not obesity (Paterson et al. 2004). Circulating corticosterone levels were not increased in liver-specific 11β-HSD1KO model indicating a minor contribution of liver 11β-HSD1 to the urinary steroid phenotype observed in the 11β-HSD1KOs and highly suggesting the importance of other tissues.

Although it is clear that 11β-HSD1 has a critical role to play in governing GC availability, its metabolic role in skeletal muscle metabolism and contribution to global homeostasis have not yet been explored.

1.4.1.1 Therapeutic inhibition of 11β-HSD1

The pharmacological inhibition of 11β-HSD1 is to great interest of many pharmaceutical companies. 11β-HSD1 has become an attractive therapeutic target for many years; therefore, the manipulation of tissue levels of glucocorticoids through targeted inhibition of cortisol metabolic pathways has been widely investigated.

Previously, human studies using the non-specific 11β-HSD inhibitor, carbenoxolone, have shown that this compound improved whole body insulin sensitivity in healthy individuals whereas in patients with type 2 diabetes, it reduced hepatic glucose production rate. Carbenoxolone has a poor selectivity for 11β-HSD1 as it also inhibits 11β-HSD2 resulting in cortisol-dependent mineralocorticoid excess and hypertension (Andrews et al. 2003;Latif et al. 2005;Walker et al. 1995). Thus, selective 11β-HSD1 inhibitors have now been developed by a number of pharmaceutical companies.

The first selective inhibitor to be described was a benzene sulphonamide, BVT2733, which has a >200-fold selectivity for inhibiting 11β-HSD1 (IC_{50} 96nM) compared to 11β-HSD2 (Barf et al. 2002). When administrated to rodents, this compound reduced fasting blood glucose and insulin levels, lowered free fatty acids, cholesterol and TAG as well as decreased total body weight (Alberts et al. 2003). The BVT2733 is highly effective at inhibiting rodent 11β-HSD1; however, it is less effective at inhibiting the human isozyme (IC50 of 3341nM) (Barf et al. 2002).

In addition, the Merc inhibitor 544, an adamantyl triazole compound, has been tested in several rodent models. It lowered fasting glucose, TAG, insulin and cholesterol when administrated to diet-induced obese mice for 11 days. It also reduced the plaque formation in mice with targeted deletion of apolipoprotein E suggesting its potential beneficial application in reducing cardiovascular disease (CVD) progression (Hermanowski-Vosatka et al. 2005).

Interestingly, another selective 11β-HSD1 inhibitor developed by Merc, Compound A, decreased hepatic steotosis in diet-induced obese rats (Berthiaume et al. 2009)

In the context of animal studies, clinical studies targeting 11β-HSD1 inhibition in man are of great importance for treatment of metabolic disease such as insulin resistance, obesity and type 2 diabetes. Recently, the Incyte selective 11β-HSD1 inhibitor, INCB013739, was administered to patients with type 2 diabetes (twice a day for 2 weeks) and completely inhibited cortisone to cortisol conversion resulting in reduced fasting glucose, total and LDL cholesterol. In addition, this compound was administrated in combination with metformin in patients with type 2 diabetes. After the 12 week trial with both drugs, the INCB13739 treatment group had reduced HbA1c and total cholesterol levels when compared to the metformin alone suggesting beneficial effects of this compound on both carbohydrate and lipid metabolism (http://www.clinicaltrials.gov/ct2/show/NCT00398619). Data from clinical studies on selective 11β-HSD1 inhibitors which can be applied in the treatments of human metabolic disease are still continuing to emerge.

1.4.2 H6PDH global knockout (H6PDHKO)

To determine the role of H6PDH in regulating 11β-HSD1 and GC metabolism, H6PDHKO mice were generated by homologous recombination in mouse embryonic stem cells to replace exons 2 and 3 with a neomycin resistance cassette. This study confirmed that H6PDH is crucial for the regulation of 11β-HSD1 oxo-reductase activity which is dependent on the supply of NADPH cofactor. It has been shown that H6PDHKO mice have a switch in 11β-HSD1 activity from oxo-reductase to dehydrogenase (Lavery et al. 2008b). There are a number of features in different tissues associated with H6PDH deficiency (Figure 1-17) (Zielinska et al. 2011).

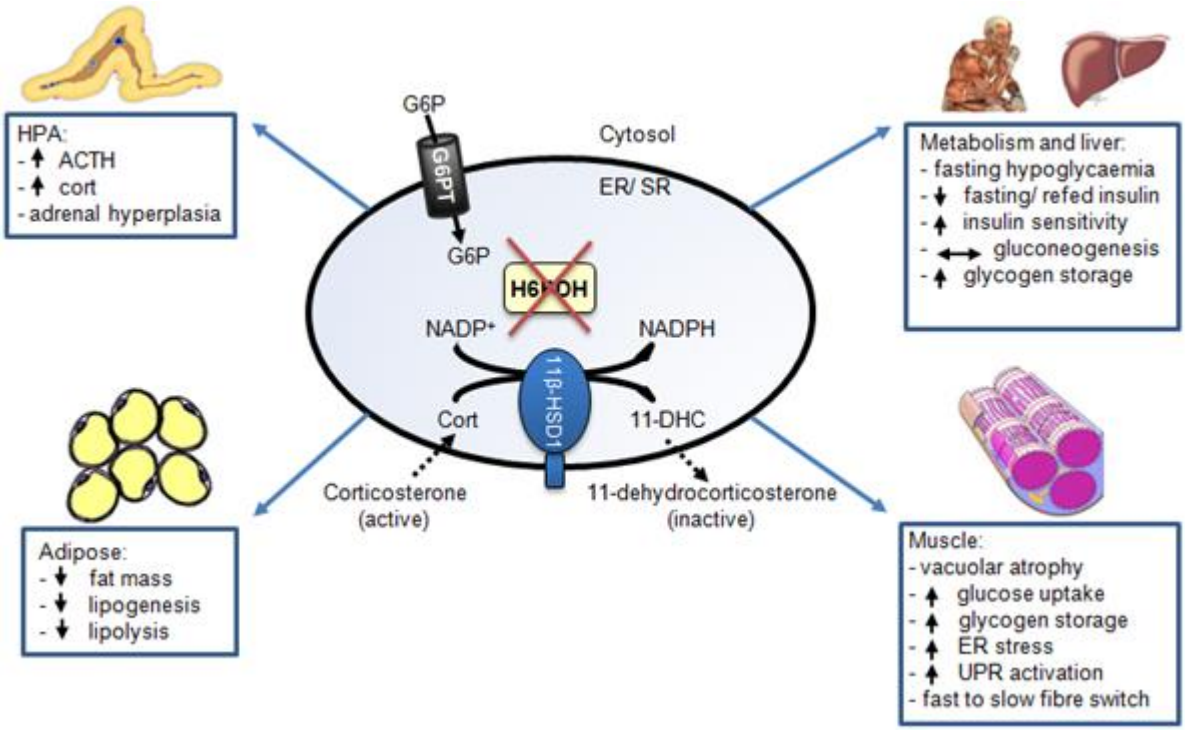

Figure 1-17 Major features present in mice tissue and system with H6PDH deficiency

In H6PDHKO mice, H6PDH does not metabolise G6P that results in no NADPH production. Therefore, 11β-HSD1 switches its activity to dehydrogenase inactivating GCs. A number of tissues and systems are affected including metabolism and liver, HPA axis, muscle and adipose tissue (Zielinska et al. 2011).

Previous work has shown that H6PDHKO mice display reduced skeletal muscle mass and locomotor activity with fasting hypoglycaemia and increased insulin sensitivity. H6PDHKO mice develop severe muscle myopathy characterised by the occurrence of large membranous vacuoles and the triad junction abnormalities (Figure 1-18) (Lavery et al. 2008b). Affected muscle indicates defects in structure and function of the SR with dysregulated proteins involved in calcium metabolism such as the ER/SR calcium ATPase (SERCA), calreticulin, and calsequestrin. In addition, microarray analysis identified a large set of differentially expressed genes enriched for networks of the ER stress and the UPR pathways, predominantly in fast-twitch muscles with the slow-twitch muscle being relatively resistant (Lavery et al. 2008b). Muscle myopathy is also associated with the switching of type II to type I muscle fibres and elevated glycogen accumulation in skeletal muscle. However, underlying mechanism of the muscle myopathy is still not fully understood and need to be further elucidated.

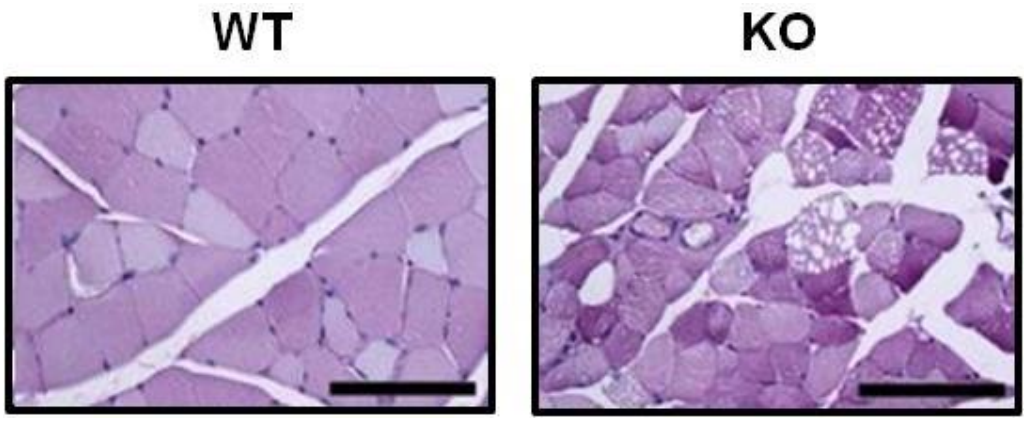

Figure 1-18 Histological defects in skeletal muscle of H6PDHKO mice

Periodic acid-Schiff-stained gastrocnemius sections comparing KO with WT muscles show the presence of vacuoles and increase in glycogen content in some KO fibres. The reference bar is 80 µM (Lavery et al. 2008b).

1.4.2.1 ER stress and the unfolded protein response pathway

A number of factors leading to impaired ER homeostasis such as glucose deprivation, disturbances in calcium and redox regulation as well as viral infection can result in ER stress and consequently in activation of the UPR pathway (Deldicque et al. 2012). The UPR is a signaling pathway that protects the cellular integrity by restoring ER folding capacity, initiating protein translation and preventing accumulation of unfolded and misfolded proteins (Deldicque 2013; Schroder and Kaufman 2005). The UPR mechanism involves the activation of three ER resident transmembrane proteins: the inositol requiring enzyme 1 (IRE1), activating transcription factor-6 (ATF6) and protein kinase R (PKR)-like ER protein kinase (PERK). These stress transducers consist of an ER-luminal part and a cytoplasmic part that sense the protein folding status in the ER and transmit this information across the ER membrane to the cytosol. They are associated with the chaperone binding immunoglobulin protein (BiP) and upon unfolded/misfolded proteins accumulation, they disassociate from BiP, consequently leading to their activation. In the chronic state of ER stress, inflammatory responses are activated mainly by Jun NH2-terminal kinase (JNK) and nuclear factor-kappa B (NF-κB). However, uncontrolled and excessive ER stress leads to apoptosis and cell death through the intrinsic and extrinsic pathways. The intrinsic pathway responds to intracellular insults such as DNA damage whereas extrinsic pathway is triggered by self-association of cell surface receptors, recruitment of caspases and attenuation of a caspase cascade (Deldicque 2013;Ron and Walter 2007).

1.4.2.2 ER stress in the skeletal muscle

ER stress is involved in the pathology of various metabolic diseases including obesity, insulin resistance and diabetes. In addition, ER stress is associated with muscle myopathies such as myotonic dystrophy type 1 (Botta et al. 2013; Ikezoe et al. 2007), dysferlin-deficient muscular dystrophy (Ikezoe et al. 2003) and myositis (Nagaraju et al. 2005). To date, a number of studies have examined the UPR activation in skeletal muscle. Both ER stress and UPR induction were observed in skeletal muscle in high-fat-fed mice, in palmitic acid-treated C2C12 muscle cells and also in humans after extreme endurance exercise (Rayavarapu et al. 2012). ER stress contributes to muscle myopathy development directly by promoting cell death or indirectly by inhibiting the mammalian target of rapamycin complex 1 (mTORC1) pathway. The mTORC1 pathway positively regulates cell growth and proliferation and by promoting a number of anabolic processes such as biosynthesis of lipids and proteins and reducing catabolic processes for instance autophagy. The mTORC1 inhibition as a consequence of ER stress, generates a state of anabolic resistance and therefore leads to decreased muscle mass (Figure 1-19) (Deldicque 2013; Laplante and Sabatini 2009).

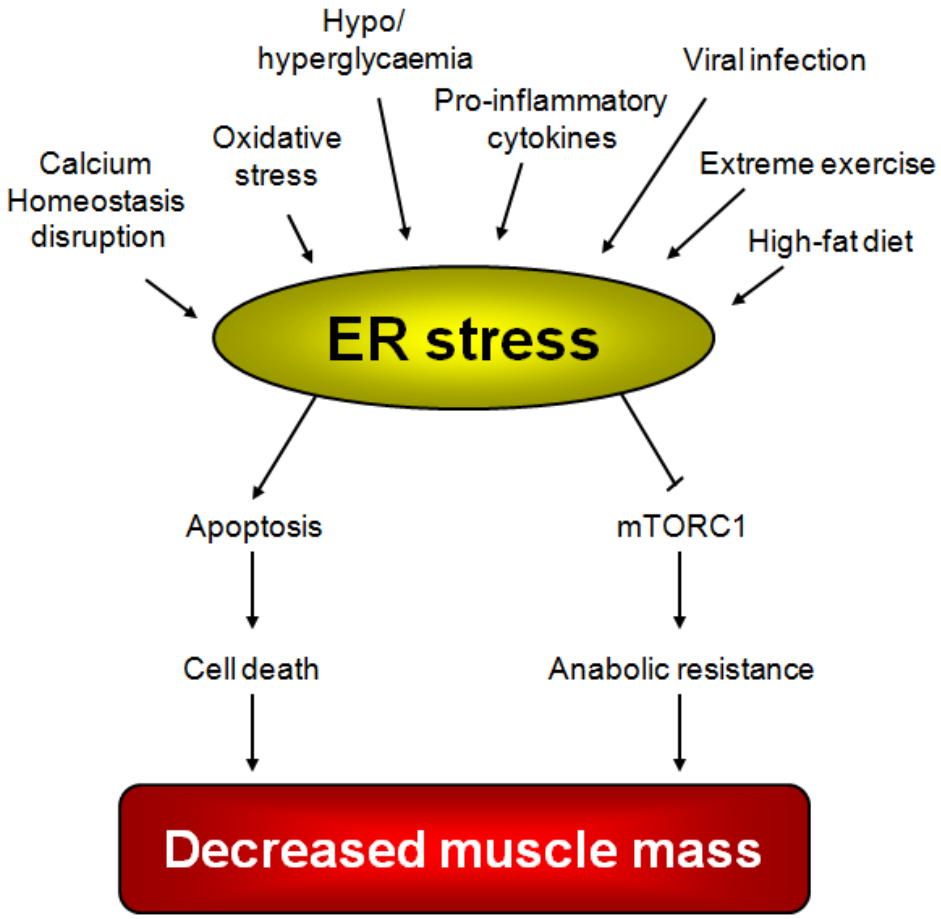

Figure 1-19 Schematic model for the involvement of ER stress in the muscle mass reduction

A number of factors lead to ER stress which can promote cell death or inhibition of mTORC1 consequently reducing muscle mass.

1.4.3 11β-HSD1/H6PDH global double knockout

In an effort to delineate further the roles that H6PDH and 11β-HSD1 play in metabolism and muscle function, a H6PDH/11β-HSD1 double KO (DKO) mouse model has been developed in which dehydrogenase activity of 11β-HSD1 seen in the H6PDHKO mouse is negated (Semjonous et al. 2011). It has been shown that DKO mouse model is a phenocopy of the salient features of the myodegeneration seen in the H6PDHKO mice displaying reduced body mass, muscle atrophy and vacuolation of type II fibre rich muscle, maintained fasting hypoglycaemia, increased muscle

glycogen deposition and elevated expression of UPR genes (Lavery et al. 2008b;Semjonous et al. 2011). Effectively, the DKO model returns GC metabolism, GC sensitivity and the HPA axis set point to levels seen in the 11β-HSD1KO mouse (Semjonous et al. 2011). Because 11β-HSD1KO mice have no reported skeletal muscle phenotype (Kotelevtsev et al. 1997b), this suggests that the mechanism eliciting myopathy in both H6PDHKO and DKO mice is 11β-HSD1 and GC independent (Semjonous et al. 2011). Consequently, this study has identified a novel role for H6PDH in muscle homeostasis through maintaining the NADPH/$NADP^+$ redox environment within the SR lumen and highlighting the importance of the G6PT/H6PDH pathway for G6P disposal in the SR.

1.4.4 H6PDH overexpression in adipose tissue

A mouse model overexpressing H6PDH under the control of the enhancer-promoter region of the adipocyte fatty acid-binding protein (*aP2*) gene (aP2/H6PDH mice) were previously generated in order to determine the role of adipose H6PDH in the pre-receptor modulation of 11β-HSD1 and metabolic phenotypes. The aP2-H6PDH mice have elevated 11β-HSD1 expression and enzyme activity correlated with increased H6PDH expression in adipose tissue (Wang et al. 2014).

Additionally, the aP2-H6PDH mice demonstrate fasting hyperglycaemia and glucose intolerance along with elevated levels of the fasting plasma insulin and free fatty acid (FFA) suggesting that these mice exhibit features of the modest metabolic syndrome and insulin resistance due to increased adipose corticosterone production (Wang et al. 2014).

Interestingly, increased mRNA levels of 11β-HSD1 and H6PDH were found in visceral and subcutaneous adipose tissues from patients with type 2 diabetes. This leads to elevated local cortisol activation and induction of abdominal adipose 11β-HSD1 activity and might contribute to the development of type 2 diabetes mellitus (T2DM) (Uckaya et al. 2008). Therefore, it suggests that H6PDH could play an important role in the pathogenesis of metabolic syndrome and T2DM.

1.5 Genetic defects in *H6PD* and *HSD11B1*

Mutations in the *H6PD* gene (encoding H6PDH) cause apparent cortisone reductase deficiency (ACRD) whereas in the *HSD11B1* gene (encoding 11β-HSD1) cause ‘‘true’’ CRD. Both CRD and ACRD are characterised by the failure to produce active glucocorticoid, cortisol, from inactive cortisone resulting in the activation of HPA axis and ACTH-mediated adrenal glucocorticoid and androgen secretion (Figure 1-20).

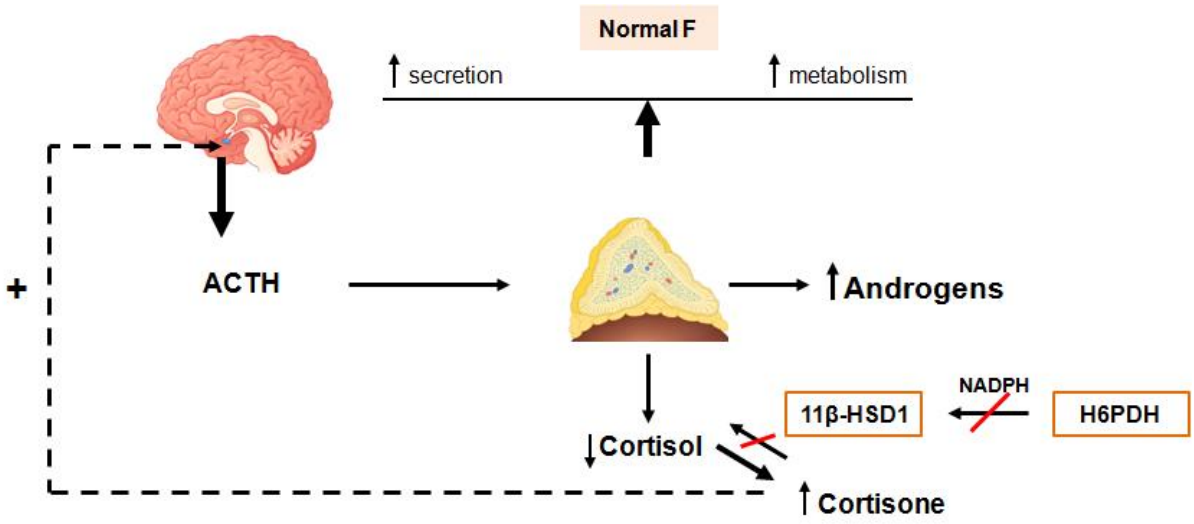

Figure 1-20 Biochemical scenario in CRD/ACRD

Mutations in 11β-HSD1 and H6PDH lead to elevated cortisol to cortisone conversion resulting in decreased cortisol feedback to the HPA axis and subsequently increased cortisol levels. Thus, increase androgen production by the adrenal glands. Circulating cortisol (F) levels remain normal due to a balance between elevated F metabolism and its increased secretion (Draper and Stewart 2005).

To date, approximately 14 cases with a spectrum of biochemical and clinical syndrome consistent with ACRD or CRD have been reported in the literature. Affected adult females present with polycystic ovary syndrome (PCOS)-like phenotype whereas children with premature adrenarche including pubarche. Urinary steroid analysis indicate increase of cortisone metabolites [tetrahydrocortisone (THE)] relative to cortisol metabolites [tetrahydrocortisol (THF+5α-THF)] together with a decrease in 5α/5β tetrahydrocortisol demonstrating impaired 11β-HSD1 activity (Lavery et al. 2008a;Lavery et al. 2013;Lawson et al. 2011). In the ER lumen, H6PDH maintains a NADPH/$NADP^+$ ratio for 11β-HSD1 oxo-reductase activity. Mutations in the *HSD11B1* gene lead to CRD and a loss of cortisol regeneration with elevations in cortisone metabolites and secondary activation of the HPA axis whereas mutations in *H6PD* cause ACRD with the loss of 11β-HSD1 oxo-reductase activity, but a gain of dehydrogenase activity and compensatory HPA axis activation seen in H6PDHKO mice (Lavery et al. 2008b;Lavery et al. 2013).

1.6 Metabolic disease and muscle

1.6.1 Type 2 diabetes

Type 2 diabetes mellitus is an endocrine disorder characterised by increased plasma glucose levels caused by peripheral insulin resistance (Larsen et al. 2008). T2DM is a progressive condition resulting from a variety of genetic and environmental factors which can affect both insulin secretion and action. According to the World Health Organisation (WHO), more than 220 million people worldwide are diagnosed with diabetes, and it is estimated that this number will increase up to 366 million by 2030

(Wild et al. 2004), mainly due to ageing population, rapidly rising obesity and physical inactivity (Froguel and Velho 2001).

Insulin secretion from the pancreas reduces glucose output by the liver, increases glucose uptake by skeletal muscle and suppresses fatty acid release from fat tissue. Patients with T2DM have impaired fasting glucose and elevated glucose production (Nielsen et al. 2000). This increase occurs in the presence of hyperinsulinaemia; therefore, hepatic insulin resistance is the driving force of hyperglycaemia in T2DM. A number of factors contribute to the pathogenesis of type 2 diabetes affecting both insulin secretion and insulin action. Decreased insulin secretion will reduce insulin signalling in its target tissues. Insulin resistance pathways have a negative effect on insulin action in adipose tissue, liver and skeletal muscle leading to increased circulating fatty acids and the hyperglycaemia of diabetes. Consequently, the raised concentrations of glucose and fatty acids in the bloodstream worsen both insulin secretion and insulin resistance (Figure 1-21) (Girard 2006;Rizza 2010).

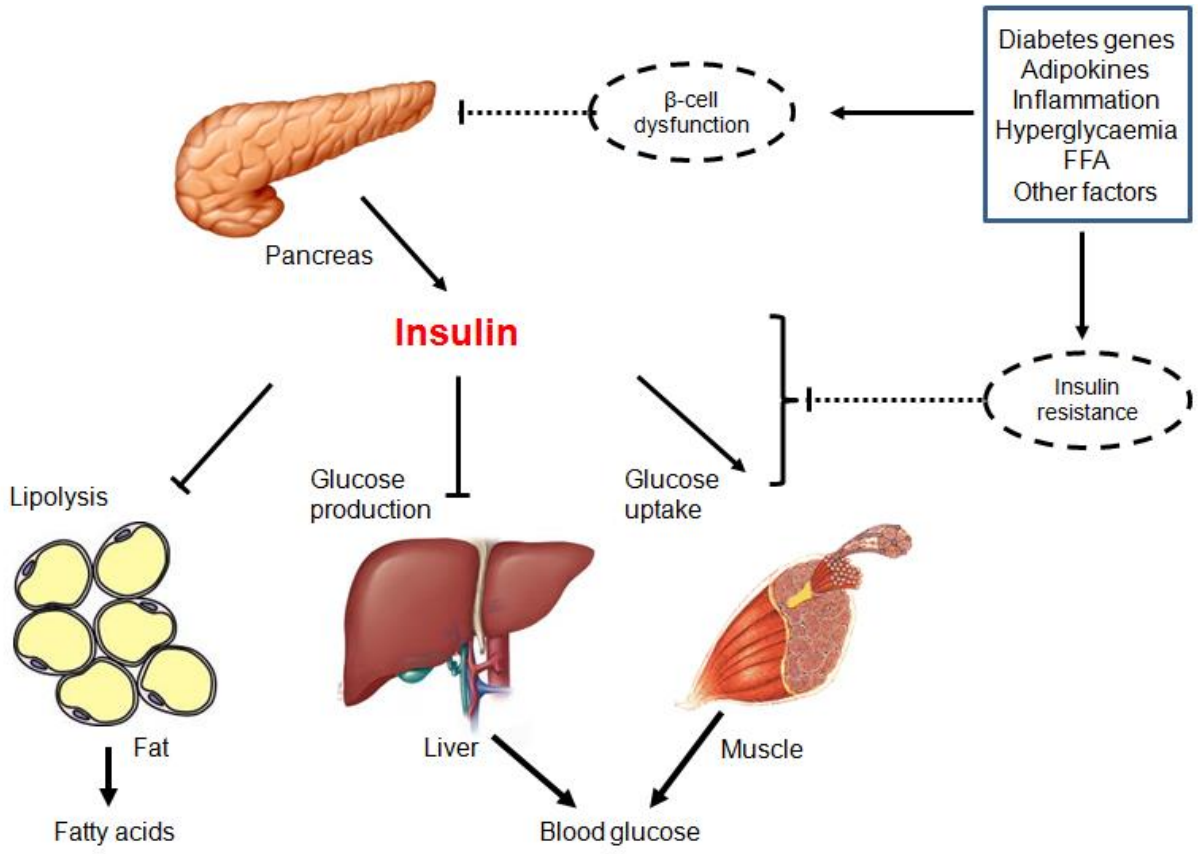

Figure 1-21 Pathophysiology of hyperglycaemia and elevated insulin resistance associated with T2DM

Diabetes increases the risk of CVD (50% of people with diabetes die of heart attack and stroke), blindness and kidney failure. Furthermore, diabetes is associated with a significantly increased risk of death compared to healthy people.

1.6.2 Skeletal muscle insulin resistance and the metabolic syndrome

Skeletal muscle as an endocrine tissue plays an important role in the pathogenesis of the metabolic syndrome. Previous studies have shown that reversing skeletal muscle insulin resistance might be a promising way to prevent the development of atherogenic dyslipidemia and non-alcoholic fatty liver disease associated with the metabolic syndrome (Jornayvaz et al. 2010).

The metabolic syndrome (Syndrome X; Insulin resistance syndrome) is a multiplex of interrelated risk factors that occur together and increase the risk of CVD, stroke and T2DM. The metabolic syndrome is associated with abdominal obesity, impaired fasting glucose, hypertension, dyslipidemia, low plasma HDL and elevated serum uric acid concentration (Larsen et al. 2008). In 1988, Reaven postulated that people with insulin resistance and hyperinsulinaemia are more likely to have hypertension, hyperlipidemia and diabetes which are the main cause of CVD (Kahn et al. 2005). However, over the years a number of organisations have published their definition of the “metabolic syndrome” and its underlying pathogenesis (Table 1-3).

Table 1-3 Criteria for clinical diagnosis of metabolic syndrome

Abbreviations: WHO (World Health Organisation), ATP III (Third Report for the National Cholesterol Education Program’s Adult Treatment Panel), AHA/NHLBI (American Heart Association/National Heart, Lung, and Blood Institute), BMI (body mass index), IGT (impaired glucose tolerance), IFG (impaired fasting glucose), T2DM (type 2 diabetes mellitus).

CLINICAL MEASURE	WHO	ATP III	AHA/NHLBI
Abdominal obesity	Waist to hip ratio: >0.9 (men) >0.85 (women) BMI>30 kg/m2	≥102 cm (m) ≥88 cm (w)	≥102 cm (m) ≥88 cm (w)
Fasting glucose	IGT, IFG, T2DM, Insulin resistance	≥100 mg/dL	≥100 mg/dL
Blood pressure	≥140/90 mmHg	≥130/85 mmHg	≥130/85 mmHg
Low HDL cholesterol	<35 mg/d L (m) <39 mg/dL (w)	<40 mg/dL (m) <50 mg/dL (w)	<40 mg/dL (m) <50 mg/dL (w)
Triglycerides	≥1.7 mmol/L	≥1.7 mmol/L	≥1.7 mmol/L
Microalbumineria	Urinary albumin excretion rate >20 µg/min albumin:creatinine ratio 30 mg/g		

The first definition of the metabolic syndrome was proposed in 1998 by the WHO. According to WHO, a subject can be diagnosed with the metabolic syndrome if glucose intolerance, impaired glucose tolerance (IGT) or diabetes and/or insulin resistance appear together with two or more of the listed criteria whereas the Third Report for the National Cholesterol Education Program's Adult Treatment Panel (ATPIII) needs three or more of the five risk factors (Grundy et al. 2005). The presence of any 3 of 5 risk factors constitutes a diagnosis of metabolic syndrome for American Heart Association/National Heart, Lung, and Blood Institute (AHA/NHLBI) (Alberti et al. 2009).

The majority of people diagnosed with the metabolic syndrome are insulin resistant. Insulin resistance is characterised by the presence of an impaired biologic response to either endogenously secreted or exogenously administrated insulin. Insulin resistance enhances the risk of the metabolic syndrome sufferers becoming type 2 diabetic which leads to increased risk factors for CVD and can cause hypertension, dyslipidemia, impaired glucose tolerance and blood vessel endothelial dysfunction (Reaven 1988;Ruderman et al. 2013).

1.6.2.1 Mitochondrial dysfunction in skeletal muscle

Skeletal muscle insulin resistance is a key contributor to the pathophysiology of T2DM. Recent studies have shown that insulin resistance, in a number of conditions such as T2DM and ageing as well as in offspring of T2DM, is associated with impaired mitochondrial oxidation in muscle (Befroy et al. 2007).

Previous studies of insulin-resistant offspring of T2DM patients have demonstrated increased plasma fatty acid concentrations (Perseghin et al. 1997) and elevated

intramyocellular lipid (Jacob et al. 1999;Perseghin et al. 1999) suggesting dysregulation of lipid metabolism in this cohort of subjects. Other studies have revealed an increase of approximately 80% in the intramyocellular lipid content correlated with reduced synthesis of mitochondrial ATP by approximately 30% in the muscle of lean, insulin-resistant offspring of T2DM patients (Petersen et al. 2004). In this study, the insulin-stimulated glucose uptake was also approximately 60% lower in the insulin-resistant cohort of subjects. These findings indicate a potentially important role for mitochondrial dysfunction in muscle in the pathogenesis of type 2 diabetes. In addition, it has been shown that decreased mitochondrial density, determined by electron microscopy, is associated with impaired insulin signaling (Morino et al. 2005).

1.6.3 GCs, atrophy and insulin resistance in the skeletal muscle

1.6.3.1 Glucocorticoids and skeletal muscle atrophy

Skeletal muscle atrophy is characterised by a decrease in muscle fibres size and is often associated with an increase in circulating GC levels (Schakman et al. 2013). Glucocorticoids catabolic effects on inducing protein breakdown, in particular through the ubiquitin- proteasome and lysosomal systems (Schakman et al. 2008) and reducing protein synthesis play a major role in the activation of muscle proteolysis. Muscle wasting process is partly attenuated by suppression of the IRS1-associated PI3K/Akt pathway (Zheng et al. 2010) leading to dephosphorylation and activation of the forkhead family of transcription factors (e.g. FOXO1) as well as inhibition of mTOR pathway (Schakman et al. 2013) resulting in increased atrogin-1 transcription and consequently accelerated protein breakdown (Sandri et al. 2004). However,

it was shown previously that endogenous GCs activate the GR which competes with IRS1 for PI3K; therefore, leading to muscle cell catabolism (Hu et al. 2009). The GC-induced muscle atrophy is also triggered by induction of muscle-specific E3 ubiquitin-ligase expression called atrogin-1 and MuRF-1. The atrogin-1 gene transcription is regulated by FOXO whereas MuRF1 by FOXO (indirect transcriptional activation) and GR itself (Waddell et al. 2008). Deletion of atrogin-1 or MuRF1 in mice results in significant muscle mass loss associated with denervation (Bodine et al. 2001). However, when these animals are exposed to GC excess, muscle atrophy is increased only in MuRF1 KO mice. The actions of GCs upon MuRF1 expression are via the association between activated GR and GRE located within the MuRF1 promoter (Waddell et al. 2008).

1.6.3.2 Glucocorticoids and insulin resistance

Type 2 diabetes and accumulation of intramyocellular lipids are associated with insulin resistance in both humans (Krssak et al. 1999) and rats (Korach-Andre et al. 2005). In addition, prolonged exposure to glucocorticoids has been linked with the development of insulin resistance inducing accumulation of lipids and their metabolites within the skeletal muscle. A previous study has shown that in high fat diet-fed mice treated with the synthetic glucocorticoid, dexamethasone, had increased intramyocellular lipid content and diacylglyceride levels in skeletal muscle coupled with insulin resistance (Gounarides et al. 2008).

In addition to the effect of exogenous glucocorticoids, pre-receptor metabolism of endogenous glucocorticoids by 11β-HSD1 is a crucial regulator of insulin sensitivity in skeletal muscle (Morgan et al. 2009). Increased expression of 11β-HSD1 has been

described in skeletal muscle of a rodent model of diabetes (Zhang et al. 2009) and myotubes isolated from patients with insulin resistance and type 2 diabetes (Abdallah et al. 2005b). Importantly, GCs elevate lipolysis and FFA generation and uptake which may be an important contributor to the insulin resistance (Morgan et al. 2009).

1.6.4 Mitochondrial myopathy

Muscle impairment can also be caused by mitochondrial dysfunction consequently leading to muscle weakness and exercise intolerance (Yamada et al. 2012). Skeletal muscle utilises oxidative ATP for energy production and highly depends on the mitochondrial respiratory chain (RC) function. A progressive dysfunction of RC can cause the development of adult-onset myopathies that can affect individuals from early infancy to late adulthood (Tyynismaa et al. 2010). Mitochondrial impairment has also been implicated in other diseases including heart failure and type 2 diabetes (Wallace et al. 1999) as well as in the ageing process (Trifunovic et al. 2004).

In a previous study, a mouse model for mitochondrial myopathy was generated by disrupting mitochondrial transcription factor A (Tfam) in skeletal muscle. The Tfam gene is ubiquitously expressed and essential for mtDNA transcription and translation; therefore, its depletion leads to loss of mtDNA transcripts, mtDNA-encoded peptides and severe deficiency of all RC subunits affecting complexes I, III, IV and V (Wredenberg et al. 2002). The muscle weakness seen in Tfam KO muscles was found to be due to decreased Ca^{2+} release from the SR during tetanic stimulation and thereby reduced activation of the contractile machinery (Aydin et al. 2009). Mutations in mtDNA cause a wide range of syndromes including mitochondrial myopathies;

however, treatment options still remain limited and further understanding of the molecular basis of these conditions need to be undertaken.

1.6.5 Duchenne muscular dystrophy (DMD)

The majority of the skeletal muscle pathologies are caused by defects either in structural or cytoskeletal proteins or in mitochondria. The most common and severe muscle dystrophy is DMD which is an X-linked recessive disorder resulting from mutations in the gene encoding dystrophin, a subsarcolemmal protein functioning within the dystrophin-associated glycoprotein complex (DGC), responsible for maintaining muscle integrity (Lynch et al. 2001;Turk et al. 2005). This gene is expressed in skeletal, cardiac and smooth muscle. The DGC complex plays a critical role by connecting the actin-based subsarcolemmal cytoskeleton to the extracellular matrix component laminin (merosin) (Chamberlain et al. 2007;Lynch et al. 2001). The DGC is localised at the Z-lines of the sarcomere and allows the transmission of force across the muscle fibre. When disrupted, it results in membrane instability and consequently leads to sarcolemmal ruptures. In addition, the extracellular calcium influx activates proteolytic activity. Subsequently, affected muscle fibres become necrotic or apoptotic followed by initiation of inflammatory processes. Cycles of both degeneration and regeneration eventually lead to irreversible muscle wasting and substitution by fibrotic and adipose tissue (Turk et al. 2005).

The DMD is characterised by severe and progressive skeletal muscle degeneration; therefore, the mdx mouse model, with a point mutation in the dystrophin gene and a lack of dystrophin expression in muscle tissues, has been utilised in a wide range of studies to investigate the underlying mechanisms and potential remedies

of this muscle wasting disease (Bulfield et al. 1984;Chamberlain et al. 2007). Currently, there are a number of clinical trials trying to find effective treatments for DMD-affected boys. One such treatment is administering glucocorticoids in order to improve walking ability and increase lifespan of DMD patients. This trial also aims to increase steroid efficacy as well as reduce side effect and toxicity of this treatment (Angelini et al. 2012).

1.6.6 Sarcopenia

Ageing and increased physical disability are associated with elevated fat mass, mainly visceral fat and lead to development of metabolic syndrome and CVD (Kim and Choi 2013). One of the most consistent physiological manifestations of ageing, observed across a wide range of species, is the progressive loss of skeletal muscle mass and function termed sarcopenia, defined as an aged-related progressive loss of muscle mass, force and strength that could lead to functional impairment, decreased mobility and consequently to mortality. In the elderly, skeletal muscle wasting and fat mass increase are correlated with the sedentary lifestyle and disability (Song et al. 2004). Skeletal muscle mass declines by up to 1% a year beginning at approximately 40 years of age. This progressive loss has been estimated at about 8% per decade until the age of 70 years and afterwards about 15% per decade (Malafarina et al. 2012;Paddon-Jones et al. 2008). Currently, sarcopenia affects more than 50 million people worldwide and predictions are that this number will increase to 200 million over the next 40 years (Kim et al. 2014).

Ageing muscle demonstrates reduction of type II fibre size with a lesser effect on type I fibre size. However, the total number of type I and type II fibres are significantly decreased with age to a similar extent (Kamel 2003).

A number of factors lead to sarcopenia including decreases in IGF-1 and GH levels, induction in proinflammatory cytokines (TNF-α, IL-1β and IL-6), long term GC treatment, neurodegenerative processes and mitochondrial dysfunction (Figure 1-22) (Sakuma and Yamaguchi 2012;Schrager et al. 2007).

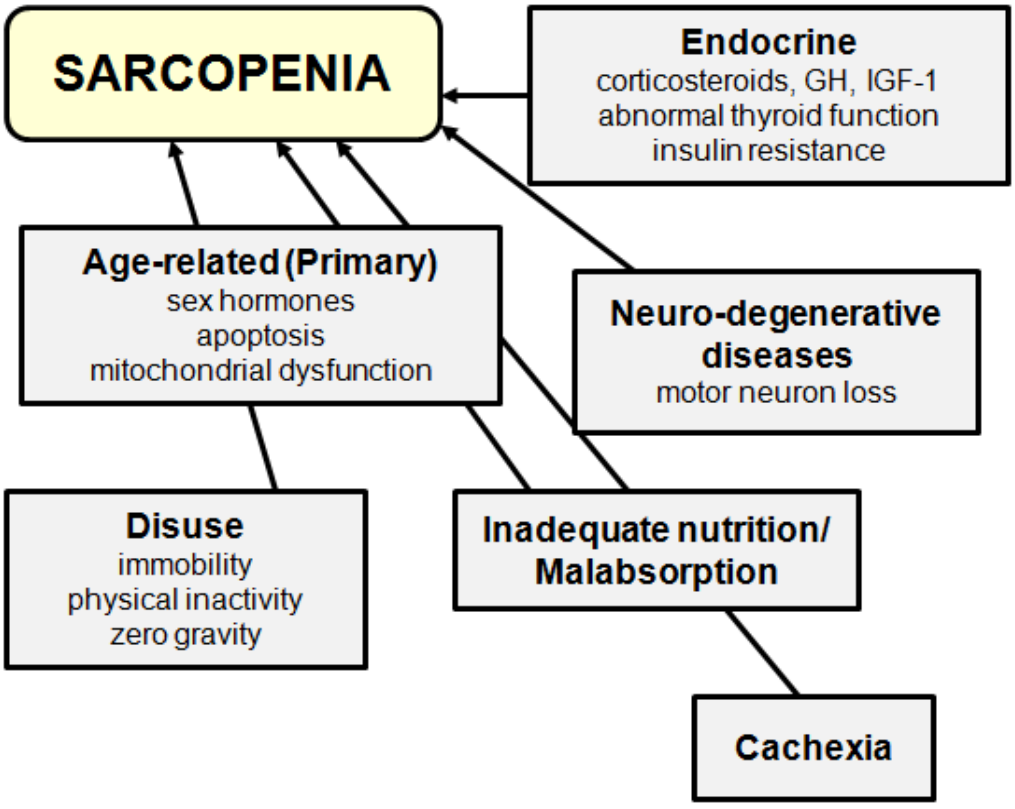

Figure 1-22 Mechanisms of sarcopenia

A number of factors lead to sarcopenia development; therefore, fully defining the physiology of ageing skeletal muscle is critical to design interventions to optimise an individual's capacity to resist sarcopenia and age-related disease**.**

Treatment of sarcopenia has become a major focus for drug discoveries in order to develop approaches to counteract its effects and thereby help in slowing down or reversing this age-related muscle decline and disability.

1.7 Thesis rationale

Skeletal muscle is a central site of energy metabolism that impacts whole body energy homeostasis. The SR is a skeletal muscle unit integrating redox balance, glucose and GC metabolism mediated by the G6PT/H6PDH/G6Pase-β/11β-HSD1 enzymatic system. Perturbation of this unit has varying impacts and associated phenotypes. This thesis will further define the roles that H6PDH and 11β-HSD1 play in local skeletal muscle homeostasis in an effort to provide insight into novel mechanisms and pathways regulating muscle metabolism.

1.8 Hypothesis

We hypothesise that H6PDH and 11β-HSD1 link the redox and metabolic status of the SR to the cytosol and therefore intermediary energy metabolism, that when depleted in muscle elicit a series of signalling responses that impact on local and systemic homeostasis. I wish to define the metabolic profiles associated with perturbation of the SR unit in skeletal muscle that will lead to better understanding of the metabolic interplay between the SR and the cytosol and the role H6PDH and 11β-HSD1 play in skeletal muscle.

1.9 Aims

- To determine the expression of G6PT/H6PDH/G6Pase-β/11β-HSD1 pathway in differentiating skeletal muscle cells. Also, to understand the role of muscle H6PDH in metabolic physiology and SR metabolism independently of other metabolic tissue using a muscle-specific knockout of H6PDH (H6MKO) mice. The H6MKO has been generated during this PhD to help to better understand H6PDH function in metabolic homeostasis and its potential role and manipulation in metabolic disease (**Chapter 3**).

- To evaluate the muscle-specific role of 11β-HSD1 and GC metabolism in determining global and tissue-specific metabolic phenotype using a muscle-specific knockout of 11β-HSD1 (HSD1MKO) (**Chapter 4**).

- To expression profile *H6PD* depleted muscle samples and attempt to discover changes in transcription that may identify factors contributing to myopathy and to establish the role of H6PDH in skeletal muscle biology (**Chapter 5**).

- To exploit metabolomics technology to evaluate muscle myopathy in the absence of H6PDH (**Chapter 6**).

Chapter 2- General Methods

Unless stated, all methods were carried out using chemicals purchased from Sigma-Aldrich Chemical Company (Poole, Dorset, UK) and cell culture plasticware from Corning (Artington, Surrey, UK).

2.1 Maintenance of tissue culture cell line C2C12

All cell culture work was undertaken in sterile conditions in a Class I biological safety cabinet (Holten LaminAir). Cell incubation was carried out at 37ºC in a Sanyo CO_2 incubator supplemented with 5% CO_2/95% air.

2.1.1 C2C12 cell line

The mouse myoblast cell line, C2C12, is a well-established model of both skeletal muscle proliferation and differentiation. They were originally generated through serial passage of myoblasts cultured from the thigh muscle of injured C3H mice collected 70 h following a crash accident (Yaffe and Saxel 1977). A subclone of these myoblasts was selected because of its ability to differentiate rapidly and express characteristic muscle proteins (Blau et al. 1985).

2.1.2 Proliferation

C2C12 myoblasts were purchased from the European Collection of Cell Cultures (Salisbury, UK). Cells were maintained in a 75 cm^3 tissue culture (TC) flask in antibiotic-free complete growth medium (GM) comprising of Dulbecco's modified eagle medium (DMEM) (PAA, Somerset, UK) supplemented with 10% (v/v) fetal calf serum (FCS), 2 mM L-glutamine and 4.5 g/L glucose. Cells were trypsinised when they reached 60-70% confluence and re-seeded into fresh flasks. Prior to experiments, cells were trypsinised and subcultured into 12-well TC plates. Proliferation medium was replaced every 48 h until cells reached 60-70% confluence.

2.1.3 Differentiation

Differentiation was initiated when myoblasts reached 60-70% confluence by replacing GM medium with DMEM supplemented with 5% horse serum. Differentiation medium (DM) was changed every 48 h. Myoblasts have formed multinucleated myotubes after 8 days of differentiation (Figure 2-1).

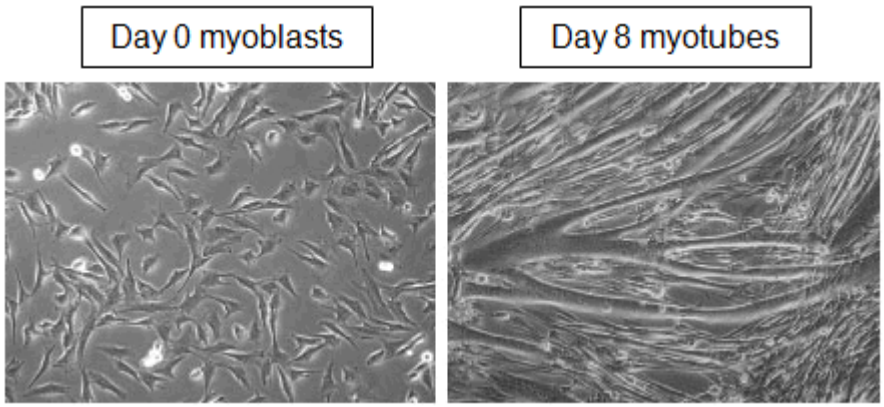

Figure 2-1 C2C12 cells have formed multinucleated myotubes after differentiation in DM for 8 days

2.1.4 Freezing down

To prepare cells for long-term storage, cells were grown in 75 cm^3 TC flasks until 60-70% confluence. They were trypsinised, re-suspended in 10 mL of proliferation medium and centrifuged at 1,000 g for 10 minutes. Medium was aspirated, and the cell pellet was re-suspended in 3 mL of FCS supplemented with 10% dimethyl sulfoxide (DMSO). Then, 1 mL of the cell mixture was transferred into a 1.5 mL cryovials and slowly cooled down to -80ºC at a rate of 1ºC/min in a cryofreezing chamber (Nalgene, Hereford, UK) containing isopropanol. Afterwards, cells were transferred to liquid nitrogen.

2.2 Murine primary skeletal muscle cell culture

2.2.1 Primary skeletal muscle cells

Skeletal myofibres were isolated from mouse extensor digitorum longus (EDL) muscle by digestion in 7 mL of DMEM supplemented with 0.2% collagenase type I in the water bath with gentle agitation at 37ºC for 90 mins. When digestion was complete, the collagenase solution was discarded, and the muscle was transferred into a Petri dish with 8 mL DMEM for further incubation at 37ºC for 20 mins. Subsequently, the Petri dish was placed under the microscope, and the muscle was gently titurated using a Pasteur pipette rinsed in 10% horse serum/DMEM. The hair-like single fibres were liberated from the muscle along with fat, tendon and other debris. Finally, single myofibres were transferred into a 12-well plate containing GM and incubated at 37ºC until proliferation.

2.2.2 Proliferation

Primary myoblasts were maintained in 12-well plates in 1 mL of DMEM supplemented with 10% horse serum, 0.5% chick embryo extract (Sera Lab, West Sussex, UK), 2 mM L-glutamine and 4.5 g/L glucose. Prior to experiments, cells were trypsinised and subcultured into 12-well TC plates and cultured until 60-70% confluence. Proliferation medium was replaced every 48 h.

2.2.3 Differentiation

Differentiation was initiated after myoblasts reached 60-70% confluence by replacing proliferating medium with DMEM supplemented with 2% horse serum and 0.5% chick embryo extract (Sera Lab, West Sussex, UK). Both proliferation and differentiation

media contained penicillin (100 IU/mL) and streptomycin (100 µg/mL). Differentiation medium was replaced every 48 h. After 8 days of differentiation, myoblasts fused to form multinucleated myotubes (Figure 2-2).

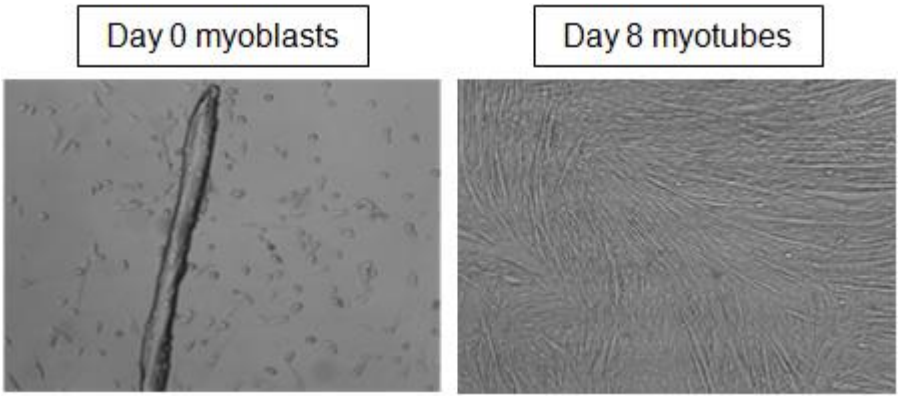

Figure 2-2 Primary myoblasts have formed multinucleated myotubes after differentiation for 8 days

2.3 RNA extraction

To extract total RNA from cultured cell monolayers or tissue explants, Chomczynski's single step procedure is applied (Chomczynski and Sacchi 1987). Cultured cells are lysed in TRI reagent that contains phenol and guanidine thiocyanate and effectively inhibits RNase activity. Subsequently, chloroform is added, and the samples are centrifuged (10,000 g at 4ºC for 15 mins) to obtain three phases. The top aqueous phase contains RNA which is precipitated with isopropanol.

For cultured cell monolayers, medium was removed from the flasks, cells were washed with phosphate-buffered saline (PBS), and 1 mL of TRI reagent was added per well (for a 12-well plate) and incubated at room temperature for 5 mins. For tissue explants, ~20 mg of tissue was homogenised in 1 mL of TRI reagent and then incubated at room temperature for 5 mins. For both cultured cell monolyers

and tissue explants, cell or tissue lysate in TRI reagent were transferred to Eppendorfs tubes, and 200 µL of chloroform was added, followed by vortexing and incubation at room temperature for 10 mins. The mixture was centrifuged at 10,000 g at 4ºC for 15 mins. The aqueous phase containing RNA was transferred to a fresh Eppendorf tube and 500 µL of isopropanol was added. The tubes were incubated on ice for 30 mins for RNA precipitation and then vortexed followed by centrifuging at 10,000 g at 4ºC for 15 mins. The RNA pellet was washed with 75% ethanol, centrifuged, air dried after ethanol was aspirated and re-suspended in 50 µL of nuclease free water.

2.3.1 RNA quantification

RNA concentration was measured using the NanoDrop ND-1000 UV-Vis Spectrophotometer (Thermofisher, Surrey, UK). The OD_{260}/OD_{280} ratio indicates the RNA purity, and only these ratios in the range of 1.8-2.0 were used. All measurements were made using 1.5 µL of RNA with respect to a blank measurement (nuclease free water).

Additionally, the integrity of the RNA was confirmed by electrophoresis on 0.8% agarose gel containing 2,000x GelRed (Cambrigde BioScience, Cambrigde, UK). The RNA separates down on gel according to its molecular mass and two abundant 28S and 18S rRNA bands are visualised under UV light.

2.4 Reverse transcription of RNA

Reverse transcription (RT) is the process in which single stranded RNA is converted to complementary DNA (cDNA). The extracted RNA is denatured losing its secondary

structure allowing random hexomers to anneal to the RNA template. Finally, the reaction is heated to a high temperature to inactivate RNA-dependent DNA polymerase and to terminate the reaction.

All RT reactions were performed using Life Technologies High-Capacity Reverse Transcription Kit (Life Technologies, Warrington, UK). To generate a 2x RT master mix, all reagents were combined as below:

Component	Volume/Reaction (µL)
10x RT Buffer	2.0
25x dNTPs mix (100 mM)	0.8
10x RT Random Primers	2.0
Multiscribe Reverse Transcriptase	1.0
RNase Inhibitor	1.0
Nuclease-free H_2O	3.2
TOTAL VOLUME PER REACTION	10.0

1 µg of RNA was diluted with nuclease free water to a final volume of 10 µL before 10 µL of 2x RT master mix was added. 20 µL of sample was loaded onto a thermal cycler (Life Technologies, Warrington, UK) and incubated at 25ºC for 10 mins followed by 37ºC for 120 mins and then 85ºC for 5 mins to terminate the reaction.

2.5 Conventional Polymerase Chain Reaction (PCR)

To amplify the regions of DNA or cDNA, oligonucleotide primers which are complementary to the 3’ and 5’ ends of this region are used. Double stranded DNA

is denatured using high temperature, and finally to allow primers annealing process, the temperature is lowered to be later increased for Taq polymerase to start the extension of oligonucleotides generating complementary DNA strands.

All conventional PCRs were carried out using New England Biolabs reagents (NEB, Herts, UK). In a 25 µL reaction, the following components were combined: 10x reaction buffer (final concentration 1x), dNTPs (200 µM), Taq DNA polymerase (0.025 units/µL), forward and reverse primers (0.4 µM) and DNA template <1,000 ng. Samples were transferred to a thermal cycler and heated to 94ºC for 2 mins (hot start), then cycled 35 times at 94ºC for 20 s, 56ºC (depending on annealing temperature of the primers) for 20 s and 72ºC for 1 min per 1 kb. Finally, samples were incubated at 72ºC for 5 mins and stored at -20ºC until required.

2.6 Relative quantitative polymerase chain reaction (qPCR)

Real-time PCR is a technique used to detect and quantify the initial amount of the template. It monitors the fluorescence emitted by a reporter during each reaction cycle which its intensity is proportional to the amount of PCR product generated. Real-time PCR quantifies the abundance of transcript. The point at which the target sequence is detected is called the cycle threshold (Ct). The Ct value of a gene of interest is subtracted from the Ct of a housekeeping gene resulting in the ΔCt value.

The oligonucleotide primers are complementary to the 5’ and 3’ ends of a region of interest amplifying cDNA. The presence of the fluorogenic probe which is chemically synthesised with a fluorescent reporter dye at the 5’ end and a quencher dye at the 3’ end allows quantification of the target transcript by fluorescence. The probe

binds to the DNA template and when the primer is extended, the probe is cleaved by the 5'-3' exonuclease activity of Taq DNA polymerase. It leads to separation of the reporter dye from the quencher dye increasing the fluorescence emitted by the latter. Then, the probe is removed from the DNA template, and the primer extension continues until it reaches the end of DNA strand.

All real-time PCR experiments were carried out using Life Technologies gene expression assays (Life Technologies, Warrington, UK). The 18S rRNA was used as a housekeeping gene at a final concentration of 25 mM each. The control reactions were carried out in separate wells from target gene expression measurements (singleplex) in 96-well plates (Life Technologies, Warrington, UK). The reactions were set up in triplicate by combining the following components: 5 µL of 2x Master Mix, 0.5 µL of either 18S mixture or 20x expression assay, 100 ng of cDNA and nuclease free water to a final volume of 10 µL per well. Plates were sealed with a clear adhesive film (Life Technologies, Warrington, UK) and finally run on 7500 real-time PCR system (Life Technologies, Warrington, UK) for 40 cycles. All data was expressed as Ct values and used to calculate ΔCt (Ct of gene of interest – Ct of 18S). They were expressed as arbitrary units (A.U. = $1000x2^{-\Delta Ct}$). Fold change was calculated using the $2^{-\Delta\Delta Ct}$ method.

2.7 11β-HSD1 enzyme activity assay

This technique allows measurement of the interconversion between the rodent inactive 11-DHC (A) and active corticosterone (B) by 11β-HSD1. This protocol was carried out on both monolayers of intact cells, microsomes and whole tissue explants.

Confluent cell monolayers were washed once with PBS, then incubated in serum free medium containing 100 nM of either 11-DHC enriched with 20,000 cpm/reaction tritiated [1,2,6,7-^{3}H(N)]-11-DHC (^{3}H-11-DHC) (for in-house synthesis see section below) or 100 nM of corticosterone enriched with 20,000 cpm/reaction of tritiated [1,2,6,7-^{3}H(N)]-corticosterone (^{3}H-corticosterone) (GE Healthcare, Bucks, UK). Incubations were carried out at 37ºC under a 5% CO_2 atmosphere for 30 mins (liver) and 2 h (quadriceps). Reaction medium was transferred to glass test tubes and 5 mL of dichloromethane was added. Steroids were extracted from medium by vortexing the tubes for 20 seconds followed by centrifugation at 1,000 g for 10 mins in order to separate aqueous from organic phases. Then the aqueous phase was aspirated, and the organic phase containing the steroids was evaporated at 55ºC using an air blowing sample concentrator (Techne, New Jersey, US). Steroids were re-suspended in 40 µL of dichloromethane, and using a Pasteur pipette they were spotted onto a silica coated thin layer chromatography plate (Thermofisher, Surrey, UK) followed by a non-radiolabelled 5 µL of 11-DHC/corticosterone (10 mM in ethanol). Each spot was separated by 1.5 cm from adjacent samples and 2 cm from the bottom of the plate. Thin layer chromatography (TLC) was used to separate the steroids in 200 mL of chloroform:absolute ethanol (92:8) mobile phase for 1.5 h. Radioactivity of the separated ^{3}H-11-DHC/^{3}H-corticosterone was measured using a Bioscan 200 imaging scanner (LabLogic, Sheffield, UK). To assign the radioactivity peaks with the correct steroids, the position of cold steroids, were visualised under UV light. The percentage conversion was calculated using region counts for the individual peaks and enzyme activity was expressed in pmoles of steroid converted per mg of protein per hour (pmol/mg/h).

Fresh tissue explants (~20 mg/well) or 100 µg muscle microsomes were added to 1 mL of serum free media and the above protocol was followed. Enzyme activity was expressed as pmoles of steroid converted per g of tissue per hour (pmol/g/h) or % conversion respectively.

2.7.1 ^{3}H -11-DHC production

Because tritiated ^{3}H-11-DHC is not commercially available, consequently it was generated from ^{3}H-corticosterone (GE Healthcare, Bucks, UK). 20 µL of ^{3}H-corticosterone (1 mCi/mL) was incubated with 250 µg of homogenised mouse placenta in 500 µL of 0.1 M potassium phosphate buffer (80.2 mL of 1 M K_2HPO_4, 19.8 mL of 1 M KH_2PO_4, 900 mL of H_2O), pH 7.4, with 500 µM NAD^+. Conversion was carried out at 37ºC in a shaking water bath overnight. Steroids were extracted by addition of 5 mL of dichloromethane. Tubes were vortexed for 20 s and centrifuged at 1,000 g for 10 mins to separate aqueous and organic phases. The aqueous phase was aspirated and the organic phase with steroids was evaporated at 55ºC using an air blowing sample concentrator (Techne, New Jersey, US). Steroids were re-suspended in 70 µL of dichloromethane, spotted onto a silica coated thin layer chromatography plate (Thermofisher, Surrey, UK) using a Pasteur pipette and separated by TLC using 200 mL of chloroform:absolute ethanol (92:8) as the mobile phase for 1.5 h. The position of ^{3}H -11-DHC was established by reading the silica plates using a Bioscan 200 imaging scanner (LabLogic, Sheffield, UK). The silica at the ^{3}H-11-DHC position was scraped into a glass tube and 300 µL of 100% ethanol was added for steroid elution. The tubes were incubated at 4ºC overnight. To separate the eluted ^{3}H-11-DHC and silica, the tubes were centrifuged at 1,000 g for

5 mins. Quality and radioactivity of ^{3}H-11-DHC were determined by separating 5 µL of stock by TLC. Number of counts was measured using the Bioscan 200 imaging scanner (Figure 2-3). Finally, the stock was diluted in ethanol to ~1,000 counts/µL which is equivalent of 1.5 pmol/µL.

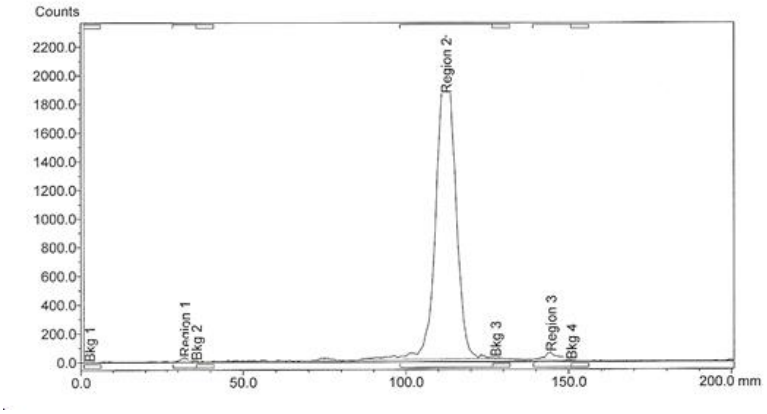

Figure 2-3 Representative of Bioscan traces of ^{3}H-11-DHC

2.8 Protein extraction

The extraction of soluble proteins from cell monolayers or tissue explants was carried out using cell lysis buffer supplemented with protease inhibitors and detergent. Centrifugation was applied to remove insoluble cell debris such as membrane lipids.

Monolayer of cells:

Cell monolayers were placed on ice and washed with cold PBS. For cells grown in 12-well plates, 40 µl of RIPA buffer (1 mM EDTA, 150 mM NaCl, 0.25% SDS, 1% NP40, 50 mM Tris pH 7.4), protease inhibitor cocktail (Roche, Sussex, UK) and phosphatase inhibitor (Thermofisher, Surrey, UK) were added. Subsequently, the cells were scraped, cell lysates were transferred to Eppendorf tubes, incubated at -80°C for 20 mins, thawed out on ice and centrifuged at 14,000 g for 15 mins at

4°C. The supernatant containing soluble proteins was transferred to fresh Eppendorf tubes and stored at -80°C prior to further protein concentration assessment (Section 2.10).

Mouse tissue explants:

Tissue was quickly harvested and snap-frozen in liquid nitrogen. To extract proteins, ~20 mg of tissue was homogenised in 1.5 mL of RIPA buffer using a mechanical homogeniser. Tissue homogenates were incubated at -80°C for 20 mins, thawed out on ice and centrifuged at 14,000 g for 15 mins at 4°C. Finally, the supernatant containing soluble proteins was collected and transferred to fresh Eppendorf tubes and either was used immediately to assess protein concentration (Section 2.10) or stored at -80°C.

2.9 Microsomal preparation

Microsomes contain lipids and proteins from the ER, Golgi, plasma membrane and transport vesicles. Murine hepatic and muscle microsomes were prepared by differential centrifugation. The extraction of microsomes from tissues was carried out using a lysis buffer supplemented with protease inhibitors.

Tissue explants were homogenised in sucrose buffer (0.25 M sucrose, 20 mM Hepes; pH 7.2) using a PowerGen 125 homogeniser (Fisher Scientific, Loughborough, UK) and centrifuged at 12,000 g at 4ºC for 15 mins. The supernatant from the first centrifugation was removed, the mitochondrial pellet was re-suspended in 25 ml of MOPs buffer (100 mM KCl, 20 mM NaCl, 1 mM $MgCl_2$, 20 mM MOPs; pH 7.2), and centrifugation was repeated at 100,000 g for 1 h. Subsequently, the

cytosolic fraction was aliquoted and stored at -80ºC whereas the microsomal pellet was washed with MOPs buffer by centrifugation at 100,000 g at 4ºC for 1 h three times, re-suspended in MOPs buffer, immediately frozen in liquid nitrogen and stored at -80ºC prior to assessment of protein concentration (up to 6 months; Section 2.10). A cocktail of protease inhibitors (1 mM phenylmethylsulfonylfluoride, 1 µM pepstatin A, 1 µM leupeptin, and 1 µg/mL aprotinin) was added to sucrose and MOPs buffers.

2.10 Measuring protein concentration

Total protein concentration from both cells monolayer and mouse tissue explants was assessed using the 96-well BioRad RC DC protein assay (BioRad, Herts, UK). This assay is based on the Lowry method, but has been modified to be reducing agent compatible (RC) and also detergent compatible (McCroskery et al. 2003). Prior to quantification, protein reacts with the copper in an alkaline copper tartrate solution. Finally, folin reacts with the copper treated protein leading to the generation of various reduced folin species of a characteristic blue colour that can absorb minimally at 405 nM and maximally at 750 nM.

Protein concentration was assessed according to the manufacturer protocol (BioRad, Herts, UK). The protein standards were made by dissolving bovine serum albumin (BSA) in RIPA buffer at final concentration 16 mg/mL. It was then serially diluted to obtain the following concentrations: 0.5, 1, 2, 4 and 8 mg/mL (Figure 2-4). 5 µL of sample or protein standards was added per well of a 96-well plate in triplicate. Subsequently, 25 µL of an alkaline copper tartrate solution (solution A) combined with surfactant solution (solution S) in a 1:50 ratio followed by 200 µL of a folin solution (solution B) was added to each well. The assay was incubated at room

temperature for 10 mins prior to absorbance being read at 690 nM on a Vector3 1420 multilable counter (PerkinElmer, Bucks, UK).

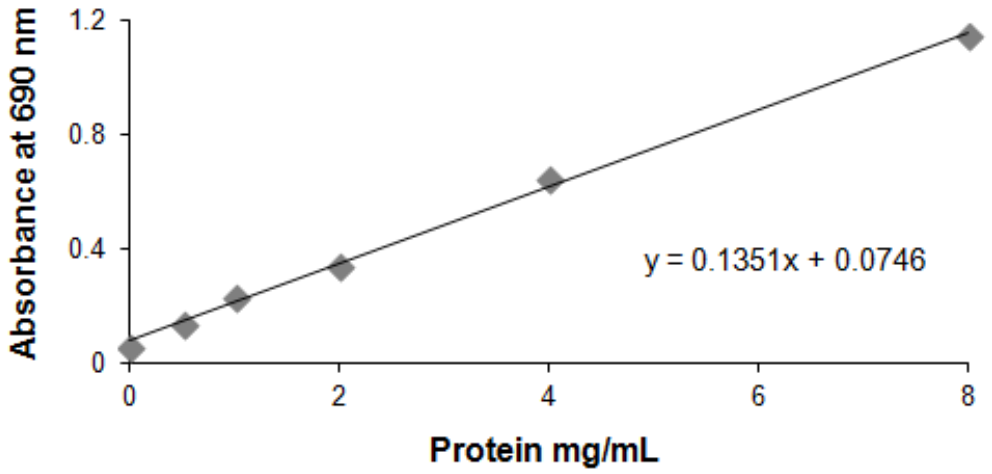

Figure 2-4 Representative BSA protein standard curve for the BioRad protein assay

2.11 Immunoblotting

Immunoblotting allows measuring the relative amounts of specific proteins in a mixed protein sample (Towbin et al. 1979). To remove all secondary and tertiary structures of proteins, proteins are boiled in a strong reducing agent. Negative charged proteins are separated according to their molecular mass using SDS-Page electrophoresis. The small proteins migrate fast and large proteins migrate slowly. Separated proteins are transferred to either a polyvinylidene difluoride (PVDF) or nitrocellulose membrane using electrical current. These membranes strongly bind proteins and any antibodies that they are exposed to. To prevent these non-specific bindings, the membrane is incubated in a blocking solution containing a generic protein such as milk or BSA. Subsequently, membranes are incubated with a primary antibody which specifically recognises the protein of interest and then with a secondary antibody

which is directed against the primary antibody and is conjugated to horseradish peroxidase (HRP). HRP catalyses a reaction involving the oxidation of luminal leading to emission of a blue light which is proportional to the amount of protein hybridised to the antibody on the membrane. Finally, the reaction is captured on a photographic film.

Between 20-40 µg of proteins or 10-25 µg of microsomes were combined with an appropriate volume of 5x loading buffer and denatured at 98ºC for 3 mins. Proteins were separated with 10-12% gradient SDS-PAGE gel (BioRad, Herts, UK) using Precision Plus Protein Standard (BioRad, Herts, UK) as a marker. The samples were run at 140 V for 1 h 30 mins, and protein transfer to nitrocellulose membrane (GE Healthcare, Bucks, UK) was conducted at 140 mA for 1 -2 h. To visualise the protein bands, the membrane was incubated in Ponceau stain with agitation for 60 s and rinsed with water. Electrophoresis and protein transfer were carried out in BioRad mini protein 3 apparatus (BioRad, Herts, UK). The membranes were blocked in 10 mL of blocking buffer containing 5% milk in PBS-0.05% Tween at room temperature for 1 h, followed by overnight incubation with the primary antibody at 4ºC. After washing with 10 mL of washing buffer (PBS-0.05% Tween) for 15 mins three times, the membranes were incubated with the secondary antibody at room temperature for 1 h. Subsequently, the membranes were washed with 10 mL of washing buffer (PBS-0.05% Tween) for 15 mins three times. Antigen-antibody complexes were detected using Enhanced Chemiluminescence (ECL; GE Healthcare, Bucks, UK). The reaction mixture (1 mL per membrane for 5 mins) was made by combining both substrate A and substrate B at a 50:50 ratio. Finally, photographic film (Perkin Elmer, Surrey, UK) was placed over the membranes

in the dark and exposed for 30 s to 30 mins followed by development on Compact X4 automatic film processor (Xograph Imageing Systems, Gloustershire, UK). To remove bound primary/secondary antibodies, the membranes were stripped by incubating them in stripping buffer (2% SDS, 100 mM β-mercaptoethanol, 50 mM Tris, pH 6.8) at 50°C for 1 h with gentle agitation. Afterwards, the membranes were washed with 10mL of washing buffer 3 times for 15 mins followed by re-probing with a different primary antibody.

2.12 H6PDH enzyme activity assay

This technique allows measuring the H6PDH activity by NADPH generation in murine hepatic and muscle microsomes.

H6PDH enzyme activity was measured by spectrophotometric detection of NADPH upon the addition of 10 mM $NADP^+$ and 10 mM G6P to hepatic microsomes (30 µg of protein) or skeletal muscle microsomes (100 µg of protein) in a total volume of 300 µL using the Ultrospec 2100pro spectrophotometer (Amersham Biosciences). Microsomes were permeabilised at 4ºC with 0.5% Triton X-100 for 30 mins to allow the free access of the cofactor and substrate to the intraluminal enzyme and incubated in the MOPs buffer at 37ºC. Absorbance readings were taken at 340 nm at 20 sec intervals for 3 mins.

2.13 NAD^+ assay

BioVision's NADH/NAD^+ Quantification Kit (Cambridge Bioscience, Cambridge, UK) provides a convenient tool for sensitive detection of the intracellular nucleotides: NADH, NAD^+ and their ratio. The NAD^+ Cycling Enzyme Mix in the kit specifically

recognises NADH/NAD^+ in an enzyme cycling reaction. The reaction specifically detects NADH and NAD^+ only. The enzyme cycling reaction significantly increases the detection sensitivity and specificity. NADt (NAD^+ and NADH) or NADH can be quantified by comparing with standard NADH.

For cultured cell monolayers: medium was removed and cells were washed with cold PBS, transferred into a micro-centrifuge tube and centrifuged at 1,500 g for 5 mins. The cells were extracted with 400 µl of NADH/NAD^+ extraction buffer by freeze/thaw two cycles (20 min on dry-ice, then 10 mins at room temperature), vortexed for 10 s and centrifuged at 16,100 g for 5 min. The extracted NADH/NAD^+ supernatant was transferred into a labelled tube.

For tissue explants: ~20 mg of tissue was washed with cold PBS and homogenised in 400 µl of NADH/NAD^+ extraction buffer in a micro-centrifuge tube followed by centrifuging at 13,200 g for 5 min. The extracted NADH/NAD^+ supernatant was transferred into a new tube. To make a standard curve, 10 µL of the 1 nmol/µL NADH standard was diluted with 990 µL NADH/NAD^+ extraction buffer in order to generate 10 pmol/µL standard NADH which was added (2, 4, 8, 10 µL) into a 96-well plate in duplicate. The final volume to 50 µL was made up with NADH/NAD^+ extraction buffer. Subsequently, 50 µL of extracted samples were transferred into a 96-well plate. To measure NADH, NAD^+ was decomposed in 200 µL of the extracted samples by heat shock at 60ºC for 30 mins before reaction. The samples were cooled down on ice, and 50 µL of NAD^+ decomposed samples were transferred into a plate. 100 µL of NAD^+ cycling mix (100 µL of NAD^+ cycling buffer and 2 µL of NAD^+ cycling enzyme mix) was added into each well to convert NAD^+ to NADH followed

by the plate incubation at room temperature for 5 mins. Finally, 10 µL of NADH developer was added into each well, and after 2 hours of incubation at room temperature, the absorbance readings nm were taken at OD 450 at 20 s intervals for 100 s.

2.14 DNA isolation

DNA is isolated from tissue explants using the phenol/chloroform extraction followed by ethanol precipitation. The aqueous phase contains DNA which is precipitated with 100% ethanol and sodium acetate solution.

Approximately 20 mg of tissue explants was collected from each animal and transferred into an Eppendorf tube containing digestion buffer which was made by combining the following components: 96 µL of 10x PCR buffer (Bioline, London, UK), 4 µL of 50 mM $MgCl_2$ (Bioline, London, UK), 5 µL of Tween-20, 885 µL of H_2O and 100 µL 2 mg/mL proteinase K (Promega, Southampton, UK). Subsequently, 100 µL of digestion buffer was added to each tissue sample and incubated in a hot block at 56ºC for 2 h or until tissues were digested. After incubation, the samples were vortexed and placed in a hot block at 99ºC for 20 mins in order to denature the proteinase K enzyme. One volume of phenol/chloroform was added to each sample followed by centrifugion at 14,000 g at 4ºC for 15 mins. The upper aqueous phase was transferred into a fresh tube and 1/10 the volume of 3 M sodium acetate solution with 2.5 volumes of 100% ethanol was added to precipitate DNA. The mixture was incubated for 30 mins on ice and centrifuged for 10 mins at 14,000 g. Subsequently, the supernatant was discarded, the pellet was washed with 1 mL of 70% ethanol and

allowed to air dry at room temperature for 5 mins. Finally, the pellet was re-suspended in 50 µL of H_2O, and DNA was stored at 4ºC until needed.

DNA concentration was measured using the NanoDrop ND-1000 UV-Vis Spectrophotometer (Thermofisher, Surrey, UK). The OD_{260}/OD_{280} ratio indicates the DNA purity, and only the ratios in the range of 1.8 were used. All measurements were made using 1.5 µL of DNA with respect to a blank consisting of nuclease free water.

2.15 Quantification of mtDNA

The NovaQUANT™ Mouse Mitochondrial to Nuclear DNA Ratio Kit (Merck Serono Ltd., Feltham, UK) compares the levels of nuclear to mitochondrial DNA in a mouse DNA sample. The mtDNA copy number to that of nuclear DNA (nDNA) is compared by real-time PCR using a set of four optimised PCR primer pairs targeting two nuclear and two mitochondrial genes. A single assay is run using four wells, whereby each well individually measures the expression of one of four gene targets. A nuclear gene 1 is compared to that of mitochondrial gene 1 and a nuclear gene 2 to mitochondrial gene 2. Finally, the ratios are calculated which are averaged to represent the mtDNA copy number per cell.

Approximately 2 ng of DNA was used in each reaction well. DNA was diluted using DNase/RNase-free water to the final volume of 10 µL. An equal volume of 2x RT2 Fast SYBR Green Mastermix (Life Technologies, Warrington, UK) was added into the tube containing DNA aliquot. Finally, 20 µl of sample mix was transferred into

each well, and the plate was sealed with a plate sealer, briefly centrifuged and run using real-time PCR (Section 2.6).

Data was analysed by averaging the copy numbers calculated from the NADH dehydrogenase, subunit 1/beclin 1 (ND1/BECN) pair and the NADH dehydrogenase, subunit 6/nebulin (ND6/NEB) pair. The Ct value from the ND1 gene was subtracted from the BECN1 Ct to obtain ΔCt1, and the ND6 Ct was subtracted from NEB to obtain ΔCt2. The average number of mitochondrial DNA copies was calculated by adding $n= 2^{\Delta Ct1}$ and $n=2^{\Delta Ct2}$ as in the table below:

Target	Ct	ΔCt	$2^{\Delta Ct}$	Average Number of Copies
NDI	18	ΔCt1=9.5	724	677
BECNI	27.5			
ND6	17.6	ΔCt2=9.3	630	
NEB	26.9			

2.16 Metabolomics technology

Metabolomics is the field of measuring all small molecules below 1,500 Da called metabolites in a biological sample in one single experiment (Adamski and Suhre 2013).

Blood from male mice (H6PDH KO and WT), aged 8 weeks old, was obtained by cardiac puncture and immediately centrifuged at 1,000 g in heparin-coated tubes. Plasma was transferred to cryotubes and snap-frozen. Subsequently, mice were sacrificed by neck dislocation using Schedule 1 method, and tissue explants (liver and quadriceps) were quickly excised from each animal to be snap-frozen in liquid nitrogen and stored at -80°C until metabolites extraction. Frozen tissues were

homogenised in the tubes containing ceramic beads of 1.4 mm diameter using extraction solvents (100% ethanol/10 mM potassium phosphate buffer; 85/15 v/v, 3 µL per mg of tissue). The Absolute*IDQ* p150 kit (Biocrates Life Sciences AG, Austria) was prepared as described by the manufacturer. A 10 µl aliquot of plasma or tissue extract was loaded onto the plate followed by drying of samples under the nitrogen stream, derivatisation of amino acids with 5% phenylisothiocyanate (PITC), drying of samples and extracting metabolites and internal standards with 5 mM ammonium acetate in methanol. Subsequently, the samples were centrifuged through the filter membrane and diluted with 600 µL MS running solvent. The final metabolites were quantified with reference to appropriate internal standards using flow injection coupled with tandem mass spectrometry (FIA-MS/MS) analysis on a 4000 QTRAP instrument (ABSciex, Germany) coupled to a high-performance liquid chromatography (HPLC) Prominence (Shimadzu Deutschland GmbH, Germany) (Adamski and Suhre 2013).

2.17 Animal work

All animal experiments and procedures were approved under the British Home Office Guidance (Animals Scientific Procedures) Act 1986 (Project Licence, PPL 30/2764). Mice were housed in standard pathogen-free conditions on a 12 h light/12 h dark cycle with access to standard rodent chow (when not fasting) and water *ad libitum.*

2.17.1 Genotyping

A sample of mouse tissue (ear clippings or tail tip) was collected from each animal and transferred into a labelled Eppendorf tube. Digestion buffer was made by

combining the following components: 96 µL of 10x PCR buffer (Bioline, London, UK), 4 µL of 50 mM $MgCl_2$ (Bioline, London, UK), 5 µL of Tween-20, 885 µL of H_2O and 100 µL of 2 mg/mL proteinase K (Promega, Southampton, UK). Subsequently, 100 µL of digestion buffer was added to each tissue sample and incubated in a hot block at 56ºC for 2 h or until tissues were digested. After incubation, the samples were vortexed and then placed in a hot block at 99ºC for 20 mins in order to denature the proteinase K enzyme. Finally, the samples were left to cool down and centrifuged at 1,000 g for 1 min. DNA was stored at 4ºC until needed.

2.17.2 Breeding scheme

Figure 2-5 shows the breeding scheme for a conditional gene targeting for all Cre/+ lines. Mice carrying the recombinase transgene and being homozygous for the floxed gene are ~12.5% of total offspring (Joyner 2001).

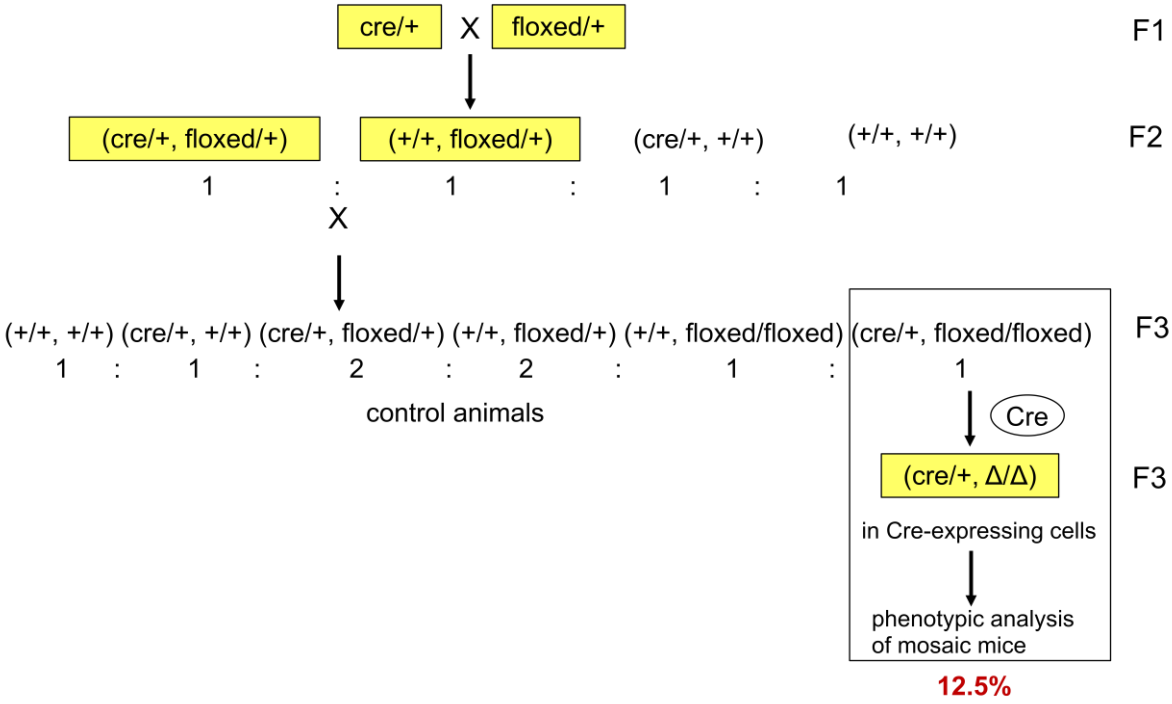

Figure 2-5 Schematic representation of the breeding strategy for the generation of conditional KO in muscle

The symbol Δ indicates deleted allele generated by recombination of the floxed locus while the symbol "+" indicates wt locus.

2.17.3 Tissue collection

Mice were sacrificed by neck dislocation (Schedule 1 method), and then tissue explants were quickly excised from each animal to be snap-frozen in liquid nitrogen for RNA/protein extraction (Section 2.3/2.8) or used fresh for 11β-HSD1 activity assay (Section 2.7).

2.18 Statistical analysis

Unpaired Student t-tests were used to compare single treatments to control using SigmaStat 3.1 (Systat Software, CA, US) whereas one way ANOVA on ranks was used to compare multiple treatments or times using SigmaStat 3.1. To perform statistical analysis on real-time PCR data, mean values of ΔCt were used.

Chapter 3- Expression and activity of the G6PT/H6PDH/G6Pase-β/11β-HSD1 metabolic unit in the SR of skeletal muscle

3.1 Introduction

Skeletal muscle is a major component of the human body that accounts for approximately 40% of the total body mass and provides support and movement to the skeleton (Smith and Muscat 2005). It plays a key role in glucose utilisation and has numerous vital metabolic functions being the major contributor to global insulin sensitivity (Larsen et al. 2008;Schuler et al. 2005).

This study focuses on investigating the G6PT(Slc37a4)/H6PDH/G6Pase-β/11β-HSD1 enzymatic pathway within the SR. G6PT transfers a substrate, G6P, from cytosol into the SR lumen which is further metabolised by either G6Pase-β to produce glucose (Gluc) and inorganic phosphate (Pi) (Shieh et al. 2003) or by H6PDH to generate a cofactor, NADPH, for 11β-HSD1 mediated GC activation. 11β-HSD1 converts cortisone (11-DHC in rodents) to the active GC, cortisol (corticosterone in rodents), and thus amplifies local GC action (Figure 3-1) (Lavery et al. 2008b). In this study, the main focus is the interaction of these enzymes in skeletal muscle and their contributions to local GC action.

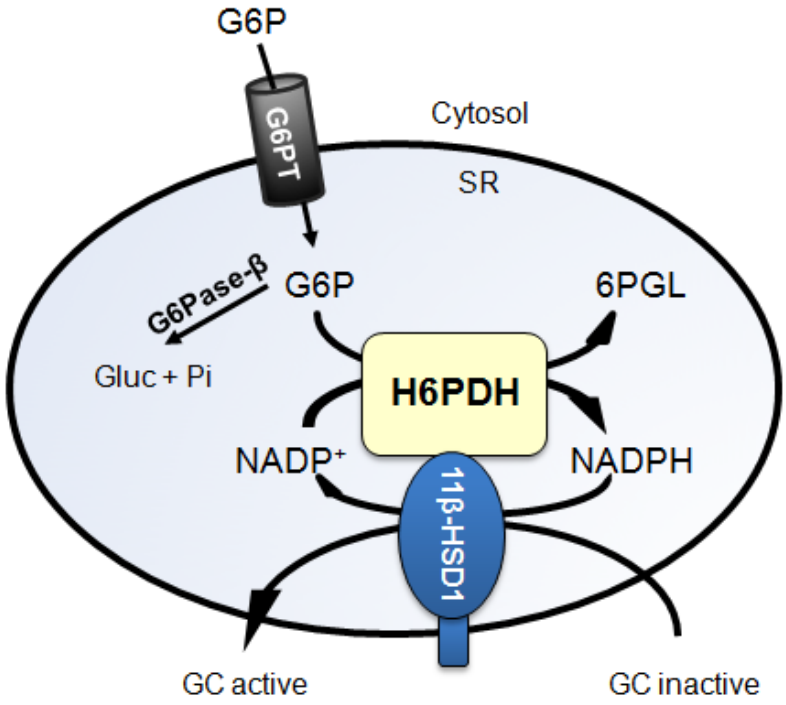

Figure 3-1 The G6PT/H6PDH/G6Pase-β/11β-HSD1 pathway in the SR of skeletal muscle

Previous investigations have shown that H6PDH global knockout (H6PDHKO) mice display fasting hypoglycaemia, increased basal- and insulin-stimulated glucose uptake as well as elevated glycogen storage (Lavery et al. 2007). The absence of H6PDH also switches the activity of 11β-HSD1 from an oxo-reductase to a dehydrogenase inactivating GCs. The H6PDHKO mice developed muscle myopathy affecting type IIb fibres and demonstrated reduced locomotor activity (Lavery et al. 2008b). Importantly, in H6PDHKO mice, the metabolic changes were accompanied by ER stress and subsequent activation of the UPR pathway with dysregulated expression of numerous genes involved in maintaining ER homeostasis (Lavery et al. 2008b;Walter and Ron 2011). In addition, H6PDHKO mice had increased 11β-HSD1 mRNA expression (Semjonous et al. 2011) and decreased

G6PT expression (Lavery et al. 2008b) in skeletal muscle. In cultured primary hepatocytes from H6PDHKO mice, G6Pase was not significantly induced; however, a trend towards up-regulation was observed (Rogoff et al. 2007). Interestingly, 11β-HSD1/H6PDH KO (DKO) mice also exhibited myopathy and retained many of the metabolic differences seen in H6PDHKO mice. The DKO phenotype has confirmed a GC and 11β-HSD1 independent role for H6PDH in controlling metabolic homeostasis and insulin sensitivity in skeletal muscle (Semjonous et al. 2011).

The first aim of this chapter is to understand the impact of H6PDH on cellular and SR G6P metabolism independently of other metabolic tissues such as liver and adipose, a muscle-specific knockout of H6PDH (H6MKO) was generated. This was to define the role of H6PDH in skeletal muscle and its impact on metabolic homeostasis as well as to determine the physiological effects of H6PDH in muscle upon glucose homeostasis and insulin sensitivity.

The aim of this chapter is also to evaluate undifferentiated myoblasts with that of differentiated myotubes and characterise the gene expression of these four pivotal enzymes involved in G6P metabolism with concurrent GC generation across myocyte differentiation using murine C2C12 and primary skeletal muscle cells.

3.2 Methods

3.2.1 C2C12 cell culture

Proliferating C2C12 myoblasts were cultured in DMEM supplemented with 10% FCS and seeded into 12-well TC plates. Differentiation was initiated when cells reached 60-70% confluence by replacing proliferation media with DMEM supplemented

with 5% horse serum and carried on for 8 days. Prior to treatment, cells were incubated in serum-free DMEM for 4 h.

3.2.2 Primary skeletal muscle cells

Skeletal myofibres were isolated from mouse EDL muscle. Primary myoblasts were maintained in 12-well TC plates in 1mL of DMEM supplemented with 10% horse serum and 0.5% chick embryo extract. Differentiation was initiated by replacing proliferating medium with DMEM supplemented with 2% horse serum and 0.5% chick embryo extract after myoblasts reached 60-70% confluence. Differentiation medium was replaced every 48 h. After 8 days of differentiation, myoblasts fused to form multinucleated myotubes.

3.2.3 Cell treatments

All cell treatments were carried out using serum free medium. GM was changed to FCS free DMEM 4 h before each treatment. Cells were treated with dexamethasone (DEX; 1 µM), insulin (1 µM), GR antagonist, Ru38486 (5 µM), and combination of DEX with insulin and DEX with Ru38486. In experiments using RU38486, cells were pre-treated with RU38486 for 10 mins before adding DEX in DMEM media. Cell treatments were carried out for 24 h.

3.2.4 RNA extraction

Total RNA was extracted on day 0, 2, 4, 6 and 8 of C2C12 differentiation or from 20 mg of tissue explants using Tri-reagent system. RNA concentration was determined

spectrophotometrically at OD_{260} and integrity assessed by agarose gel electrophoresis. 1µg of RNA was used for reverse transcription (see Section 2.4).

3.2.5 Real-time PCR

Primers and probes for all genes were supplied by Life Technologies; 11β-HSD1 (Mm00476182_m1), H6PDH (Mm00557617_m1), G6PT (Mm00484574_m1), G6Pase-β (Mm00616234_m1), α-actin (Mm00808218_g1), myogenin (Mm00440387_m1), HSPa5 also known as BiP (Mm00517691_m1) and DDIT3 (Mm00492097_m1). mRNA levels were determined using the ABI 7500 sequence detection system (Life Technologies, Warrington, UK). Reactions were performed in singleplex in triplicates as described in Section 2.6 and normalised against the 18S rRNA housekeeping gene.

3.2.6 H6PDH enzyme activity assay

The H6PDH activity was measured in 30 µg of liver and 100 µg of muscle microsomes from H6PDH KO and WT mice. Detection of NADPH was recorded upon the addition of 10 mM $NADP^+$ and 10 mM G6P using the Ultrospec 2100pro spectrophotometer (Amersham Biosciences, Chalfont St Giles, UK). Absorbance readings were taken at 340 nm at 20 sec intervals for 3 mins.

3.2.7 11β-HSD1 activity assay

Mouse tissue explants (~20 mg) were incubated with 100 nM 11-DHC or corticosterone supplemented with a tritiated tracer. Steroid incubation took place for 4 h for muscle tissue and 30 mins for liver. Subsequently, steroids were extracted

using dichloromethane, separated using a mobile phase consisting of chloroform/absolute ethanol (92:8) by thin layer chromatography and scanned using a Bioscan 200 imaging scanner (LabLogic, Sheffield, UK). 11β-HSD1 activity was expressed as pmol of corticosterone or 11-DHC generated per g of tissue per hour of incubation.

3.2.8 Histology

Quadriceps muscle was harvested from H6PDH global KO mice and then fixed in 10% neutral buffered formalin. Each muscle from both KO and WT mice (n=3 for each genotype) was paraffin embedded and cut into 5 µm sections to be stained by hematoxylin and eosin (H&E) to provide a histological detail of muscle structure. Muscle tissue was analysed from mice of 4 and 7 weeks of age.

3.2.9 Immunoblotting

Microsomes were extracted from tissue explants, and their concentration was determined as described in Section 2.10. For H6PDH immunoblotting, 10 µg of microsomal protein was resolved on 10% SDS-PAGE gels. Proteins were transferred to nitrocellulose membranes for 1 h at 100 V, and then primary, H6PDH (Santa Cruz Biotechnology, Heidelberg, Germany), and secondary antibodies (Dako, Glostrop, UK) were used at a dilution of 1:1,000 and 1:25,000 respectively. Membranes were re-probed for BiP antibody (BD Biosciences, Oxford, UK) used as a loading control at a dilution of 1:1,000. Bands were visualised using ECL detection kit (GE Healthcare, Bucks, UK).

3.2.10 Rodent protocol

All animal experiments and procedures were carried out in accordance with the British Home Office Guidance (Animals Scientific Procedures) Act 1986 (Project Licence, PPL 30/2764). Mice were housed in standard pathogen-free conditions on a 12 h light/12 h dark cycle with access to standard rodent chow (when not fasting) and water *ad libitum.*

On the day of experiment, mice were sacrificed by cervical dislocation. Liver, skeletal muscle (quadriceps, tibialis anterior (TA), soleus), heart, kidney and lung were removed and snap-frozen in liquid nitrogen for characterisation of DNA recombination and mRNA expression. To measure 11β-HSD1 activity, tissue explants were freshly harvested in the serum-free DMEM and immediately used for the assay.

3.2.11 Genotyping

The H6PDH knockout 1st allele mice were purchased from the EUCOMM (The European Mouse Mutant Archive – EMMA, Munich, Germany) programme that employs a KO 1st allele strategy in which a SA-βgeo-pA reporter cassette (SA, splice acceptor; βgeo, β-galactosidase/neomycin phosphotransferase fusion gene; pA, bovine growth hormone polyadenylation sequence) flanked by FRT (flippase recognition target) sequence is inserted into the 1st intron of H6PDH inactivating the gene. This global knockout was called H6KO. At the same time target exon was floxed by the LoxP sites. A conditional allele was generated by Flp recombinase expression to remove the reporter gene (data not shown). The Cre recombinase

expression is under the control of the *Acta1* promoter, and will excise exon 3 coding the catalytic domain of the conditional *H6PD* allele in skeletal muscle (Figure 3-2).

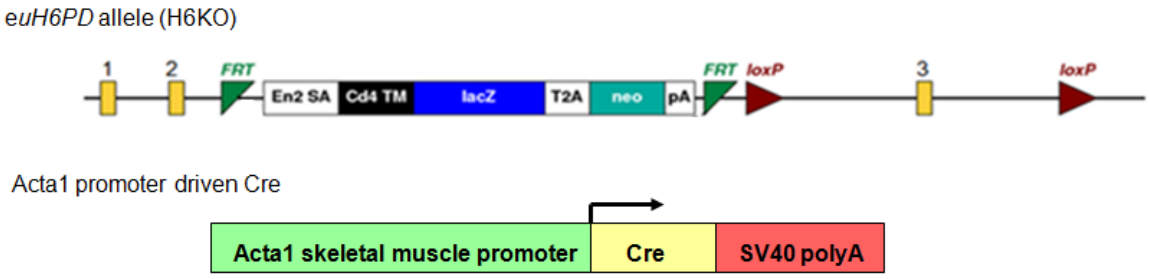

Figure 3-2 A schematic representation of the H6KO allele and Acta1-Cre

The H6KO allele will be crossed with a Flp deleted strain in order to generate a conditional allele which after breeding with muscle-specific Cre mice (Acta-Cre), will generate H6MKO mice.

To generate H6MKO, floxed homozygous H6KO mice on a C57BL/6 background were crossed with Acta1-Cre transgenic mice (C57BL/6 background, targeting Cre expression to skeletal muscle and heart). This generated mice devoid of H6PDH activity in skeletal muscle cells. Genotyping PCR was carried out on ear clip DNA using following gene specific primers (5′-3′) (Figure 3-3):

	Primers	Sequence	Product size
KO allele	Ef4685	TTTGCACGGGCCTCAGGGCTGG	747
	L3r4688	TGGCTTTGGGAGGGAGTGGCCC	
	CreF	GTAGTTATTCGGATCATCAGCTACAC	402
	CreR	GCTGCCACGACCAAGTGACAGCAATG	

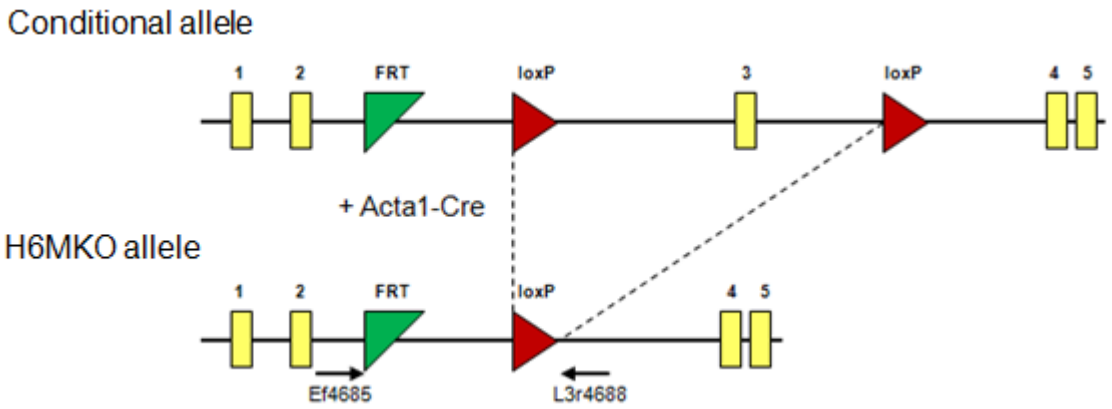

Figure 3-3 Primers used for H6MKO genotyping

The Ef4685 and L3r4688 primers were used to confirm successful deletion of exon 3 which inactivated *H6PD* function whereas the CreF/R primers confirmed gene knockout specific to skeletal muscle.

3.2.11.1 Fasting blood glucose measurement

Mice were fasted for 16 h (n=6/group), and then blood samples were taken by tail nick. Blood glucose was measured using a Onetouch Ultra glucometer.

3.2.11.2 Analysis of urinary GC metabolites

Urine was collected from 8- to 14-wk-old female mice on filter paper from four members of each group (H6MKO and WT). Subsequently, the samples were analysed by repetitive scanning using GC/MS instrument at the Steroid Mass Spectrometry Core Facility within CEDAM, University of Birmingham. Corticosterone

metabolites were identified through interpretation of their mass spectra. Individual components were quantified by relating the peak areas on the TIC (total-ion-current) chromatograms to the peak area of the stigmasterol internal standard. Individual steroids were quantified as a percentage of the total corticosterone metabolites (Lavery et al. 2006).

3.2.12 Statistical analysis

Statistical comparisons were performed using Prism 4 (GraphPad, CA). Data were presented with statistical significance defined as $P<0.05$. Where data were normally distributed, unpaired Student t-tests were used to compare single treatments to control whilst one way ANOVA on ranks was used to compare multiple treatments or times using SigmaStat 3.1 (Systat Software, CA, US). To perform statistical analysis on real-time PCR data, mean values of A.U. were used.

3.3 Results

3.3.1 11β-HSD1, H6PDH, G6PT and G6Pase-β pathway expression during C2C12 differentiation

To show that C2C12 cell line was differentiating correctly according to the muscle-specific profile differentiation markers, α-actin ($p<0.05$ for day 4 and 6 vs. day 0) and myogenin ($p<0.01$ for day 6 vs. day 0; $p<0.001$ for day 2, 4 and 8 vs. day 0), significantly increased their mRNA expression reaching the highest peak at day 4 (Figure 3-4).

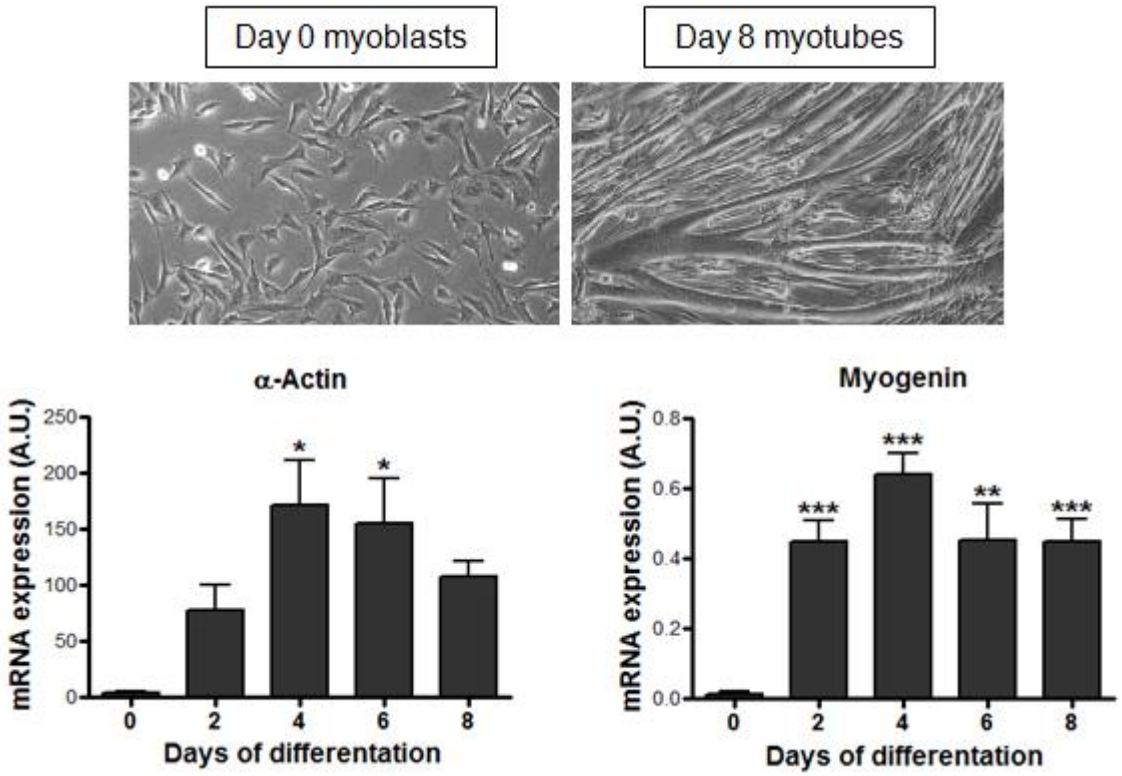

Figure 3-4 The mRNA expression of differentiation markers: α-actin and myogenin

*p<0.05; **<0.01; *** p<0.001 vs. control: day 0 myoblasts. All data are the mean A.U. values ±SEM from n=4 experiments by ANOVA (Newman-Keuls post test).

11β-HSD1 significantly increased its mRNA expression during differentiation ($p<0.05$ for day 6 vs. day 4; $p<0.01$ for day 4 vs. day 0 and $p<0.001$ for day 8 vs. day 0, 2, 4 and 6). H6PDH expression was also elevated in mature myotubes ($p<0.05$ for day 8 vs. day 0 and for day 6 vs. day 4; $p<0.01$ for day 8 vs. day 4). There was no significant change in the gene expression of G6PT and G6Pase-β (Figure 3-5).

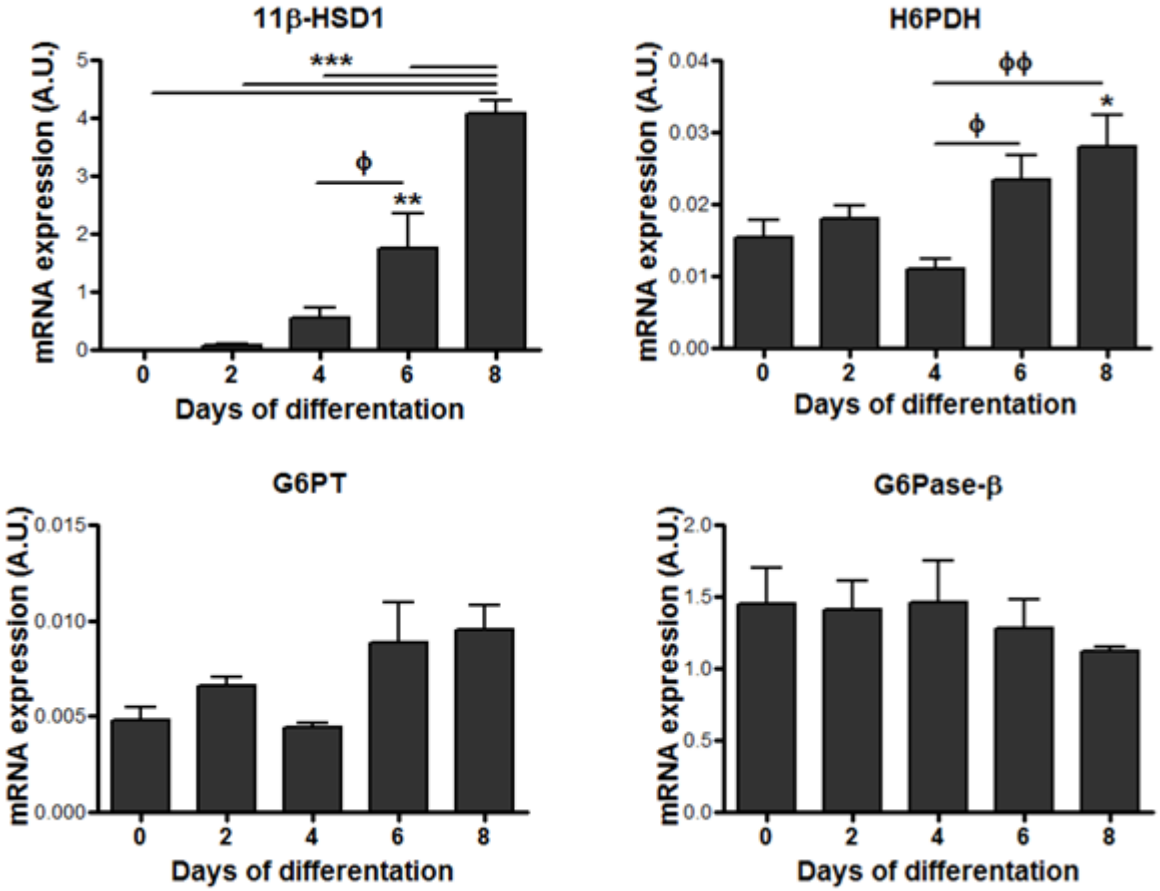

Figure 3-5 Changes in expression of 11β-HSD1, H6PDH, G6PT and G6Pase-β across C2C12 differentiation

**<0.01; *** p<0.001 vs. control: day 0 myoblasts and ϕ<0.05; ϕϕ<0.01 vs. day 4. All data are the mean A.U. values ±SEM from n=4 experiments by ANOVA (Newman-Keuls post test).

3.3.2 11β-HSD1, H6PDH, G6PT and G6Pase-β pathway expression during primary skeletal muscle cells differentiation

Similarly to C2C12, primary skeletal muscle cells were able to differentiate correctly across an 8 day period; however, to a lesser degree. The muscle-specific profile differentiation markers, α-actin mRNA ($p<0.05$ for day 8 vs. day 2; $p<0.01$ for day 8 vs. day 0 and day 6 and for day 4 vs. day 2; $p<0.001$ for day 8 vs. day 4)

and myogenin mRNA ($p<0.05$ for day 8 vs. day 2, 4 and 6; and $p<0.01$ for day 8 vs. day 0) were significantly elevated reaching the highest peak at day 8 (Figure 3-6).

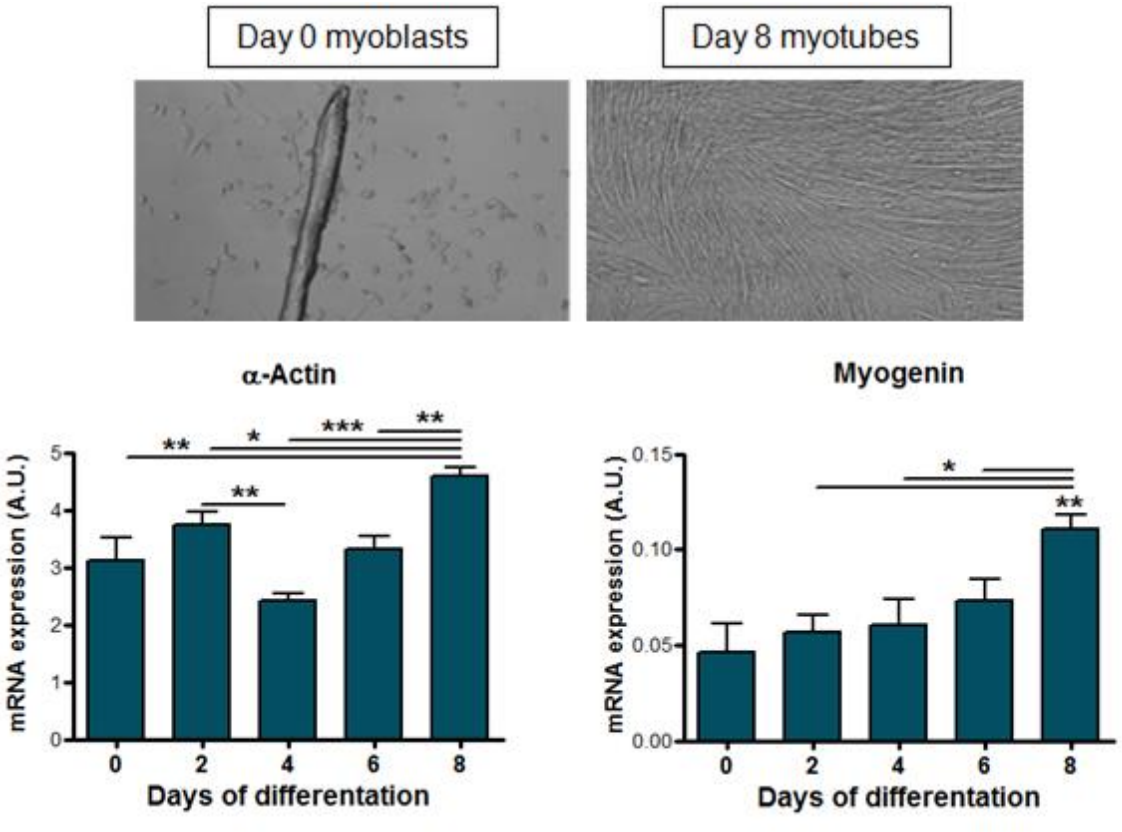

Figure 3-6 The mRNA expression of differentiation markers: α-actin and myogenin across primary muscle cells differentiation

*<0.05, **<0.01 and *** p<0.001. All data are the mean A.U. values ±SEM from n=4 experiments by ANOVA (Newman-Keuls post test).

11β-HSD1 significantly increased its mRNA expression reaching the highest peak at day 8 ($p<0.05$ for day 8 vs. day 0; $p<0.01$ for day 8 vs. day 4) whereas H6PDH mRNA expression was elevated in mature myotubes at day 6 and 8 ($p<0.05$ for day 8 vs. day 4; $p<0.01$ for day 6 vs. day 0, 2 and 4). Similarly to C2C12, G6PT and G6Pase-β did not change their mRNA expression over the 8 day differentiation time course (Figure 3-7).

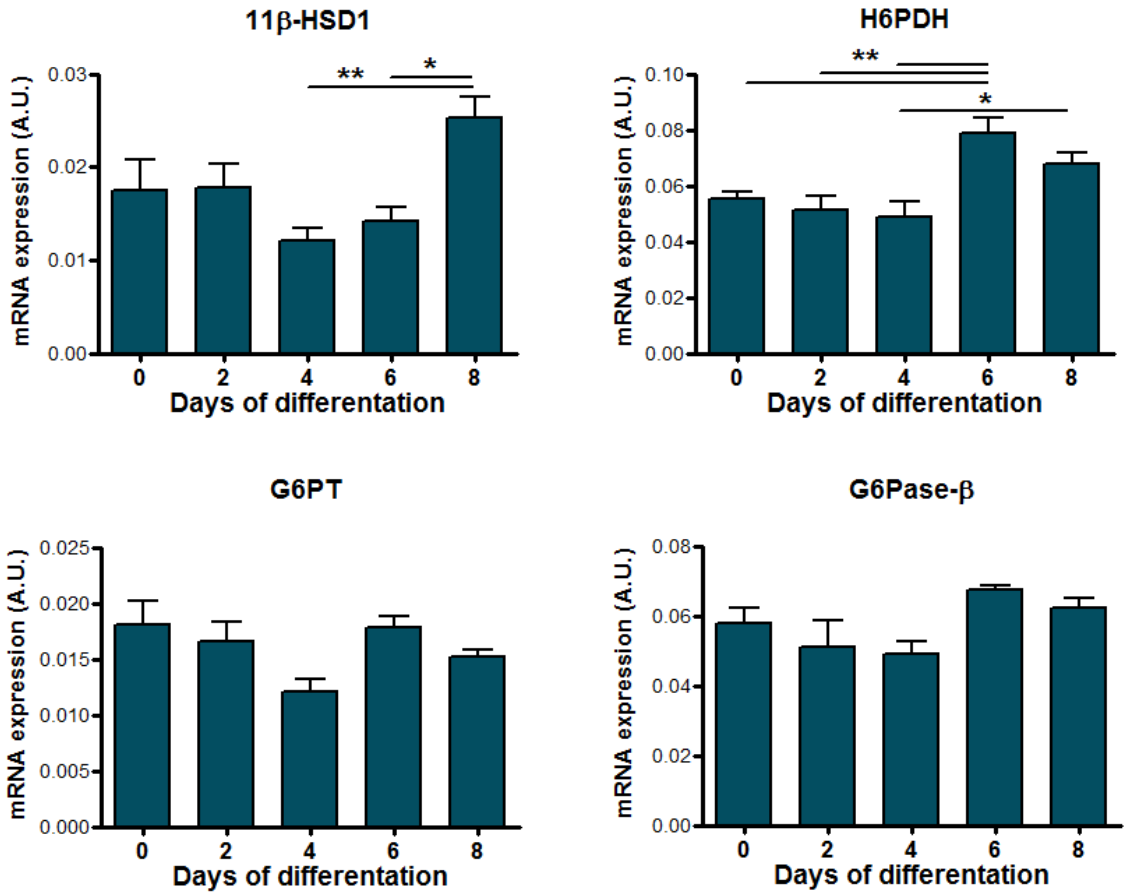

Figure 3-7 Changes in expression of 11β-HSD1, H6PDH, G6PT and G6Pase-β across primary muscle cells differentiation

*<0.05; **<0.01 day 8 vs. day 6 and 4 respectively for 11β-HSD1; *<0.05 day 6 vs. day 4 and **<0.01 day 6 vs. day 0, 2 and 4 for H6PDH. All data are the mean A.U. values ±SEM from n=4 experiments by ANOVA (Newman-Keuls post test).

3.3.3 C2C12 myoblasts gene expression in response to GC and insulin treatment

To investigate the regulation of G6PT/H6PDH/G6Pase-β/11β-HSD1 pathway, we studied their response to both GC and insulin, important regulators of muscle glucose metabolism (Figure 3-8).

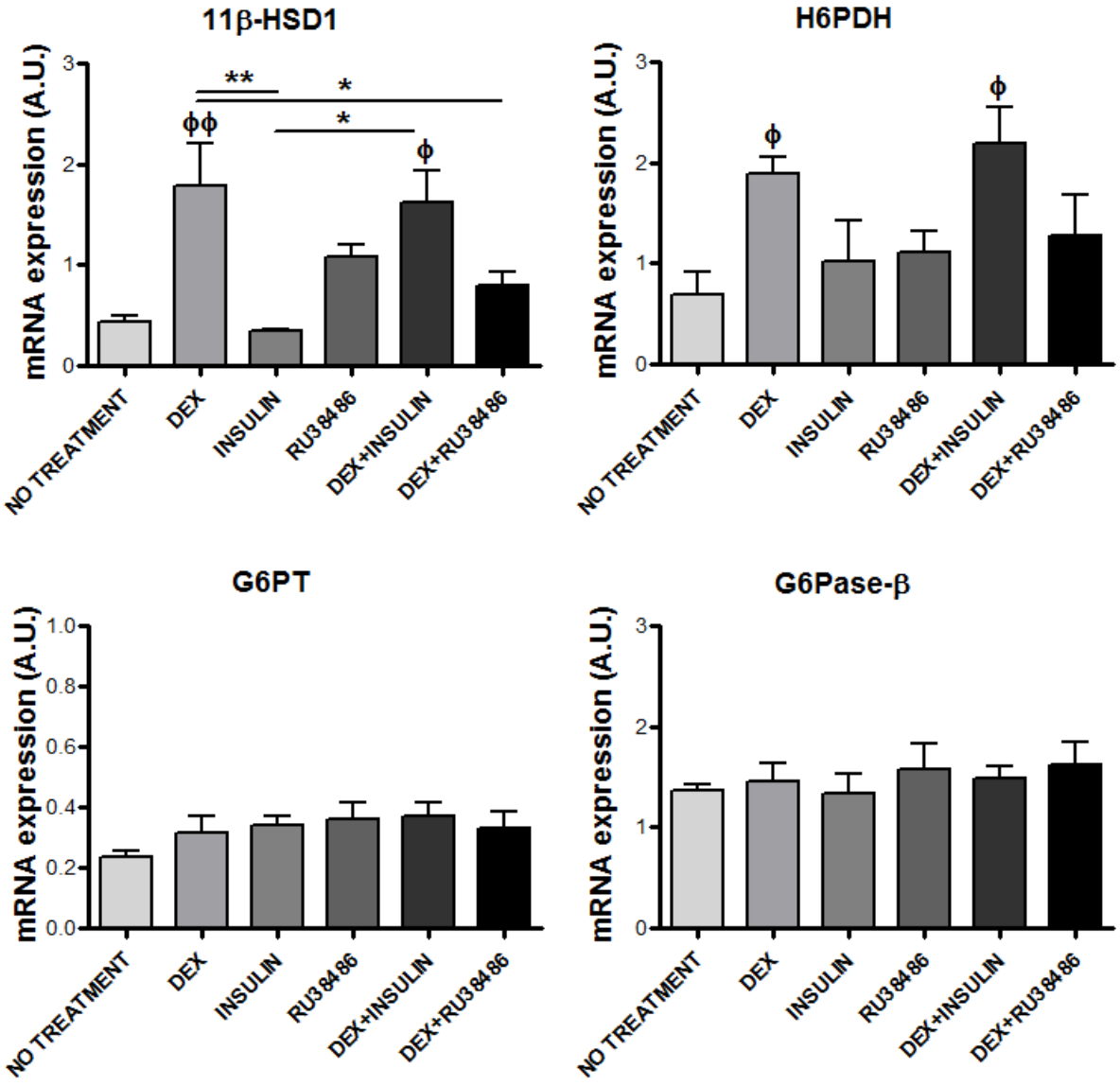

Figure 3-8 The mRNA expression of key components involved in GC metabolism in C2C12 myoblasts

11β-HSD1, H6PDH, G6PT and G6Pase-β expression measured using real-time PCR following treatment with DEX (1 μM, 24 h) with or without GR antagonist, Ru38486, insulin (*<0.05; **<0.01; ϕ<0.05 and ϕϕ<0.01 vs. no treatment). All data are the mean A.U. values ±SEM from n=3 experiments by ANOVA (Newman-Keuls post test).

Treatment of undifferentiated C2C12 myoblasts with DEX significantly increased 11β-HSD1 mRNA expression ($p<0.01$). Insulin had no effect. Moreover, combination of DEX with insulin also increased 11β-HSD1 expression ($p<0.05$) while DEX

combined with Ru38486 decreased ($p<0.05$). H6PDH mRNA expression of C2C12 myoblasts was significantly greater when treated with DEX ($p<0.05$) and DEX combined with insulin ($p<0.05$). This was probably due to DEX effect, as insulin on its own did not have any effect. G6PT and G6Pase-β did not change their mRNA expression in response to GC and insulin treatments.

3.3.4 C2C12 myotubes gene expression in response to GC and insulin treatment

In C2C12 myotubes differentiated for 5 days, 11β-HSD1 mRNA expression was not significantly changed after treatment with DEX, Ru38486, DEX combined with insulin or Ru38486. No effect of Ru38486 treatment on 11β-HSD1 mRNA expression suggests that GC inhibitor did not work properly. Additionally, combination of DEX and insulin significantly increased H6PDH mRNA expression ($p<0.01$) when compared to no treated cells. Similarly to myoblasts, G6PT and G6Pase-β did not change their mRNA expression in response to GC and insulin treatments (Figure 3-9).

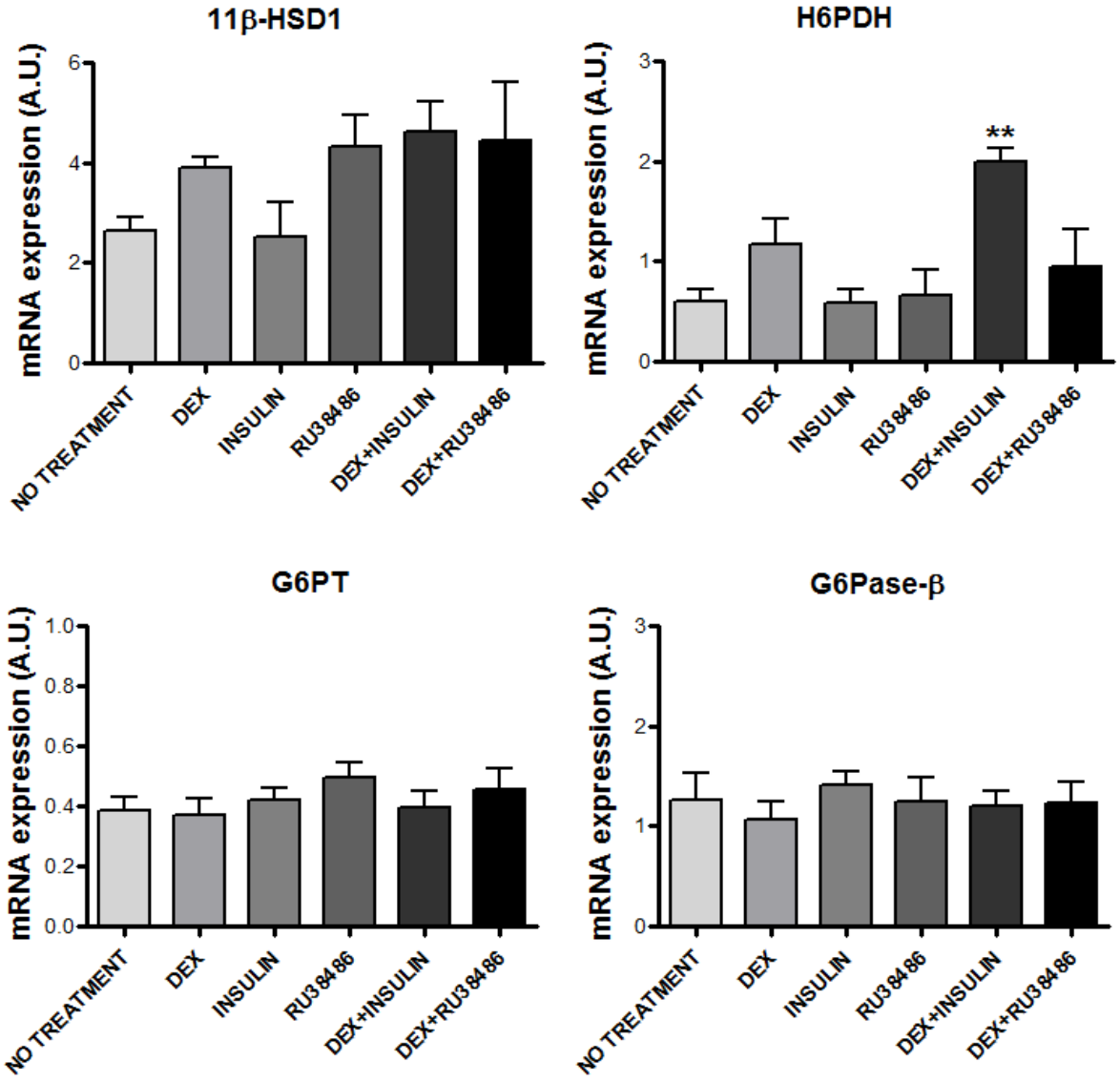

Figure 3-9 The mRNA expression of key components involved in GC metabolism in C2C12 myotubes

11β-HSD1, H6PDH, G6PT and G6Pase-β expression measured using real-time PCR following a 24 h treatment with DEX (1 μM) with or without GR antagonist, Ru38486 (5 μM), insulin (1 μM) with or without DEX and Ru38486 (** $p<0.01$ vs. no treatment). All data are the mean A.U. values ±SEM from n=3 experiments by ANOVA (Newman-Keuls post test).

Increased expression of differentiation markers (α-actin, myogenin) during the transition from proliferating to differentiating C2C12 and primary skeletal muscle cells was shown in order to confirm their ability to differentiate. C2C12 cells had greater

expression of these genes compared to primary cells suggesting that the time of maturation from myoblasts to myotubes varies between different cell models. Elevated mRNA expression of 11β-HSD1 and H6PDH in response to differentiation signals might highlight the importance of these genes in skeletal muscle development and underline their central role within SR. To investigate further the role of H6PDH as the redox regulator of glucose and GC metabolism within the SR of skeletal muscle, H6PDH muscle-specific mouse model (H6MKO) was generated and compared to the global H6KO mice.

3.3.5 H6MKO generation and evaluation

3.3.5.1 H6PDH global KO (H6KO) characterisation

Firstly, a novel knockout *H6PD* allele (H6KO), in which initial recombination of the LacZ reporter cassette into intron 2 is intended to completely knockout *H6PD* gene, was evaluated. Characterisation of 11β-HSD1 activity and muscle function in H6KO is important as these mice are expected to recapitulate the phenotype of previously generated H6PDH global knockout (H6PDHKO) mice and could not be used for H6MKO generation (Lavery et al. 2006).

H6PDH mRNA expression in muscle and liver were significantly decreased when compared to wild type mice (Figure 3-10).

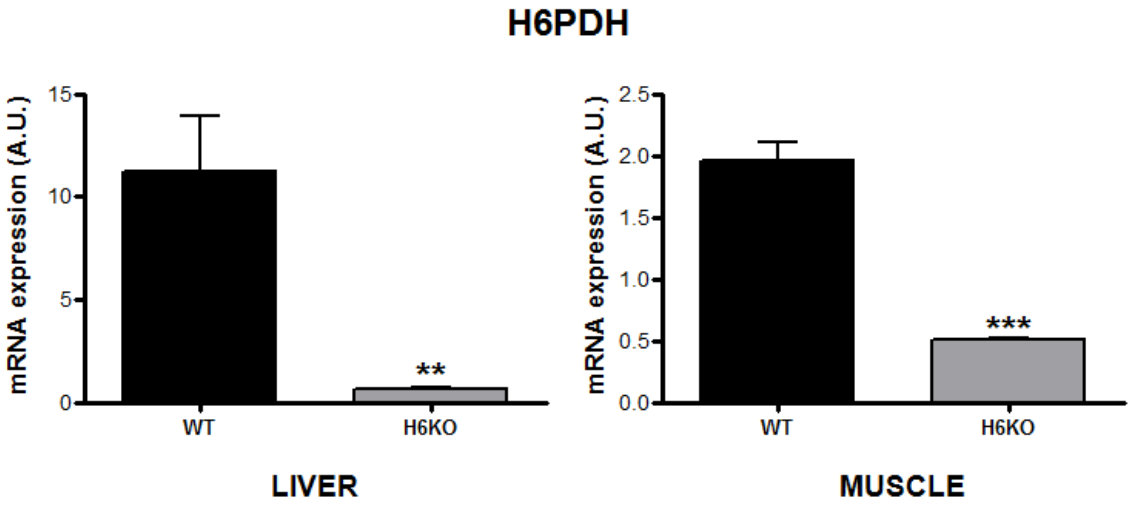

Figure 3-10 Successful H6PDH knock down in H6KO mice

Measurement of H6PDH mRNA gene expression in A.U. by real-time PCR in quadriceps and liver explants from 7-8 weeks old H6KO mice. ** $p<0.01$ vs. WT liver, *** $p<0.001$ vs. WT muscle; n=4/group. All data are the mean A.U. values ±SEM.

Additionally, hepatic and skeletal muscle microsomes were used to assess H6PDH enzyme activity in H6KO and WT mice using G6P as a substrate and $NADP^+$ cofactor for murine H6PDH. High level of activity in WT mice and no activity in the hepatic microsomes from H6KO mice were recorded; however, residual H6PDH activity was still detected in skeletal muscle microsomes from H6KO mice (Figure 3-11).

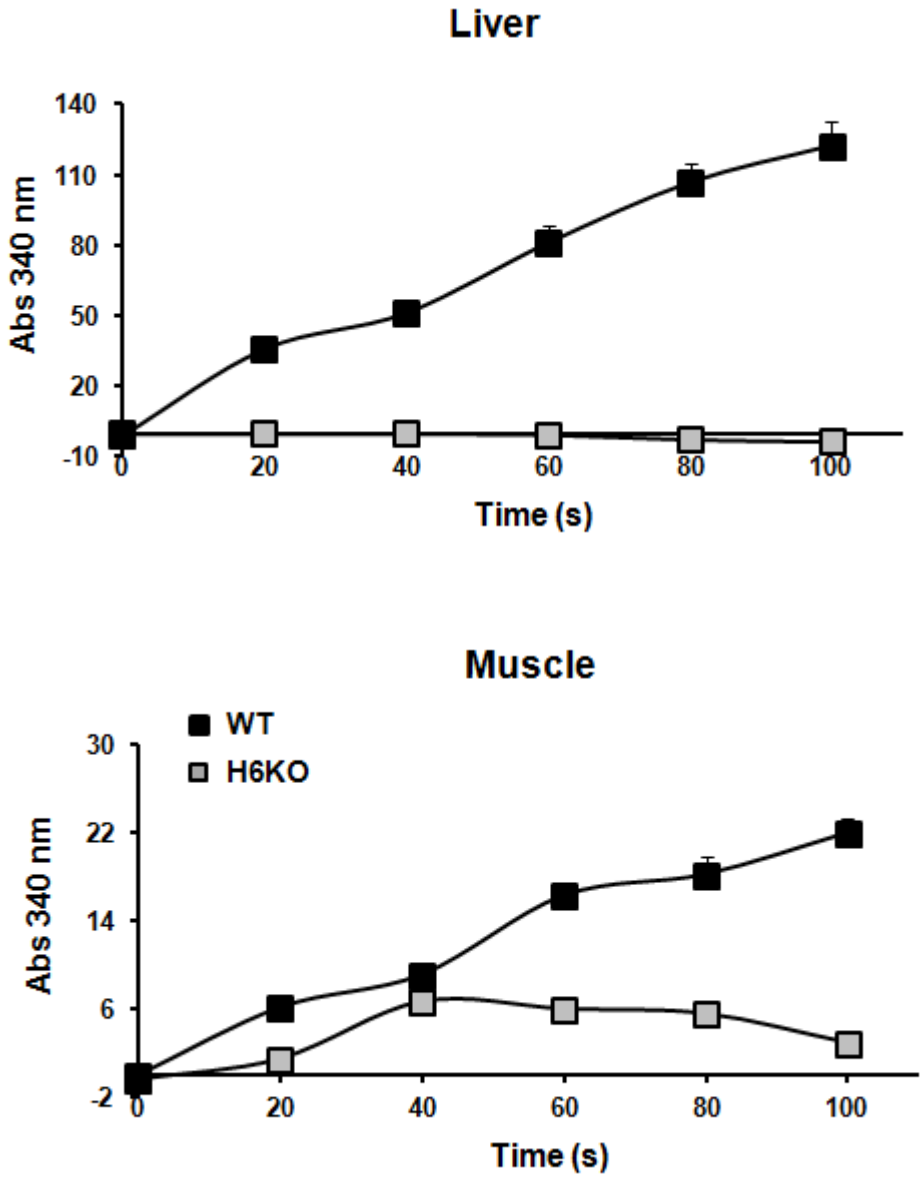

Figure 3-11 Residual H6PDH enzyme activity in H6KO muscle microsomes

H6PDH activity was determined spectrophotometrically by measuring the production of NADPH at 340 nm in the reaction containing the H6PDH-specific substrate G6P with readings taken at 20 s intervals for 3 mins. All data are the mean values ±SEM (n=3/group).

The 11β-HSD1 activity in muscle and liver explants in H6KO was switched off as previously described in H6PDHKO mice (Lavery et al. 2006) (Figure 3-12). In liver and muscle (quadriceps), there was a reduction of an oxo-reductase activity whereas there was a significant increase of a dehydrogenase activity in liver and subtle,

but not significant in muscle. These data suggest that the H6KO mice endorse anticipated 11β-HSD1 biochemistry.

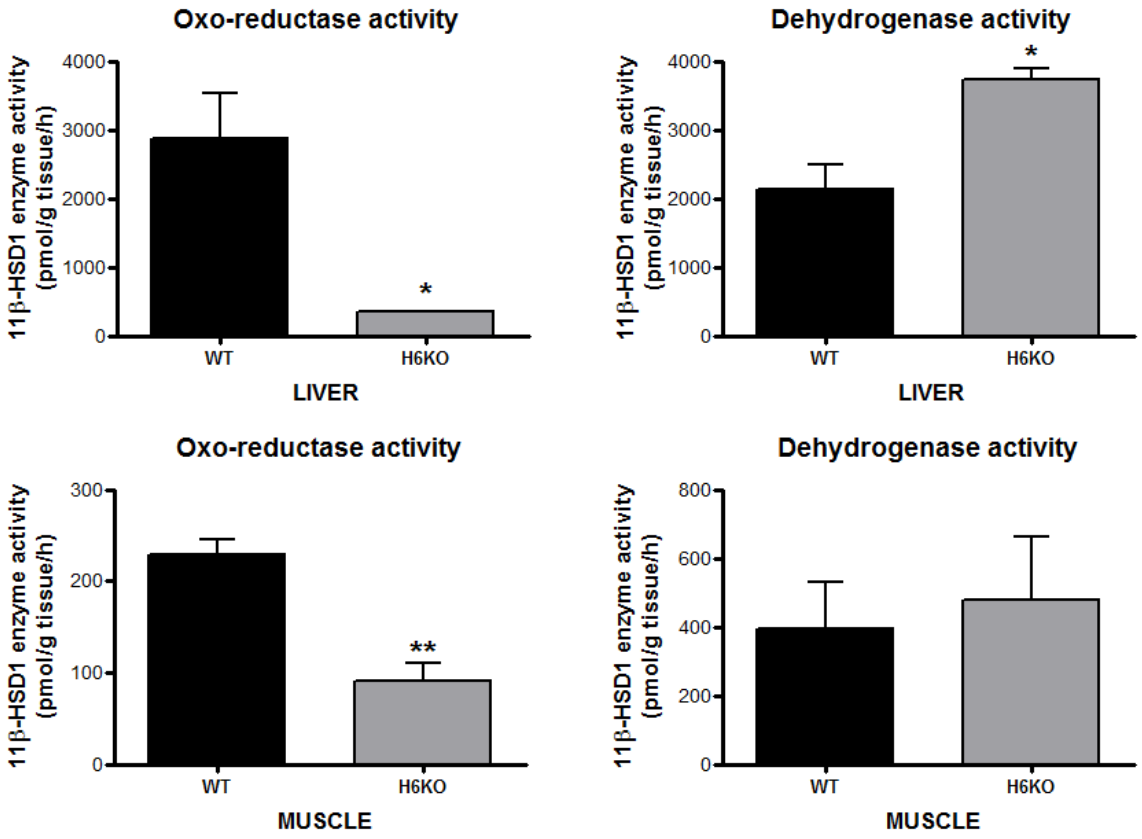

Figure 3-12 H6KO mice displayed reduced oxo-reductase and increased dehydrogenase 11β-HSD1 activity

The 11β-HSD1 enzyme activity in liver and muscle explants from H6KO and WT mice. * $p<0.05$, ** $p<0.01$ vs. WT. All data are the mean values ±SEM (n=3/group).

In addition, the visual appearance of TA, consisting of type IIb fibres, was markedly changed in 7-10 weeks old H6KO mice compared with WT. H&E staining of H6KO TA muscle showed elevated atrophic and vacuolated type fibres (Figure 3-13B) whilst no such histological features were evident in WT mice (Figure 3-13A). The H6KO mice which were 7 or more weeks of age presented the features of the myopathy seen in previously generated H6PDHKO mice. Unlike TA, soleus muscle

from H6KO mice did not present the full phenotype of myopathy, and centralised nuclei were the only feature seen in its sections (Figure 3-13D) when compared to WT soleus (Figure 3-13C).

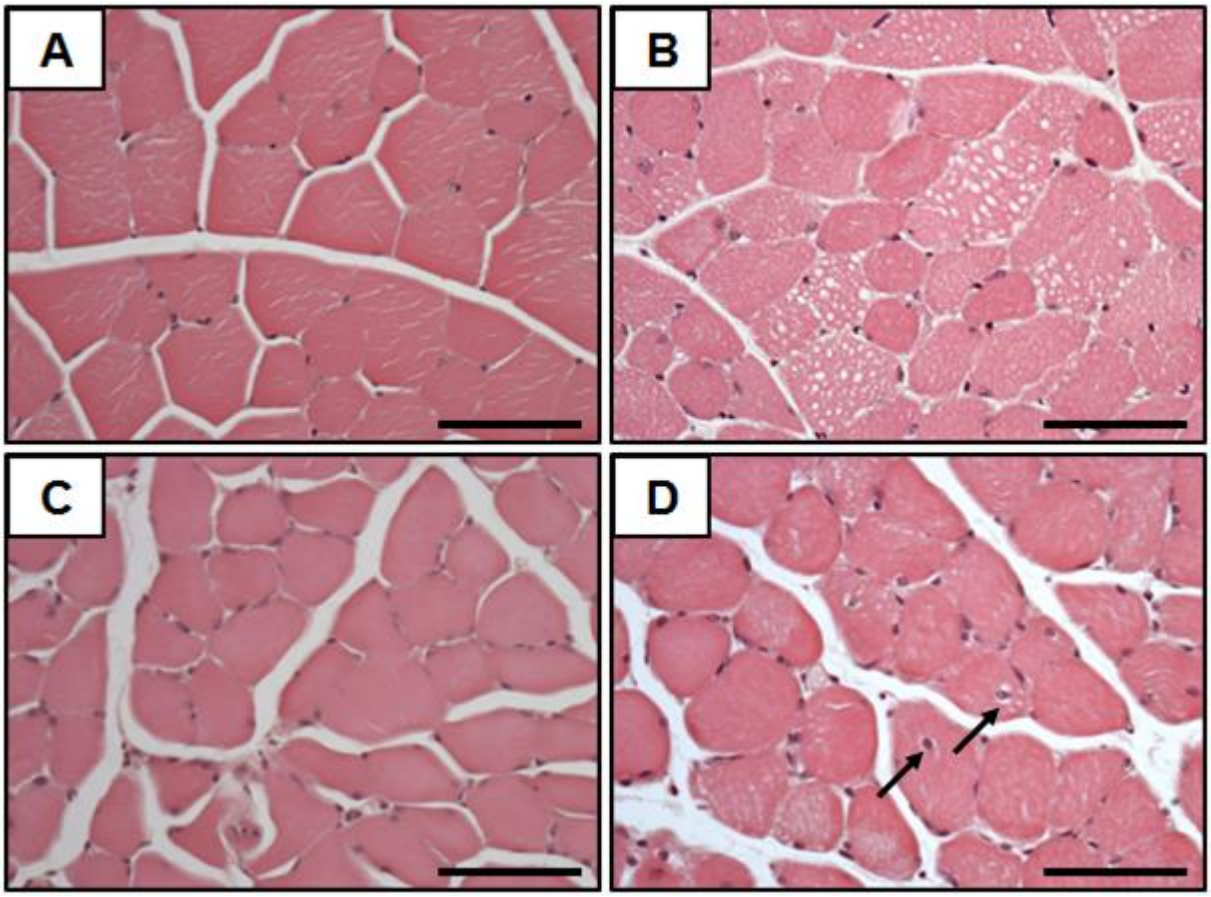

Figure 3-13 Histological defects in skeletal muscle of H6KO mice

Muscle sections of TA (A and B) and soleus (C and D) from WT (A and C) and H6KO (B and D) mice at 7-10 weeks stained with H&E. Vacuoles are present predominantly in type IIb fibres (B) when compared to control (A) and type I fibres which have only centralized nuclei shown by arrows (D) (each representative image is from n=3/group). The reference bar is 80 µM.

We measured the H6KO myopathy markers associated with ER stress and activation of the UPR pathway. ER stress indicators, DNA damage-inducible transcript 3 (DDIT3) and Heat Shock 70 kDa Protein 5 (HSPa5) (Figure 3-14), were elevated in quadriceps from the H6KO mice at 8 weeks of age.

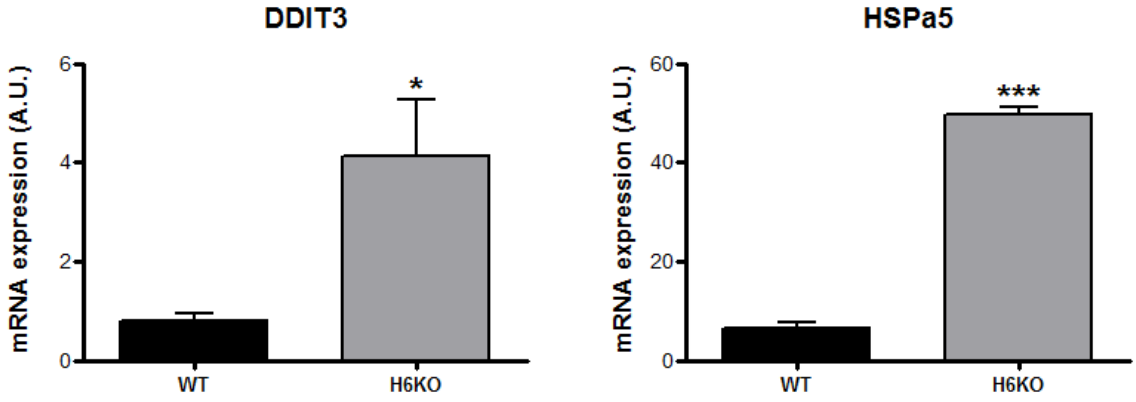

Figure 3-14 Increased ER stress response in H6KO muscle

Induction of ER stress markers, DDIT3 and HSPa5, in muscle (quadriceps) from 8 weeks old H6KO and WT mice. All data are the mean A.U. values ±SEM from n=4/group experiments (* $p<0.05$, *** $p<0.001$ vs. WT).

3.3.5.2 Characterisation of H6MKO mouse model

H6PDH is an enzyme responsible for the NADPH production within the ER/SR lumen. However, it is also an important, 11β-HSD1 independent, regulator of the SR metabolic function. To eliminate the muscle-specific GC effects seen in H6PDH global KO mice, H6PDH muscle-specific mouse model (H6MKO) was generated.

The expression of Cre recombinase used to produce H6MKO model is under the control of the *Acta1* (alpha actin) promoter and is expected to excise exon 3 coding the catalytic domain of the conditional *H6PD* allele in skeletal muscle (Figure 3-15).

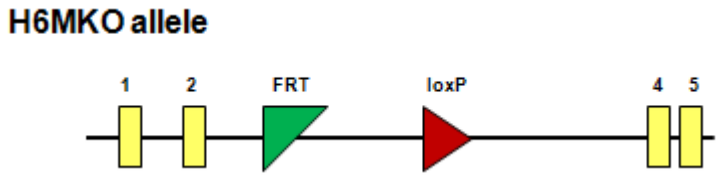

Figure 3-15 Generated H6MKO allele with exon 3 being removed by Acta1-Cre recombinase activity

To validate H6MKO model (Cre/+;fl/fl), we assessed DNA recombination between the LoxP sites using genomic DNA from an ear clip (Figure 3-16).

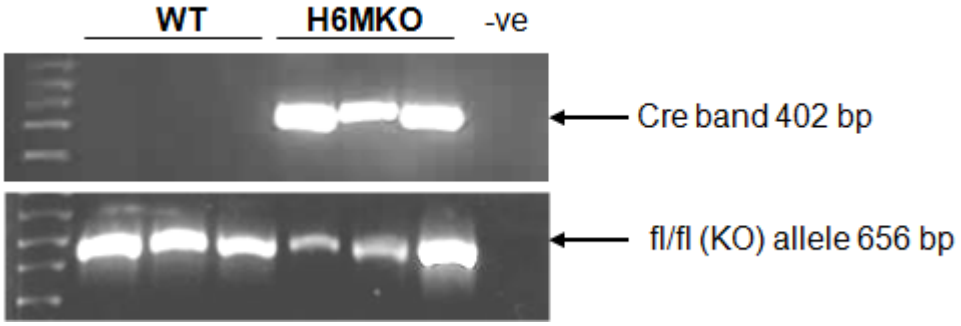

Figure 3-16 PCR detection of a Cre band and a KO allele using DNA isolated from an ear clip

Initial characterisation of H6MKO mice using genomic DNA isolated from a range of tissues showed that recombination of the conditional to the KO allele is skeletal muscle-specific (Figure 3-17). Skeletal muscle (quadriceps and TA) was the only tissue to show recombination for removal of exon 3, with other tissues (including liver and kidney) remaining normal for floxed exon 3 *H6PD* allele.

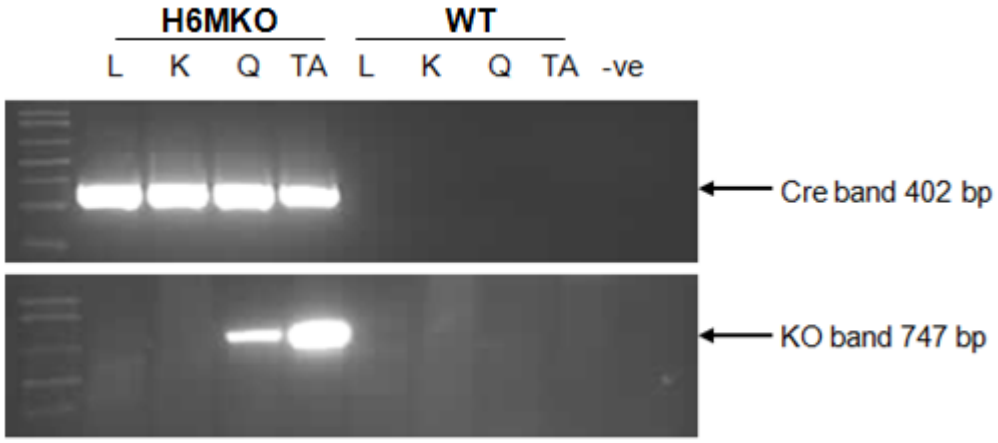

Figure 3-17 Successful DNA recombination skeletal muscle-specific

L-liver, K-kidney, Q-quadriceps, TA-tibialis anterior.

After successful DNA recombination specific to skeletal muscle, H6PDH mRNA expression was assessed in the quadriceps and TA muscles of 14 weeks old H6MKO and WT mice by real-time PCR and was shown to be approximately 27% and 22% in the H6MKO compared to WT mice respectively (Figure 3-18A). Additionally, H6PDH protein was not detected in muscle (quadriceps) of H6MKO mice (Figure 3-18B).

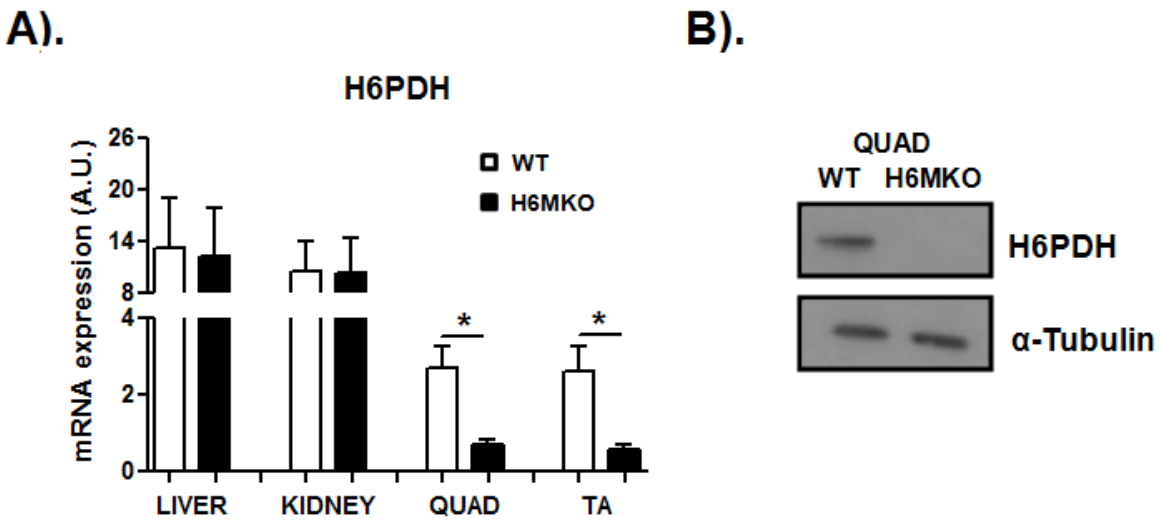

Figure 3-18 H6PDH mRNA and protein expression measured in tissue explants from H6MKO and WT mice

H6PDH mRNA expression in muscle (quadriceps and TA) showed significant reduction in H6MKO mice (A). All data are the mean A.U. values ±SEM (*<0.05; n=4/group). No H6PDH protein expression in muscle of H6MKO mice (B); α-tubulin was used as a loading control.

In addition, the expression of ER stress markers was measured in a number of muscle tissues from H6MKO and WT mice of 14 weeks of age. There was a significant induction in DDIT3 and HSPa5 expression in quadriceps and TA muscles from H6MKO mice whereas in soleus muscle, there was a significant increase of DDIT3 expression and no change in HSPa5 expression (Figure 3-19).

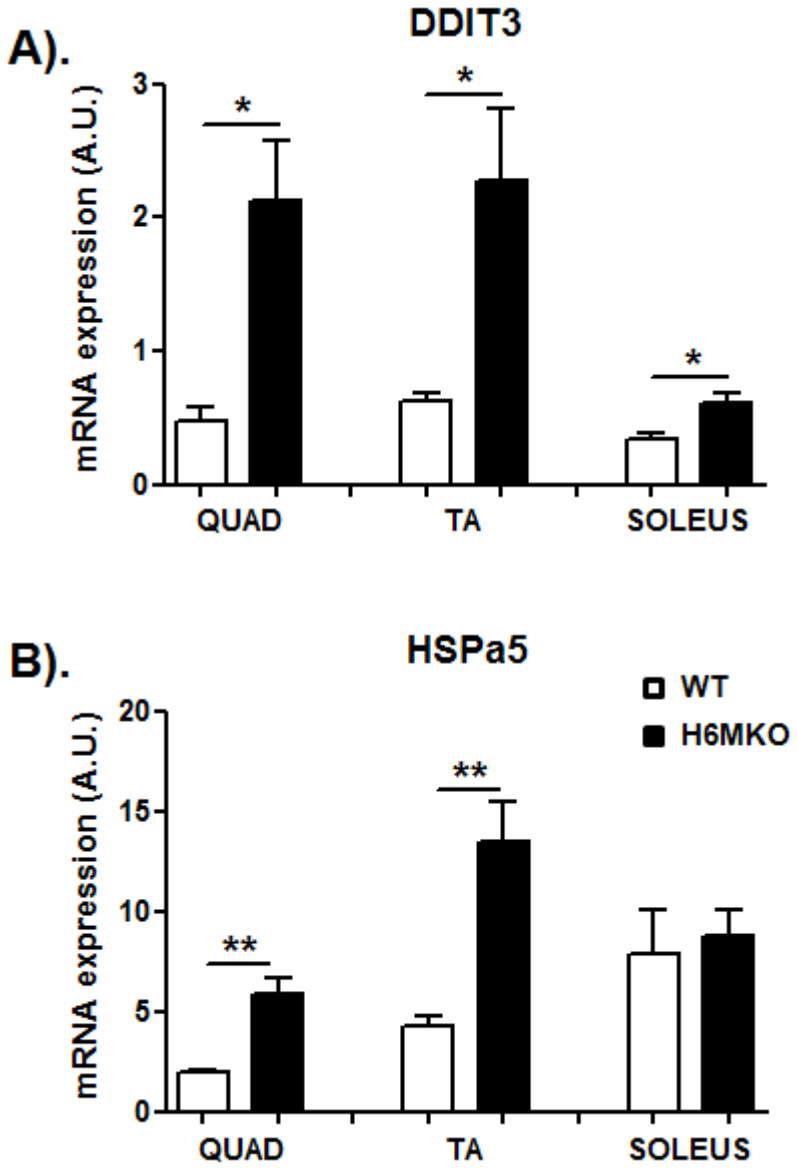

Figure 3-19 Increased expression of ER stress markers in H6MKO mice

Significant induction of DDIT3 mRNA expression in quadriceps, tibialis anterior (TA) and soleus muscle from H6MKO mice (A); elevated HSPa5 mRNA expression in quadriceps and TA whilst no change observed in soleus muscle from H6MKO mice (B). All data are the mean A.U. values ±SEM from n=4/group (*<0.05, **<0.01 vs WT).

3.3.5.3 Blood glucose

H6MKO and matching WT mice were exposed to 16 h fasting in order to determine blood glucose levels. H6MKO mice displayed slightly decreased glucose level as WT mice in the fasting state. This did not reach statistical significance (Figure 3-20).

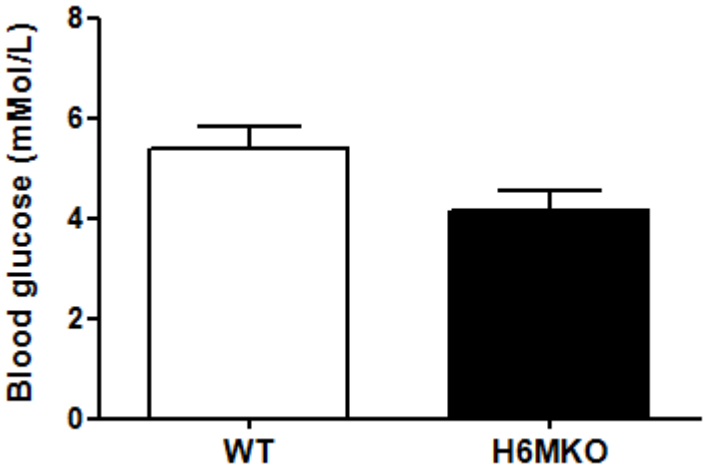

Figure 3-20 Lack of significant difference in fasting blood glucose in H6MKO compared to WT mice

Blood glucose concentration was determined after 16 h of food deprivation. All data are the mean values ±SEM from n=6/group (8-12 wk).

3.3.5.4 Urinary GC analysis

To assess systemic GC metabolism in H6MKO mice, we examined urinary GC metabolites derived from inactive 11-DHC or active corticosterone. Previously, we have demonstrated that H6PDHKO mice (both male and female) excreted the majority of their GC as metabolites of 11-DHC compared with WT (Figure 3-21B). Surprisingly, in urine from H6MKO mice, the proportion of 11-DHC metabolites was similar to WT (Figure 3-21A) suggesting that lack of H6PDH and subsequently NADPH cofactor for oxo-reductase activity of 11β-HSD1 enzyme in skeletal muscle was not sufficient enough to change the proportion of 11-DHC or corticosterone

metabolites. This supports that urinary ratio might be more driven by H6PDH-11β-HSD1 enzyme complex from other tissues.

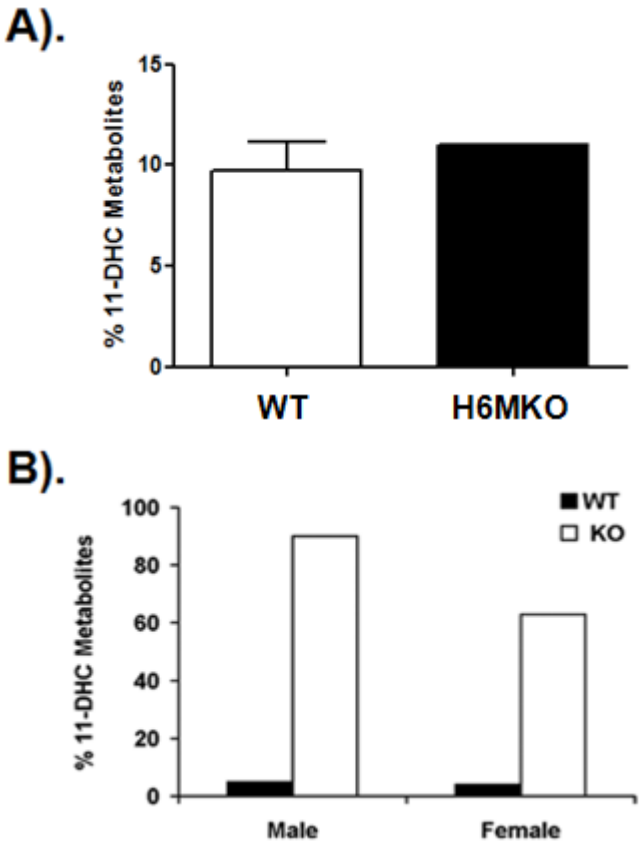

Figure 3-21 Analysis of urinary steroid metabolites

11-DHC metabolites as percent of corticosteroid metabolites in female H6MKO and WT mice. H6MKO mice excreted approximately 11% of corticosteroids as metabolites of 11-DHC whereas WT mice >9% (A). All data are the mean values ±SEM from n=4/group (8-12 wk). Both male and female H6PDHKO mice excreted >90% and >60% of corticosteroids as metabolites of 11-DHC respectively (B) (Lavery et al. 2007).

The H6MKO mouse model was generated and fully characterised using Acta1-Cre mouse line in order to evaluate the H6PDH role in muscle metabolism independently of other metabolic tissues. Despite the successful H6PDH knockout specific to the skeletal muscle, the preliminary fasting blood glucose and urine analysis measured in H6MKO mice were indistinguishable from WT mice highlighting the importance of the cross talk between adipose tissue and liver, but also could be due to an insufficient

number of mice tested. Consequently, further research was carried out utilising global H6KO mouse colony.

3.4 Discussion

The aim of this chapter was to assess the expression of the SR G6PT/H6PDH/11β-HSD1 axis in models of differentiating skeletal muscle cells. Additionally, a further enzyme G6Pase-β was also examined in term of its expression. Furthermore, I also established some basic regulation by insulin and GC, as major determinants of muscle energy homeostasis. These four enzymes are involved in G6P metabolism within the SR ultimately influencing the SR NADPH/$NADP^+$ ratio and GC metabolism.

I have shown that across C2C12 myocytes and primary myoblasts differentiation, there was a significant increase in differentiation markers (α-actin, myogenin) during the transition from proliferating to differentiating muscle cells. However, this was observed to a lesser degree in primary myoblasts. Myogenin is a muscle-specific basic helix-loop-helix (bHLH) transcription factor inducing myogenesis, and α-actin is involved in muscle contraction (Moran et al. 2002). I have also shown increased 11β-HSD1 and H6PDH mRNA expression across differentiation. Both these genes are involved in GC activation within the ER/SR lumen. Increased expression of 11β-HSD1 during differentiation process suggests intracellular GC role in the differentiation of skeletal myoblasts to mature myotubes (Biedasek et al. 2011). Thus it would appear that there was a coordinated up-regulation of 11β-HSD1 and H6PDH in response to differentiation signals, which were not present for G6PT and G6Pase-β. Therefore, these data might confirm the importance of these genes in skeletal muscle development.

Treatment of both C2C12 myoblasts and myotubes with DEX significantly enhanced the expression of 11β-HSD1 which generates active GCs. Expression of H6PDH was also significantly elevated in both myoblasts and myotubes. This indicates that DEX increases 11β-HSD1 enzyme expression suggesting that systemic GCs can enhance 11β-HSD1 expression in the skeletal muscle which may have consequences for ageing and inflammatory aspects. Furthermore, treatment of C2C12 with DEX and GC antagonist, Ru38486, showed decrease in the 11β-HSD1 and H6PDH expression in C2C12 myoblasts compared to the treatment with DEX only. In differentiated C2C12 myotubes, co-incubation with Ru38486 did not change 11β-HSD1 expression and partially, but not significantly, blocked DEX effects upon H6PDH expression. C2C12 treatments did not change G6PT and G6pase-β expression neither in myoblasts nor in myotubes. It shows that active GC level may not affect G6P transport into the ER/SR lumen by G6PT or its utilisation by G6Pase-β to produce glucose and inorganic phosphate in muscle. The Ru38486 inhibitor was not sufficient enough to completely reverse DEX effect. This is a GR antagonist to a lesser extent as it also shares progesterone receptor-blocking activity. Other methods involving inhibition of GR receptor could be carried out such as knocking down of GR in the cell culture or using another available GR antagonist (guggulsterone). However, similarly to Ru38486, guggulsterone is not GR-specific as it also inhibits mineralocorticoid, androgen and progesterone receptors.

These data confirm that both C2C12 and primary muscle cells are good models to study glucose and GC metabolism in skeletal muscle.

Secondly, to address further the important role of H6PDH in the regulation of 11β-HSD1 and muscle SR redox, we established H6MKO mice to compare with

global H6KO mice. Fasting glycaemia and urinary GC metabolite excretion were measured. The H6KO mice recapitulated myopathy and ER stress seen in previously generated H6PDHKO mice (Lavery et al. 2008b); therefore, I have proceeded with further breeding in order to generate H6MKO mouse model. Subsequently, the H6MKO model was generated and characterised. I have shown a successful DNA recombination, significant knockout of *H6PD* gene on mRNA and protein level as well as partial and residual H6PDH activity in hepatic and muscle microsomes respectively. In addition, there was also induction in mRNA expression of DDIT3 and HSPa5 suggesting the presence of ER stress which leads to myopathy development. Although fasting glucose analysis showed no significant differences between H6MKO and WT mice, a slight reduction in blood glucose levels in H6MKO mice was recorded. This lack of power could be due to not sufficient number of mice in the study. Importantly, a previous study demonstrated lowered fasting glucose levels in H6PDHKO mice as an indicator of relative hypoglycaemia ($P < 0.001$) (Lavery et al. 2007). H6MKO mice have the same level of 11-DHC metabolites in urine as WT mice. Although skeletal muscle is a major component of the human body, the expression of SR enzymes was not observed to the same level as in other metabolic tissue such as liver. Low expression of H6PDH was not sufficient to increase dehydrogenase activity intracellularly, and this might clarify why there was no induction of 11-DHC metabolites in H6MKO mice. While skeletal muscle phenotype was fully recapitulated, the global GC metabolism did not differ from WT and most likely could be determined by other tissues. Due to lack of time and resources, further experiments using H6MKO colony could not be continued. Beside basic phenotyping and measurement of fasting blood glucose levels and urinary

metabolites, it would be interesting to carry out glucose and insulin tolerance tests, muscle strength test and also apply high fat diet experiments to investigate muscle H6PDH role in obesity.

Further study was continued using global H6KO mouse model to analyse the underlying mechanisms of myopathy and insulin sensitivity development in the absence of H6PDH.

We propose that further investigation of the associated role of H6PDH-11β-HSD1 in the skeletal muscle may be valuable in understanding its function in homeostasis and its potential role and manipulation in metabolic disease such as T2DM and insulin resistance. Therefore, the aim of next chapter was to generate an 11β-HSD1 muscle-specific KO mouse mode.

Chapter 4- Evaluating the muscle-specific role of 11β-HSD1

4.1 Introduction

The occurrence of obesity, T2DM and insulin resistance has now reached epidemic proportions and still continues to rise. On average, obesity is associated with a decreased life expectancy of at least 9 years increasing obesity-related health problems such as insulin resistance, a major risk factor for T2DM and CVD that increase morbidity and mortality (Kopelman et al. 2007). However, despite the magnitude of the clinical problems, the precise molecular mechanisms that contribute to pathogenesis of obesity-related insulin resistance and its pathologies remain unknown.

Skeletal muscles play a key role in glucose utilisation accounting for 80-90% of peripheral glucose uptake, and they are also the major contributors to global insulin sensitivity. The effects of GC excess upon skeletal muscle are exemplified in patients with Cushing's syndrome who, in addition to the classic phenotype of central obesity and insulin resistance (leading to T2DM in some), also develop profound proximal myopathy affecting predominantly type II fibres (Khaleeli et al. 1983). Furthermore, intracellular GC generation is increased as it has been shown that expression and activity of 11β-HSD1 are elevated in skeletal muscle of diabetic individuals and pharmacological inhibition of 11β-HSD1 is insulin sensitising (Biedasek et al. 2011;Morgan et al. 2009). To date, the precise mechanisms underpinning this observation have not been identified.

GCs have potent effects upon carbohydrate and lipid metabolism. Previous studies have mainly focussed on their role in hepatic carbohydrate metabolism where they drive gluconeogenesis. In adipose tissue, GC effects are complicated; the lipolytic action of GC is well described (Slavin et al. 1994), but they can also redistribute into

visceral site as seen in Cushing's syndrome. So far, the action of GCs upon carbohydrate and lipid metabolism in skeletal muscle has not been explored in detail. Skeletal muscle could play as important role as the liver and adipose tissue when considering the metabolic development of insulin resistance, and therefore the mechanisms by which GC metabolism can influence muscle phenotype requires a full investigation.

Observations in patients with Cushing's syndrome provide an insight into the pathogenic action of excess endogenous GCs in humans. However, in the vast majority of cases of simple obesity and insulin resistance, circulating GC levels are not elevated (Fraser et al. 1999). In key metabolic target tissues such as liver, adipose and muscle, local GC availability is controlled by a series of enzymes that either regenerate or inactivate cortisol. Intracellular glucocorticoid metabolism is mediated by 11β-HSD1, which activates cortisol from hormonally inactive cortisone in humans and 11-DHC to corticosterone in rodents. The 11β-HSD1 active site is within the ER/SR lumen where it is dependent upon the cofactor provider, the enzyme H6PDH, to maintain a high $NADPH/NADP^+$ ratio required to support its oxo-reductase activity (Figure 4-1) (Lavery et al. 2008a).

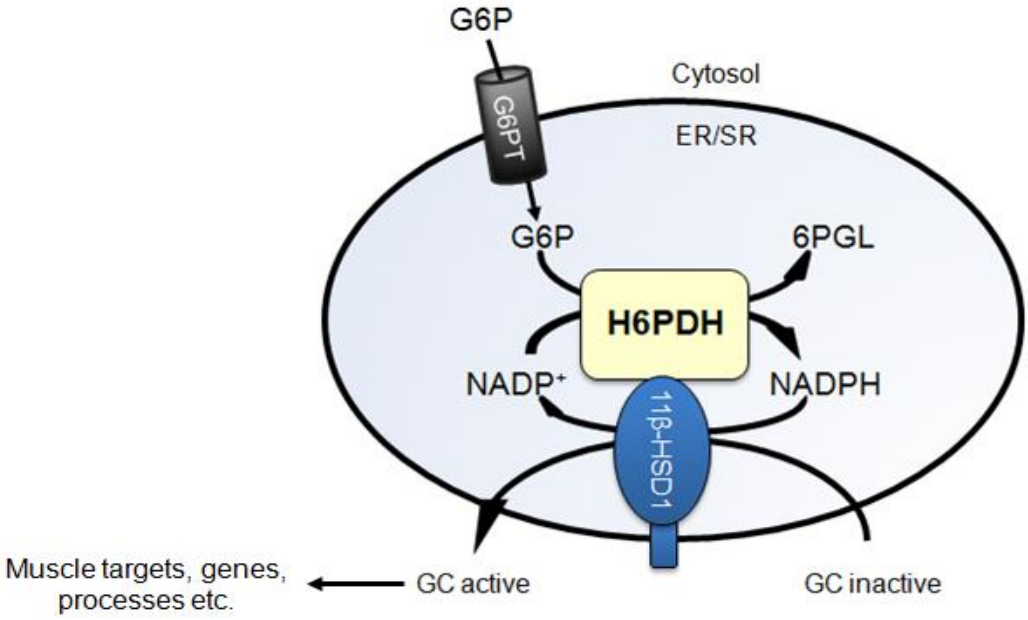

Figure 4-1 Schematic representation of the G6PT/H6PDH/11β-HSD1 pathway in the ER/SR

Interestingly, a recent study of healthy old and young people has found a significant association between increased muscle 11β-HSD1 expression and lower quadriceps strength. Elevated cortisol generation within muscle by 11β-HSD1 might contribute to loss of muscle strength with age, a key component of sarcopenia. Therefore, inhibition of 11β-HSD1 could be beneficial in preventing or delaying sarcopenia in order to increase healthspan (Kilgour et al. 2013).

Experiments in transgenic mouse models have helped with better understanding of 11β-HSD1 function *in vivo* in a number of metabolically important tissues such as liver (Lavery et al. 2012) and adipose (Bujalska et al. 2007). Over-expression of 11β-HSD1 in adipose causes all features of metabolic syndrome including obesity whereas over-expression in liver leads to insulin resistance without obesity (Paterson et al. 2004). Importantly, circulating corticosterone levels were not

increased in either models suggesting elevated intracellular GC availability underpins the observed phenotypes. Conversely, mice lacking 11β-HSD1 globally have lower tissue GC levels and display a cardio-protective phenotype on high fat diet (Masuzaki et al. 2001;Morton et al. 2001).

The rodent model of Cushing syndrome and exogenous GC excess has been recently generated (Morgan et al. 2014). WT mice administrated with corticosterone (Cort) in drinking water displayed decreased grip strength paralleled to reduced mass of type IIb fibre-rich muscles but not the type I fibre-rich soleus muscles. In addition, Cort-treated mice had increased mRNA expression of several key atrophy markers including MuRF1 and atrogin1 as well as FoxO1, a transcription factor that regulates muscle mass. Interestingly, 11β-HSD1 global knockout mice were protected from skeletal muscle myopathy induced by Cort administration (Morgan et al. 2014).

The functional importance of 11β-HSD1 was further shown using the selective 11β-HSD1 inhibitor, A1, which was able to abolish the actions of 11-DHC in rodents and cortisone in humans promoting serine-307 phosphorylation of IRS1 and threonine-308 phosphorylation of Akt/PKB (Morgan et al. 2009). Phosphorylation of IRS1 negatively regulates its function by decreasing its affinity for the insulin receptor and increasing proteasomal degradation. These data show the importance of 11β-HSD1 as a critical regulator of skeletal muscle insulin sensitivity and provide a new tool to investigate the role of GCs and 11β-HSD1 selective inhibitors in insulin resistance. Moreover, gene expression analysis using an *in vivo* rodent model has suggested that this may be mediated by alterations in lipid metabolism such as decreased lipogenesis, lipolysis and FFA availability (Morgan et al. 2009).

Deletion of 11β-HSD1 specifically in the liver in 11β-HSD1 LKO mice has shown subtle stimulation of the HPA axis increasing systemic GC production whereas their metabolic parameters are relatively minor. The LKO mouse model suggests the importance of other GC target tissues in determining global metabolic phenotype (Lavery et al. 2012). To investigate the role of 11β-HSD1 and GC availability in skeletal muscle, we have generated 11β-HSD1 muscle-specific knockout mice (HSD1MKO). We hypothesise that 11β-HSD1 inhibition within skeletal muscle plays as important role in the insulin sensitisation process as liver and adipose.

On the basis of previous findings, we assume that inhibition of 11β-HSD1 in rodent skeletal muscle and abolishment of pre-receptor GC regeneration within the myocyte, will enhance insulin sensitivity, glucose utilisation and decrease intramuscular triglyceride accumulation and mobilisation ameliorating obesity and diabetes upon high fat feeding. We also hypothesise that muscle 11β-HSD1 contribute significantly to systemic GC levels and can impact upon metabolic GC biomarkers.

In order to assess the skeletal muscle-specific contribution to the metabolic phenotype seen in 11β-HSD1 global knockout (HSD1GKO) mice, I have generated HSD1MKO mouse model using Cre-LoxP technology.

4.2 Methods

4.2.1 Primary skeletal muscle cells

Primary cultures derived from skeletal muscle consisting mainly of myoblasts and myofibroblasts were isolated from mouse EDL muscle. Primary cells were maintained in 12-well TC plates in 1mL of DMEM supplemented with 10% horse serum and 0.5% chick embryo extract. Most of the myofibroblasts attached to the plate

surface during initial incubation period (2 hours). They were cultured until they reached 80% confluence to be subsequently used for 11β-HSD1 activity assessment. Myoblasts were transferred to a new 12-well plate and when they reached 60-70% confluence, differentiation was initiated by replacing proliferating medium with DMEM supplemented with 2% horse serum and 0.5% chick embryo extract. Differentiation medium was replaced every 48 h. After 8 days of differentiation, myoblasts fused to form multinucleated myotubes.

4.2.2 RNA extraction

Total RNA was extracted from 20 mg of tissue using Tri-reagent system. RNA concentration was determined spectrophotometrically at OD_{260} and integrity assessed by agarose gel electrophoresis. 1µg of RNA was used for reverse transcription (see Section 2.4).

4.2.3 Real-time PCR

11β-HSD1 (Mm00476182_m1) mRNA level was determined using the ABI 7500 sequence detection system (Life Technologies, Warrington, UK). Primers and probes for all genes were supplied by Life Technologies. Reactions were performed in singleplex in triplicates as described in Section 2.6 and normalised against the 18S rRNA housekeeping gene.

4.2.4 11β-HSD1 activity assay

Tissue explants (~20 mg), 100 µg of muscle microsomes, confluent primary myofibroblasts or differentiated myotubes were incubated with 100 nM 11-DHC

supplemented with a tritiated tracer. Steroid incubation was carried out for 4 h for muscle tissue explants, microsomes and primary cells whilst 30 mins for liver. Subsequently, steroids were extracted using dichloromethane, separated using a mobile phase consisting of chloroform/absolute ethanol (92:8) by thin layer chromatography, and scanned using a Bioscan 200 imaging scanner (LabLogic, Sheffield, UK). 11β-HSD1 activity was expressed as pmol of corticosterone generated per g of tissue per hour of incubation or as a % conversion.

4.2.5 Microsomes preparation

Liver and skeletal muscle microsomes were prepared from 4- to 8-weeks old mice by differential centrifugation techniques as described in Section 2.9. The microsomal pellet was re-suspended in MOPs buffer and then immediately frozen in liquid nitrogen and stored at -80ºC (up to 6 months) prior to assessment of protein concentration.

4.2.6 Rodent protocol

All animal experiments and procedures were carried out in accordance with the British Home Office Guidance (Animals Scientific Procedures) Act 1986 (Project Licence, PPL 30/2764). Mice were housed in standard pathogen-free conditions on a 12 h light/12 h dark cycle with access to standard rodent chow (when not fasting) and water *ad libitum.*

On the day of experiment, mice were sacrificed by cervical dislocation, then liver, skeletal muscle (quadriceps, TA, soleus), heart, kidney and lung were removed and snap-frozen in liquid nitrogen for characterisation of DNA recombination and mRNA

expression. To measure 11β-HSD1 activity, tissue was freshly harvested in the serum-free DMEM and used directly for the assay.

4.2.7 Generation of 11β-HSD1 muscle-specific knockout (HSD1MKO)

The Cre/LoxP technology can be used to delete loxP-flanked chromosomal DNA sequences in selected tissue of transgenic animals (Rao and Monks 2009). To generate HSD1MKO mouse model, I have used three different muscle-specific Cre lines.

Firstly, we have purchased a transgenic mouse expressing Cre recombinase under the control of a skeletal muscle-specific promoter from the *mef2c* gene. The Cre expression in this transgenic line is exclusively restricted to all skeletal muscle from early in development. Secondly, as an alternate method, the Acta1-Cre transgenic was purchased from the Jackson Laboratory (Maine, US). The Acta1-Cre transgenic mice have Cre recombinase gene driven by the *Acta1* promoter that encodes α-skeletal muscle actin expressed as the major component of the thin filament in skeletal muscle (Saito et al. 2011a). This Cre activity is restricted to skeletal muscle tissue and heart. These mice have been used to breed with the conditional 11β-HSD1 all on the C57BL/6 background to generate the HSD1MKO mice. Thirdly, I have also tested muscle creatine kinase Cre (MCK-Cre) transgenic mouse line that have Cre recombinase gene driven by the *MCK* promoter.

4.2.7.1 Genotyping

The following primers were used for genotyping of HSD1MKO mice to confirm the presence of the Cre transgene:

Primers	Sequence	Product size
CreF	GTAGTTATTCGGATCATCAGCTACAC	402
CreR	GCTGCCACGACCAAGTGACAGCAATG	

PCR detection of the *HSD11B1* KO alleles was carried out using P1+P2 primers which give a 138 bp product for a WT allele and a 172 bp product for a conditional allele containing a 3′ LoxP site (Lox+/+). After a P2 binding site is removed and P1+P3 are brought into proximity producing a 279 bp KO band confirming successful Cre recombination and exon 5 removal. The occurrence of two bands represents het (both KO and WT bands are present). The following primers were used:

Primers	Sequence	Product size
P1	GGGAGCTTGCTTACAGCATC	P1+P2: 138 (WT)
P2	CATTCTCAAGGTAGATTGAACTCTG	P1+P2: 172 (Conditional)
P3	TCCATGCAATCAACTTCTCG	P1+P3: 279 (KO)

PCR reactions were carried out as in Section 2.5, and 2.2 % agarose gel was run to confirm the size of the product.

4.3 Results

4.3.1 HSD1MKO validation

To characterise the HSD1MKO mice model, DNA, RNA and 11β-HSD1 enzyme activity work were assessed.

In the first strategy, the Cre cDNA was cloned under the control of the *mef2c* skeletal muscle promoter to design *mef2c*-73k-Cre construct (Heidt and Black 2005); however, DNA extraction from tissue explants did not show successful recombination of this gene in skeletal muscle tissue. I have repeated these experiments three times (including mRNA screening and 11β-HSD1 activity assays), and after getting the same results, the colony was closed down (data not shown). As the Mef2c-Cre in these experiments appeared to be no functional, a second strategy was carried out; we purchased Acta1-Cre transgenic mice expressing Cre recombinase under the control of *Acta1* (alpha actin) promoter (Figure 4-2A) (Saito et al. 2011b) from the Jackson Laboratory. I assessed recombination between the LoxP sites using genomic DNA isolated from an ear clip (Figure 4-2B) as previously shown in liver (Figure 4-2C) in our group (Lavery et al. 2012).

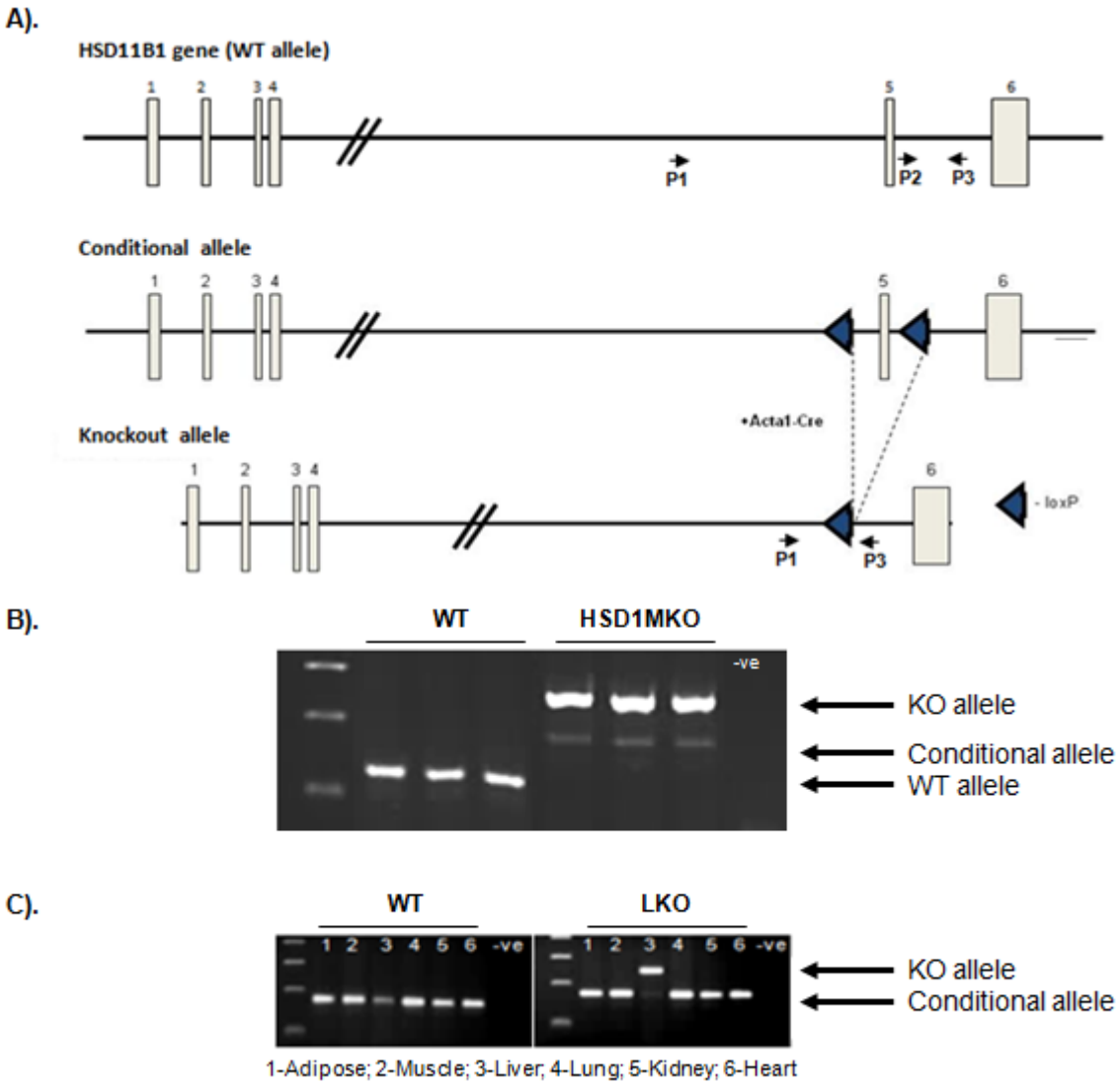

Figure 4-2 Targeting strategy and HSD1MKO validation

Targeting strategy for HSD1MKO generation. The exon 5 of a conditional allele was flanked with LoxP sites and bred with the muscle-specific Acta1-Cre mice to design knockout allele (A). PCR detection of a knockout allele validating the HSD1MKO model. PCR products derived from HSD1 primer sets on DNA isolated from an ear clip (B) (n=3/group). Successful knockout of 11β-HSD1 in liver (C) (Lavery et al. 2012).

Initial characterisation of HSD1MKO mouse line has shown that recombination of a conditional to a KO allele is skeletal muscle-specific. Skeletal muscle (quadriceps, soleus and TA) was the only tissue to show recombination for removal of exon 5 whilst other tissues (including liver, lung, kidney and also heart although it expresses *Acta1* gene) remained normal for floxed exon 5 *HSD11B1* alleles (Figure 4-3).

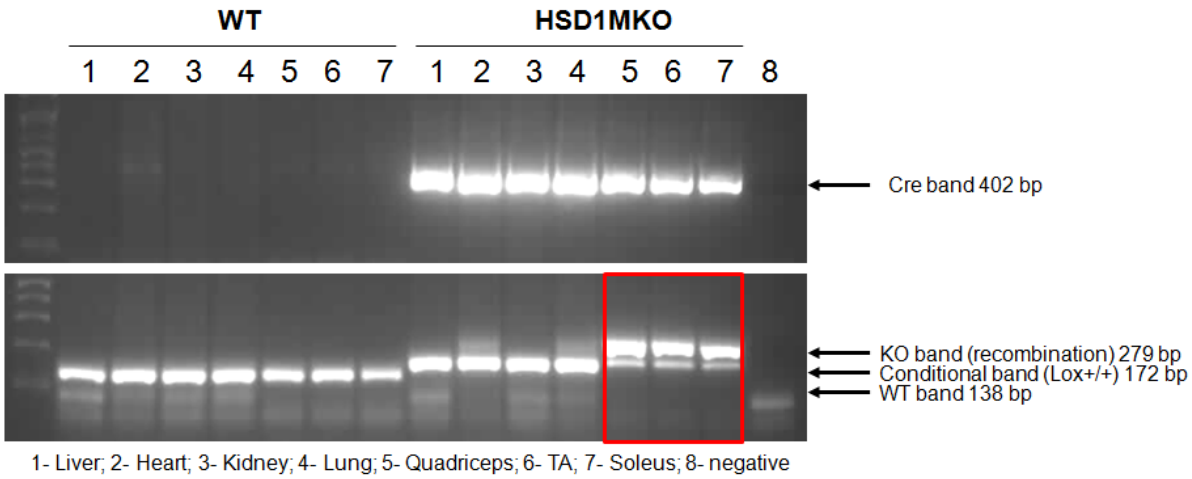

Figure 4-3 Genomic DNA recombination is specific to the skeletal muscle (quadriceps, TA, soleus)

Abbreviations: TA (tibialis anterior).

Following successful DNA recombination specific to skeletal muscle, 11β-HSD1 mRNA expression was assessed in the quadriceps muscle by real-time PCR. Unexpectedly, there was no significant difference between HSD1MKO and WT mice on mRNA level (Figure 4-4).

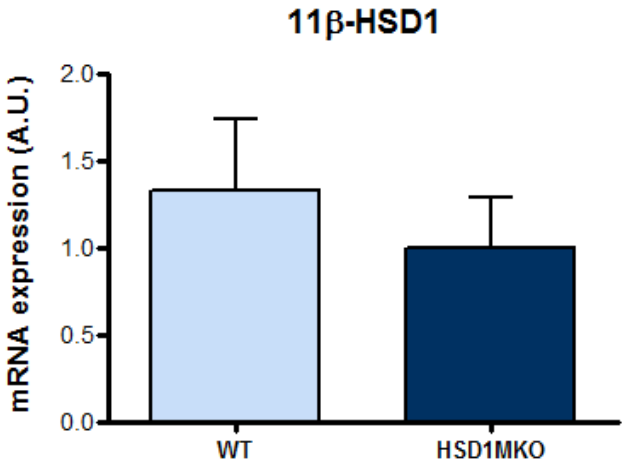

Figure 4-4 11β-HSD1 mRNA expression measured in quadriceps explants

There was no significant reduction of 11β-HSD1 expression in muscle from HSD1MKO mice. All data are the mean A.U. values ±SEM from n=7-8/group.

Additionally, validation of the HSD1MKO model at the mRNA level was also carried out in a number of tissues (liver, heart, lung, kidney, quadriceps, soleus and TA), and 11β-HSD1 expression was compared to the same tissue collected from WT mice (Figure 4-5). However, there was no significant reduction in 11β-HSD1 mRNA expression in quadriceps, TA and soleus muscle tissues.

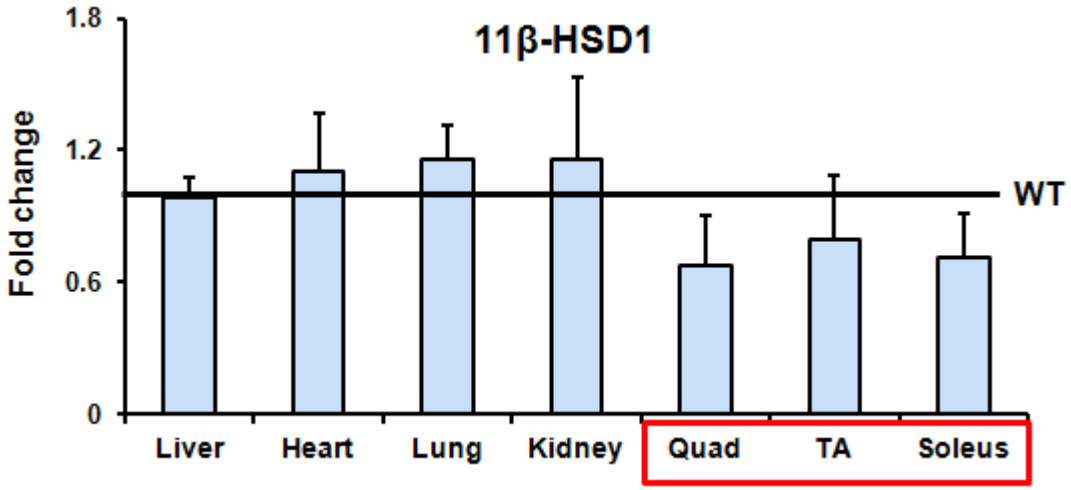

Figure 4-5 11β-HSD1 mRNA expression measured in tissue explants from HSD1MKO and WT mice

11β-HSD1 expression in the muscle tissues showed no significant difference between HSD1MKO and WT mice. All data are the mean fold change values ±SEM from n=7-8/group for quadriceps (quad), n=4/group for other tissues. Abbreviations: TA (tibialis anterior).

To further characterise the HSD1MKO model, the 11β-HSD1 oxo-reductase activity was measured in quadriceps explants from HSD1MKO and WT mice (Figure 4-6). Again, there was no significant difference between HSD1MKO and WT muscle explants in the ability to reduce 11-DHC to corticosterone. This confirmed the mRNA data, but did not corroborate with the level of recombination seen at the DNA level.

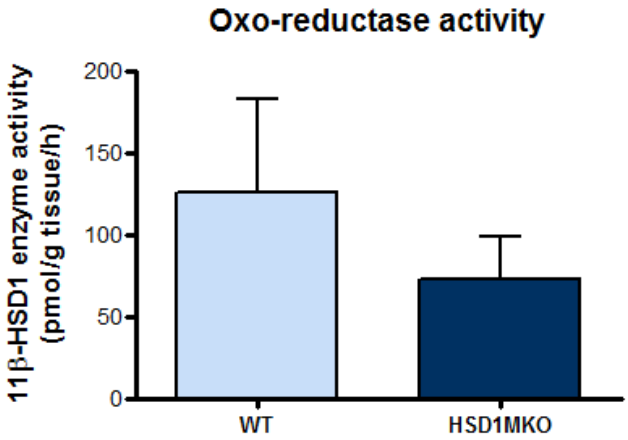

Figure 4-6 The 11β-HSD1 enzyme activity in quadriceps muscle explants

Representative activity traces. All data are the mean values ±SEM from n=3/group in triplicate.

To further validate our model, the oxo-reductase activity of 11β-HSD1 in the SR was measured in microsomes prepared from skeletal muscles. The activity was measured in intact microsomes pre-incubated with or without 10 mM G6P and 10 mM NADPH for 30 mins. Previously, we have shown that in the presence of the substrate, conversion of 11-DHC to corticosterone was elevated in WT mice (Lavery et al. 2006). As expected, the activity seen in HSD1MKO and WT microsomes pre-incubated with G6P and NADPH was increased; however, disappointly, there was no significant difference in activity between HSD1MKO and WT mice (Figure 4-7).

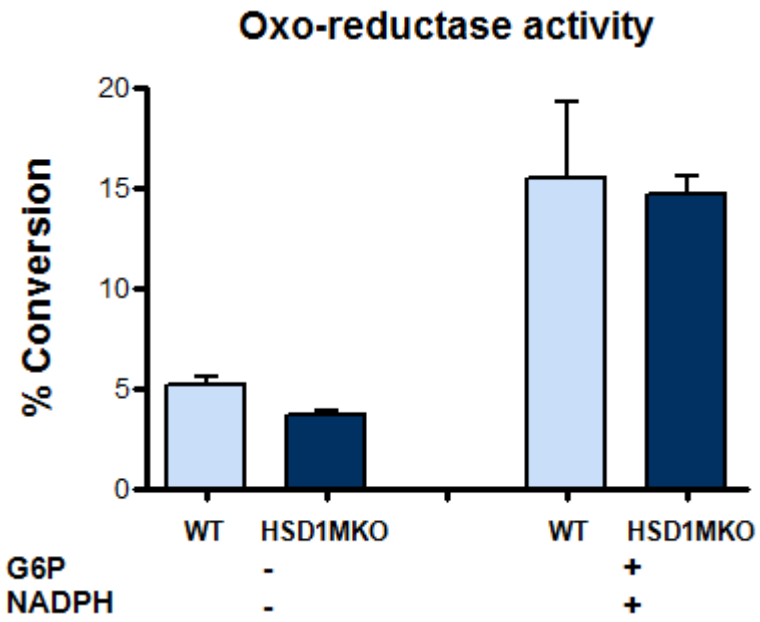

Figure 4-7 Measurement of 11β-HSD1 oxo-reductase activity in muscle microsomes derived from HSD1MKO and WT mice

Below each graph is indicated whether microsomes were intact or pre-incubated with G6P and NADPH. All data are the mean values ±SEM from n=3/group in triplicate.

In addition, 11β-HSD1 activity was also measured in myotubes and myofibroblasts using murine primary skeletal muscle cells. Again, there was no significant difference between HSD1MKO and WT cells in the ability to reduce 11-DHC to corticosterone (Figure 4-8). Despite successful recombination at the DNA level, this supports the mRNA data and activity measured in both muscle explants and muscle microsomes.

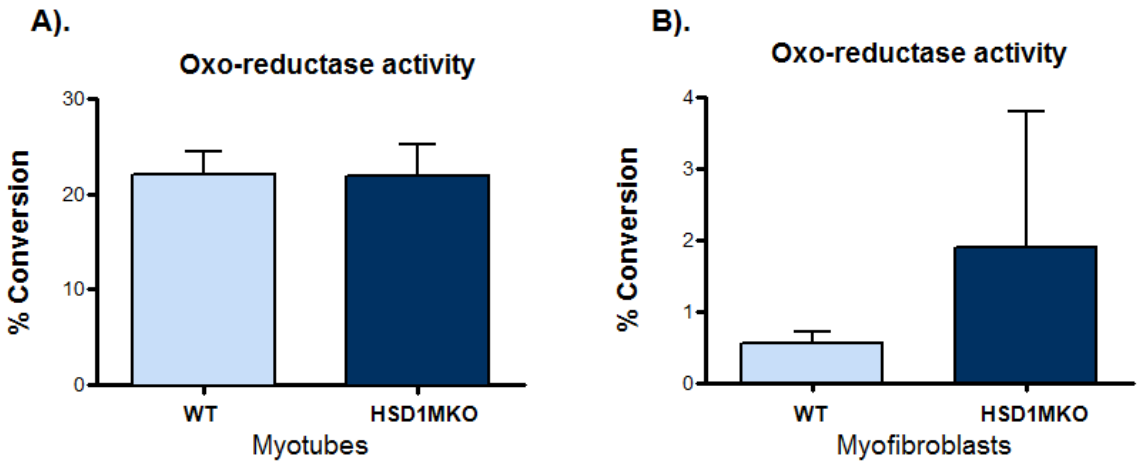

Figure 4-8 Measurement of 11β-HSD1 oxo-reductase activity

11-DHC reduction in primary myotubes (A) and in primary myofibroblasts (B) derived from HSD1MKO and WT male mice. All data are the mean values ±SEM from n=3/group in triplicate.

The HSD1MKO mouse model was generated using Acta1-Cre mouse line and characterised in order to study GC-dependent mechanism affecting muscle metabolism. However, the line was closed down due to only partial and no significant loss of 11β-HSD1 expression. As third strategy, I have tested a muscle-specific MCK-Cre line, expressing Cre recombinase in skeletal muscle under the control of the muscle creatine kinase promoter (MCK-Cre mice). Again, a successful recombination on DNA levels was achieved whilst 11β-HSD1 mRNA expression and 11β-HSD1 oxo-reductase activity remained unchanged when compared to WT mice (data not shown).

4.4 Discussion

Previous studies using transgenic animal models have highlighted the critical role of 11β-HSD1 in the regulation of metabolic phenotype in different tissues. Overexpression of 11β-HSD1 in liver leads to insulin resistance and hypertension

(Paterson et al. 2004) whereas overexpression in adipose tissue results in visceral obesity, insulin resistance, hypertension and dyslipidemia (Masuzaki et al. 2001). Interestingly, circulating corticosterone levels were not elevated in both models suggesting that increased intracellular GC availability underpins the observed phenotypes. Consequently, this has led to the development of selective 11β-HSD1 inhibitors as a potential novel therapy for patients with diabetes, obesity, and hypertension (Rosenstock et al. 2010).

The HSD1GKO mice are protected from the adverse metabolic consequences of exogenous GC administration including skeletal myopathy (Morgan et al. 2014). As muscle is a prime determinant of insulin sensitivity playing a major role in glucose and lipid homeostasis, we believe that inhibiting 11β-HSD1 in muscle would be of great importance. Thus, selective 11β-HSD1 inhibitors are a promising therapy to limit the side effects associated with GC excess. To further examine 11β-HSD1 and GC availability in skeletal muscle, a muscle-specific knockout of 11β-HSD1 was generated by expressing Cre recombinase under the control of three different skeletal muscle-specific promoters from the *mef2c*, *Acta1* and *MCK* genes. According to actual knowledge, the Cre expression in these transgenic lines should be completely restricted to skeletal muscle and heart from early stage in development and should be present in all types of skeletal muscles including fast and slow fibers (Agrawal et al. 2012;Bruning et al. 1998;Heidt and Black 2005). However, mRNA expression (sequences of primers and probes covered deleted exon 5) and 11β-HSD1 activity ($p=0.4385$) were still present in skeletal muscle tissues of the knockouts despite high level recombination at DNA level (see Figure 4-3). This was in contrast to previously demonstrated efficiency with our successful knockout of

11β-HSD1 restricted only to liver (Lavery et al. 2012). As muscles are highly heterogeneous tissues, we hypothesised that there could be additional non-myocyte cell types highly expressing 11β-HSD1 present within skeletal muscle tissue such myofibroblasts, satellite cells and stromal cells (Figure 4-9).

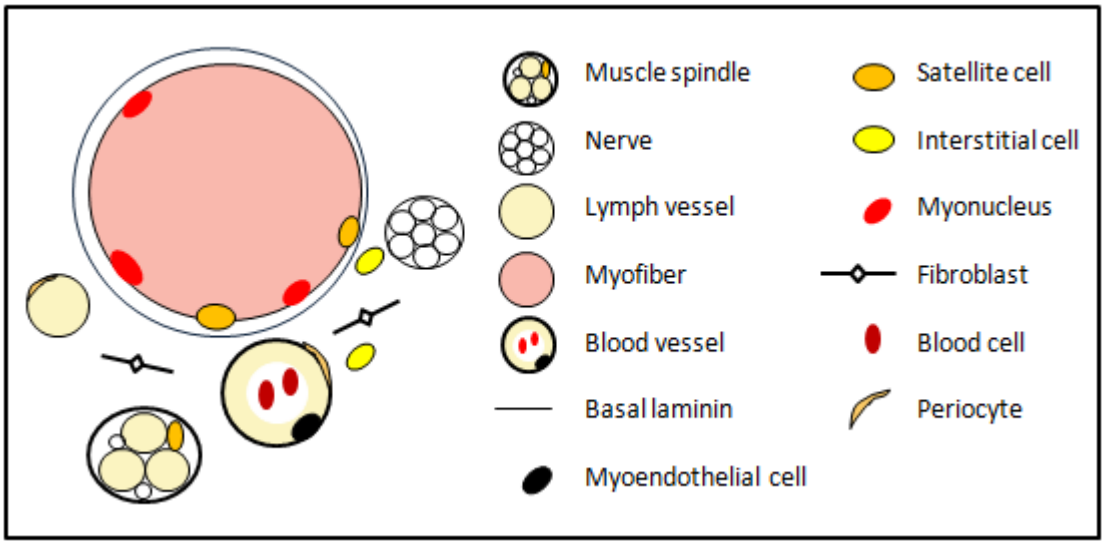

Figure 4-9 The constituent cell types of skeletal muscle

To validate the genotype, myotubes and myofibroblasts were isolated from the EDL muscle and 11β-HSD1 activity was measured. Despite correct validation on genetic level, there was still oxo-reductase activity in HSD1MKO myotubes to similar level seen in WT. Initial characterisation of HSD1MKO mouse model demonstrated that skeletal muscle was the only tissue to show recombination for removal of exon 5; however, the high levels of 11β-HSD1 expression in different muscle types and 11β-HSD1 activity still remained in the muscle explants, muscle microsomes and primary myotubes/myofibroblasts. Disappointingly, despite using three different Cre mouse lines, we were unable to generate a successful mouse model with 11β-HSD1 activity depleted only in skeletal muscle. This could be due to the nature of muscle

tissue precluding it complete depletion; however we believe, there is still potential of applying 11β-HSD1 inhibitors to protect from myoatrophy caused by GC administration and excess.

Regardless of successful DNA recombination to similar level seen in LKO mouse model, high expression of mRNA (muscle explants) and activity (muscle explants, muscle microsomes and primary myotubes) was still detected. Cre mediated recombination is never 100% and being a syncytialised cell type, it could be that high NADPH cofactor and remaining functional *HSD11B1* gene in some nuclei of muscle fibres were sufficient enough to reduce 11-DHC almost to the same level seen in WT mice across the cell. If successful, this would have been an excellent model to determine a number of important points regarding 11β-HSD1, examining its function in the regulation of muscle glucocorticoid production and muscle energy metabolism in health and disease.

We propose that GC metabolism in skeletal muscle is controlled by 11β-HSD1 to lesser degree than in other tissues. Urine analysis from our H6MKO mouse model confirms that pre-receptor GC metabolism in muscle is not sufficient to increase extracellular circulating GC level as previously seen in H6PDHKO, HSD1GKO and DKO mice (Semjonous et al. 2011). This has been probably caused by the contribution of all organs as systemic GCs were also not changed in LKO mice (Lavery et al. 2012).

Chapter 5- Novel stress response in *H6PD* depleted skeletal muscle

5.1 Introduction

H6PDH plays an important role in maintaining NADPH levels and redox environment within the SR regulating skeletal muscle SR NADPH/$NADP^+$ ratio and local GC generation (Lavery et al. 2006;Lavery et al. 2008b). In an effort to outline further the roles that H6PDH and 11β-HSD1 play in metabolism and muscle function, a H6PDH/11β-HSD1 DKO mouse has been developed in which the dehydrogenase activity of 11β-HSD1 seen in the H6PDHKO mouse was negated. Effectively, the DKO model has returned GC metabolism, GC sensitivity and the HPA axis set point to levels seen in the 11β-HSD1KO mouse. Critically, in contrast to the 11β-HSD1KO mice, DKO mice have phenocopied the salient features of H6PDHKO mice displaying type IIb fibre myopathy associated with reduced skeletal muscle mass and poor force generation contributing to decreased locomotor activity. The H6PDHKO mice have also displayed insulin sensitisation, increased muscle glycogen deposition and maintained fasting hypoglycaemia (Figure 5-1) (Lavery et al. 2008b; Semjonous et al. 2011). These findings are consistent with an 11β-HSD1 and GC independent function of H6PDH in which SR G6P metabolism and $NADP^+$/NADPH redox status are important for maintaining muscle homeostasis.

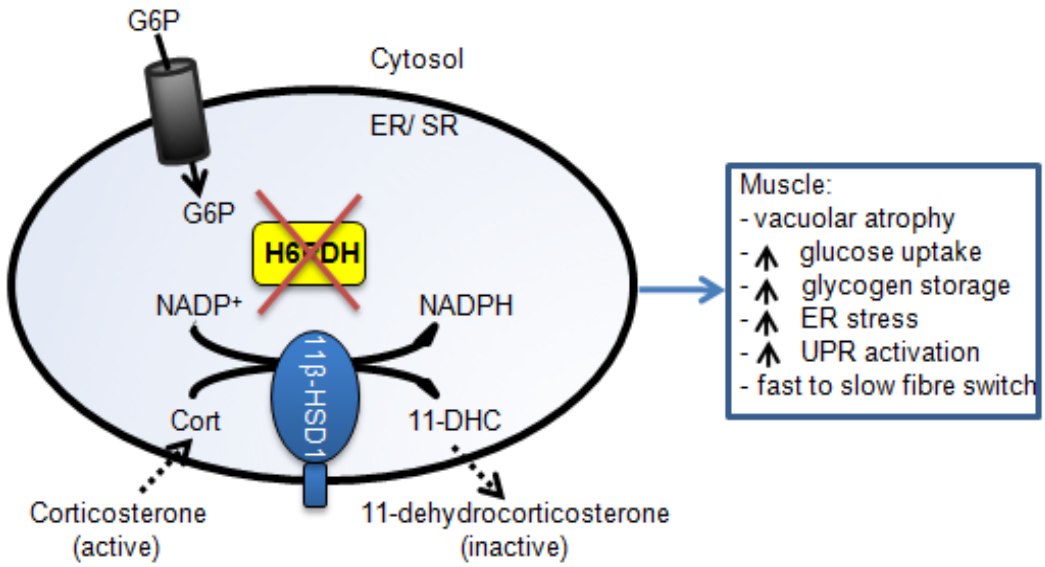

Figure 5-1 Model of H6PDH deficiency and skeletal muscle myopathy

The H6PDHKO mice display a number of metabolic changes including skeletal muscle myopathy, increased glucose uptake, ER stress and subsequently elevated UPR activation.

In addition, H6PDH deletion disrupts the ER redox balance and eventually, in H6PDHKO mice, ER stress responses and the UPR pathway are triggered and regulated by the expression of numerous genes involved in maintaining ER homeostasis (Figure 5-2) (Lavery et al. 2008b;Walter and Ron 2011).

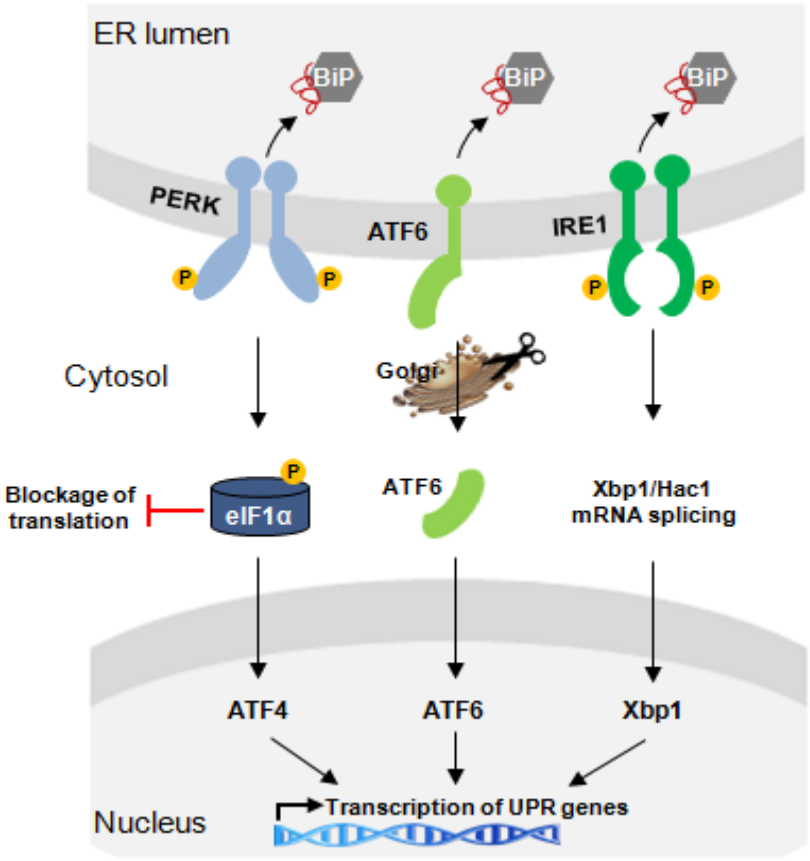

Figure 5-2 A model for the activation of the UPR in the H6PDHKO mice

The loss of H6PDH and consequently change in NADPH/$NADP^+$ ratio affects the redox balance of the ER resulting in unfolded protein accumulation and activation of the PERK, ATF6 and IRE1 pathways. They slow general protein translation and increase the expression of specific chaperones, degradative proteins and enzymatic pathways that expands SR volume. Abbreviations: BiP (binding immunoglobulin protein), PERK (PKR-like ER protein kinase), ATF6 (activating transcription factor -6), IRE1 (inositol requiring enzyme 1), eIF1α (eukaryotic initiation factors 1α), XBP1 (X-box-binding protein 1).

In H6PDHKO mice, there is a complex interplay of GCs, insulin sensitivity and ER stress, as explained earlier. The majority of metabolic and structural changes appear to be age-related and secondary to an initial early life triggers when the ER stress/UPR pathways are initiated. A number of integrated factors might be involved including change in GC metabolism, increase of SR redox sensitivity or metabolic changes affecting intermediary metabolism. H6PDH contributes to the NADPH

content and SR redox environment (Rogoff et al. 2010). Microsomes from H6PDHKO SR are more oxidised than WT SR microsomes, as shown by an increased $NADP^+$/NADPH ratio (Zielinska et al. 2011).

Previously, bioinformatic analysis of microarray data, using the Affymetrix human mouse genome 430 2.0 oligonucleotide array set and complied with the Minimum Information about a Microarray Experiment standard, generated from the TA and soleus muscles of 4 weeks old H6PDHKO mice identified a large set of differentially expressed genes (>300) that group into a number of pathways such as structural components, polyamine biosynthesis, purine salvage, intermediary metabolism and most prominently ER/SR stress and the UPR. The ER/SR stress and UPR activation affect the normal protein-folding environment of the ER/SR and consequently their transit through the ER/SR. This is an important determinant of myopathy progression in H6PDHKO mice (Lavery et al. 2008b). Because myopathy does not develop from birth, it is important to identify the preceding triggers initiating ER stress that might be informative to protein response. An analysis of changes in the expression of the top ranked de-regulated genes indicated that a number of metabolic pathways precede changes in the UPR pathway by 1 to 2 days post weaning. This analysis was based on just the top 2 de-regulated metabolic and UPR genes (Figure 5-3).

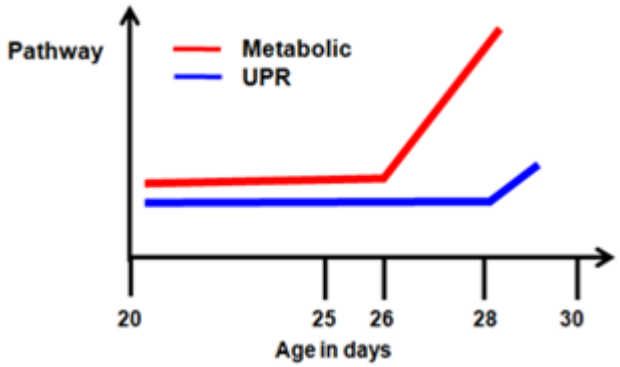

Figure 5-3 Bioinformatics analysis of microarray data in the H6PDHKO mice (unpublished data)

I wish to extend this analysis and by qPCR screening additionally assess an extended panel of the most up- or down-regulated genes, not involved in the ER or UPR stress response. The aim of this chapter is to generate genes expression profile in order to determine early changes in transcription which might be potential indicators of perturbations leading to the development of myopathy and SR stress in *H6PD* depleted muscle.

5.2 Methods

5.2.1 C2C12 cell culture

Proliferating C2C12 myoblasts were cultured in DMEM supplemented with 10% FCS and seeded into 12-well TC plates. Differentiation was initiated when cells reached 60-70% confluence by replacing GM with DMEM medium supplemented with 5% horse serum and was carried on for 8 days.

5.2.2 Cell treatments

C2C12 treatment was commenced upon differentiation day 4 when cells fused to form myotubes. Cells were grown for 24 h in glucose-free GM and also in the presence of different glucose concentrations such as 25 mM, 12.5 mM and 4 mM.

All cell treatments were carried out using serum free medium. GM was changed to FCS-free DMEM 4 h before each treatment. Cells were treated with DEX (1 µM) and insulin (1 µM) for 24 h.

5.2.3 RNA extraction

Total RNA was extracted on day 0, 2, 4, 6 and 8 of C2C12 differentiation and also from ~20 mg of tissue explants using Tri-reagent system. RNA concentration was determined spectrophotometrically at OD_{260} and its integrity assessed by agarose gel electrophoresis. 1 µg of RNA was used for reverse transcription (see Section 2.3).

5.2.4 Real-time PCR

Gene expressions have been measured using Life Technologies primers and probes; AMPD1 (Mm01308676_m1), AMD1 (Mm04207265_gH), SMOX (Mm00461100_m1), FRZB (Mm00441378_m1), MYH2 (Mm01332564_m1), PYCR1 (Mm00522674_m1), EEF2 (Mm01171434_g1), PRRX1 (Mm00440932_m1), ENO3 (Mm00468267_m1), MTHFD2 (Mm00485276_m1), NMRK2 (Mm01172895_m1), NAMPT (Mm00451938_m1), NMNAT1 (Mm01257929_m1), NADSYN1 (Mm00513448_m1), NMRK1 (Mm00521050_m1), AFMID (Mm00510774_m1), NMNAT2 (Mm00615393_m1), NMNAT3 (Mm00513791_m1), INDO (Mm00492586_m1), QPRT (Mm00504998_g1) and NAPRT1 (Mm01205844_g1). mRNA levels were determined

using the ABI 7500 sequence detection system (Life Technologies, Warrington, UK). Reactions were performed in singleplex in triplicates as described in Section 2.6 and normalised against the 18S rRNA housekeeping gene.

5.2.5 Cell fractions preparation

The microsomal, cytosolic and mitochondrial fractions were prepared from skeletal muscle of 14 weeks old WT mice by differential centrifugation techniques as described in Section 2.9. The supernatant from the first centrifugation was removed and the mitochondrial pellet was re-suspended in MOPs buffer. Followed by the centrifugation at 100,000 g for 1 h, the cytosolic supernatant was collected. The microsomal pellet was re-suspended in MOPs buffer after a series of washes. All cell fractions were immediately frozen in liquid nitrogen and then stored at -80ºC (up to 6 months) prior to assessment of protein concentration.

5.2.6 Immunoblotting

Proteins were extracted from C2C12 cells and tissue explants. Their concentration was determined as described in Section 2.10. For nicotinamide riboside kinase 2 (NMRK2) and nicotinamide phosphoribosyltransferase (NAMPT), 25 µg of protein whereas for NMRK2, NAMPT and BiP, 25 µg of microsomal, cytosolic and mitochondrial fractions were resolved on 10% SDS-PAGE gels. Proteins were transferred to nitrocellulose membranes at 140 mA for 1 h 30 mins. Primary NMRK2 (1:1,000) and NAMPT (1:1,000) antibodies were purchased from Generon Ltd Marketplace, UK whereas secondary antibodies from Dako, Glostrop, UK were used at a dilution of 1:10,000 and 1:1,000 respectively. The BiP antibody (BD Biosciences,

Oxford, UK) was used at a dilution of 1:1,000. Membranes were re-probed for α-Tubulin and primary and secondary antibodies used at a dilution of 1:1,000 (Abcam, Cambridge, UK). Bands were visualised using ECL detection kit (GE Healthcare, Bucks, UK).

5.2.7 NAD^+ assay

The NADH/NAD^+ supernatant was extracted from C2C12 cells grown in the medium containing different glucose concentrations and from ~20 mg of muscle tissue explants. A BioVision's NADH/NAD^+ Quantification Kit was used to detect NADH, NAD^+ and their ratio as described in the Section 2.13. The readings at OD 450 nm were taken after 2 hours of incubation at room temperature.

5.2.8 Histology

Quadriceps muscle was harvested from mice and then fixed in 10% neutral buffered formalin. Each muscle, from both 3 and 8 weeks old H6KO and WT mice (n=3 for each age), was paraffin embedded and cut into 5 μm sections to be stained by H&E to provide histological details of muscle structure.

5.2.9 Rodent protocol

Mice were housed in standard conditions on a 12 h / 12 h light-dark cycle with access to standard rodent chow and water *ad libitum.* All procedures were carried out in accordance with the UK Animals (Scientific Procedures) Act, 1986. On the day of experiment mice were sacrificed by cervical dislocation, then liver and skeletal

muscle (quadriceps, TA, soleus) tissues were removed, snap-frozen in liquid nitrogen and stored at -80ºC.

5.2.10 Statistical analysis

Where data were normally distributed, unpaired Student t-tests were used to compare single treatments to control using SigmaStat 3.1 (Systat Software, CA, US). One way ANOVA on ranks was used to compare multiple treatments, doses or times using SigmaStat 3.1. Statistical analysis on PCR data was performed on mean ΔCt values.

5.3 Results

5.3.1 Defining early metabolic factors leading to myopathy development through transcriptional profiling

To identify novel stress response genes, involved in the perturbation of the SR redox environment, that initiate ER stress, the analysis were extended to additional panel of the most up- or down-regulated genes, not involved in the ER or UPR stress response (Table 5-1). I have evaluated the H6KO muscle at 3 weeks of age, when no ER stress and myopathy are evident (Figure 5-4A) and compared these to 8 week old myopathy-affected muscle (Figure 5-4B) in order to define the earliest changes that precede myopathy.

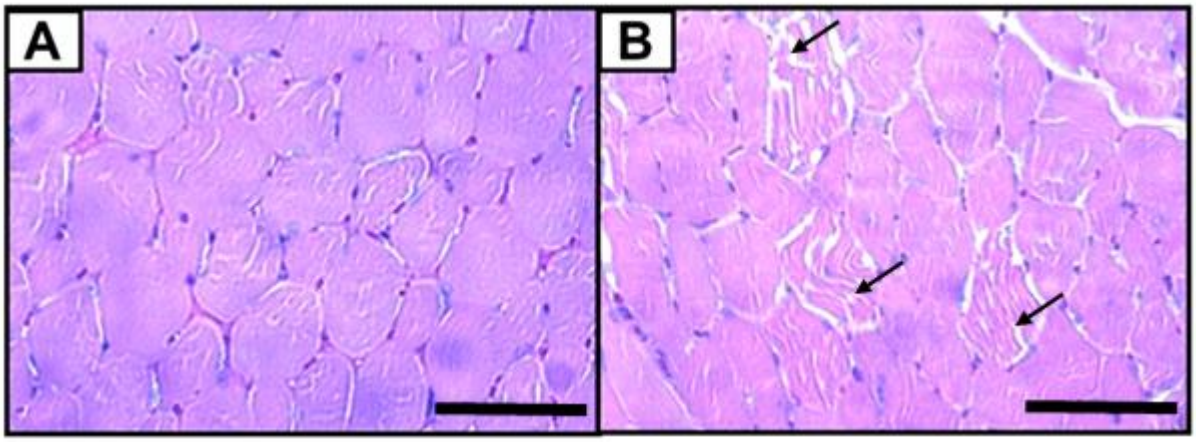

Figure 5-4 Histological defects in skeletal muscle of H6KO

Quadriceps sections stained with H&E show vacuoles present predominantly in type IIb fibres in 8 weeks old H6KO mice shown by black arrows (B) when compared to 3 weeks old mice (A) (representative image shown from n=3/group). The reference bar is 80 µM.

Unlike at 8 weeks old H6KO mice, at 3 weeks only 5 genes: AMD1, PYCR1, MTHFD2 and MYH2 were moderately, albeit significantly differentially expressed, though not to the same degree as at 8 weeks (Table 5-1). However, the most striking and highly significant difference observed at 3 weeks was elevated expression (~85-fold increase) of the gene, NMRK2, also known as muscle integrin binding protein (MIBP) or integrin binding protein 1 beta 3 (ITG1BP3) (Bieganowski and Brenner 2004).

Table 5-1 Gene expression in quadriceps from H6KO and WT mice

Data are presented as A.U., mean ± standard deviation (SD). ↔ No significant change in expression, ↓ gene down-regulated, ↑ gene up-regulated compared to WT; n=4. Abbreviations: AMPD1 [adenosine monophosphate deaminase 1 (isoform M)], AMD1 (adenosylmethionine decarboxylase 1), SMOX (spermine oxidase), FRZB (frizzled-related protein), MYH2 (myosin, heavy polypeptide 2, skeletal muscle, adult), PYCR1 (pyrroline-5-carboxylate reductase 1), EEF2 (eukaryotic translation elongation factor 2), PRRX1 (paired related homeobox 1), ENO3 (enolase 3, beta muscle), MTHFD2 [methylenetetrahydrofolate dehydrogenase (NAD^+ dependent)].

Gene Symbol	mRNA expression (A.U.±SD)		P value	mRNA expression (A.U.±SD)		P value
	3 weeks old			8 weeks old		
	WT	KO		WT	KO	
AMPD1	90.4±24.1	76.5±12.9	↔	59.4±7.8	5.2±1.8	3. 1E-13 ↓
AMD1	4.5±0.6	3.3±0.3	0.03 ↓	46.1±8.1	6.2±0.2	6.13E-05 ↓
SMOX	6.9±3.6	3.9±1.4	↔	21.3±7.4	7.4±0.8	0.0097 ↓
FRZB	1.4±0.3	2.2±0.6	↔	0.5±0.1	0.2±0.05	0.00015 ↓
MYH2	8.7±3.0	33.7±9.4	0.01 ↑	5.7±2.6	24.6±4.1	0.00024 ↓
PYCR1	0.7±0.05	0.9±0.1	0.003 ↑	0.4±0.05	2.0±0.3	1.1E-05 ↑
EEF2	49.9±20.9	93.0±18.0	↔	54.1±3.9	116.7±7.9	7.67E-06 ↑
PRRX1	3.6±0.8	5.5±1.0	↔	3.3±0.2	0.08±0.04	1.32E-08 ↓
ENO3	254.7±47.4	259.2±96.9	↔	228.3±33.8	173.1±9.3	0.019 ↓
MTHFD2	4.5±0.6	3.3±0.3	0.03 ↓	0.3±0.03	4.2±0.4	1.43E-06 ↑
NMRK2	0.7±0.2	66.9±7.0	**2.69E-11** ↑	5.73±2.34	83.27±15.9	1.05E-10 ↑

5.3.2 NMRK2 as the most up-regulated gene in 3 week old H6KO mice

To further revaluate the NMRK2 mRNA data in the muscle of 3 weeks old H6KO mice, we examined NMRK2 protein expression (25 kDa) by Western immunoblotting. Protein expression of NMRK2 was also significantly increased compared to age matched WT controls (Figure 5-5).

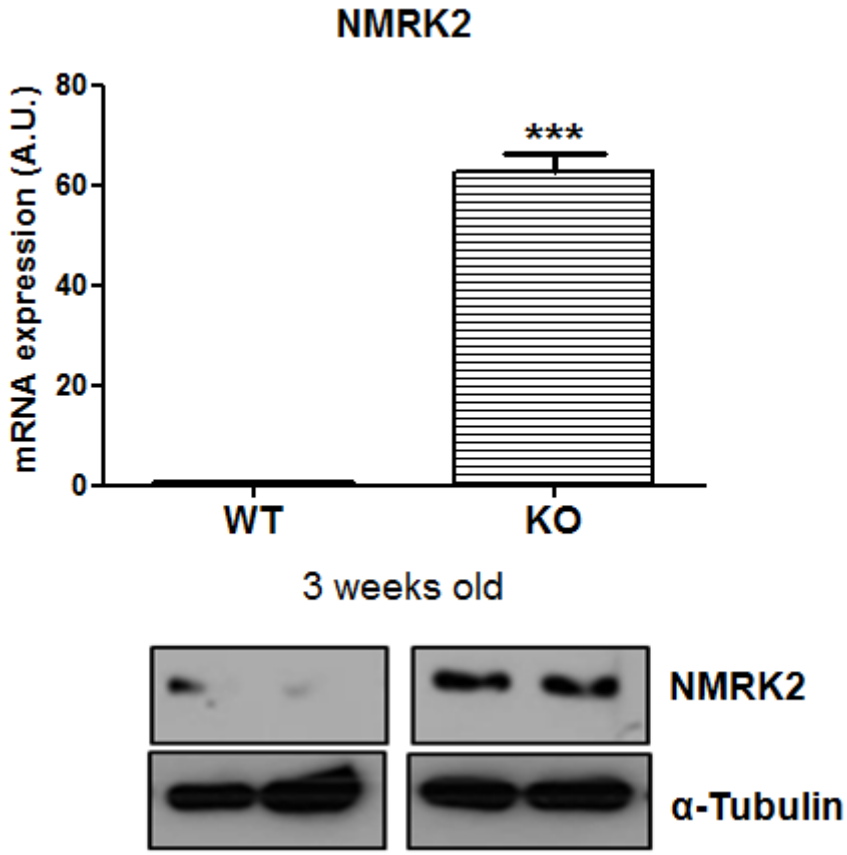

Figure 5-5 NMRK2 mRNA and protein level induction in the 3 weeks of age H6KO mice compared to WT mice

α-Tubulin was used as a loading control. All data are the mean A.U. values ±SEM from n=4/group (***<0.001).

5.3.3 Elevated cellular NAD^+ content associated with increased NMRK2

A major pathway proposed to determine skeletal muscle NAD^+ cellular content is the NMRK2 mediated salvage of nicotinamide riboside (NR)

(Bieganowski and Brenner 2004). NMRK2 was highly up-regulated in H6KO mice; therefore, we measured tissue level of NAD^+. This assay demonstrated that indeed NAD^+ levels were also increased associated with elevated expression of NMRK2 due to deficiency of H6PDH (Figure 5-6).

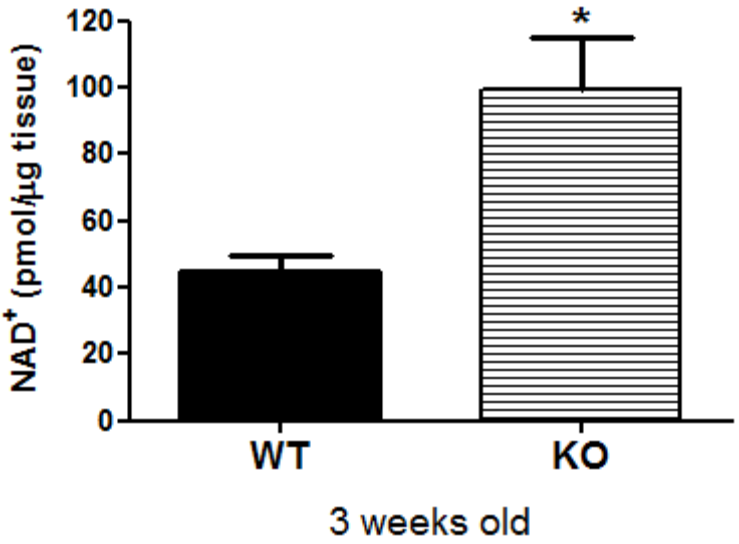

Figure 5-6 Increase in cellular NAD^+ content in H6KO mice when compared to WT mice

NAD^+ induction in pre-myopathy affected quadriceps muscle. All data are the mean values ±SEM from n=4/group (*<0.05).

5.3.4 NAMPT and NMNAT1 expression increased in H6KO mice

NMRK2 expression and NAD^+ content were highly up-regulated in muscle of H6KO mice; thus, we assessed the mRNA expression of other genes involved in NAD^+ metabolism such as NAMPT and nicotinamide mononucleotide adenylyltransferase 1 (NMNAT1) (Figure 5-7).

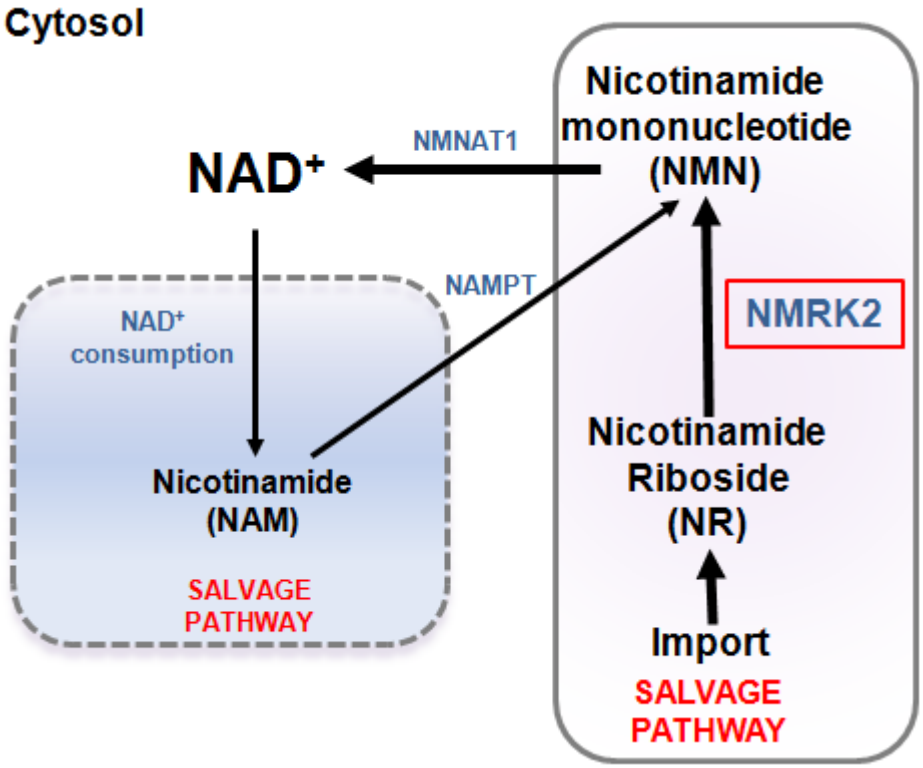

Figure 5-7 Schematic pathway of NAMPT, NMNAT1 and NMRK2 activity leading to NAD^+ generation

The major route to NAD^+ in muscle is via NAMPT salvage of NAM, and the NMRK2 mediated salvage of NR.

There was a significant up-regulation of both NAMPT and NMNAT1 in 3 weeks old H6KO mice when compared to matching WT; however, not to the same degree as NMRK2 (Figure 5-8).

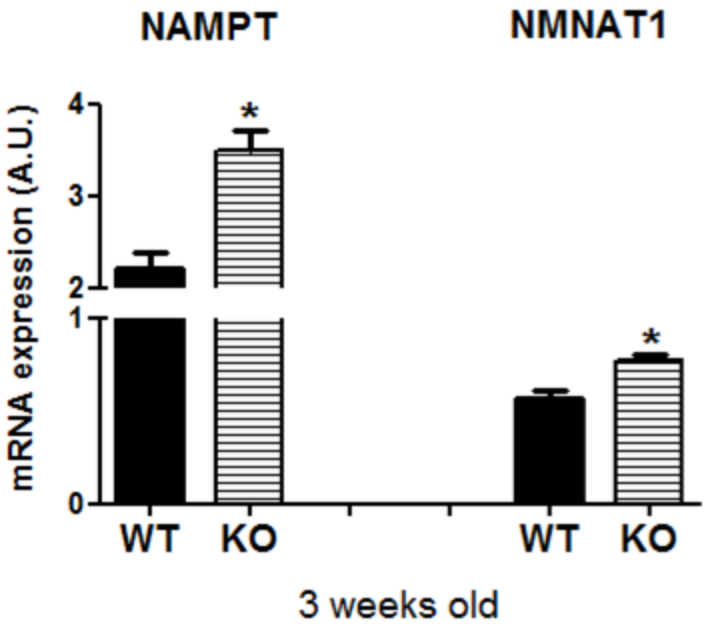

Figure 5-8 Induction of NAMPT and NMNAT1 mRNA expression in H6KO mice

NAMPT and NMNAT1 mRNA expression was increased in quadriceps muscle from H6KO mice when compared to WT mice. All data are the mean A.U. values ±SEM from n=4/group (*<0.05).

5.3.5 NMRK2 is critically involved in NAD^+ salvage

NMRK2 expression is restricted to skeletal muscle, and to a lower degree heart playing a role in NAD^+ metabolism (Bieganowski and Brenner 2004). NAD^+ is an essential redox coenzyme and is generated by a number of routes, including through the salvage of the dietary vitamin NR. To examine the relative importance of NMRK2 in muscle NAD^+ metabolism, we screened the expression of all known genes involved in NAD^+ metabolism in the slow twitch rich soleus, and fast twitch rich TA muscle, with the results displayed as a heat map in Figure 5-9. The microarray results showed that, in soleus and TA skeletal muscles, NMRK2 was the most highly expressed gene followed by NAMPT. Interestingly, NAD synthetase 1 (NADSYN1), a key rate limiting enzyme in NAD^+ classical *de novo* and the Preiss-Handler pathways,

was not expressed in soleus and TA muscle tissues. These data suggest that the NMRK2 and NAMPT mediated NAD^+ salvage pathways are predominantly responsible for regulating NAD^+ content in skeletal muscle.

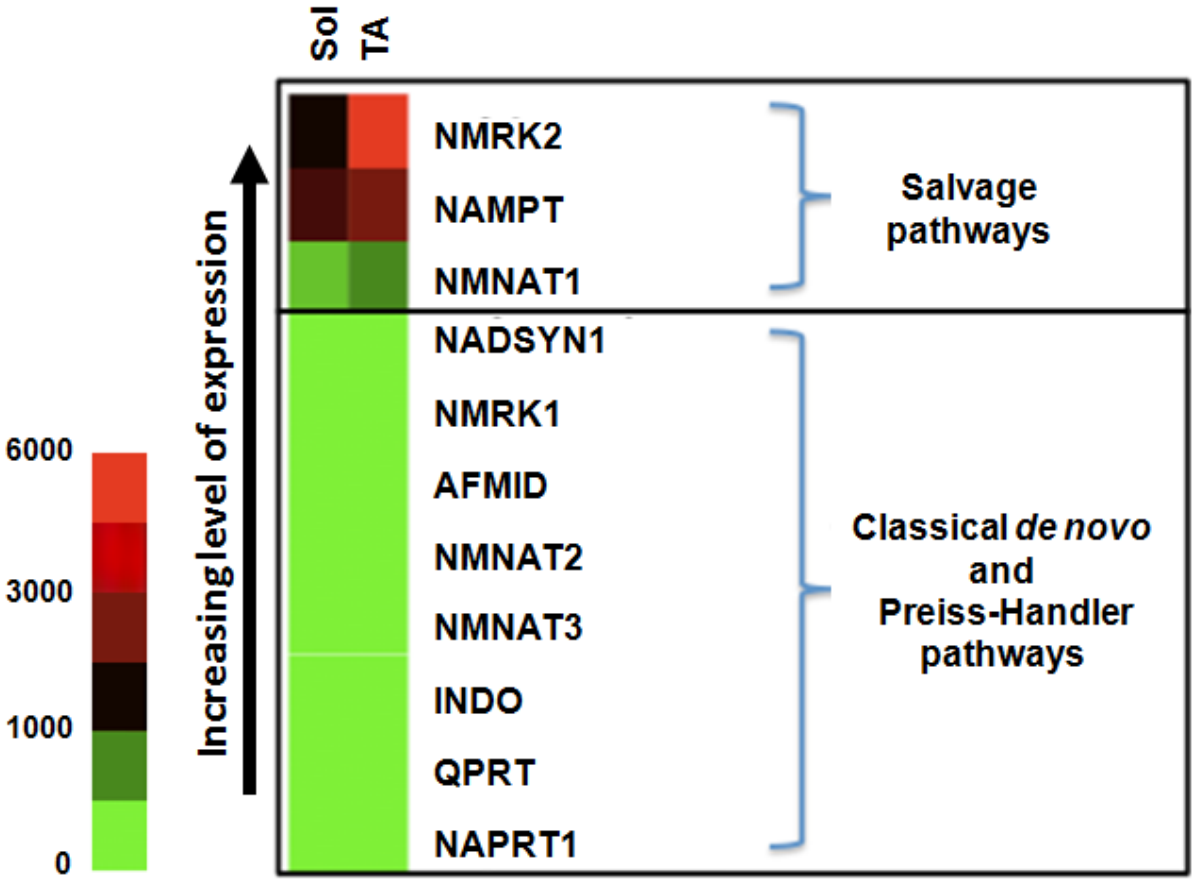

Figure 5-9 *De novo*, Preiss-Handler and salvage routes to NAD^+ synthesis in soleus (sol) and TA muscle

Only the salvage routes were expressed, and NMRK2 appeared at the mRNA level to be the most abundantly expressed with fast twitch TA muscle having the greatest expression. Abbreviations: AFMID (Arylformamidase), INDO (Indoleamine 2,3-dioxygenase 1), QPRT (Quinolinate phosphoribosyltransferase), NAPRT1 (Nicotinate phosphoribosyltransferase domain containing 1).

A 5-fold enrichment of NMRK2 mRNA in the more glycolytic type IIb fibre rich TA compared to type I fibre rich soleus is shown in Figure 5-10. This correlates with the fibre type affected most severely by myopathy in H6KO mice. NMRK2 expression

is more prominent in fast-twitch muscle fibres that have a higher metabolic capacity compared to slow-twitch muscle fibres (Chang et al. 2014) suggesting type IIb fibres are more sensitive to change in NAD^+ content.

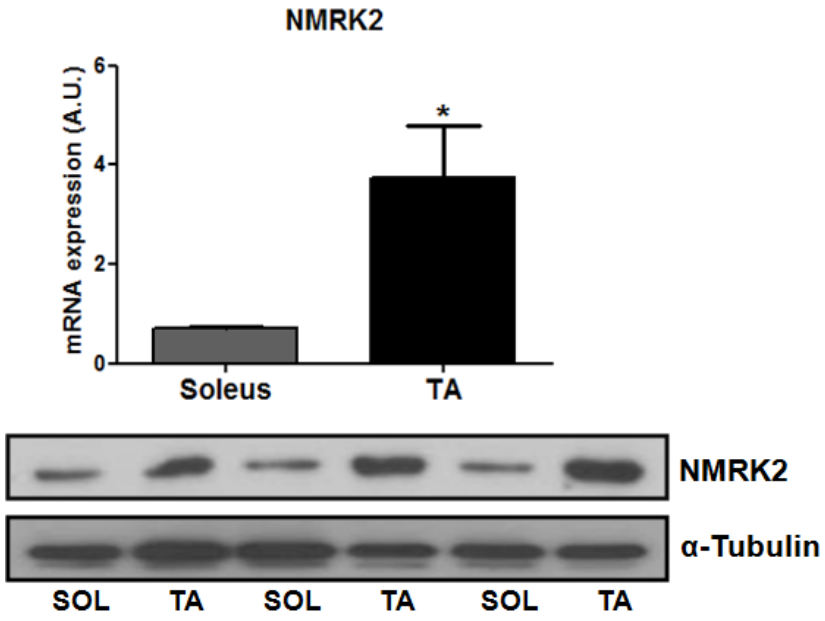

Figure 5-10 NMRK2 was enriched in type II fibre rich TA muscle

NMRK2 mRNA and protein expression was greatly increased in TA muscle compared to soleus muscle from 3 weeks old WT mice. α-Tubulin was used as a loading control. All data are the mean A.U. values ±SEM from n=3/group (*<0.05). Abbreviations: SOL (soleus), TA (tibialis anterior).

The salvage of NAM through the NAMPT and the salvage of NR through NMRK2 are the major routes of NAD^+ biosynthesis in skeletal muscle. Therefore, I also examined NAMPT expression in TA and soleus muscles. There was increase; however, not significant in NAMPT mRNA and protein expression in TA compared to soleus muscle (Figure 5-11) suggesting that NMRK2 salvage pathway contributes more to NAD^+ synthesis in fast twitch muscle type than NAMPT.

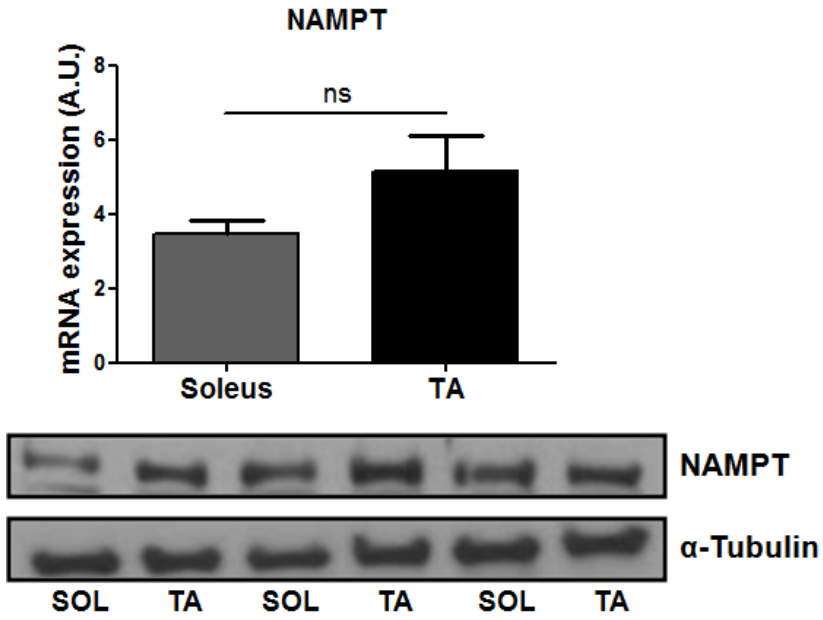

Figure 5-11 NAMPT mRNA and protein expression in TA muscle

There was no significant difference in NAMPT mRNA and protein expression between soleus and TA muscles. α-Tubulin was used as a loading control. All data are the mean A.U. values ±SEM from n=3/group (*<0.05). Abbreviations: SOL (soleus), TA (tibialis anterior), NS (not significant).

5.3.6 NMRK2 expression is restricted to cytosol

To localise NMRK2 pathway to a cell-specific compartment, I have investigated the expression of NMRK2 within different cell fractions including microsomes, cytosol and mitochondria as well as I used whole muscle tissue (TA) as a positive control. I have shown that NMRK2 was prominently expressed in the cytosolic fraction whereas NAMPT expression was most highly expressed in cytosol and to a lower degree in mitochondria (Figure 5-12). I applied BiP as a positive control as its expression is believed to be restricted to microsomes; however, I still found a subtle BiP expression in mitochondria, probably due to its presence in the mitochondria associated-ER membranes (MAMs) formed between the ER and the mitochondria (Giorgi et al. 2011).

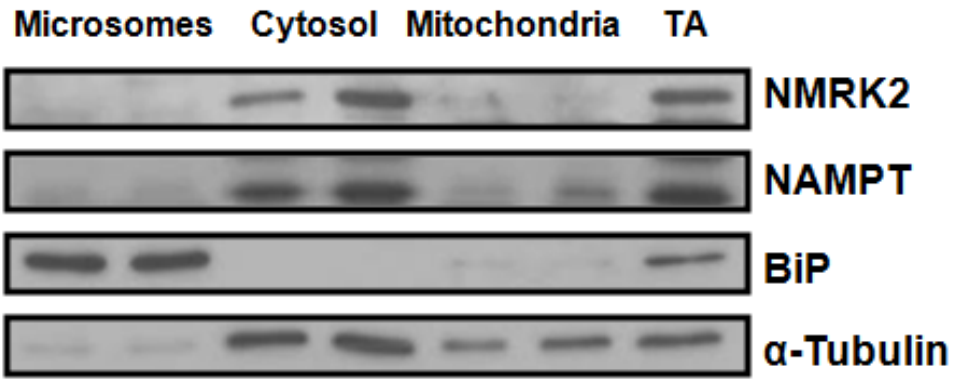

Figure 5-12 NMRK2 expression restricted to cytosolic fraction of skeletal muscle

BiP and α-Tubulin were used as positive controls for microsomes and all fractions respectively.

5.3.7 NMRK2 and NAMPT expression across C2C12 differentiation

The C2C12 differentiating muscle cell line was used as a good model to study muscle metabolism; therefore, I assessed NMRK2 expression patterns as C2C12s differentiated from myoblasts to myotubes across 8 day period. The NMRK2 mRNA and protein expression was low in undifferentiated myoblasts at day 0 and was already significantly increased by day 2 and further elevated across the 8 days of myotubes differentiation. This induction appeared to plateau once the C2C12 cells have fully differentiated and formed myotubes (between days 4-6). These results corroborate that NMRK2 pathway was up-regulated across muscle cells differentiation and may be important for their normal development (Figure 5-13).

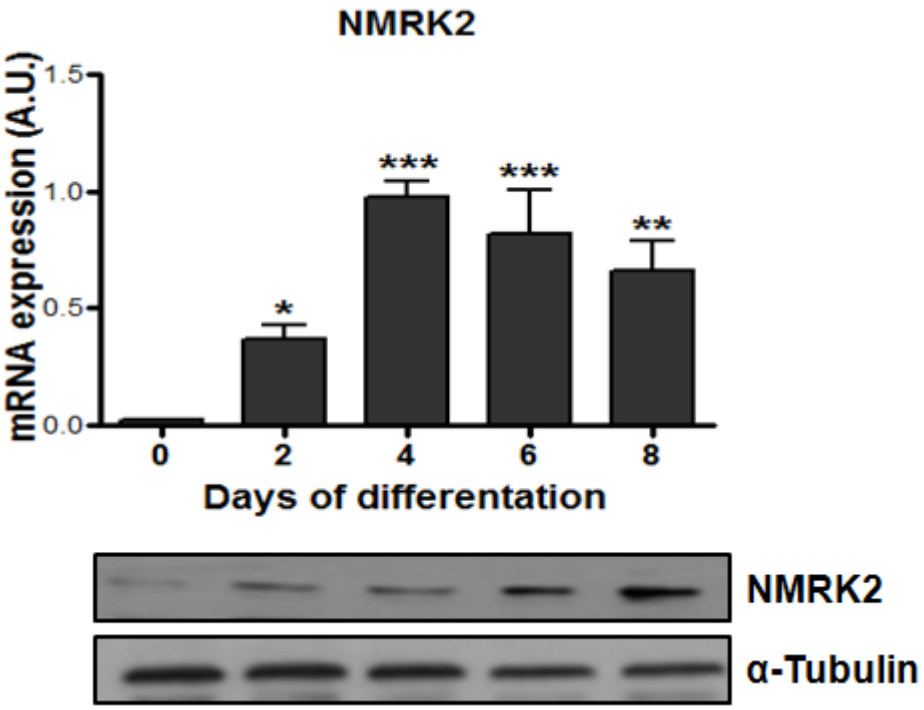

Figure 5-13 NMRK2 mRNA and protein induction across C2C12 cell differentiation

α-Tubulin was used as a loading control. All data are the mean A.U. values ±SEM from n=4 (*<0.05, **<0.01, ***<0.001 vs. day 0.) by ANOVA (Newman-Keuls post test).

.

In addition, I measured NAMPT mRNA and protein expression in C2C12 over the 8 day differentiation time course. In contrast to NMRK2, expression of NAMPT was already present in myoblasts at day 0 and was continuously expressed at a similar level across the 8 day of muscle cells differentiation (Figure 5-14) suggesting that NAMPT is similarly expressed in both myoblasts and mature muscle cells and may not be essential for differentiation and development of C2C12 muscle cell line.

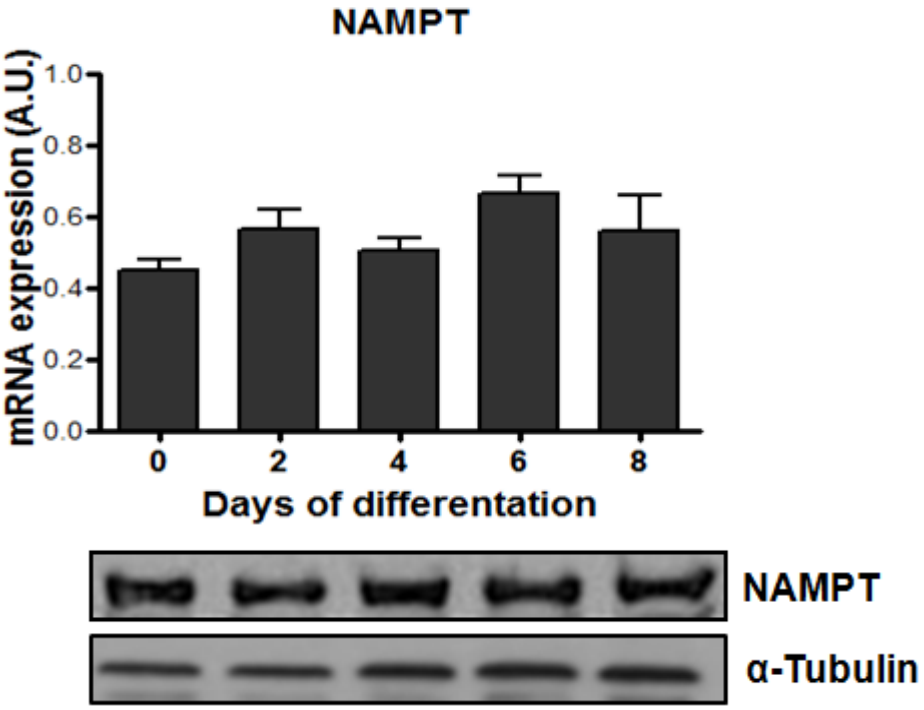

Figure 5-14 NAMPT mRNA and protein expression across C2C12 cell differentiation

NAMPT mRNA and protein expression did not change across differentiating C2C12. α-Tubulin was used as a loading control. All data are the mean A.U. values ±SEM from n=4 by ANOVA (Newman-Keuls post test).

5.3.8 Changes of NMRK2 and NAMPT expression in C2C12 cells followed by insulin and GC treatment

To identify modification of NMRK2 and NAMPT expression by hormonal factors relevant to this study, C2C12 myoblasts were differentiated for 5 days until they formed myotubes and then treated with DEX or insulin for 24 hours. DEX increased NMRK2 ($p=0.2033$) and NAMPT ($p=0.3847$) mRNA expression; however, these changes were not statistically significant. Treatment with insulin did not alter NMRK2 or NAMPT mRNA expression (Figure 5-15).

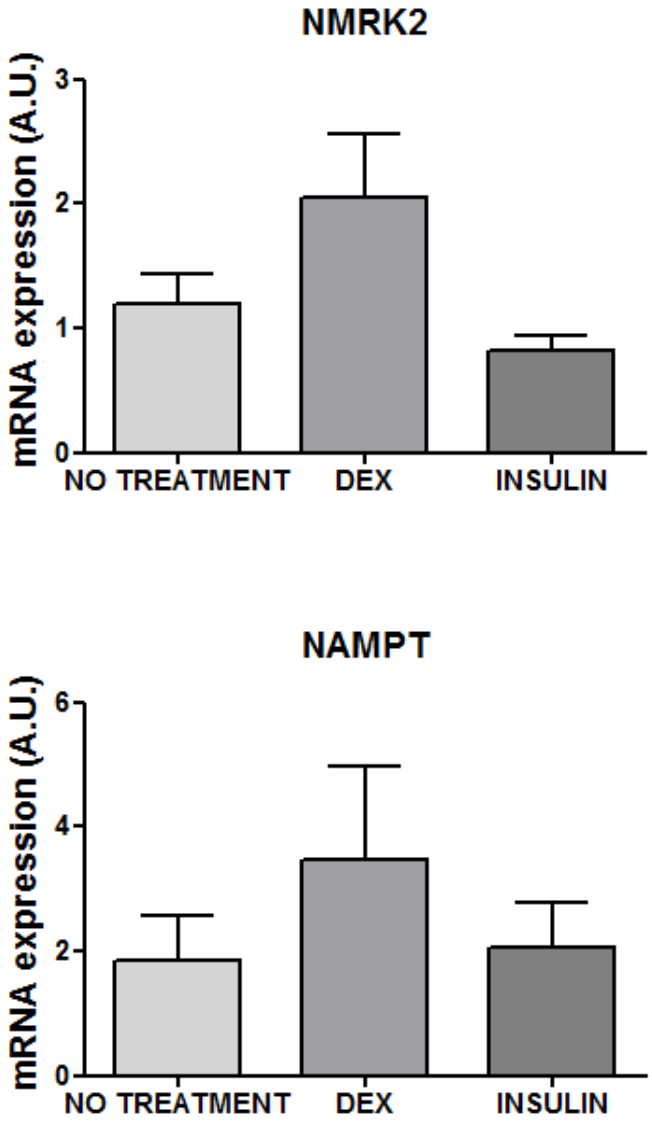

Figure 5-15 NMRK2 and NAMPT regulations by DEX and insulin in C2C12 myotubes

No significant differences in NMRK2 and NAMPT mRNA expression after DEX and insulin treatment. All data are the mean A.U. values ±SEM from n=3 by ANOVA (Newman-Keuls post test).

5.3.9 NMRK2 expression in glucose-deprived C2C12

These analyses were extended to assess other systems that have been previously shown to increase muscle cell NAD^+ content (Fulco et al. 2008). One such method is to restrict glucose availability in C2C12 muscle cells in culture.

Following 24 hour glucose restriction in C2C12 myotubes growth media from optimised 25 mM glucose to 4 mM, a dose-dependent increase in NMRK2 mRNA and protein expression was recorded. Measurement of monolayer cellular NAD^+ content indeed showed a correlation with increased NAD^+ levels (Figure 5-16). This implies that NMRK2 can be up-regulated during metabolic stress and further lead to increase of cellular NAD^+ biosynthesis in order to maintain NAD^+ content.

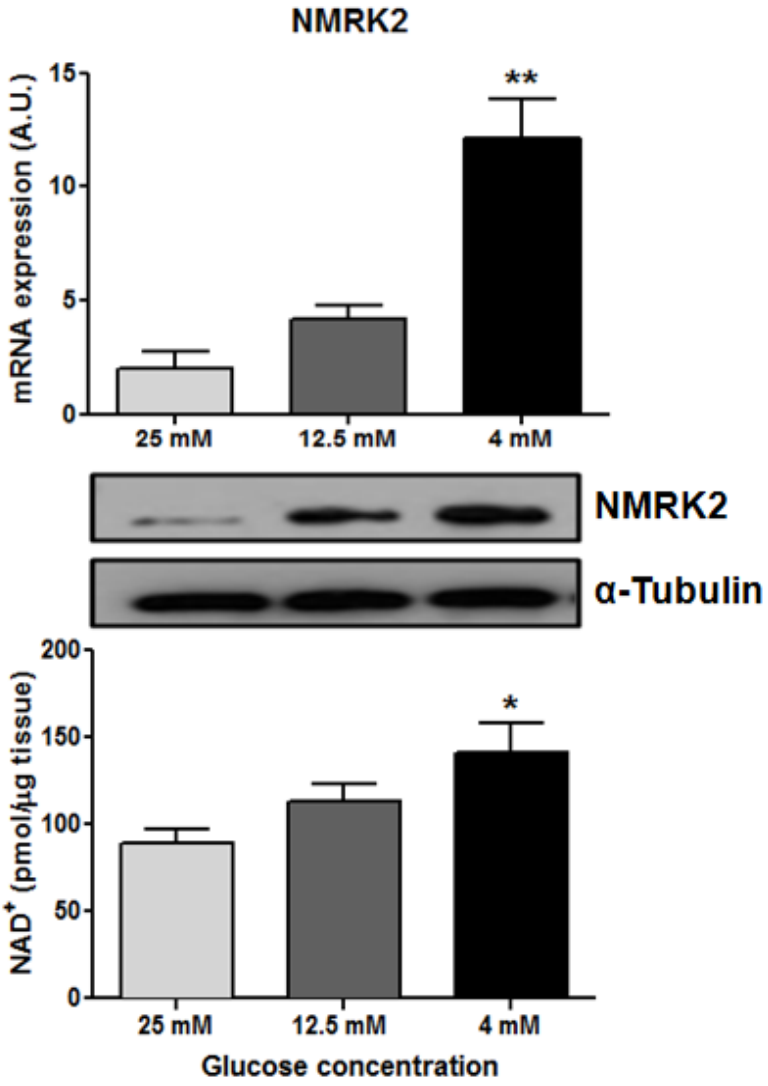

Figure 5-16 Glucose restriction in C2C12 myotubes increased NMRK2 mRNA and protein expression which was associated with elevated NAD^+ levels

By ANOVA, *<0.05 vs. control (25 mM), **<0.01 vs. control (25 mM) and 12.5 mM. α-Tubulin was used as a loading control. All data are the mean A.U. values ±SEM from n=4 by ANOVA (Newman-Keuls post test).

5.4 Discussion

To identify novel factors responding to altered SR redox caused by H6PDH deficiency, I have screened for differentially expressed genes in H6KO muscle prior to myopathy, SR stress and UPR activation as well as after the development of muscle wasting and fibrosis. I have identified a potential novel stress response pathway that may sense and respond to perturbation of the SR redox environment. The most differentially-expressed gene, being 85-fold over-represented in H6KO muscle without yet of signs of myopathy compared to controls, was NMRK2. Adaptation to H6PDH depletion involved early induction of NMRK2 expression which I found was restricted to cytosol of muscle and was preferentially expressed in glycolytic fast fibres such as TA, severely affected by myopathy in H6KO mice compared to soleus type I slow twitch fibres. This implicates a fibre type-specific relationship for NMRK2 expression that was higher in fast twitch muscle to regulate glycolytic metabolism and to replenish energy demands loss during anaerobic exercise. NMRK2 salvage and phosphorylation of NR, an essential vitamin, can elevate cellular NAD^+ content as in H6KO mice. NMRK2 has emerged as a skeletal muscle-specific pathway capable of regulating NAD^+ biosynthesis which is subject to subcellular compartmentalisation, and these data suggest that NAD^+ biosynthesis and NMRK2 are mechanisms for increasing $NAD^+/NADP^+$ flux in response to redox perturbations in the SR.

NMRK2 has only recently been identified as an enzyme that metabolises a newly identified dietary vitamin precursor, NR, found in food, particularly in milk and grains to cycle NAD^+ salvage and is continuously delivered to muscle once absorbed into the circulation (Bogan et al. 2008). NAD^+ is an essential redox co-enzyme that can

also be consumed by the sirtuins family of protein deactylases which can signal to improve mitochondrial function and insulin sensitivity (Tempel et al. 2007). However, skeletal muscle-specific overexpression of SIRT1 did not increase whole-body energy expenditure or insulin sensitivity in young mice (White et al. 2013). NMRK2 acts as a kinase phosphorylating NR to NMN which is subsequently converted to NAD^+ by the enzyme NMNAT1 (Figure 5-17) (Bieganowski and Brenner 2004).

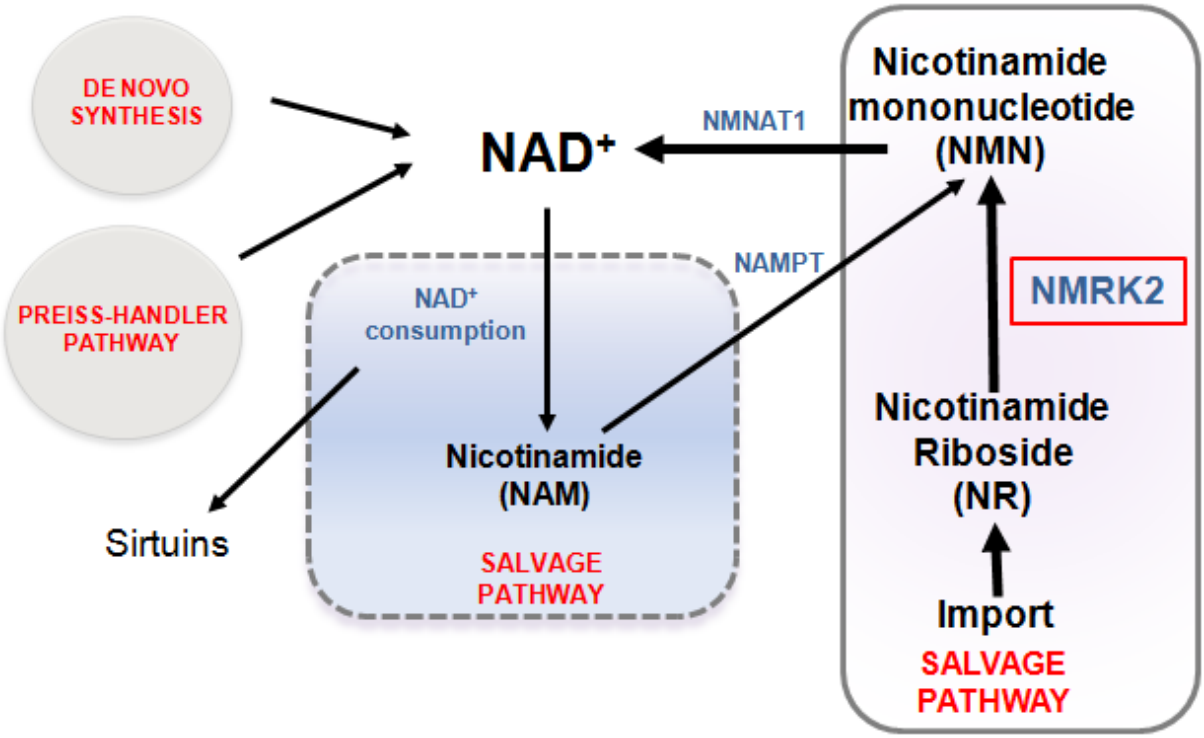

Figure 5-17 Schematic synthesis pathways of NAD^+

Two major routes to NAD^+ in skeletal muscle are via NAMPT salvage of NAM and NMRK2 salvage of NR. The boxed sections represent active pathways in skeletal muscle, with the solid rectangle detailing the NMRK2 route to NAD^+ synthesis.

NMRK2 belongs to the NMRK family of proteins which is found in most eukaryotes, from yeast to humans (Bieganowski and Brenner 2004). There are two isoforms of this enzyme in humans and rodents, NMRK1 and NMRK2. The amino acid sequences of these enzymes are highly conserved. NMRK belongs

to the deoxynucleoside kinase and nucleoside monophosphate (NMP) kinase superfamily although the sequence conservation is very low (less than 20% identity) (Khan et al. 2007). In humans, NMRK2 consists of 230 amino acids with a high activity against NR, and in the mouse NMRK2 is highly homologous to the human protein but with a C-terminal amino acid truncation containing 195 amino acids.

A previous study in zebrafish has demonstrated a potential role for NMRK2 in muscle morphogenesis. The NMRK2 orthologue in zebrafish was shown to potentiate laminin polymerisation, possibly through NAD^+ dependent ADP-ribosylation and subcellular localisation of the integrin-associated adaptor protein paxillin (Goody et al. 2010). Additionally, in dystrophic zebrafish lines NMRK2b-mediated NAD^+ synthesis is necessary for normal myogenesis with supplementation of NAD^+ significantly reducing muscle degeneration and improving muscle structure (Goody et al. 2012). The translational importance of the NMRK2 for skeletal muscle metabolic function was shown recently as mice fed NR demonstrated widespread metabolic remodelling in skeletal muscle. This response was mediated by induced NAD^+ in skeletal muscle, consequently activating SIRT1 and SIRT3 culminating in elevated oxidative metabolism and protection against high-fat diet-induced obesity (Canto et al. 2012). Taken together, manipulation of NAD^+ precursors and enzymes involved in NAD^+ biosynthesis, as potential future therapeutic approaches for treatment of a broad spectrum of muscular disorders, could improve muscle metabolic function and insulin sensitivity.

NAD^+ consumption by SIRT signalling demonstrates the necessity to maintain appropriate NAD^+ pools within the cell, particularly during periods of metabolic stress.

This shows the importance of NAD^+ biosynthesis pathways, which still remain poorly defined in skeletal muscle, to synthesise and replenish cellular NAD^+.

NMRK2 mediated NAD^+ salvage also works concurrent with the NAMPT pathway. Both NAMPT and NMRK2 generate NMN, the common precursor molecule converted into NAD^+ by NMNAT1. In H6KO mice, the expression of NAMPT and NMNAT1 was significantly increased; however, not to the same level as NMRK2. The expression of NMRK2 and NAMPT, as the main muscle NAD^+ salvage pathways, was also examined across C2C12 cell differentiation. NMRK2 expression was significantly elevated from day 2 to reach the greatest level on day 4 of myofibrillar differentiation whereas NAMPT was continuously expressed.

NMRK2 mediated NAD^+ salvage, from NR, has provided a novel pathway for energy homeostasis in skeletal muscle. Muscle glucose restriction increases NAD^+ level (Fulco et al. 2008) and here I demonstrate glucose restriction, with a concurrent increase in NAD^+ content, enhanced NMRK2 pathway as a novel mechanism leading to elevated NAD^+ content. This NMRK2 and subsequently NAD^+ induction along with increased fast twitch fibre expression further support that the salvage of NR through NMRK2 plays an important role in maintaining NAD^+ levels during metabolic stress, such as calorie restriction, in order to prevent NAD^+ depletion and large shifts in cellular redox status.

These data suggest NMRK2 can act as a stress response gene to increase the availability of NAD^+. As NAD^+ can be converted to $NADP^+$ through NAD^+ kinase, there is a possibility the NMRK2 mediated NAD^+ salvage pathway in muscle is sensing changes in the SR NADPH/$NADP^+$ ratio in H6KO mice (Figure 5-18). NAD^+

is a substrate for the SIRT family of deacetylases, with SIRT1 and SIRT3 activation leading to enhanced muscle oxidative metabolism (Bieganowski and Brenner 2004). In H6KO mice, higher NAD^+ content may increase SIRT activation and alter metabolism resulting in increased insulin sensitivity, and this theory is being explored in this model.

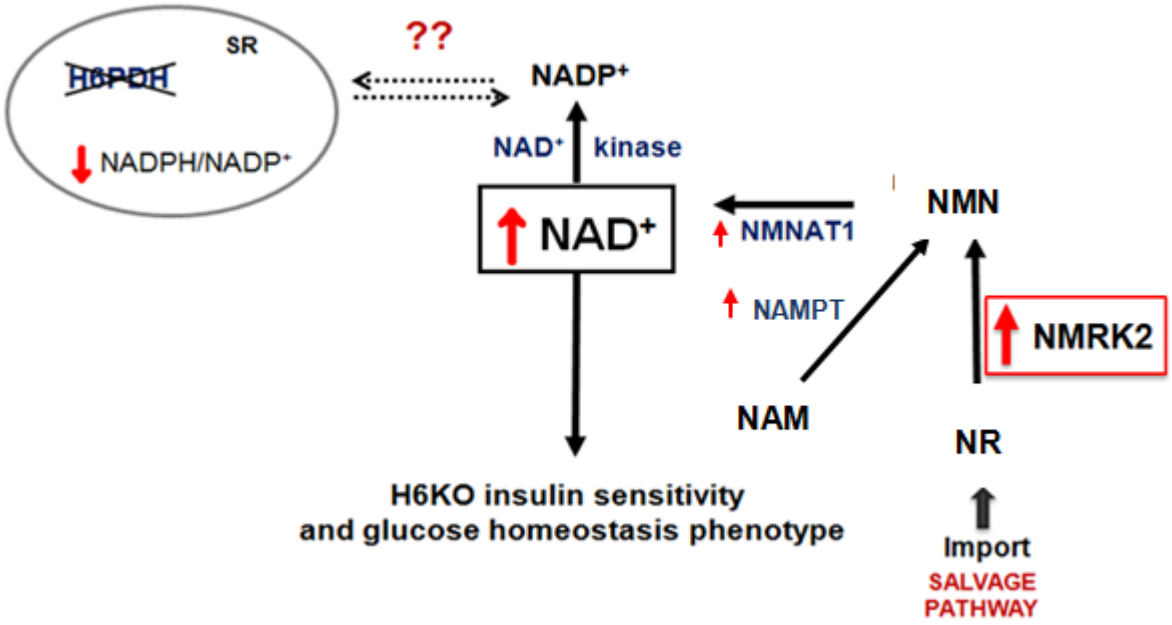

Figure 5-18 Summary of the association of NAD^+ salvage through the NMRK2 pathway with H6PDH deficiency

Enhanced NMRK2, NAMPT and NMNAT1 expression increase NAD^+ content which may lead to changes in muscle metabolism.

Microarrays in healthy tibialis anterior (type IIb fibre rich) and soleus (type I fibre rich) muscle imply that both NMRK2 and NAMPT salvage pathways are the primary routes involved in NAD^+ replenishment in skeletal muscle. NMRK2 is muscle-specific whereas NAMPT is ubiquitously expressed suggesting an important role for NMRK2 in skeletal muscle NAD^+ bioavailability. Increased NMRK2 mediated NR salvage and consequently NAD^+ metabolism in H6KO mice may be critical for establishing and maintaining SR NAD(P)(H) and regulating SR resident metabolism.

Skeletal muscle-specific expression of NMRK2 may play an important role in maintaining cellular NAD^+ pools in muscle by increasing its levels especially during metabolic stress. Whereas NAMPT mediated salvage could maintain basal NAD^+ content, but would be unable to retain appropriate NAD^+ levels under cellular stress. Therefore, NMRK2 expression may be increased to enhance NAD^+ salvage to maintain cellular redox status and ensure downstream metabolic adaptations occur.

In this chapter, I have identified the potential importance of the skeletal muscle-specific route to NAD^+ salvage and synthesis through the activity of the NMRK2 pathway. This novel adaptive mechanism responds to SR perturbation in H6KO mice. NMRK2 salvages NR for the ultimate generation of NAD^+. Delivering NR to muscle can elevate NAD^+ bioavailability, increase mitochondrial function and stimulate insulin sensitivity, which suggests that NMRK2 plays a pivotal role in the physiology of muscle energy metabolism (Canto et al. 2012). Defining the importance of muscle NAD^+ salvage pathways (particularly through NMRK2) to the maintenance of intracellular NAD^+ provision and the regulation of energy metabolism will extend our understanding of muscle physiology. This will illuminate strategies to 'boost' NAD^+ dependent energy metabolism to delay or prevent muscle diseases such as sarcopenia and prolong healthspan.

Skeletal muscle NMRK2 mediated NAD^+ salvage is important to the ability of muscle to adapt to fluctuating cellular and subcellular NAD^+ requirements, and that salvage pathways can be further manipulated to increase levels of NAD^+ during ageing and exercise as a mean to prevent or delay sarcopenia and increase healthspan. Measurements of NAD^+ and related metabolites could serve as an indicator of muscle metabolic status in health or disease. Liquid chromatography/mass

spectrometry methods should be applied to study NAD^+ metabolism in mouse muscle cells, tissue, subcellular fractions (e.g. mitochondria, SR) and blood during lifespan or/and in response to exercise. To determine the importance of NMRK2 and NAMPT to the ability of muscle to regulate NAD^+ availability and therefore mitochondrial function and energy homeostasis, NMRK2 muscle-specific KOs should be generated, and the consequences for age related sarcopenia and response to exercise further examined in this model.

Chapter 6- Metabolomic profiling of *H6PD* depleted muscle

6.1 Introduction

H6PDH is an important factor in setting the redox status of the ER/SR lumen by generating NADPH. In H6KO mice, alterations in SR redox lead to SR stress and consequently to activation of the UPR pathways in skeletal muscle as a result of perturbed SR homeostasis (Lavery et al. 2008b). The role of H6PDH in muscle SR is still enigmatic as are the underlying mechanisms leading to myoatrophy in its absence. I wish to examine aspects of the metabolic profile associated with H6PDH deficiency in muscle by applying metabolomics technology.

Metabolomics reveals changes in metabolite levels which are a driving force in the manifestation of phenotypes. Applying this technology in my study may help to identify biomarkers of muscle mass reduction and provide functional observations of muscle metabolic and energetic state due to *H6PD* depletion. This set of data should help with better understanding the correlation of muscle myopathy with metabolic changes and SR stress in the absence of H6PDH.

In Chapter 5, I screened for differentially expressed genes in H6KO muscle prior to myopathy and SR stress, and identified NMRK2 gene as a novel stress marker and highlighted its potential as an adaptive mechanism. In addition to this expression profiling, I applied targeted metabolomics to identify perturbations of the metabolic homeostasis and thereby to offer an access to biomarkers of metabolic pathways that are impacted by H6PDH depletion leading to myopathy development.

6.2 Methods

6.2.1 Rodent protocol

Mice were housed in standard conditions on a 12 h / 12 h light-dark cycle with access to standard rodent chow and water *ad libitum.* All procedures were carried out in accordance with the UK Animals (Scientific Procedures) Act, 1986. Male mice (H6KO and WT), aged 8 weeks old, were sacrificed by cervical dislocation (Schedule 1 method). All cardiac blood was collected for plasma isolation. Tissue explants (liver and quadriceps muscle) were removed, snap-frozen in liquid nitrogen and then stored at -80°C until metabolite extraction.

6.2.2 Method

Liver, quadriceps muscle and plasma were collected from H6KO and matching WT control mice. Frozen tissue explants were homogenised in the tubes containing ceramic beads of 1.4 mm diameter using extraction solvents (Section 2-16). The Absolute*IDQ* p150 kit (Biocrates Life Sciences AG, Austria) was prepared as described by the manufacturer. A 10 µl aliquot of plasma or tissue extract was used for PITC-derivatisation of amino acids, extraction with organic solvent and several liquid handling steps. Metabolites were quantified with a reference to appropriate internal standards using FIA-MS/MS on a 4000 QTRAP instrument (AB Sciex, Germany) coupled to a HPLC Promincence (Shimadzu Deutschland GmbH, Germany).

The application areas of the AbsoluteIDQ p150 kit are diverse because of the broad metabolite spectrum. In total, 163 metabolites divided into 6 groups were measured (Table 6-1).

Table 6-1 List of metabolites measured and their application areas

Taken from http://www.biocrates.com/products/research-products/absoluteidq-p150-kit.

Metabolite Class	Number of Analytes Measured	Biological Relevance (selected example)
Sugars	Sum of Hexose (90-95% Glucose)	Carbohydrate metabolism
Amino Acids	13 Proteinogenic Amino Acids + Ornithine	Amino acids metabolism, urea-cycle, activity of gluconeogenesis and glycolysis, insulin sensitivity/resistance
Acylcarnitine	41	Energy metabolism, fatty acid transport and mitochondrial fatty acid oxidation, ketosis, oxidative stress
Sphingomyelin	15	Signalling cascades, membrane damage
Phosphatidylcholine	77	Dyslipidemia, fatty acid profile, activity of destaurases
Lyso-Phosphatidylcholine	15	Degradation of phospholipids, signalling cascade, fatty acid profile

6.2.3 Experiment set up

The metabolomic analysis was conducted in collaboration with Prof. Jerzy Adamski from the German Research Center for Environmental Health in Munich, Germany. We applied the AbsoluteIDQ p150 kit to generate a metabolic profile in liver, quadriceps muscle and blood plasma from H6KO mice and matching controls. Mice were collected at 8 weeks of age at 10 am in the fed state. At this age, all phenotypes were fulminating in the H6KO showing evidence of SR stress, the UPR activation and myopathy. The experiment was set up as shown in Figure 6-1.

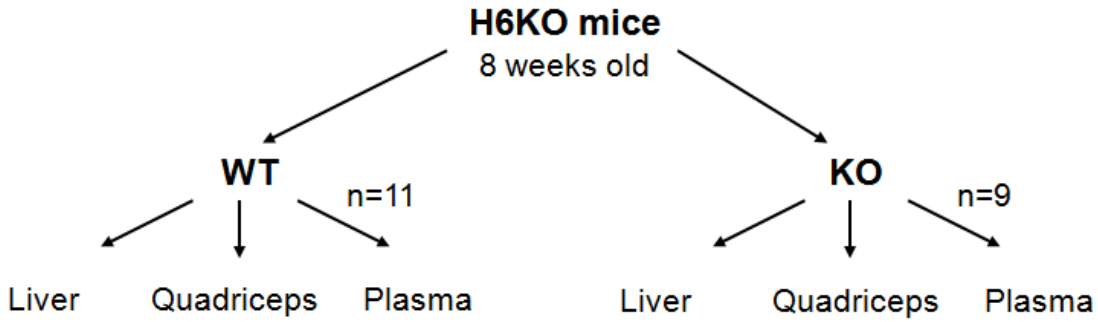

Figure 6-1 Schematic representation of targeted metabolomics set up

Liver, quadriceps muscle explants and blood plasma were collected from each animal (n=11 and n=9 for H6KO and WT respectively).

6.2.4 RNA extraction

Total RNA was extracted from ~20 mg of tissue explants using Tri-reagent system. RNA concentration was determined spectrophotometrically at OD_{260} and its integrity assessed by agarose gel electrophoresis. 1 µg of RNA was used for reverse transcription (see Section 2.4).

6.2.5 Real-time PCR

The sequence of all primers was as below:

CYTC: FWD: 5'-GCAAGCATAAGACTGGACCAAA-3'

REV: 5'-TTGTTGGCATCTGTGTAAGAGAATC-3'

COX1: FWD: 5'-TTCGCCATCATATTCGTAGG-3'

REV: 5'-TGTGGTGTAAGCATCTGGGT-3'

COX4: FWD: 5'- GTGCTGATCTGGGAGAAGAGCTA-3'

REV: 5'-GGTTGCCCTCATGTCCAGCAT-3'

COX5: FWD: 5'-TTCAAGCAGAGGAGATGGTG-3'

REV: 5'-CCAAACACGACAACTCCAAC-3'

CS: FWD: 5'-CCGTGCTCATGGACTTGGGCCTT-3'

REV: 5'-CCCCTGGCCCAACGTAGATGCTC-3'

The mRNA levels were determined using the ABI 7500 sequence detection system (Life Technologies, Warrington, UK). Primers for all genes were supplied by Eurofins Genomics (Valiant Way, UK). Reactions were performed in singleplex in triplicates as described in Section 2.6 using SYBR® Green master mix from Life Technologies and normalised against the 18S rRNA housekeeping gene system (Life Technologies, Warrington, UK).

6.2.6 Quantification of mitochondrial DNA (mtDNA)

DNA (~2 ng) from quadriceps muscle of 12-14 weeks old H6KO and matching controls was used to compare the mtDNA copy number to that of nDNA by real-time PCR using a set of four optimised PCR primers specific to cytochrome-b (mitochondrial) and β-globulin (nuclear). The number of mitochondrial DNA copies was calculated by using the following formula $n= 2^{\Delta Ct}$ [ΔCt=Ct (nDNA)-Ct (mtDNA)].

6.2.7 Statistical analysis

Where data were normally distributed, unpaired Student t-test was used to compare single treatments to control using SigmaStat 3.1 (Systat Software, CA, US).

6.3 Results

6.3.1 Lack of metabolic phenotype in liver and plasma

There were no significant changes in metabolic profile in blood plasma from H6KO mice when compared to WT. In liver used as a control, out of 163 metabolites analysed, only the ratio of hydroxylated to non-hydroxylated ceramide phosphocholines (sphingomyelins) was decreased and isovalerylcarnitine content was increased in H6KO mice. We believe, these changes do not contribute to the metabolic phenotype observed in H6KO mice.

6.3.2 Metabolic changes in muscle of H6KO mice

H6KO quadriceps muscle had pronounced metabolomic phenotype in comparison to that of liver and plasma. Table 6-2 shows the absolute quantification for each metabolite in its class and significant changes. The list of all 163 metabolites and their alterations in quadriceps muscle due to H6PDH deficiency is supplemented in the Appendix (Table S-1).

Table 6-2 Number of metabolites changed in H6PDH depleted muscle

Metabolite Class	Number of Analytes Measured	Number of Metabolites Changed
Hexose	Sum of Hexose (90-95% Glucose)	0
Amino Acids	13 Proteinogenic Amino Acids + Ornithine	7
Acylcarnitine	41	6
Sphingomyelin	15	4
Phosphatidylcholine	77	40
LysoPhosphatidylcholine	15	8
Total number of metabolites analyses: 163 Total number of metabolites changed: 65		

6.3.2.1 Increased amino acids content in muscle of H6KO mice

Differences in amino acids content and their potential role in development of the phenotype seen in H6KO mice were assessed. Out of 13 proteinogenic amino acids analysed, glutamine (Gln; $p<0.001$), arginine (Arg; $p<0.001$), proline (Pro; $p<0.01$), tryptophan (Trp; $p<0.01$) and glycine (Gly; $p<0.05$) were significantly elevated (Figure 6-2). This suggests muscle breakdown that increases amino acids levels.

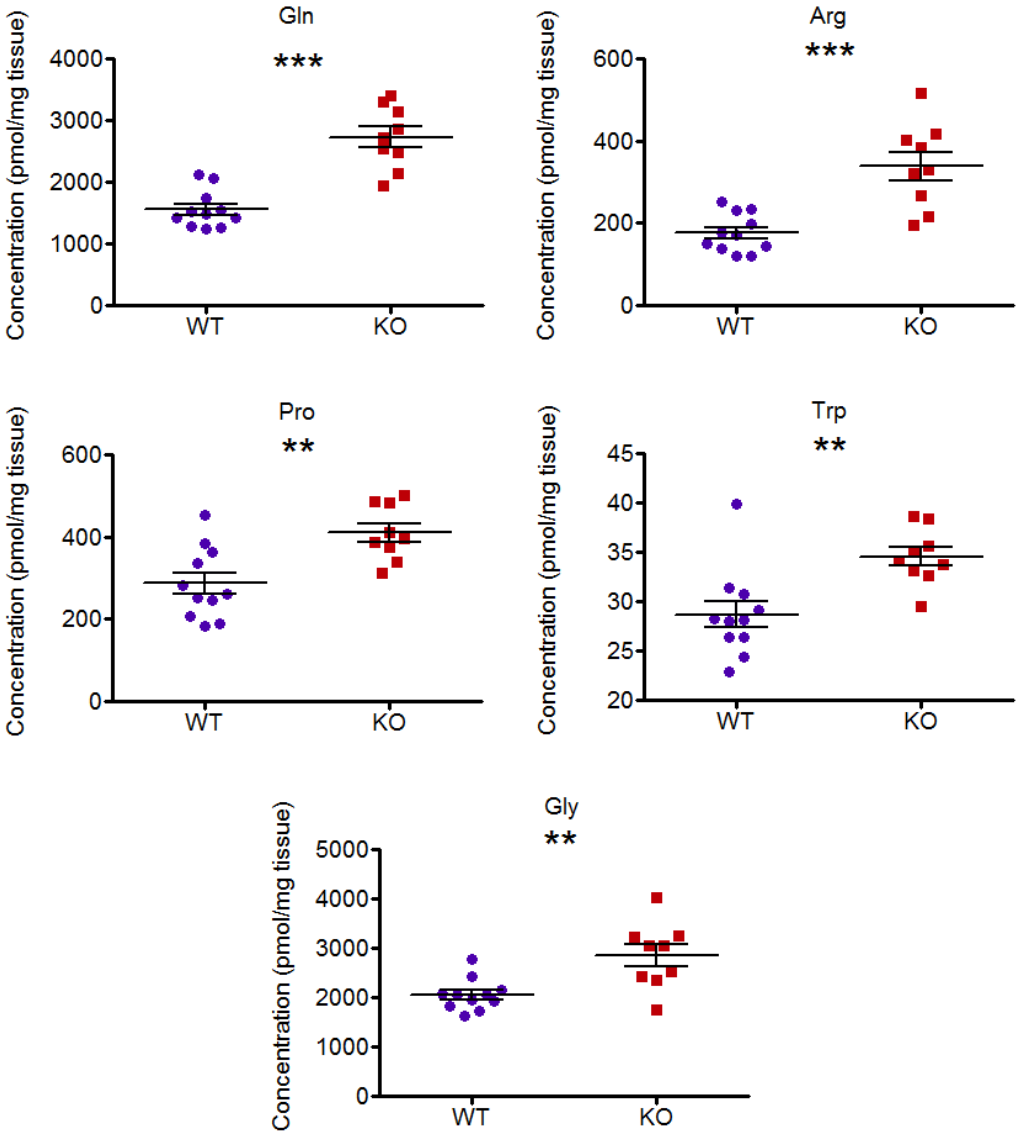

Figure 6-2 Changes in amino acids content in atrophic muscle

Gln, Arg, Pro, Trp and Gly were significantly increased in H6KO mice compared to WT. All data are the mean values ±SEM (*<0.05; **<0.01; ***<0.001).

6.3.2.2 H6PDH depleted muscle has reduced arginase activity

An Orn/Arg ratio, representing greatly impaired arginase activity, was significantly decreased in H6KO mice ($p<0.001$) compared to WT (Figure 6-3A). These changes reflect a diminished ornithine (Orn) level ($p<0.05$) (Figure 6-3B). Depletion in arginase activity, together with decreased mRNA expression of SMOX and AMD1 shown in Table 5-1, may affect synthesis of downstream targets such as growth signals (polyamines).

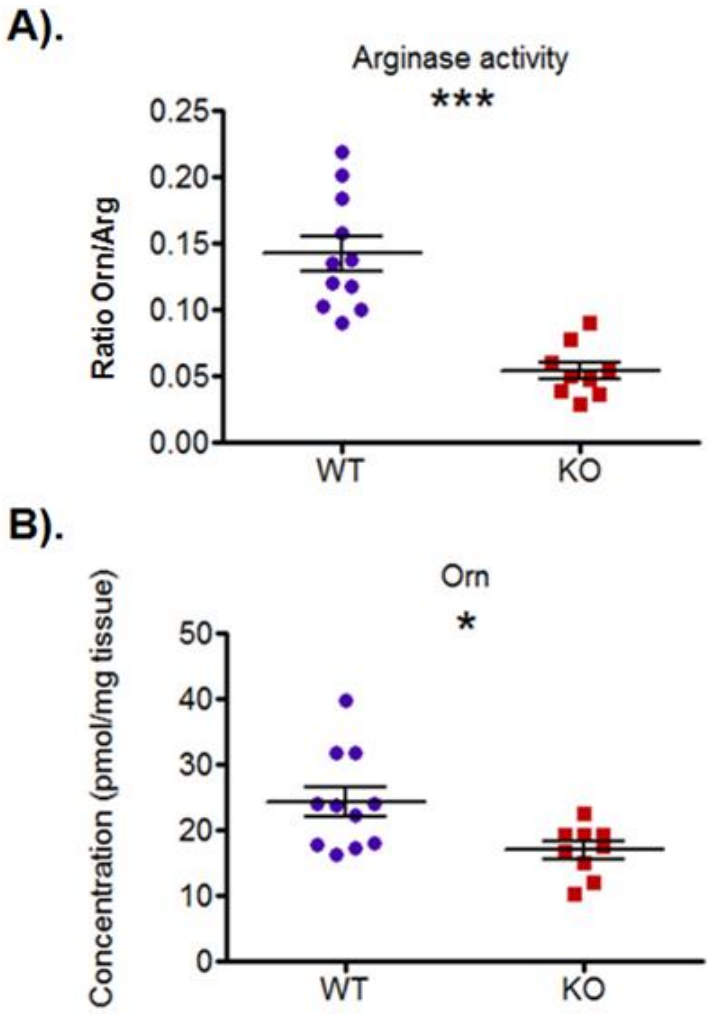

Figure 6-3 Impaired arginase activity in *H6PD* depleted muscle

Decreased ornithine content in H6KO mice (A); reduction in Orn/Arg ratio, an indicator of arginase activity, in H6KO mice (B). All data are the mean values ±SEM (*<0.05; ***<0.001).

In H6KO muscle, there was also significant decline in branched-chain amino acids content such as leucine/isoleucine (xLeu) ($p<0.05$) (Figure 6-4). This could represent muscle undergoing breakdown of amino acids that can directly enter energetic pathways.

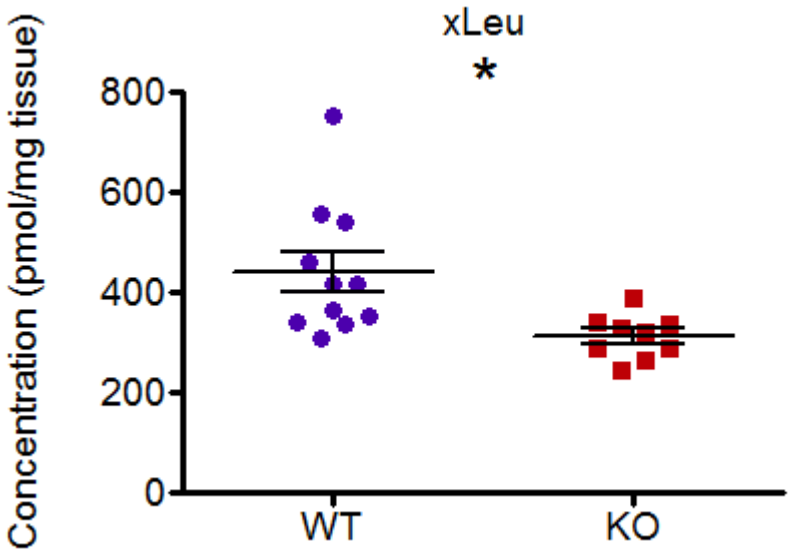

Figure 6-4 Alterations in branched-chain amino acids

The sum of leucine and isoleucine was lowered in H6KO mice compared to WT. All data are the mean values ±SEM (*<0.05).

6.3.2.3 Increased acylcarnitines content in *H6PD* depleted muscle

The screening of 40 acylcarnitines showed six being significantly elevated including acetylcarnitine (C2), butyrylcarnitine (C4), valerylcarnitine (C5), decanoylcarnitine (C10:1), malonylcarnitine/hydroxybutyrylcarnitine (C3-DC/C4-OH) as well as fumarylcarnitine/hexanoylcarnitine (C4:1-DC/C6) (Figure 6-5). Acylcarnitines represent byproducts of fat, glucose and amino acid mitochondrial oxidation. This work contributes to increasing evidence that elevated acylcarnitines may act

as biomarkers of defects in fat metabolism and may be an indication of mitochondrial dysfunction (Sampey et al. 2012).

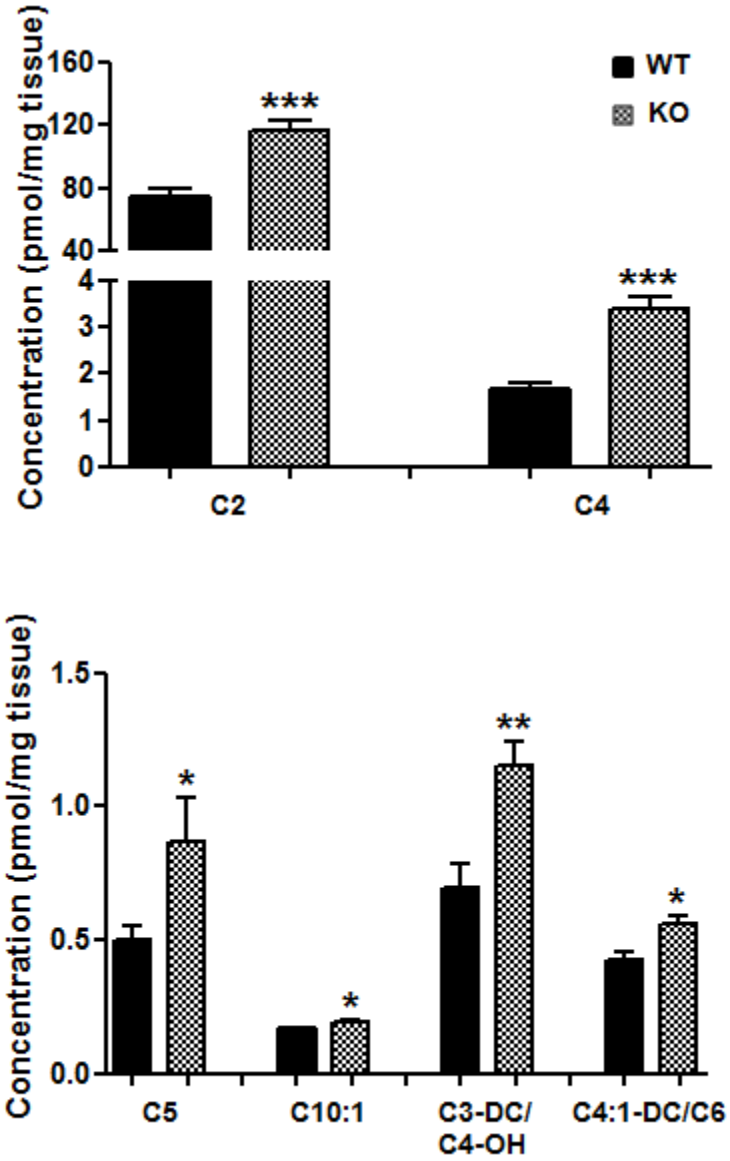

Figure 6-5 Increased acylcarnitines level in H6KO mice

Out of 40 acylcarnitines, C2, C4, C5, C10:1, C3-DC/C4-OH and C4:1-DC/C6 were significantly up-regulated in myopathy-affected muscle. All data are the mean values ±SEM (*<0.05; **<0.005; ***<0.001).

These elevations of acylcarnitines were concomitant with a significant induction of acetylcarnitine to free carnitine ratio (C2/C0; $p<0.05$), and short chain acylcarnitines

to free carnitine ratio [(C2+C3)/C0; p<0.01] in atrophic muscle (Figure 6-6). Both ratios are indication of defects in β-oxidation activity (http://www.biocrates.com/images/Produktfolder_MetaDis_Einzelseiten.pdf).

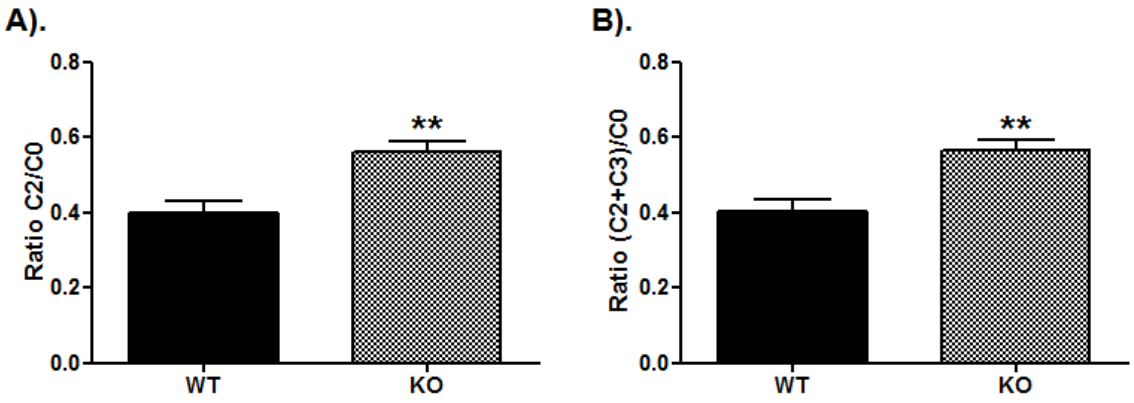

Figure 6-6 Induction of acylcarnitines ratios

The ratios of acetylcarnitine to free carnitine (A) and short chain acylcarnitines to free carnitine (B) were significantly increased in quadriceps muscle due to H6PDH deficiency. All data are the mean values ±SEM (**<0.005).

6.3.2.4 Alterations of membrane lipids content in H6KO mice

In muscle, the most obvious effect was on the membrane lipids; many of the lipids were about 50% greater than the control. One reason for this is that in H6KO muscle cell, the membrane lipids are being scavenged for oxidation and building up as C2-C6 acylcarnitines were elevated.

Additionally, the majority of lysoPhosphatidylcholines was increased (Figure 6-7) and the level of 40 phosphatidylcholines was also dysregulated in H6KO mice (Table 1 in Appendix).

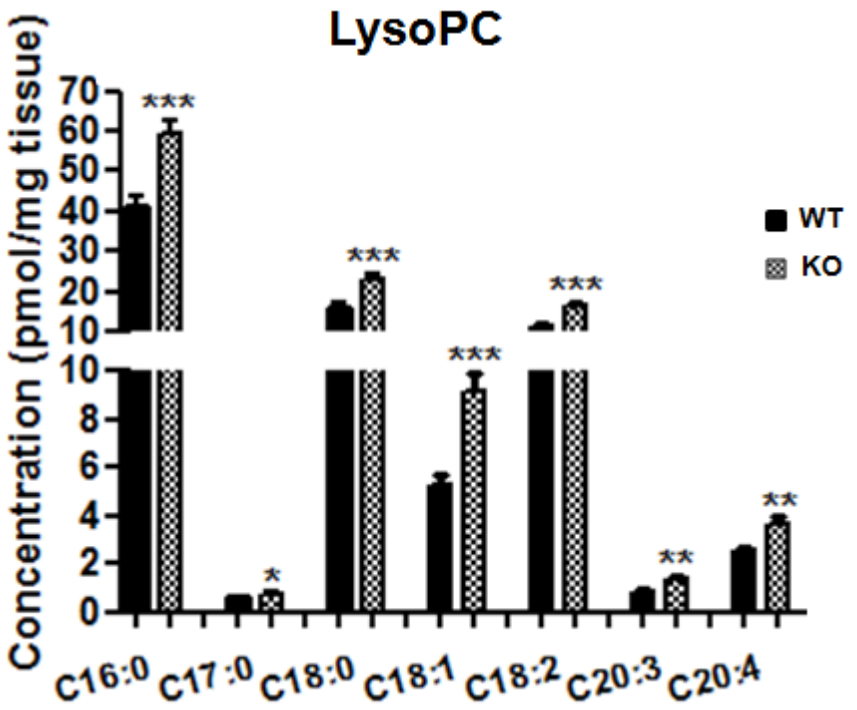

Figure 6-7 Changes in lysoPhosphatidylcholine (lysoPC) content in muscle from H6KO mice

The levels of C16:0, C17:0, C18:0, C18:1, C18:2, C20:3 and C20:4 were elevated in H6KO mice. All data are the mean values ±SEM (*<0.05; **<0.01; ***<0.001).

Total phosphatidylcholine (PC) content was depleted (Figure 6-8A) suggesting they might be salvaged at the membrane for energy leading to induction of total lysoPC content (Figure 6-8B). As expected, the ratio of total lysoPC/total PC was significantly increased in H6KO mice (Figure 6-8C) indicating perturbation of membrane lipids, potentially causing membrane leakage and further interactions between muscle SR and cytosol.

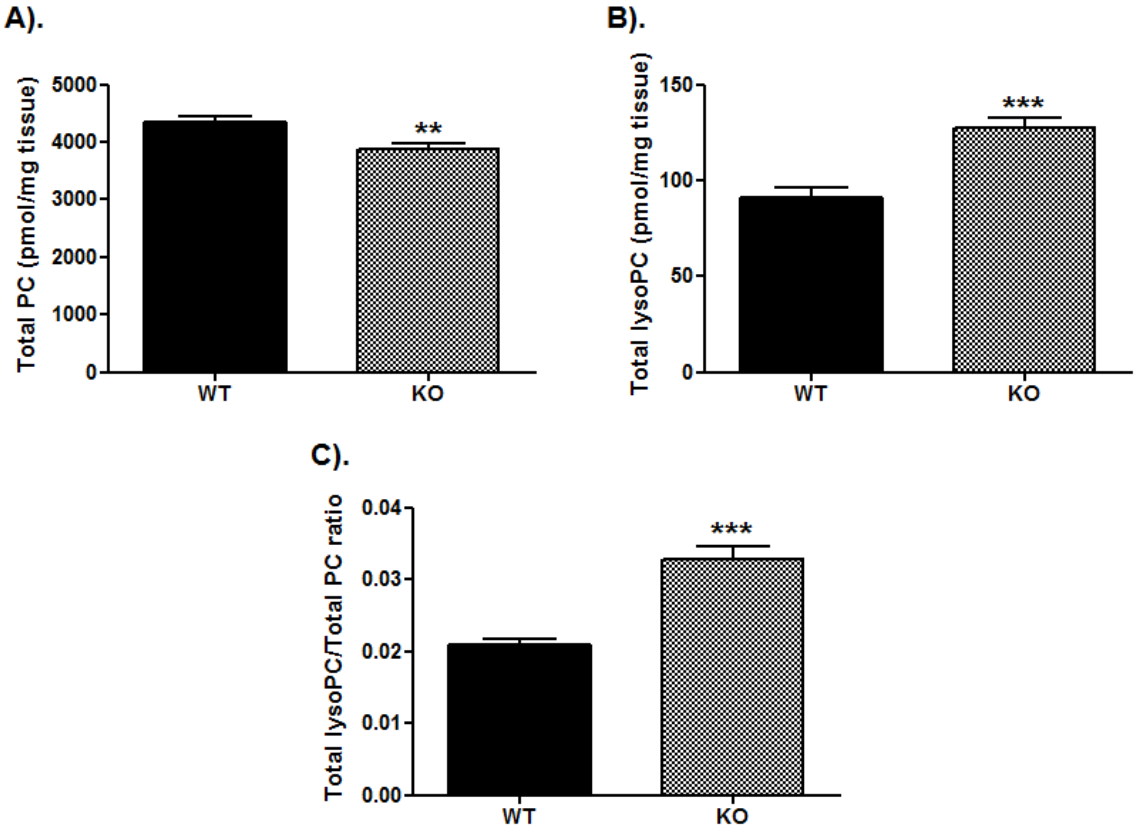

Figure 6-8 Changes in total lysoPC and total PC content

Decreased total PC content (A) was correlated with increased total lysoPC level (B) leading to induction of total lysoPC/total PC ratio in *H6PD* depleted muscle. All data are the mean values ±SEM (**<0.01; ***<0.001).

6.3.3 Elevated mitochondrial biogenesis in atrophic muscle

Here, we demonstrate that skeletal myopathy is associated with a range of metabolic and energetic changes within muscle cell reflecting alterations in metabolite content. Metabolomic profiling revealed dysregulation of amino acids and lipid metabolism that potentially affect mitochondrial function.

PGC-1α, a key regulator of energy metabolism, was previously shown to be increased in H6KO mice (Lavery et al. 2008b). In addition, I measured the mRNA expression of pyruvate dehydrogenase kinase, isozyme 4 (PDK4), a downstream

target of PGC-1α. I found induction in PDK4 mRNA expression in *H6PD* depleted muscle (Figure 6-9).

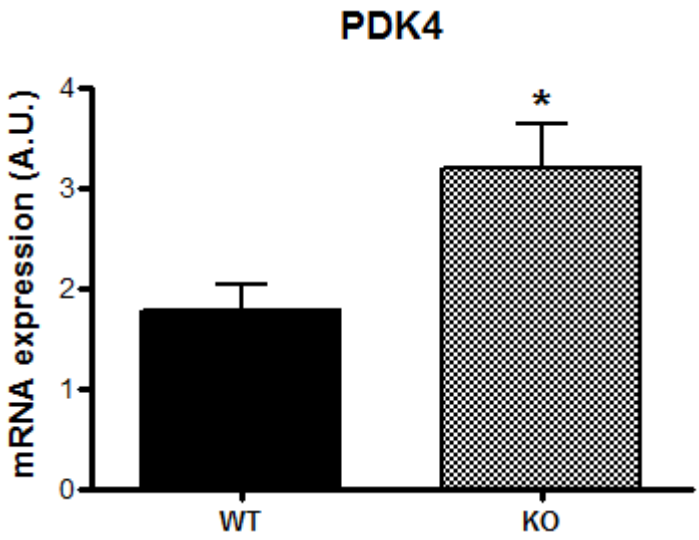

Figure 6-9 Increased PDK4 mRNA expression in H6KO mice

All data are the mean A.U. values ±SEM from n=8-9/group (*<0.05).

Mitochondrion is a major site for energy production, β-oxidation and energy metabolism. Alterations in lipid metabolism and amino acids content may affect energy metabolism; therefore, I determined mitochondrial abundance in *H6PD* depleted muscle. The changes in mtDNA may provide insight into the processes that either initiate or propagate mitochondrial dysfunction that is implicated in a vast array of diseases and conditions including cancer and ageing (Phillips et al. 2014).

The mitochondrial DNA to nuclear DNA ratio (mtDNA:nDNA) as an estimate for the number of mtDNA copy number was significantly increased in quadriceps explants from H6KO mice compared to WT ($p<0.001$) (Figure 6-10).

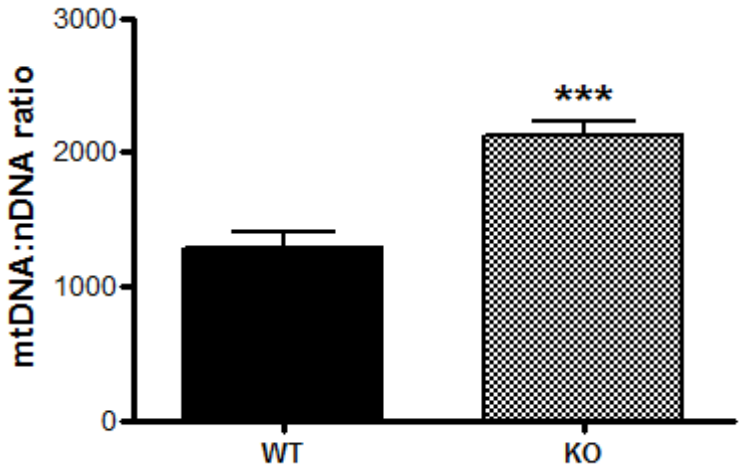

Figure 6-10 Elevated mtDNA:nDNA ratio in H6KO mice

All data are the mean values ±SEM from n=10/group (***<0.001 vs. WT).

Additionally, the mRNA expression of a number of mitochondrial- and nuclear-encoded genes was measured in myopathy-affected muscle. There was a significant induction in mRNA expression of mitochondrial-encoded genes including cytochrome C oxidase (COX) subunit 1, 4 and 5 (Figure 6-11A) as well as in the mRNA expression of nuclear-encoded genes such as cytochrome C (CYTC) and citrate synthase (CS) expression (Figure 6-11B). This was correlated with elevated mtDNA copy number in H6KO mice.

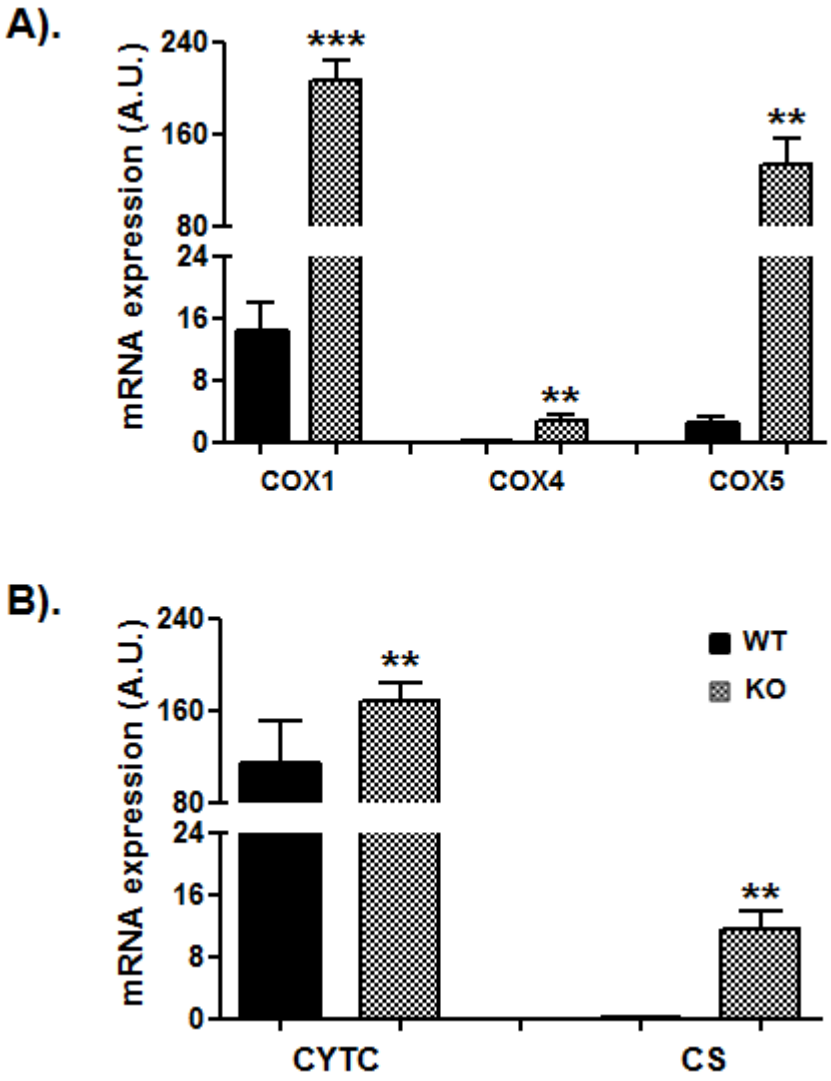

Figure 6-11 Increased expression of mitochondrial genes

Elevated expression of mitochondrial-encoded genes: COX 1, 4 and 5 (A); Increased mRNA expression of nuclear-encoded genes: CYTC and CS (B). All data are the mean values ±SEM from n=8-9/group (*<0.05, **<0.01, ***<0.001 vs. WT).

6.4 Discussion

In Chapter 5, I identified a large set of significantly dysregulated genes in H6KO mice. They group into a number of common pathways such as structural, polyamine biosynthesis, purine salvage, intermediary metabolism and ER/SR stress. NMRK2 expression was the most up-regulated in H6KO mice which was associated

with elevated muscle NAD^+ content. A previous study has shown that despite myopathy, these mice had enhanced glycogen storage, insulin sensitivity and protection from diet-induced insulin resistance (Lavery et al. 2007). H6KO muscle also displayed elevated mitochondrial biogenesis with increased expression of mitochondrial encoded genes and increased mitochondrial copy number; all phenotypes consistent with NAD^+ dependent SIRT1 and SIRT3 activity (Canto et al. 2012).

The metabolomics results are combined in Figure 6-12.

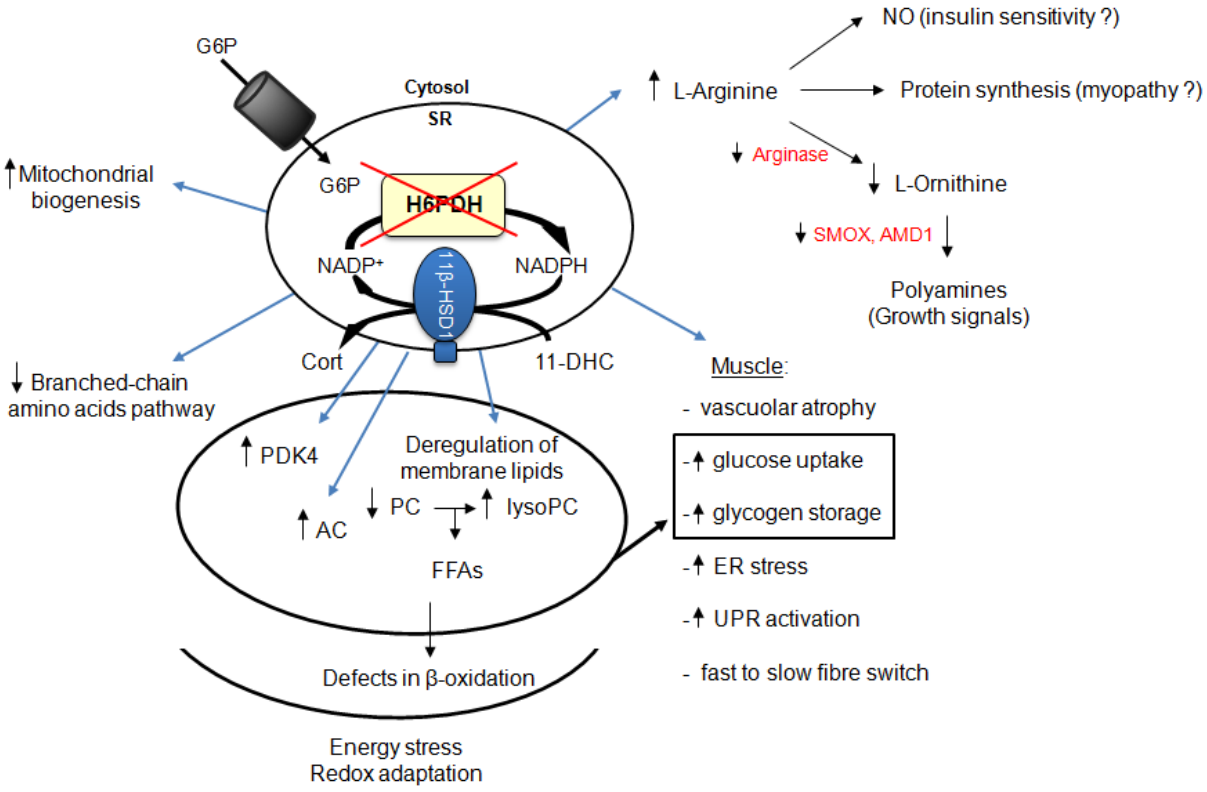

Figure 6-12 Summary of metabolomic changes due to H6PDH deficiency

Changes in AC and lipids content in association with increased PDK4 mRNA expression might lead to energy stress in H6KO mice whereas reduction of arginase activity and decreased mRNA expression of SMOX and AMD1 may impinge on growth signals (polyamines). Abbreviations: AC (acylcarnitines), FFA (free fatty acid), NO (nitric oxide), PC (phosphatidylcholine).

H6PDH deficiency impacts on amino acids metabolism that could contribute to aspects of the phenotype such as insulin sensitisation through elevated arginine and subsequent nitric oxide (NO) content. It has been previously shown that impaired NO bioavailability is correlated with the development of insulin resistance (Sydow et al. 2005) and endothelial NO synthesis and insulin sensitivity are positively related in healthy humans (Petrie et al. 1996). Also, decreased arginase activity and consequently ornithine content in association with reduced SMOX and AMD1 mRNA expression might lead to diminished growth signals such as polyamines.

We propose that changes in protein synthesis and amino acid accumulation may lead to reduction in muscle mass (Lecker et al. 2006) and as a consequence influence ER stress, and also that increased glutamine may be associated with disrupted urea cycle and changes in amino acids content shown in patients with urea cycle disorder (Serrano et al. 2011).

In H6KO mice, changes in ER/SR redox balance may affect cytosolic NADH/NAD^+ redox leading to mitochondrial biogenesis activation as a potential rescue mechanism. I have identified a novel NMRK2 mediated stress response pathway and a number of alterations in metabolites of which many are membrane lipids. There are also other pathways that could be influenced by these redox changes such as TCA cycle; however, they need to be analysed further to confirm if any changes that occur are associated with *H6PD* depletion.

In this chapter, metabolomics technology was applied in order to identify the factors, at the metabolic levels, contributing to muscle wasting seen in H6KO mice. I have recorded a number of metabolite changes including amino acids, acylcarnitines and

lipids that might contribute to dysregulation of redox metabolism, energy homeostasis and mitochondrial function; however, additional work needs to be carried out to investigate the downstream targets of changed pathways such acetyl-CoA, lactate and pyruvate. Despite the underlying mechanisms and factors directly leading to myopathy development in H6KO mice were not found, applying targeted metabolomics technology has provided insight into perturbations of energetic homeostasis in skeletal muscle.

Chapter 7- Discussion and Future Directions

The SR lumen contains a fully functional metabolic unit that regulates GC and energy metabolism in skeletal muscle. In this thesis, I have characterised the expression profile of the SR enzyme system, G6PT/H6PDH/G6Pase-β/11β-HSD1, across muscle cell differentiation and after GC and insulin treatments. I have shown that across C2C12 myocytes and primary myoblasts differentiation, there was a significant increase in 11β-HSD1 expression and a slight induction of H6PDH expression. Both these genes are involved in GC metabolism within the ER/SR lumen confirming their importance in differentiation of skeletal myoblasts to mature myotubes; therefore, in skeletal muscle development which was previously published for 11β-HSD1 (Biedasek et al. 2011). Increased mRNA expression of 11β-HSD1 after GC treatment indicates its essential role as a main regulator of GC metabolism in the SR. Thus it would appear that there is a coordinated up-regulation of 11β-HSD1 and H6PDH in response to differentiation signals which are not present for G6PT and G6Pase-β. In line with H6MKO, it makes this system important for regulation of steroids. However, when we knocked out H6PDH in muscle, it has appeared to be a phenocopy of global KO (Lavery et al. 2008b) developing SR stress and myopathy, but there were no changes in urinary 11-DHC metabolites suggesting that systemic features are potentially driven by contribution of other tissues. Expression of G6Pase-β in differentiating muscle cells was shown here for the first time. This would have a vital role in glucose recycling for energy metabolism in skeletal muscle.

I have also generated HSD1MKO mouse model in order to evaluate the muscle-specific role of 11β-HSD1 and GC metabolism in determining global metabolic phenotype. Using three different Cre lines, I successfully recombined the *HSD11B1* gene to a KO; however, 11β-HSD1 mRNA expression and activity remained at the

same level seen in WT. We cannot explain this phenomenon, but this could be due to the nature of muscle cells or a biological principle that makes it difficult to test. The HSD1MKO mouse model would have been an excellent model to determine 11β-HSD1 function in the regulation of muscle GC and energy metabolism in health and disease. Though global 11β-HSD1 has not reported direct muscle phenotype (Semjonous et al. 2011), and when treated with Cort, these mice were protected from the reduced grip strength, decreased lean mass and diminished myofiber diameter. Moreover, Cort-mediated induction of muscle atrophy markers MuRF1, atrogin1 and FoxO1 was also blunted in HSD1GKO animals (Morgan et al. 2014). It would have been a great opportunity to test a range of muscle-specific GC and 11β-HSD1 mediated phenotypes; however, despite successful recombination, the colony has been discontinued.

H6KO mice developed skeletal myopathy; however, the precise underpinning molecular mechanisms are still unknown. To assess the future importance of H6PDH in muscle metabolism, further investigations were needed in order to find the basis of this muscle wasting associated with other metabolic changes such as increased insulin sensitivity and glycogen storage. In Chapter 5, I identified important NAD^+ biosynthesis genes with NMRK2 being the most up-regulated gene in muscle of young H6KO mice without yet any signs of myopathy compared to WT controls. We believe, this adaptation to *H6PD* depletion involves early induction of NMRK2 expression which was also greater in TA muscle that is affected by myopathy in H6KO mice when compared to soleus muscle protected from most atrophic changes. This implicates a fibre type-specific relationship for NMRK2 expression that was higher in fast twitch muscle to regulate glycolytic metabolism. In addition, microarrays

in WT TA and soleus muscle implied that both NMRK2 and NAMPT salvage pathways are the only routes involved in NAD^+ replenishment in skeletal muscle (Lavery et al. 2008b). Whilst NAMPT was ubiquitously expressed, NMRK2 was a muscle-specific gene suggesting it may play an important role in skeletal muscle NAD^+ bioavailability. Elevated NMRK2 mediated NR salvage and consequently NAD^+ metabolism in H6KO mice may be critical for establishing and maintaining SR NAD(P)(H) as well as regulating SR resident metabolism.

NMRK2 as a skeletal muscle-specific pathway is capable of regulating NAD^+ biosynthesis through NR phosphorylation (Canto et al. 2012). Thus, NAD^+ biosynthesis and NMRK2 may be mechanisms for increasing $NAD^+/NADP^+$ flux in response to redox perturbations within the SR seen in H6KO mice.

I also determined NMRK2 and NAMPT expression across muscle cells differentiation. NMRK2 expression appeared to be switched on and significantly increased from day 2 to day 4 of myofibrillar differentiation whereas NAMPT appeared to be continuously expressed. Skeletal muscle-specific expression of NMRK2 suggests it may play an important role in maintaining NAD^+ pools in muscle to maintain cellular redox status and ensure that downstream metabolic adaptations occur.

NMRK2 mediated NAD^+ salvage has provided a novel pathway for energy homeostasis in skeletal muscle. NMRK2 protein expression increased during glucose restriction followed by an increase in NAD^+ content. This NMRK2 and subsequently NAD^+ inductions along with elevated fast twitch fibre expression further support that the salvage of NR through NMRK2 plays an important role in maintaining NAD^+ levels during metabolic stress such as calorie restriction in order to prevent NAD^+

depletion and large shifts in cellular redox status. Additional evidence supporting the potential importance of NMRK2 in metabolic adaptation has been shown through its elevated expression in SK-Hep1 cancer cells (Hwang and Kim 2009). This induction of NMRK2 expression may allow such cells to exhibit a shift towards glucose-dependent metabolism to drive cell growth.

Despite myopathy, increased NMRK2 expression in H6KO was associated with elevated muscle cellular NAD^+ content with enhanced glycogen storage, insulin sensitivity and protection from diet-induced insulin resistance. Interestingly, H6KO muscle displayed increased expression of mitochondrial encoded genes and elevated mitochondrial copy number. We propose that NMRK2 can act as a stress response gene to increase the availability of NAD^+ in skeletal muscle. The NAD^+ salvage pathway in muscle responds to changes in the SR NADPH/$NADP^+$ ratio seen in H6KO mice suggesting the likelihood of the crosstalk between the SR and cytosol which has not been identified before.

In Chapter 6, I investigated the association of muscle myopathy with metabolic changes and SR stress in the absence of H6PDH by applying metabolomics technology on H6KO mice and relevant WT controls. H6PDH deficiency caused a change in metabolic pathways consistent with increased amino acid and that could contribute to aspects of the phenotype in H6KO mice such as insulin sensitisation through elevated arginine and subsequent NO content. Changes in protein synthesis and amino acid accumulation could lead to a reduction in muscle mass (Lecker et al. 2006) and consequently may influence ER/SR stress. In addition to amino acids disruption, there were also defects in β-oxidation in H6PDH depleted

muscle which needs to be further analysed. Interestingly, in humans, high acetylcarnitine to carnitine ratio has been observed in patients with carnitine palmitoyltransferase II deficiency characterised by muscle pain and weakness consequently leading to the breakdown of muscle tissue (Wieser 1993). Our metabolomics data have revealed a number of metabolomic changes in skeletal muscle. This technology endorses the theory that energy stress could potentially be a signal for NMRK2 mediated salvage pathway and mitochondria. These data are being analysed in conjunction with the microarray data (Lavery et al. 2008b) in order to provide an insight into homeostatic responses on amino acid metabolism and β-oxidation during metabolic stress in skeletal muscle of H6KO mice.

Although I did not identify drivers of the phenotype seen in H6KO mice, I looked at responses over time such as energy deprivation that leads to other pathways activation. One of the most important early changes is compensatory mechanism of increased NMRK2 to generate more NAD^+ cofactor. Overall this thesis has led me to propose that in the *H6PD* depleted muscle, activation of SR stress pathways and perturbed SR NADPH/$NADP^+$ redox homeostasis may be associated with high up-regulation of cytosolic NMRK2 and consequently increased cellular NAD^+ content. A number of metabolite alterations may contribute to H6KO phenotype such as muscle wasting or insulin sensitivity which makes this model very complex (Figure 7-1).

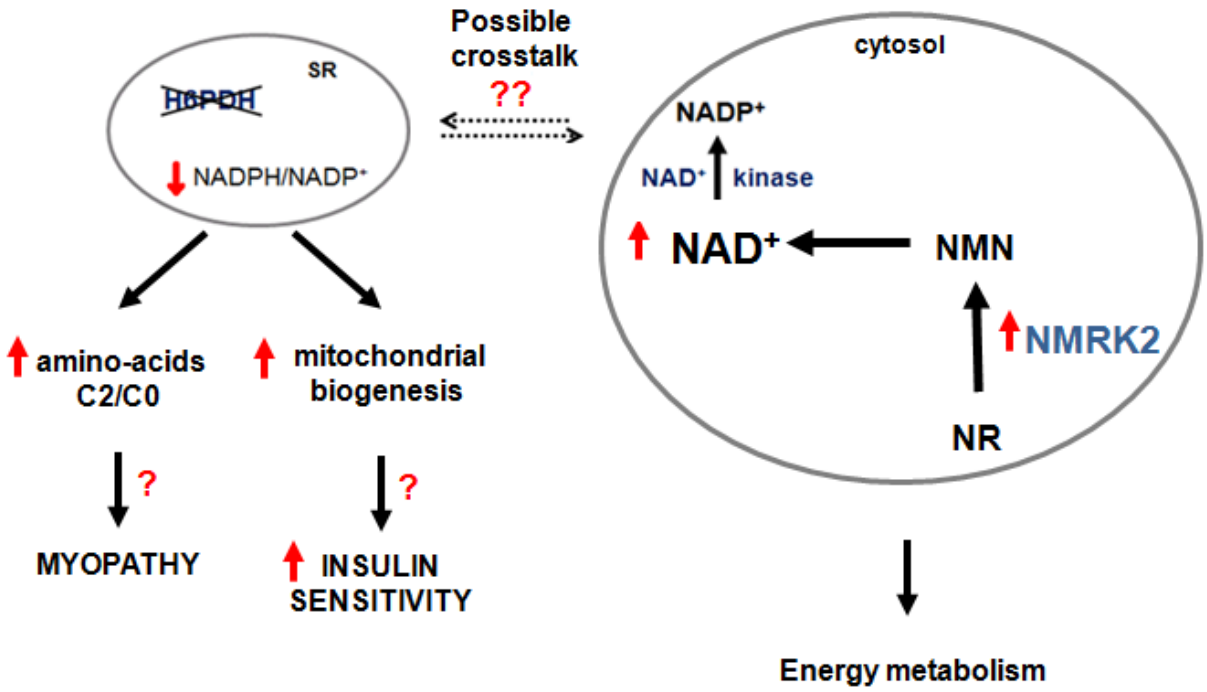

Figure 7-1 Changes within skeletal muscle due to H6PDH deficiency

Therefore, pathways governing NAD^+ bioavailability, particularly NMRK2 may be critical for establishing and maintaining SR NAD(P)(H) and regulating SR resident metabolism. As we believe, there is a crosstalk between the SR and cytosol. Additional analysis need to be undertaken in order to investigate downstream targets involved in myopathy development in H6KO mice.

The SR and energy metabolism need to be further investigated by implementing targeted LC/MS based metabolomics for the quantitative analysis of NAD^+ metabolites in skeletal muscle. Measurements of NAD^+ and related metabolites could serve as an indicator of muscle metabolic status in health or disease. As NAD^+ and related metabolites are converted to one or more other metabolites during metabolic stress, a single measurement of NAD^+ can be misleading, and the routine and accurate quantification of cellular NAD^+ metabolites, representing multiple

biosynthetic routes and breakdown pathways, is necessary to progress in this field. This will demonstrate new biological relationships between pathways that determine NAD^+ bioavailability and metabolism.

I demonstrated that NMRK2 is enriched in fast-twitch glycolytic vs. oxidative muscle. The fast-twitch muscle displayed the greatest phenotypic change in H6KO mouse line. Using Affymetrix genome arrays and tissues from a KO mouse line and treatments, the transcriptomic profiles in TA and soleus muscle should be further analysed in order to integrate this with NAD^+ metabolome and physiological data to understand the normal physiology of NMRK2 enrichment in glycolytic muscle. Identifying NMRK2 and NAD^+ sensitive pathways in type II glycolytic fibres will provide insight into their preferential loss in ageing muscle and also give understanding of the molecular basis of fibre type specific metabolism.

To support metabolomics analysis, mitochondrial respiration and β-oxidation should be measured from isolated mitochondria from TA and soleus muscles. Additionally, mRNA and protein expression of mitochondrial enzymes involved in β-oxidation as well as electron transport chain complexes I-IV, citrate synthase activities and protein abundances should be examined in mitochondrial preparations. To further understand the downstream NAD^+ metabolism, the SIRT 1 and 3 activities need to be determined in total cellular, nuclear and mitochondrial extracts as well as protein deacetylation should be evaluated of known SIRT substrates. These data could help with better understanding of insulin sensitivity in myopathy-affected muscle. Fully defining the physiology of skeletal muscle is critical to design interventions to optimise an individual's capacity to resist muscle-wasting diseases.

In this thesis, I have investigated a complex skeletal muscle unit, sarcoplasmic reticulum, which is a site of GC metabolism and other metabolic pathways including glucose utilisation as well as protein folding and trafficking. I have applied a number of transgenic mouse models to examine how the perturbations of SR genes can affect energetic and metabolic homeostasis. My main aim was to identify the role of H6PDH in muscle SR which is more enigmatic as H6KO mice develop an 11β-HSD1 and GC- independent type IIb fibre skeletal muscle myopathy and activation of SR stress pathways that we believe is a result of perturbed SR NADPH/$NADP^+$ redox homeostasis as well as the underlying factors or pathways leading to development of atrophic muscle which to date is still unknown. During my PhD, I have characterised a novel stress response salvage pathway in skeletal muscle leading to activation of NMRK2 which consequently increased cellular NAD^+ content. These data suggest that NAD^+ biosynthesis and NMRK2 are mechanisms for increasing NAD^+/$NADP^+$ flux in response to redox perturbations in the SR. I hypothesise that skeletal muscle NMRK2 mediated NAD^+ salvage is important to the ability of muscle to adapt to fluctuating cellular and subcellular NAD^+ requirements, and that salvage pathways can be manipulated to increase levels of NAD^+ during metabolic stress such as ageing and exercise as means to prevent or delay sarcopenia and increase healthspan. Additionally, I have highlighted a number of alternations in lipid membrane content suggesting a possible crosstalk between the SR and cytosol which to date is still unidentified. Further experiments need to be carried out to investigate novel mechanisms and pathways linking NMRK2 expression, SR redox and the control of muscle energy metabolism and mitochondrial function in order to

improve skeletal muscle physiology to make extended lifespan health and disease-free.

Conference Proceedings

Oral presentations:

Zielinska AE, Doig CL, Lavery GG 'Increased expression of NRK2 links an NAD+ salvage pathway to the metabolic and redox status of the sarcoplasmic reticulum in skeletal muscle of H6PDKO mice'- Annual Meeting of the American Endocrine Society, San Francisco, USA, 2013.

Zielinska AE, Doig CL, McCabe EL, Stewart PM, Lavery GG 'A hypomorphic *H6PD* allele is sufficient to rescue the skeletal myopathy but not the lack of 11β-HSD type 1-mediated glucocorticoid regeneration phenotypes of H6PDKO mice'- British Endocrine Society Annual Scientific Meeting, Harrogate, March 2012.

Zielinska AE & Lavery GG. 'Pre-receptor glucocorticoid metabolism and glucose flux in the endoplasmic reticulum'- Young Active Research in Endocrinology (YARE), Stockholm, October 2011.

Poster presentations:

Zielinska AE, Doig CL, Lavery GG 'NRK2 links an NAD^+ salvage pathway to the metabolic status of the sarcoplasmic reticulum in skeletal muscle'- College of Medical and Dental Sciences Graduate Festival of Research, University of Birmingham, Birmingham, April 2014 (3^{rd} prize award).

Zielinska AE, Doig CL, Stewart PM, Adamski J, Lavery GG 'H6PDH deficiency in muscle impacts amino acid metabolism' - British Endocrine Society Annual Scientific Meeting, Liverpool, March 2014.

Zielinska AE, Doig CL, Lavery GG 'Increased expression of NRK2 links an NAD^+ salvage pathway to the metabolic and redox status of the sarcoplasmic reticulum in skeletal muscle of H6PDKO mice'- International Early-Career Symposium, Clinical and Translational Physiology, Birmingham, July 2013.

Zielinska AE, Doig CL, McCabe EL, Saqib K, Morgan SA, Stewart PM, Lavery GG 'Glucocorticoid Regeneration in Skeletal Muscle Is Not Restricted to the Myocyte; Evaluation of the Skeletal Muscle-Specific 11β-Hydroxysteroid Dehydrogenase Type 1 Knockout Mouse'- Annual Meeting of the American Endocrine Society, Houston, June 2012.

Appendix

Table S-1 Overview of all detected metabolites using the AbsoluteIDQ p150 kit and their change in H6PDH depleted muscle

For each metabolite analysed, the metabolites class, short name and full biological name are given. Significant alterations show p<0.05 when comparing H6KO mice to WT. ↔ No significant, ↓ decreased and ↑ increased metabolite concentration.

Metabolite Class	Short Name	Full Biochemical Name	Change in H6KO
Sugars	H1	Hexose	↔
Amino acids	Arg	Arginine	↑ p=0.00018
	Gln	Glutamine	↑ p=4.44E-06
	Gly	Glycine	↑ p=0.0024
	His	Histidine	↔
	Met	Methionine	↔
	Orn	Ornithine	↓ p=0.016
	Phe	Phenylalanine	↔
	Pro	Proline	↑ p=0.0027
	Ser	Serine	↔
	Thr	Threonine	↔
	Trp	Tryptophan	↑ p=0.0032
	Tyr	Tyrosine	↔
	Val	Valine	↔
	xLeu	xLeucine (Leucine/Isoleucine)	↓ 0.012
Acylcarnitines	C0	DL-Carnitine	↔
	C2	Acetyl-L-carnitine	↑ p=5.63E-05
	C3	Propionyl-L-carnitine	↔
	C3:1	Propenyl-L-carnitine	↔
	C4	Butyryl-L-carnitine	↑ p=1.59E-05
	C4:1	Butenyl-L-carnitine	↔
	C5	Valeryl-L-carnitine	↑ p=0.034
	C5:1	Tiglyl-L-carnitine	↔
	C6:1	Hexenoyl-L-carnitine	↔
	C8	Octanoyl-L-carnitine	↔
	C8:1	Octenoyl-L-carnitine	↔
	C9	Nonayl-L-carnitine	↔
	C10	Decanoyl-L-carnitine	↔
	C10:1	Decanoyl-L-carnitine	↑ p=0.033
	C10:2	Decanoyl-L-carnitine	↔
	C12	Decanoyl-L-carnitine	↔
	C12:1	Decanoyl-L-carnitine	↔
	C14	Tetradecanoyl-L-carnitine	↔
	C14:1	Tetradecenoyl-L-carnitine	↔
	C14:2	Tetradecadienyl-L-carnitine	↔
	C16	Hexadecanoyl-L-carnitine	↔
	C16:1	Hexadecenoyl-L-carnitine	↔
	C16:2	Hexadecadienyl-L-carnitine	↔

Acylcarnitines	C18	Octadecanoyl-L-carnitine	↔
	C18:1	Octadecenoyl-L-carnitine	↔
	C18:2	Octadecadienyl-L-carnitine	↔
	C3-OH	Hydroxypropionyl-L-carnitine	↔
	C3-DC/C4-OH	Malonyl-L-carnitine/Hydroxybutyryl-L-carnitine	↑ p=0.0024
	C5-DC/C6-OH	Glutaryl-L-carnitine/ Hydroxyhexanoyl-L-carnitine	↔
	C5-M-DC	Methylglutaryl-L-carnitine	↔
	C3-DC-M/C5-OH	Methylmalonyl-L-carnitine/Hydroxyvaleryl-L-carnitine	↔
	C5:1-DC	Glutaconyl-L-carnitine	↔
	C4:1-DC/C6	Fumaryl-L-carnitine/Hexanoyl-L-carnitine	↑ p=0.0095
	C7-DC	Pimelyl-L-carnitine	↔
	C12-DC	Dodecanedioyl-L-carnitine	↔
	C14:1-OH	Hydroxytetradecenoyl-L-carnitine	↔
	C14:2-OH	Hydroxytetradecadienyl-L-carnitine	↔
	C16-OH	Hydroxyhexadecanoyl-L-carnitine	↔
	C16:1-OH	Hydroxyhexadecenoyl-L-carnitine	↔
	C16:2-OH	Hydroxyhexadecadienyl-L-carnitine	↔
	C18:1-OH	Hydroxyoctadecenoyl-L-carnitine	↔
Sphingomyelin	SM C16:0	Sphingomyeline C 16:0	↑ p=3.59E-06
	SM C16:1	Sphingomyeline C 16:1	↑ p=0.00054
	SM C18:0	Sphingomyeline C 18:0	↔
	SM C18:1	Sphingomyeline C 18:1	↑ p=0.0031
	SM C20:2	Sphingomyeline C 20:2	↔
	SM C22:3	Sphingomyeline C 22:3	↔
	SM C24:0	Sphingomyeline C 24:0	↔
	SM C24:1	Sphingomyeline C 24:1	↔
	SM C26:0	Sphingomyeline C 26:0	↔
	SM C26:1	Sphingomyeline C 26:1	↔
	SM (OH) C14:1	Hydroxysphingomyeline C14:1	↔
	SM (OH) C16:1	Hydroxysphingomyeline C 16:1	↔
	SM (OH) C22:1	Hydroxysphingomyeline C 22:1	↔
	SM (OH) C22:2	Hydroxysphingomyeline C 22:2	↑ p=0.045
	SM (OH) C24:1	Hydroxysphingomyeline C 24:1	↔
Phosphati-dylcholine	PC aa C24:0	Phosphatidylcholine diacyl C 24:0	↔
	PC aa C26:0	Phosphatidylcholine diacyl C 26:0	↔
	PC aa C28:1	Phosphatidylcholine diacyl C 28:1	↔
	PC aa C30:0	Phosphatidylcholine diacyl C 30:0	↓ p=4.06E-08
	PC aa C30:2	Phosphatidylcholine diacyl C 30:2	↓ p=0.00069
	PC aa C32:0	Phosphatidylcholine diacyl C 32:0	↓ p=0.0028
	PC aa C32:1	Phosphatidylcholine diacyl C 32:1	↓ p=2.33E-05
	PC aa C32:2	Phosphatidylcholine diacyl C 32:2	↓ p=0.0019
	PC aa C32:3	Phosphatidylcholine diacyl C 32:3	↓ p=3.79E-13

Phosphatidylcholine	PC aa C34:1	Phosphatidylcholine diacyl C 34:1	↔
	PC aa C34:2	Phosphatidylcholine diacyl C 34:2	↔
	PC aa C34:3	Phosphatidylcholine diacyl C 34:3	↔
	PC aa C34:4	Phosphatidylcholine diacyl C 34:4	↓ p=0.049
	PC aa C36:0	Phosphatidylcholine diacyl C 36:0	↔
	PC aa C36:1	Phosphatidylcholine diacyl C 36:1	↔
	PC aa C36:2	Phosphatidylcholine diacyl C 36:2	↑ p=0.00015
	PC aa C36:3	Phosphatidylcholine diacyl C 36:3	↑ p=0.0022
	PC aa C36:4	Phosphatidylcholine diacyl C 36:4	↔
	PC aa C36:5	Phosphatidylcholine diacyl C 36:5	↔
	PC aa C36:6	Phosphatidylcholine diacyl C 36:6	↓ p=0.00093
	PC aa C38:0	Phosphatidylcholine diacyl C 38:0	↔
	PC aa C38:1	Phosphatidylcholine diacyl C 38:1	↔
	PC aa C38:3	Phosphatidylcholine diacyl C 38:3	↑ p=0.045
	PC aa C38:4	Phosphatidylcholine diacyl C 38:4	↔
	PC aa C38:5	Phosphatidylcholine diacyl C 38:5	↓ p=1.11E-06
	PC aa C38:6	Phosphatidylcholine diacyl C 38:6	↓ p=3.95E-05
	PC aa C40:1	Phosphatidylcholine diacyl C 40:1	↔
	PC aa C40:2	Phosphatidylcholine diacyl C 40:2	↔
	PC aa C40:3	Phosphatidylcholine diacyl C 40:3	↔
	PC aa C40:4	Phosphatidylcholine diacyl C 40:4	↓ p=0.021
	PC aa C40:5	Phosphatidylcholine diacyl C 40:5	↓ p=4.68E-05
	PC aa C40:6	Phosphatidylcholine diacyl C 40:6	↓ p=0.0025
	PC aa C42:0	Phosphatidylcholine diacyl C 42:0	↓ p=0.025
	PC aa C42:1	Phosphatidylcholine diacyl C 42:1	↔
	PC aa C42:2	Phosphatidylcholine diacyl C 42:2	↓ p=0.024
	PC aa C42:4	Phosphatidylcholine diacyl C 42:4	↔
	PC aa C42:5	Phosphatidylcholine diacyl C 42:5	↔
	PC aa C42:6	Phosphatidylcholine diacyl C42:6	↓ p=0.0011
	PC ae C30:0	Phosphatidylcholine acyl-alkyl C 30:0	↓ p=0.00094
	PC ae C30:1	Phosphatidylcholine acyl-alkyl C 30:1	↔
	PC ae C30:2	Phosphatidylcholine acyl-alkyl C 30:2	↔
	PC ae C32:1	Phosphatidylcholine acyl-alkyl C 32:1	↔
	PC ae C32:2	Phosphatidylcholine acyl-alkyl C 32:2	↔
	PC ae C34:0	Phosphatidylcholine acyl-alkyl C 34:0	↓ p=0.01
	PC ae C34:1	Phosphatidylcholine acyl-alkyl C 34:1	↔
	PC ae C34:2	Phosphatidylcholine acyl-alkyl C34:2	↔
	PC ae C34:3	Phosphatidylcholine acyl-alkyl C 34:3	↑ p=0.00029
	PC ae C36:0	Phosphatidylcholine acyl-alkyl C 36:0	↔
	PC ae C36:1	Phosphatidylcholine acyl-alkyl C 36:1	↔
	PC ae C36:2	Phosphatidylcholine acyl-alkyl C 36:2	↑ p=0.0037
	PC ae C36:3	Phosphatidylcholine acyl-alkyl C 36:3	↑ p=0.00019
	PC ae C36:4	Phosphatidylcholine acyl-alkyl C36:4	↔
	PC ae C36:5	Phosphatidylcholine acyl-alkyl C 36:5	↑ p=7.48E-05
	PC ae C38:0	Phosphatidylcholine acyl-alkyl C 38:0	↓ p=8.96E-07
	PC ae C38:1	Phosphatidylcholine acyl-alkyl C 38:1	↓ p=0.028

Phosphatidylcholine	PC ae C38:2	Phosphatidylcholine acyl-alkyl C 38:2	↑ p=0.00012
	PC ae C38:3	Phosphatidylcholine acyl-alkyl C 38:3	↔
	PC ae C38:4	Phosphatidylcholine acyl-alkyl C 38:4	↔
	PC ae C38:5	Phosphatidylcholine acyl-alkyl C 38:5	↔
	PC ae C38:6	Phosphatidylcholine acyl-alkyl C38:6	↔
	PC ae C40:0	Phosphatidylcholine acyl-alkyl C 40:0	↓ p=0.011
	PC ae C40:1	Phosphatidylcholine acyl-alkyl C 40:1	↓ p=0.0016
	PC ae C40:2	Phosphatidylcholine acyl-alkyl C 40:2	↓ p=0.008
	PC ae C40:3	Phosphatidylcholine acyl-alkyl C 40:3	↔
	PC ae C40:4	Phosphatidylcholine acyl-alkyl C40:4	↔
	PC ae C40:5	Phosphatidylcholine acyl-alkyl C 40:5	↓ p=0.0092
	PC ae C40:6	Phosphatidylcholine acyl-alkyl C 40:6	↓ p=0.035
	PC ae C42:0	Phosphatidylcholine acyl-alkyl C 42:0	↔
	PC ae C42:1	Phosphatidylcholine acyl-alkyl C 42:1	↔
	PC ae C42:2	Phosphatidylcholine acyl-alkyl C 42:2	↓ p=0.011
	PC ae C42:3	Phosphatidylcholine acyl-alkyl C 42:3	↓ p=0.00045
	PC ae C42:4	Phosphatidylcholine acyl-alkyl C 42:4	↓ p=0.016
	PC ae C42:5	Phosphatidylcholine acyl-alkyl C 42:5	↓ p=0.0021
	PC ae C44:3	Phosphatidylcholine acyl-alkyl C 44:3	↓ p=7.64E-07
	PC ae C44:4	Phosphatidylcholine acyl-alkyl C 44:4	↓ p=0.012
	PC ae C44:5	Phosphatidylcholine acyl-alkyl C 44:5	↓ p=0.032
	PC ae C44:6	Phosphatidylcholine acyl-alkyl C 44:6	↔
LysoPhosphatidylcholine	lysoPC a C14:0	lysoPhosphatidylcholine acyl C14:0	↔
	lysoPC a C16:0	lysoPhosphatidylcholine acyl C16:0	↑ p=0.00021
	lysoPC a C16:1	lysoPhosphatidylcholine acyl C16:1	↔
	lysoPC a C17:0	lysoPhosphatidylcholine acyl C17:0	↑ p=0.047
	lysoPC a C18:0	lysoPhosphatidylcholine acyl C18:0	↑ p=0.00039
	lysoPC a C18:1	lysoPhosphatidylcholine acyl C18:1	↑ p=0.00021
	lysoPC a C18:2	lysoPhosphatidylcholine acyl C18:2	↑ p=0.00056
	lysoPC a C20:3	lysoPhosphatidylcholine acyl C20:3	↑ p=0.0019
	lysoPC a C20:4	lysoPhosphatidylcholine acyl C20:4	↑ p=0.0025
	lysoPC a C24:0	lysoPhosphatidylcholine acyl C24:0	↓ p=0.0024
	lysoPC a C26:0	lysoPhosphatidylcholine acyl C26:0	↔
	lysoPC a C26:1	lysoPhosphatidylcholine acyl C26:1	↔
	lysoPC a C28:0	lysoPhosphatidylcholine acyl C28:0	↔
	lysoPC a C28:1	lysoPhosphatidylcholine acyl C28:1	↔
	lysoPC a C6:0	lysoPhosphatidylcholine acyl C6:0	↔

References

Abdallah, B.M., Beck-Nielsen, H., & Gaster, M. 2005. Increased expression of 11β-hydroxysteroid dehydrogenase type 1 in type 2 diabetic myotubes. *Eur.J.Clin.Invest*, 35, (10) 627-634.

Adamski, J. & Suhre, K. 2013. Metabolomics platforms for genome wide association studies--linking the genome to the metabolome. *Curr.Opin.Biotechnol.*, 24, (1) 39-47.

Adi, S., Bin-Abbas, B., Wu, N.Y., & Rosenthal, S.M. 2002. Early stimulation and late inhibition of extracellular signal-regulated kinase 1/2 phosphorylation by IGF-I: a potential mechanism mediating the switch in IGF-I action on skeletal muscle cell differentiation. *Endocrinology*, 143, (2) 511-516.

Agrawal, P.B., Joshi, M., Savic, T., Chen, Z., & Beggs, A.H. 2012. Normal myofibrillar development followed by progressive sarcomeric disruption with actin accumulations in a mouse Cfl2 knockout demonstrates requirement of cofilin-2 for muscle maintenance. *Hum.Mol.Genet.*, 21, (10) 2341-2356.

Alberti, K.G., Eckel, R.H., Grundy, S.M., Zimmet, P.Z., Cleeman, J.I., Donato, K.A., Fruchart, J.C., James, W.P., Loria, C.M., & Smith, S.C., Jr. 2009. Harmonizing the metabolic syndrome: a joint interim statement of the International Diabetes Federation Task Force on Epidemiology and Prevention; National Heart, Lung, and Blood Institute; American Heart Association; World Heart Federation; International Atherosclerosis Society; and International Association for the Study of Obesity. *Circulation*, 120, (16) 1640-1645.

Alberts, P., Nilsson, C., Selen, G., Engblom, L.O., Edling, N.H., Norling, S., Klingstrom, G., Larsson, C., Forsgren, M., Ashkzari, M., Nilsson, C.E., Fiedler, M., Bergqvist, E., Ohman, B., Bjorkstrand, E., & Abrahmsen, L.B. 2003. Selective inhibition of 11 β-hydroxysteroid dehydrogenase type 1 improves hepatic insulin sensitivity in hyperglycemic mice strains. *Endocrinology*, 144, (11) 4755-4762.

Andrews, R.C., Rooyackers, O., & Walker, B.R. 2003. Effects of the 11 β-hydroxysteroid dehydrogenase inhibitor carbenoxolone on insulin sensitivity in men with type 2 diabetes. *J.Clin.Endocrinol.Metab*, 88, (1) 285-291.

Angelini, C. & Peterle, E. 2012. Old and new therapeutic developments in steroid treatment in Duchenne muscular dystrophy. *Acta Myol.* 31 (1) 9-15.

Angione, A.R., Jiang, C., Pan, D., Wang, Y.X., & Kuang, S. 2011. PPARdelta regulates satellite cell proliferation and skeletal muscle regeneration. *Skelet.Muscle*, 1, (1) 33.

Arlt, W. & Stewart, P.M. 2005. Adrenal corticosteroid biosynthesis, metabolism, and action. *Endocrinol.Metab Clin.North Am.*, 34, (2) 293-313.

Armstrong, D.L., Masiowski, M.L., & Wood, P.A. 1993. Pathologic characterization of short-chain acyl-CoA dehydrogenase deficiency in BALB/cByJ mice. *Am.J.Med.Genet.*, 47, (6) 884-892.

Aydin, J., Andersson, D.C., Hanninen, S.L., Wredenberg, A., Tavi, P., Park, C.B., Larsson, N.G., Bruton, J.D., & Westerblad, H. 2009. Increased mitochondrial Ca2+ and decreased sarcoplasmic reticulum Ca2+ in mitochondrial myopathy. *Hum.Mol.Genet.*, 18, (2) 278-288.

Bali, D.S., Chen, Y.T., & Goldstein, J.L. 1993. Glycogen Storage Disease Type I. University of Washington, Seattle (WA).

Banhegyi, G., Csala, M., & Benedetti, A. 2009. Hexose-6-phosphate dehydrogenase: linking endocrinology and metabolism in the endoplasmic reticulum. *J.Mol.Endocrinol.*, 42, (4) 283-289.

Barf, T., Vallgarda, J., Emond, R., Haggstrom, C., Kurz, G., Nygren, A., Larwood, V., Mosialou, E., Axelsson, K., Olsson, R., Engblom, L., Edling, N., Ronquist-Nii, Y., Ohman, B., Alberts, P., & Abrahmsen, L. 2002. Arylsulfonamidothiazoles as a new class of potential antidiabetic drugs. Discovery of potent and selective inhibitors of the 11β-hydroxysteroid dehydrogenase type 1. *J.Med.Chem.*, 45, (18) 3813-3815.

Barnes, P.J. 1998. Anti-inflammatory actions of glucocorticoids: molecular mechanisms. *Clin.Sci.(Lond)*, 94, (6) 557-572.

Befroy, D.E., Petersen, K.F., Dufour, S., Mason, G.F., de Graaf, R.A., Rothman, D.L., & Shulman, G.I. 2007. Impaired mitochondrial substrate oxidation in muscle of insulin-resistant offspring of type 2 diabetic patients. *Diabetes*, 56, (5) 1376-1381.

Berthiaume, M., Laplante, M., Festuccia, W.T., Berger, J.P., Thieringer, R., & Deshaies, Y. 2009. Additive action of 11β-HSD1 inhibition and PPAR-gamma agonism on hepatic steatosis and triglyceridemia in diet-induced obese rats. *Int.J.Obes.(Lond)*, 33, (5) 601-604.

Bhat, B.G., Hosea, N., Fanjul, A., Herrera, J., Chapman, J., Thalacker, F., Stewart, P.M., & Rejto, P.A. 2008. Demonstration of proof of mechanism and pharmacokinetics and pharmacodynamic relationship with 4'-cyano-biphenyl-4-sulfonic acid (6-amino-pyridin-2-yl)-amide (PF-915275), an inhibitor of 11 - hydroxysteroid dehydrogenase type 1, in cynomolgus monkeys. *J.Pharmacol.Exp.Ther.*, 324, (1) 299-305.

Biedasek, K., Andres, J., Mai, K., Adams, S., Spuler, S., Fielitz, J., & Spranger, J. 2011. Skeletal muscle 11β-HSD1 controls glucocorticoid-induced proteolysis and expression of E3 ubiquitin ligases atrogin-1 and MuRF-1. *PLoS.One.*, 6, (1) e16674.

Bieganowski, P. & Brenner, C. 2004. Discoveries of nicotinamide riboside as a nutrient and conserved NRK genes establish a Preiss-Handler independent route to NAD+ in fungi and humans. *Cell*, 117, (4) 495-502.

Billeter, R., Weber, H., Lutz, H., Howald, H., Eppenberger, H.M., & Jenny, E. 1980. Myosin types in human skeletal muscle fibres. *Histochemistry*, 65, (3) 249-259.

Blau, H.M., Pavlath, G.K., Hardeman, E.C., Chiu, C.P., Silberstein, L., Webster, S.G., Miller, S.C., & Webster, C. 1985. Plasticity of the differentiated state. *Science*, 230, (4727) 758-766.

Bloemberg, D. & Quadrilatero, J. 2012. Rapid determination of myosin heavy chain expression in rat, mouse, and human skeletal muscle using multicolor immunofluorescence analysis. *PLoS.One.*, 7, (4) e35273.

Bodine, S.C., Latres, E., Baumhueter, S., Lai, V.K., Nunez, L., Clarke, B.A., Poueymirou, W.T., Panaro, F.J., Na, E., Dharmarajan, K., Pan, Z.Q., Valenzuela, D.M., DeChiara, T.M., Stitt, T.N., Yancopoulos, G.D., & Glass, D.J. 2001. Identification of ubiquitin ligases required for skeletal muscle atrophy. *Science*, 294, (5547) 1704-1708.

Botta, A., Malena, A., Loro, E., Del, M.G., Suman, M., Pantic, B., Szabadkai, G., & Vergani, L. 2013. Altered Ca2+ homeostasis and endoplasmic reticulum stress in myotonic dystrophy type 1 muscle cells. *Genes (Basel)*, 4, (2) 275-292.

Bottinelli, R. & Reggiani, C. 2000. Human skeletal muscle fibres: molecular and functional diversity. *Prog.Biophys.Mol.Biol.*, 73, (2-4) 195-262.

Bronk, J. R. 1999. Human metabolism: Functional Diversity and Integration. Addison Wesley Longman. Harlow.

Brooks, S.V. 2003. Current topics for teaching skeletal muscle physiology. *Adv.Physiol Educ.*, 27, (1-4) 171-182.

Bruce, C.R., Hoy, A.J., Turner, N., Watt, M.J., Allen, T.L., Carpenter, K., Cooney, G.J., Febbraio, M.A., & Kraegen, E.W. 2009. Overexpression of carnitine palmitoyltransferase-1 in skeletal muscle is sufficient to enhance fatty acid oxidation and improve high-fat diet-induced insulin resistance. *Diabetes*, 58, (3) 550-558.

Bruce, C.R., Thrush, A.B., Mertz, V.A., Bezaire, V., Chabowski, A., Heigenhauser, G.J., & Dyck, D.J. 2006. Endurance training in obese humans improves glucose tolerance and mitochondrial fatty acid oxidation and alters muscle lipid content. *Am.J.Physiol Endocrinol.Metab*, 291, (1) E99-E107.

Bruning, J.C., Michael, M.D., Winnay, J.N., Hayashi, T., Horsch, D., Accili, D., Goodyear, L.J., & Kahn, C.R. 1998. A muscle-specific insulin receptor knockout exhibits features of the metabolic syndrome of NIDDM without altering glucose tolerance. *Mol.Cell*, 2, (5) 559-569.

Bujalska, I.J., Durrani, O.M., Abbott, J., Onyimba, C.U., Khosla, P., Moosavi, A.H., Reuser, T.T., Stewart, P.M., Tomlinson, J.W., Walker, E.A., & Rauz, S. 2007. Characterisation of 11β-hydroxysteroid dehydrogenase 1 in human orbital adipose tissue: a comparison with subcutaneous and omental fat. *J.Endocrinol.*, 192, (2) 279-288.

Bulfield, G., Siller, W.G., Wight, P.A., & Moore, K.J. 1984. X chromosome-linked muscular dystrophy (mdx) in the mouse. *Proc.Natl.Acad.Sci.U.S.A*, 81, (4) 1189-1192.

Burton, D.A., Stokes, K., & Hall, G.M. 2003. Physiological effects of exercise. *Contin Educ Anaesth Crit Care Pain*, 4, (6) 185-188.

Canto, C., Houtkooper, R.H., Pirinen, E., Youn, D.Y., Oosterveer, M.H., Cen, Y., Fernandez-Marcos, P.J., Yamamoto, H., Andreux, P.A., Cettour-Rose, P., Gademann, K., Rinsch, C., Schoonjans, K., Sauve, A.A., & Auwerx, J. 2012. The NAD(+) precursor nicotinamide riboside enhances oxidative metabolism and protects against high-fat diet-induced obesity. *Cell Metab*, 15, (6) 838-847.

Chamberlain, J.S., Metzger, J., Reyes, M., Townsend, D., & Faulkner, J.A. 2007. Dystrophin-deficient mdx mice display a reduced life span and are susceptible to spontaneous rhabdomyosarcoma. *FASEB J.*, 21, (9) 2195-2204.

Chang, C.C., Yang, M.H., Tung, H.C., Chang, C.Y., Tsai, Y.L., Huang, J.P., Yen, T.H., & Hung, L.M. 2014. Resveratrol exhibits differential protective effects on fast- and slow-twitch muscles in streptozotocin-induced diabetic rats. *J.Diabetes*, 6, (1) 60-67.

Chen, L.Y., Pan, C.J., Shieh, J.J., & Chou, J.Y. 2002. Structure-function analysis of the glucose-6-phosphate transporter deficient in glycogen storage disease type Ib. *Hum.Mol.Genet.*, 11, (25) 3199-3207.

Chen, L.Y., Shieh, J.J., Lin, B., Pan, C.J., Gao, J.L., Murphy, P.M., Roe, T.F., Moses, S., Ward, J.M., Lee, E.J., Westphal, H., Mansfield, B.C., & Chou, J.Y. 2003a. Impaired glucose homeostasis, neutrophil trafficking and function in mice lacking the glucose-6-phosphate transporter. *Hum.Mol.Genet.*, 12, (19) 2547-2558.

Chen, W., Zhang, X., Birsoy, K., & Roeder, R.G. 2010. A muscle-specific knockout implicates nuclear receptor coactivator MED1 in the regulation of glucose and energy metabolism. *Proc.Natl.Acad.Sci.U.S.A*, 107, (22) 10196-10201.

Chomczynski, P. & Sacchi, N. 1987. Single-step method of RNA isolation by acid guanidinium thiocyanate-phenol-chloroform extraction. *Anal.Biochem.*, 162, (1) 156-159.

Cottrell, E.C., Seckl, J.R., Holmes, M.C., & Wyrwoll, C.S. 2013. Foetal and placental 11β-HSD2: a hub for developmental programming. *Acta Physiol (Oxf)*., 210, (2):288-295.

Csala, M., Banhegyi, G., & Benedetti, A. 2006. Endoplasmic reticulum: a metabolic compartment. *FEBS Lett.*, 580, (9) 2160-2165.

Dagher, Z., Ruderman, N., Tornheim, K., & Ido, Y. 2001. Acute regulation of fatty acid oxidation and amp-activated protein kinase in human umbilical vein endothelial cells. *Circ.Res.*, 88, (12) 1276-1282.

Dash, R.K., Li, Y., Kim, J., Beard, D.A., Saidel, G.M., & Cabrera, M.E. 2008. Metabolic dynamics in skeletal muscle during acute reduction in blood flow and oxygen supply to mitochondria: in-silico studies using a multi-scale, top-down integrated model. *PLoS.One.*, 3, (9) e3168.

Day, K., Shefer, G., Shearer, A., & Yablonka-Reuveni, Z. 2010. The depletion of skeletal muscle satellite cells with age is concomitant with reduced capacity of single progenitors to produce reserve progeny. *Dev.Biol.*, 340, (2) 330-343.

Deldicque, L. 2013. Endoplasmic reticulum stress in human skeletal muscle: any contribution to sarcopenia? *Front Physiol*, 4, 236.

Deldicque, L., Hespel, P., & Francaux, M. 2012. Endoplasmic reticulum stress in skeletal muscle: origin and metabolic consequences. *Exerc.Sport Sci.Rev.*, 40, (1) 43-49.

Dobbins, R.L., Szczepaniak, L.S., Bentley, B., Esser, V., Myhill, J., & McGarry, J.D. 2001. Prolonged inhibition of muscle carnitine palmitoyltransferase-1 promotes intramyocellular lipid accumulation and insulin resistance in rats. *Diabetes*, 50, (1) 123-130.

Dolinsky, V.W., Douglas, D.N., Lehner, R., & Vance, D.E. 2004. Regulation of the enzymes of hepatic microsomal triacylglycerol lipolysis and re-esterification by the glucocorticoid dexamethasone. *Biochem.J.*, 378, (Pt 3) 967-974.

Draper, N. & Stewart, P.M. 2005. 11β-hydroxysteroid dehydrogenase and the pre-receptor regulation of corticosteroid hormone action. *J.Endocrinol.*, 186, (2) 251-271.

Edwards, C.R., Stewart, P.M., Burt, D., Brett, L., McIntyre, M.A., Sutanto, W.S., De Kloet, E.R. & Monder, C. 1988. Localisation of 11β-hydroxysteroid dehydrogenase--tissue specific protector of the mineralocorticoid receptor. *Lancet* 2, 986-9.

Engert, J.C., Berglund, E.B., & Rosenthal, N. 1996. Proliferation precedes differentiation in IGF-I-stimulated myogenesis. *J.Cell Biol.*, 135, (2) 431-440.

Farah, C.S. & Reinach, F.C. 1995. The troponin complex and regulation of muscle contraction. *FASEB J.*, 9, (9) 755-767.

Fink, B., Thanzami, V., Seydel, H., & Manning, J.T. 2006. Digit ratio and hand-grip strength in German and Mizos men: cross-cultural evidence for an organizing effect of prenatal testosterone on strength. *Am.J.Hum.Biol.*, 18, (6) 776-782.

Flanagan-Steet, H., Hannon, K., McAvoy, M.J., Hullinger, R., & Olwin, B.B. 2000. Loss of FGF receptor 1 signaling reduces skeletal muscle mass and disrupts myofibre organization in the developing limb. *Dev.Biol.*, 218, (1) 21-37.

Fraser, R., Ingram, M.C., Anderson, N.H., Morrison, C., Davies, E., & Connell, J.M. 1999. Cortisol effects on body mass, blood pressure, and cholesterol in the general population. *Hypertension*, 33, (6) 1364-1368.

Froguel, P. & Velho, G. 2001. Genetic determinants of type 2 diabetes. *Recent Prog.Horm.Res.*, 56, 91-105.

Frost, R.A. & Lang, C.H. 2007. Protein kinase B/Akt: a nexus of growth factor and cytokine signaling in determining muscle mass. *J.Appl.Physiol (1985.)*, 103, (1) 378-387.

Fulco, M., Cen, Y., Zhao, P., Hoffman, E.P., McBurney, M.W., Sauve, A.A., & Sartorelli, V. 2008. Glucose restriction inhibits skeletal myoblast differentiation by activating SIRT1 through AMPK-mediated regulation of Nampt. *Dev.Cell,* 14 (5) 661-673.

Gathercole, L.L., Lavery, G.G., Morgan, S.A., Cooper, M.S., Sinclair, A.J., Tomlinson, J.W., & Stewart, P.M. 2013. 11β-hydroxysteroid dehydrogenase 1: translational and therapeutic aspects. *Endocr.Rev.*, 34, (4) 525-555.

Geeves, M.A. & Holmes, K.C. 1999. Structural mechanism of muscle contraction. *Annu.Rev.Biochem.*, 68, 687-728.

Gerich, J.E., Meyer, C., Woerle, H.J., & Stumvoll, M. 2001. Renal gluconeogenesis: its importance in human glucose homeostasis. *Diabetes Care*, 24, (2) 382-391.

Giorgi, C., Wieckowski, M.R., Pandolfi, P.P., & Pinton, P. 2011. Mitochondria associated membranes (MAMs) as critical hubs for apoptosis. *Commun.Integr.Biol.*, 4, (3) 334-335.

Girard, J. 2006. Insulin's effect on the liver: "direct or indirect?" continues to be the question. *J.Clin.Invest*, 116, (2) 302-304.

Goldspink, G. 1999. Changes in muscle mass and phenotype and the expression of autocrine and systemic growth factors by muscle in response to stretch and overload. *J.Anat.*, 194 (Pt 3), 323-334.

Goody, M.F., Kelly, M.W., Lessard, K.N., Khalil, A., & Henry, C.A. 2010. Nrk2b-mediated NAD+ production regulates cell adhesion and is required for muscle morphogenesis in vivo: Nrk2b and NAD+ in muscle morphogenesis. *Dev.Biol.*, 344, (2) 809-826.

Goody, M.F., Kelly, M.W., Reynolds, C.J., Khalil, A., Crawford, B.D., & Henry, C.A. 2012. NAD+ biosynthesis ameliorates a zebrafish model of muscular dystrophy. *PLoS.Biol.*, 10, (10) e1001409.

Gounarides, J.S., Korach-Andre, M., Killary, K., Argentieri, G., Turner, O., & Laurent, D. 2008. Effect of dexamethasone on glucose tolerance and fat metabolism in a diet-induced obesity mouse model. *Endocrinology*, 149, (2) 758-766.

Greenhaff, P.L. 2001. The creatine-phosphocreatine system: there's more than one song in its repertoire. *J.Physiol*, 537, (Pt 3) 657.

Grundy, S.M., Cleeman, J.I., Daniels, S.R., Donato, K.A., Eckel, R.H., Franklin, B.A., Gordon, D.J., Krauss, R.M., Savage, P.J., Smith, S.C., Jr., Spertus, J.A., & Costa, F. 2005. Diagnosis and management of the metabolic syndrome: an American Heart Association/National Heart, Lung, and Blood Institute Scientific Statement. *Circulation*, 112, (17) 2735-2752.

Hafezi-Moghadam, A., Simoncini, T., Yang, Z., Limbourg, F.P., Plumier, J.C., Rebsamen, M.C., Hsieh, C.M., Chui, D.S., Thomas, K.L., Prorock, A.J., Laubach, V.E., Moskowitz, M.A., French, B.A., Ley, K., & Liao, J.K. 2002. Acute cardiovascular protective effects of corticosteroids are mediated by non-transcriptional activation of endothelial nitric oxide synthase. *Nat Med.*, 8, (5) 473-9.

Hamalainen, N. & Pette, D. 1993. The histochemical profiles of fast fibre types IIB, IID, and IIA in skeletal muscles of mouse, rat, and rabbit. *J.Histochem.Cytochem.*, 41, (5) 733-743.

Heidt, A.B. & Black, B.L. 2005. Transgenic mice that express Cre recombinase under control of a skeletal muscle-specific promoter from mef2c. *Genesis.*, 42, (1) 28-32.

Hermanowski-Vosatka, A., Balkovec, J.M., Cheng, K., Chen, H.Y., Hernandez, M., Koo, G.C., Le Grand, C.B., Li, Z., Metzger, J.M., Mundt, S.S., Noonan, H., Nunes, C.N., Olson, S.H., Pikounis, B., Ren, N., Robertson, N., Schaeffer, J.M., Shah, K., Springer, M.S., Strack, A.M., Strowski, M., Wu, K., Wu, T., Xiao, J., Zhang, B.B., Wright, S.D., & Thieringer, R. 2005. 11β-HSD1 inhibition ameliorates metabolic syndrome and prevents progression of atherosclerosis in mice. *J.Exp.Med.*, 202, (4) 517-527.

Hewitt, K.N., Walker, E.A., & Stewart, P.M. 2005. Minireview: hexose-6-phosphate dehydrogenase and redox control of 11β-hydroxysteroid dehydrogenase type 1 activity. Endocrinology, 146, (6) 2539-2543.

Houtkooper, R.H., Canto, C., Wanders, R.J., & Auwerx, J. 2010. The secret life of NAD+: an old metabolite controlling new metabolic signaling pathways. *Endocr.Rev.*, 31, (2) 194-223.

Hu, Z., Wang, H., Lee, I.H., Du, J., & Mitch, W.E. 2009. Endogenous glucocorticoids and impaired insulin signaling are both required to stimulate muscle wasting under pathophysiological conditions in mice. *J.Clin.Invest*, 119, (10) 3059-3069.

Hwang, E.-S., & Kim, G.H. 2009. Allyl isothiocyanate influences cell adhesion, migration and metalloproteinase gene expression in SK-Hep1 cells. *Exp.Biol.Med.* 234, (1) 105-111.

Ikezoe, K., Furuya, H., Ohyagi, Y., Osoegawa, M., Nishino, I., Nonaka, I., & Kira, J. 2003. Dysferlin expression in tubular aggregates: their possible relationship to endoplasmic reticulum stress. *Acta Neuropathol.*, 105, (6) 603-609.

Ikezoe, K., Nakamori, M., Furuya, H., Arahata, H., Kanemoto, S., Kimura, T., Imaizumi, K., Takahashi, M.P., Sakoda, S., Fujii, N., & Kira, J. 2007. Endoplasmic reticulum stress in myotonic dystrophy type 1 muscle. *Acta Neuropathol.*, 114, (5) 527-535.

Itoh, E., Iida, K., Kim, D.S., del Rincon, J.P., Coschigano, K.T., Kopchick, J.J., & Thorner, M.O. 2004. Lack of contribution of 11βHSD1 and glucocorticoid action to reduced muscle mass associated with reduced growth hormone action. *Growth Horm.IGF.Res.*, 14, (6) 462-466.

Jacob, S., Machann, J., Rett, K., Brechtel, K., Volk, A., Renn, W., Maerker, E., Matthaei, S., Schick, F., Claussen, C.D., & Haring, H.U. 1999. Association of increased intramyocellular lipid content with insulin resistance in lean nondiabetic offspring of type 2 diabetic subjects. *Diabetes*, 48, (5) 1113-1119.

Jang, C., Obeyesekere, V.R., Dilley, R.J., Krozowski, Z., Inder, W.J., & Alford, F.P. 2007. Altered activity of 11β-hydroxysteroid dehydrogenase types 1 and 2 in skeletal muscle confers metabolic protection in subjects with type 2 diabetes. *J.Clin.Endocrinol.Metab*, 92, (8) 3314-3320.

Jarvis, J.C., Mokrusch, T., Kwende, M.M., Sutherland, H., & Salmons, S. 1996. Fast-to-slow transformation in stimulated rat muscle. *Muscle Nerve*, 19, (11) 1469-1475.

Jin, X., Kim, J.G., Oh, M.J., Oh, H.Y., Sohn, Y.W., Pian, X., Yin, J.L., Beck, S., Lee, N., Son, J., Kim, H., Yan, C., Wang, J.H., Choi, Y.J., & Whang, K.Y. 2007. Opposite roles of MRF4 and MyoD in cell proliferation and myogenic differentiation. *Biochem.Biophys.Res.Commun.*, 364, (3) 476-482.

Jing, E., Emanuelli, B., Hirschey, M.D., Boucher, J., Lee, K.Y., Lombard, D., Verdin, E.M., & Kahn, C.R. 2011. Sirtuin-3 (Sirt3) regulates skeletal muscle metabolism and insulin signaling via altered mitochondrial oxidation and reactive oxygen species production. *Proc.Natl.Acad.Sci.U.S.A*, 108, (35) 14608-14613.

Jornayvaz, F.R., Samuel, V.T., & Shulman, G.I. 2010. The role of muscle insulin resistance in the pathogenesis of atherogenic dyslipidemia and nonalcoholic fatty liver disease associated with the metabolic syndrome. *Annu.Rev.Nutr.*, 30, 273-290.

Joyner, A.L. 2001. Gene targeting: a practical approach. Oxford University Press. Oxford.

Kahn, R., Buse, J., Ferrannini, E., & Stern, M. 2005. The metabolic syndrome: time for a critical appraisal: joint statement from the American Diabetes Association and the European Association for the Study of Diabetes. *Diabetes Care*, 28, (9) 2289-2304.

Kambadur, R., Sharma, M., Smith, T.P., & Bass, J.J. 1997. Mutations in myostatin (GDF8) in double-muscled Belgian Blue and Piedmontese cattle. *Genome Res.*, 7, (9) 910-916.

Kamel, H.K. 2003. Sarcopenia and ageing. *Nutr.Rev.*, 61, (5 Pt 1) 157-167.

Khaleeli, A.A., Betteridge, D.J., Edwards, R.H., Round, J.M., & Ross, E.J. 1983. Effect of treatment of Cushing's syndrome on skeletal muscle structure and function. *Clin.Endocrinol.(Oxf)*, 19, (4) 547-556.

Khan, J.A., Xiang, S., & Tong, L. 2007. Crystal structure of human nicotinamide riboside kinase. *Structure.*, 15, (8) 1005-1013.

Kilgour, A.H., Gallagher, I.J., MacLullich, A.M., Andrew, R., Gray, C.D., Hyde, P., Wackerhage, H., Husi, H., Ross, J.A., Starr, J.M., Chapman, K.E., Fearon, K.C., Walker, B.R., & Greig, C.A. 2013. Increased skeletal muscle 11βHSD1 mRNA is associated with lower muscle strength in ageing. *PLoS.One.*, 8, (12) e84057.

Kim, J.Y., Hickner, R.C., Cortright, R.L., Dohm, G.L., & Houmard, J.A. 2000. Lipid oxidation is reduced in obese human skeletal muscle. *Am.J.Physiol Endocrinol.Metab*, 279, (5) E1039-E1044.

Kim, K.S., Park, K.S., Kim, M.J., Kim, S.K., Cho, Y.W., & Park, S.W. 2014. Type 2 diabetes is associated with low muscle mass in older adults. *Geriatr.Gerontol.Int.*, 14 Suppl 1, 115-121.

Kim, T.N. & Choi, K.M. 2013. Sarcopenia: Definition, Epidemiology, and Pathophysiology. *J.Bone Metab*, 20, (1) 1-10.

Kockskamper, J., Zima, A.V., & Blatter, L.A. 2005. Modulation of sarcoplasmic reticulum Ca2+ release by glycolysis in cat atrial myocytes. *J.Physiol*, 564, (Pt 3) 697-714.

Kopelman, P., Jebb, S.A., & Butland, B. 2007. Executive summary: Foresight 'Tackling Obesities: Future Choices' project. *Obes.Rev.*, 8 Suppl 1, vi-ix.

Korach-Andre, M., Gounarides, J., Deacon, R., Beil, M., Sun, D., Gao, J., & Laurent, D. 2005. Age and muscle-type modulated role of intramyocellular lipids in the progression of insulin resistance in nondiabetic Zucker rats. *Metabolism*, 54, (4) 522-528.

Košir, R., Zmrzljak, U.P., Bele, T., Acimovic, J., Perse, M., Majdic, G., Prehn, C., Adamski, J., & Rozman, D. 2012. Circadian expression of steroidogenic cytochromes P450 in the mouse adrenal gland--involvement of cAMP-responsive element modulator in epigenetic regulation of Cyp17a1. *FEBS J.*, 279, (9) 1584-93.

Kotelevtsev, Y., Holmes, M.C., Burchell, A., Houston, P.M., Schmoll, D., Jamieson, P., Best, R., Brown, R., Edwards, C.R., Seckl, J.R., & Mullins, J.J. 1997a. 11β-hydroxysteroid dehydrogenase type 1 knockout mice show attenuated glucocorticoid-inducible responses and resist hyperglycaemia on obesity or stress. *Proc.Natl.Acad.Sci.U.S.A*, 94, (26) 14924-14929.

Kraus-Friedmann, N. 1984. Hormonal regulation of hepatic gluconeogenesis. *Physiol Rev.*, 64, (1) 170-259.

Krssak, M., Falk, P.K., Dresner, A., DiPietro, L., Vogel, S.M., Rothman, D.L., Roden, M., & Shulman, G.I. 1999. Intramyocellular lipid concentrations are correlated with insulin sensitivity in humans: a 1H NMR spectroscopy study. *Diabetologia*, 42, (1) 113-116.

Labeit, S., Kolmerer, B., & Linke, W.A. 1997. The giant protein titin. Emerging roles in physiology and pathophysiology. *Circ.Res.*, 80, (2) 290-294.

Lakshmi, V. & Monder, C. 1988. Purification and characterization of the corticosteroid 11β-dehydrogenase component of the rat liver 11β-hydroxysteroid dehydrogenase complex. *Endocrinology*, 123, (5) 2390-2398.

Laplante, M. & Sabatini, D.M. 2009. mTOR signaling at a glance. *J.Cell Sci.*, 122, (Pt 20) 3589-3594.

Larsen, P.R., Kronenberg, H.M., Melmed, S., & Polonsky, K.S. 2008. Williams Textbook of Endocrinology. Elsevier Saunders. Philadelphia (PA).

Latif, S.A., Pardo, H.A., Hardy, M.P., & Morris, D.J. 2005. Endogenous selective inhibitors of 11β-hydroxysteroid dehydrogenase isoforms 1 and 2 of adrenal origin. *Mol.Cell Endocrinol.*, 243, (1-2) 43-50.

Lavery, G.G., Hauton, D., Hewitt, K.N., Brice, S.M., Sherlock, M., Walker, E.A., & Stewart, P.M. 2007. Hypoglycaemia with enhanced hepatic glycogen synthesis in recombinant mice lacking hexose-6-phosphate dehydrogenase. *Endocrinology*, 148, (12) 6100-6106.

Lavery, G.G., Idkowiak, J., Sherlock, M., Bujalska, I., Ride, J.P., Saqib, K., Hartmann, M.F., Hughes, B., Wudy, S.A., De, S.J., Arlt, W., Krone, N., Shackleton, C.H., Walker, E.A., & Stewart, P.M. 2013. Novel H6PDH mutations in two girls with premature adrenarche: 'apparent' and 'true' CRD can be differentiated by urinary steroid profiling. *Eur.J.Endocrinol.*, 168, (2) K19-K26.

Lavery, G.G., Walker, E.A., Draper, N., Jeyasuria, P., Marcos, J., Shackleton, C.H., Parker, K.L., White, P.C., & Stewart, P.M. 2006. Hexose-6-phosphate dehydrogenase knock-out mice lack 11β-hydroxysteroid dehydrogenase type 1-mediated glucocorticoid generation. *J.Biol.Chem.*, 281, (10) 6546-6551.

Lavery, G.G., Walker, E.A., Tiganescu, A., Ride, J.P., Shackleton, C.H., Tomlinson, J.W., Connell, J.M., Ray, D.W., Biason-Lauber, A., Malunowicz, E.M., Arlt, W., & Stewart, P.M. 2008a. Steroid biomarkers and genetic studies reveal inactivating mutations in hexose-6-phosphate dehydrogenase in patients with cortisone reductase deficiency. *J.Clin.Endocrinol.Metab*, 93, (10) 3827-3832.

Lavery, G.G., Walker, E.A., Turan, N., Rogoff, D., Ryder, J.W., Shelton, J.M., Richardson, J.A., Falciani, F., White, P.C., Stewart, P.M., Parker, K.L., & McMillan, D.R. 2008b. Deletion of hexose-6-phosphate dehydrogenase activates the unfolded protein response pathway and induces skeletal myopathy. *J.Biol.Chem.*, 283, (13) 8453-8461.

Lavery, G.G., Zielinska, A.E., Gathercole, L.L., Hughes, B., Semjonous, N., Guest, P., Saqib, K., Sherlock, M., Reynolds, G., Morgan, S.A., Tomlinson, J.W., Walker, E.A., Rabbitt, E.H., & Stewart, P.M. 2012. Lack of significant metabolic abnormalities in mice with liver-specific disruption of 11β-hydroxysteroid dehydrogenase type 1. *Endocrinology,* 153, (7) 3236-3248.

Lawson, A.J., Walker, E.A., Lavery, G.G., Bujalska, I.J., Hughes, B., Arlt, W., Stewart, P.M., & Ride, J.P. 2011. Cortisone-reductase deficiency associated with heterozygous mutations in 11β-hydroxysteroid dehydrogenase type 1. *Proc.Natl.Acad.Sci.U.S.A*, 108, (10) 4111-4116.

Lecker, S.H., Goldberg, A.L., & Mitch, W.E. 2006. Protein degradation by the ubiquitin–proteasome pathway in normal and disease states. *J.Am.Soc.Nephrol.* 17, 71807-1819.

Liu, R., Jin, P., LiqunYu, Wang, Y., Han, L., Shi, T., & Li, X. 2014. Impaired mitochondrial dynamics and bioenergetics in diabetic skeletal muscle. *PLoS.One.*, 9, (3) e92810.

Liu, L., Wang, Y.X., Zhou, J., Long, F., Sun, H.W., Liu, Y., Chen, Y.Z. & Jiang, C.L. 2005. Rapid non-genomic inhibitory effects of glucocorticoids on human neutrophil degranulation. *Inflamm Res.*, 54, (1) 37-41.

Long, W., Wei, L., & Barrett, E.J. 2001. Dexamethasone inhibits the stimulation of muscle protein synthesis and PHAS-I and p70 S6-kinase phosphorylation. *Am.J.Physiol Endocrinol.Metab*, 280, (4) E570-E575.

Lopaschuk, G.D., Ussher, J.R., Folmes, C.D., Jaswal, J.S., & Stanley, W.C. 2010. Myocardial fatty acid metabolism in health and disease. *Physiol Rev.*, 90, (1) 207-258.

Lynch, G.S., Hinkle, R.T., Chamberlain, J.S., Brooks, S.V., & Faulkner, J.A. 2001. Force and power output of fast and slow skeletal muscles from mdx mice 6-28 months old. *J.Physiol*, 535, (Pt 2) 591-600.

Maina, F., Casagranda, F., Audero, E., Simeone, A., Comoglio, P.M., Klein, R., & Ponzetto, C. 1996. Uncoupling of Grb2 from the Met receptor in vivo reveals complex roles in muscle development. *Cell*, 87, (3) 531-542.

Malafarina, V., Uriz-Otano, F., Iniesta, R., & Gil-Guerrero, L. 2012. Sarcopenia in the elderly: diagnosis, physiopathology and treatment. *Maturitas*, 71, (2) 109-114.

Mason, P.J., Stevens, D., Diez, A., Knight, S.W., Scopes, D.A., & Vulliamy, T.J. 1999. Human hexose-6-phosphate dehydrogenase (glucose 1-dehydrogenase) encoded at 1p36: coding sequence and expression. *Blood Cells Mol.Dis.*, 25, (1) 30-37.

Masuzaki, H., Paterson, J., Shinyama, H., Morton, N.M., Mullins, J.J., Seckl, J.R., & Flier, J.S. 2001. A transgenic model of visceral obesity and the metabolic syndrome. *Science*, 294, (5549) 2166-2170.

McCroskery, S., Thomas, M., Maxwell, L., Sharma, M., & Kambadur, R. 2003. Myostatin negatively regulates satellite cell activation and self-renewal. *J.Cell Biol.*, 162, (6) 1135-1147.

Moran, J.L., Li, Y., Hill, A.A., Mounts, W.M., & Miller, C.P. 2002. Gene expression changes during mouse skeletal myoblast differentiation revealed by transcriptional profiling. *Physiol Genomics*, 10, (2) 103-111.

Morgan, J.E. & Partridge, T.A. 2003. Muscle satellite cells. *Int.J.Biochem.Cell Biol.*, 35, (8) 1151-1156.

Morgan, S.A., McCabe, E.L., Gathercole, L.L., Hassan-Smith, Z.K., Larner, D.P., Bujalska, I.J., Stewart, P.M., Tomlinson, J.W., & Lavery, G.G. 2014. 11β-HSD1 is the major regulator of the tissue-specific effects of circulating glucocorticoid excess. *Proc.Natl.Acad.Sci.U.S.A*, 111, (24) E2482-E2491.

Morgan, S.A., Sherlock, M., Gathercole, L.L., Lavery, G.G., Lenaghan, C., Bujalska, I.J., Laber, D., Yu, A., Convey, G., Mayers, R., Hegyi, K., Sethi, J.K., Stewart, P.M., Smith, D.M., & Tomlinson, J.W. 2009. 11β-hydroxysteroid dehydrogenase type 1 regulates glucocorticoid-induced insulin resistance in skeletal muscle. *Diabetes*, 58, (11) 2506-2515.

Morino, K., Petersen, K.F., Dufour, S., Befroy, D., Frattini, J., Shatzkes, N., Neschen, S., White, M.F., Bilz, S., Sono, S., Pypaert, M., & Shulman, G.I. 2005. Reduced mitochondrial density and increased IRS-1 serine phosphorylation in muscle of insulin-resistant offspring of type 2 diabetic parents. *J.Clin.Invest*, 115, (12) 3587-3593.

Morton, N.M., Holmes, M.C., Fievet, C., Staels, B., Tailleux, A., Mullins, J.J., & Seckl, J.R. 2001. Improved lipid and lipoprotein profile, hepatic insulin sensitivity, and glucose tolerance in 11β-hydroxysteroid dehydrogenase type 1 null mice. *J.Biol.Chem.*, 276, (44) 41293-41300.

Morton, N.M., Ramage, L., & Seckl, J.R. 2004. Down-regulation of adipose 11β-hydroxysteroid dehydrogenase type 1 by high-fat feeding in mice: a potential adaptive mechanism counteracting metabolic disease. *Endocrinology*, 145, (6) 2707-2712.

Mussig, K., Fiedler, H., Staiger, H., Weigert, C., Lehmann, R., Schleicher, E.D., & Haring, H.U. 2005. Insulin-induced stimulation of JNK and the PI 3-kinase/mTOR pathway leads to phosphorylation of serine 318 of IRS-1 in C2C12 myotubes. *Biochem.Biophys.Res.Commun.*, 335, (3) 819-825.

Nagaraju, K., Casciola-Rosen, L., Lundberg, I., Rawat, R., Cutting, S., Thapliyal, R., Chang, J., Dwivedi, S., Mitsak, M., Chen, Y.W., Plotz, P., Rosen, A., Hoffman, E., & Raben, N. 2005. Activation of the endoplasmic reticulum stress response in autoimmune myositis: potential role in muscle fibre damage and dysfunction. *Arthritis Rheum.*, 52, (6) 1824-1835.

Nielsen, M.F., Nyholm, B., Caumo, A., Chandramouli, V., Schumann, W.C., Cobelli, C., Landau, B.R., Rizza, R.A., & Schmitz, O. 2000. Prandial glucose effectiveness and fasting gluconeogenesis in insulin-resistant first-degree relatives of patients with type 2 diabetes. *Diabetes*, 49, (12) 2135-2141.

Nixon, M., Upreti, R., & Andrew, R. 2012. 5alpha-Reduced glucocorticoids: a story of natural selection. *J.Endocrinol.,* 212, (2) 111-127.

Odermatt, A., Arnold, P., & Frey, F.J. 2001. The intracellular localization of the mineralocorticoid receptor is regulated by 11β-hydroxysteroid dehydrogenase type 2. *J.Biol.Chem.*, 276, (30) 28484-28492.

Outten, C.E. & Culotta, V.C. 2003. A novel NADH kinase is the mitochondrial source of NADPH in Saccharomyces cerevisiae. *EMBO J.*, 22, (9) 2015-2024.

Paddon-Jones, D., Short, K.R., Campbell, W.W., Volpi, E., & Wolfe, R.R. 2008. Role of dietary protein in the sarcopenia of ageing. *Am.J.Clin.Nutr.*, 87, (5) 1562S-1566S.

Pan, C.J., Chen, S.Y., Lee, S., & Chou, J.Y. 2009. Structure-function study of the glucose-6-phosphate transporter, an eukaryotic antiporter deficient in glycogen storage disease type Ib. *Mol.Genet.Metab*, 96, (1) 32-37.

Patergnani, S., Suski, J.M., Agnoletto, C., Bononi, A., Bonora, M., De, M.E., Giorgi, C., Marchi, S., Missiroli, S., Poletti, F., Rimessi, A., Duszynski, J., Wieckowski, M.R., & Pinton, P. 2011. Calcium signaling around Mitochondria Associated Membranes (MAMs). *Cell Commun.Signal.*, 9, 19.

Paterson, J.M., Morton, N.M., Fievet, C., Kenyon, C.J., Holmes, M.C., Staels, B., Seckl, J.R., & Mullins, J.J. 2004. Metabolic syndrome without obesity: Hepatic overexpression of 11β-hydroxysteroid dehydrogenase type 1 in transgenic mice. *Proc.Natl.Acad.Sci.U.S.A*, 101, (18) 7088-7093.

Peckett, A.J., Wright, D.C., & Riddell, M.C. 2011. The effects of glucocorticoids on adipose tissue lipid metabolism. *Metabolism*, 60, (11) 1500-1510.

Peppa, M., Koliaki, C., Nikolopoulos, P., & Raptis, S.A. 2010. Skeletal muscle insulin resistance in endocrine disease. *J.Biomed.Biotechnol.*, 2010, 527850.

Perseghin, G., Ghosh, S., Gerow, K., & Shulman, G.I. 1997. Metabolic defects in lean nondiabetic offspring of NIDDM parents: a cross-sectional study. *Diabetes*, 46, (6) 1001-1009.

Perseghin, G., Scifo, P., De, C.F., Pagliato, E., Battezzati, A., Arcelloni, C., Vanzulli, A., Testolin, G., Pozza, G., Del, M.A., & Luzi, L. 1999. Intramyocellular triglyceride content is a determinant of in vivo insulin resistance in humans: a 1H-13C nuclear magnetic resonance spectroscopy assessment in offspring of type 2 diabetic parents. *Diabetes*, 48, (8) 1600-1606.

Petersen, K.F., Dufour, S., Befroy, D., Garcia, R., & Shulman, G.I. 2004. Impaired mitochondrial activity in the insulin-resistant offspring of patients with type 2 diabetes. *N.Engl.J.Med.*, 350, (7) 664-671.

Petrie, J.R., Ueda, S., Webb, D.J., Elliott, H.L., & Connell, J.M. 1996. Endothelial nitric oxide production and insulin sensitivity. A physiological link with implications for pathogenesis of cardiovascular disease. *Circulation*, 93, (7) 1331-1333.

Phillips, N.R., Sprouse, M.L., & Roby, R.K. 2014. Simultaneous quantification of mitochondrial DNA copy number and deletion ratio: a multiplex real-time PCR assay. *Sci.Rep.*, 4, 3887.

Pratt, W.B. & Toft, D.O. 1997. Steroid receptor interactions with heat shock protein and immunophilin chaperones. *Endocr.Rev.*, 18(3):306-60.

Rando, T.A. & Blau, H.M. 1994. Primary mouse myoblast purification, characterization, and transplantation for cell-mediated gene therapy. *J.Cell Biol.*, 125, (6) 1275-1287.

Rao, P. & Monks, D.A. 2009. A tetracycline-inducible and skeletal muscle-specific Cre recombinase transgenic mouse. *Dev.Neurobiol.*, 69, (6) 401-406.

Rayavarapu, S., Coley, W., & Nagaraju, K. 2012. Endoplasmic reticulum stress in skeletal muscle homeostasis and disease. *Curr.Rheumatol.Rep.*, 14, (3) 238-243.

Reaven, G.M. 1988. Banting lecture 1988. Role of insulin resistance in human disease. *Diabetes*, 37, (12) 1595-1607.

Rizza, R.A. 2010. Pathogenesis of fasting and postprandial hyperglycaemia in type 2 diabetes: implications for therapy. *Diabetes*, 59, (11) 2697-2707.

Rogoff, D., Black, K., McMillan, D.R., & White, P.C. 2010. Contribution of hexose-6-phosphate dehydrogenase to NADPH content and redox environment in the endoplasmic reticulum. *Redox.Rep.*, 15, (2) 64-70.

Rogoff, D., Ryder, J.W., Black, K., Yan, Z., Burgess, S.C., McMillan, D.R., & White, P.C. 2007. Abnormalities of glucose homeostasis and the hypothalamic-pituitary-adrenal axis in mice lacking hexose-6-phosphate dehydrogenase. *Endocrinology*, 148, (10) 5072-5080.

Ron, D. & Walter, P. 2007. Signal integration in the endoplasmic reticulum unfolded protein response. *Nat.Rev.Mol.Cell Biol.*, 8, (7) 519-529.

Rosenstock, J., Banarer, S., Fonseca, V.A., Inzucchi, S.E., Sun, W., Yao, W., Hollis, G., Flores, R., Levy, R., Williams, W.V., Seckl, J.R., & Huber, R. 2010. The 11β-hydroxysteroid dehydrogenase type 1 inhibitor INCB13739 improves hyperglycaemia in patients with type 2 diabetes inadequately controlled by metformin monotherapy. *Diabetes Care*, 33, (7) 1516-1522.

Rosol, T.J., Yarrington, J.T., Latendresse, J., & Capen, C.C. 2001. Adrenal gland: structure, function, and mechanisms of toxicity. *Toxicol.Pathol.*, 29, (1) 41-48.

Rossi, A.E. & Dirksen, R.T. 2006. Sarcoplasmic reticulum: the dynamic calcium governor of muscle. *Muscle Nerve*, 33, (6) 715-731.

Ruderman, N.B., Carling, D., Prentki, M., & Cacicedo, J.M. 2013. AMPK, insulin resistance, and the metabolic syndrome. *J.Clin.Invest*, 123, (7) 2764-2772.

Saito, Y., Komaki, H., Hattori, A., Takeuchi, F., Sasaki, M., Kawabata, K., Mitsuhashi, S., Tominaga, K., Hayashi, Y.K., Nowak, K.J., Laing, N.G., Nonaka, I., & Nishino, I. 2011a. Extramuscular manifestations in children with severe congenital myopathy due to ACTA1 gene mutations. *Neuromuscul.Disord.*, 21, (7) 489-493.

Sakuma, K. & Yamaguchi, A. 2012. Sarcopenia and age-related endocrine function. *Int.J.Endocrinol.*, 2012, 127362.

Salomonsson, S., Grundtman, C., Zhang, S.J., Lanner, J.T., Li, C., Katz, A., Wedderburn, L.R., Nagaraju, K., Lundberg, I.E., & Westerblad, H. 2009. Upregulation of MHC class I in transgenic mice results in reduced force-generating capacity in slow-twitch muscle. *Muscle Nerve*, 39, (5) 674-682.

Sampey, B.P., Freemerman, A.J., Zhang, J., Kuan, P.F., Galanko, J.A., O'Connell, T.M., Ilkayeva, O.R., Muehlbauer, M.J., Stevens, R.D., Newgard, C.B., Brauer, H.A., Troester, M.A., & Makowski, L. 2012. Metabolomic profiling reveals mitochondrial-derived lipid biomarkers that drive obesity-associated inflammation. *PLoS.One*, 7, (6) e38812.

Sandri, M., Sandri, C., Gilbert, A., Skurk, C., Calabria, E., Picard, A., Walsh, K., Schiaffino, S., Lecker, S.H., & Goldberg, A.L. 2004. Foxo transcription factors induce the atrophy-related ubiquitin ligase atrogin-1 and cause skeletal muscle atrophy. *Cell*, 117, (3) 399-412.

Sanger, F. 1959. Chemistry of insulin; determination of the structure of insulin opens the way to greater understanding of life processes. *Science*, 129, (3359) 1340-1344.

Schakman, O., Gilson, H., & Thissen, J.P. 2008. Mechanisms of glucocorticoid-induced myopathy. *J.Endocrinol.*, 197, (1) 1-10.

Schakman, O., Kalista, S., Barbe, C., Loumaye, A., & Thissen, J.P. 2013. Glucocorticoid-induced skeletal muscle atrophy. *Int.J.Biochem.Cell Biol.*, 45, (10) 2163-2172.

Schleicher, E.D. & Weigert, C. 2000. Role of the hexosamine biosynthetic pathway in diabetic nephropathy. *Kidney Int.Suppl*, 77, S13-S18.

Schrager, M.A., Metter, E.J., Simonsick, E., Ble, A., Bandinelli, S., Lauretani, F., & Ferrucci, L. 2007. Sarcopenic obesity and inflammation in the InCHIANTI study. *J.Appl.Physiol (1985.)*, 102, (3) 919-925.

Schroder, M. & Kaufman, R.J. 2005. The mammalian unfolded protein response. *Annu.Rev.Biochem.*, 74, 739-789.

Schuler, M., Ali, F., Metzger, E., Chambon, P., & Metzger, D. 2005. Temporally controlled targeted somatic mutagenesis in skeletal muscles of the mouse. *Genesis.*, 41, (4) 165-170.

Seale, P. & Rudnicki, M.A. 2000. A new look at the origin, function, and "stem-cell" status of muscle satellite cells. *Dev.Biol.*, 218, (2) 115-124.

Seckl, J.R. 2004. 11β-hydroxysteroid dehydrogenases: changing glucocorticoid action. *Curr.Opin.Pharmacol.*, 4, (6) 597-602.

Semjonous, N.M., Sherlock, M., Jeyasuria, P., Parker, K.L., Walker, E.A., Stewart, P.M., & Lavery, G.G. 2011. Hexose-6-phosphate dehydrogenase contributes to skeletal muscle homeostasis independent of 11β-hydroxysteroid dehydrogenase type 1. *Endocrinology*, 152, (1) 93-102.

Senesi, S., Csala, M., Marcolongo, P., Fulceri, R., Mandl, J., Banhegyi, G., & Benedetti, A. 2010. Hexose-6-phosphate dehydrogenase in the endoplasmic reticulum. *Biol.Chem.*, 391, (1) 1-8.

Serrano' M., Ormazábal, A., Vilaseca, M.A., Lambruschini, N., Garcia-Romero, R., Meavilla, S., Perez-Dueñas, B., Pineda, M., Garcia-Cazorla, A., Campistol, J., & Artuch, R. 2011. Assessment of plasma ammonia and glutamine concentrations in urea cycle disorders. *Clinical Biochemistry*, 44, 742–744.

Shieh, J.J., Pan, C.J., Mansfield, B.C., & Chou, J.Y. 2003. A glucose-6-phosphate hydrolase, widely expressed outside the liver, can explain age-dependent resolution of hypoglycaemia in glycogen storage disease type Ia. *J.Biol.Chem.*, 278, (47) 47098-47103.

Sipila, S. & Poutamo, J. 2003. Muscle performance, sex hormones and training in peri-menopausal and post-menopausal women. *Scand.J.Med.Sci.Sports*, 13, (1) 19-25.

Slavin, B.G., Ong, J.M., & Kern, P.A. 1994. Hormonal regulation of hormone-sensitive lipase activity and mRNA levels in isolated rat adipocytes. *J.Lipid Res.*, 35, (9) 1535-1541.

Smerdu, V., Karsch-Mizrachi, I., Campione, M., Leinwand, L., & Schiaffino, S. 1994. Type IIx myosin heavy chain transcripts are expressed in type IIb fibres of human skeletal muscle. *Am.J.Physiol*, 267, (6 Pt 1) C1723-C1728.

Smith, A.G. & Muscat, G.E. 2005. Skeletal muscle and nuclear hormone receptors: implications for cardiovascular and metabolic disease. *Int.J.Biochem.Cell Biol.*, 37, (10) 2047-2063.

Song, M.Y., Ruts, E., Kim, J., Janumala, I., Heymsfield, S., & Gallagher, D. 2004. Sarcopenia and increased adipose tissue infiltration of muscle in elderly African American women. *Am.J.Clin.Nutr.*, 79, (5) 874-880.

Song, Y.L., Foster, W.R., Shuster, D.J., Nadler, S.G., Salter-Cid, L., & Sasseville, V.G. 2011. Transcriptional profiling of liver and effect of glucocorticoids in a rat adjuvant-induced arthritis model. *Vet.Pathol.*, 48, (4) 885-895.

Spangenburg, E.E. & Booth, F.W. 2003. Molecular regulation of individual skeletal muscle fibre types. *Acta Physiol Scand.*, 178, (4) 413-424.

Sun, C., Zhang, F., Ge, X., Yan, T., Chen, X., Shi, X., & Zhai, Q. 2007. SIRT1 improves insulin sensitivity under insulin-resistant conditions by repressing PTP1B. *Cell Metab*, 6, (4) 307-319.

Sydow, K., Mondon, C.E., & Cooke, J.P. 2005. Insulin resistance: potential role of the endogenous nitric oxide synthase inhibitor ADMA. *Vasc.Med.*, 10 Suppl 1, S35-S43.

Tajsharghi, H. 2008. Thick and thin filament gene mutations in striated muscle diseases. *Int.J.Mol.Sci.*, 9, (7) 1259-1275.

Tarasov, A.I., Griffiths, E.J., & Rutter, G.A. 2012. Regulation of ATP production by mitochondrial Ca(2+). *Cell Calcium*, 52, (1) 28-35.

Tasic Dimov, D. & Dimov, I. 2007. Muscle fibre types and fibre morphometry in the soleus muscle of the rat. *Facta Universitatis*.14, (3) 121-127.

Tempel, W., Rabeh, W.M., Bogan, K.L., Belenky, P., Wojcik, M., Seidle, H.F., Nedyalkova, L., Yang, T., Sauve, A.A., Park, H.W., & Brenner, C. 2007. Nicotinamide riboside kinase structures reveal new pathways to NAD+. *PLoS.Biol.*, 5, (10) e263.

Tennakoon, J.B., Shi, Y., Han, J.J., Tsouko, E., White, M.A., Burns, A.R., Zhang, A., Xia, X., Ilkayeva, O.R., Xin, L., Ittmann, M.M., Rick, F.G., Schally, A.V., & Frigo, D.E. 2013. Androgens regulate prostate cancer cell growth via an AMPK-PGC-1alpha-mediated metabolic switch. *Oncogene*.

Thomas, M., Langley, B., Berry, C., Sharma, M., Kirk, S., Bass, J., & Kambadur, R. 2000. Myostatin, a negative regulator of muscle growth, functions by inhibiting myoblast proliferation. *J.Biol.Chem.*, 275, (51) 40235-40243.

Tomlinson, J.W., Walker, E.A., Bujalska, I.J., Draper, N., Lavery, G.G., Cooper, M.S., Hewison, M., & Stewart, P.M. 2004. 11β-hydroxysteroid dehydrogenase type 1: a tissue-specific regulator of glucocorticoid response. *Endocr.Rev.*, 25, (5) 831-866.

Towbin, H., Staehelin, T., & Gordon, J. 1979. Electrophoretic transfer of proteins from polyacrylamide gels to nitrocellulose sheets: procedure and some applications. *Proc.Natl.Acad.Sci.U.S.A*, 76, (9) 4350-4354.

Trifunovic, A., Wredenberg, A., Falkenberg, M., Spelbrink, J.N., Rovio, A.T., Bruder, C.E., Bohlooly, Y., Gidlof, S., Oldfors, A., Wibom, R., Tornell, J., Jacobs, H.T., & Larsson, N.G. 2004. Premature ageing in mice expressing defective mitochondrial DNA polymerase. *Nature*, 429, (6990) 417-423.

Tsouko, E., Khan, A.S., White, M.A., Han, J.J., Shi, Y., Merchant, F.A., Sharpe, M.A., Xin, L., & Frigo, D.E. 2014. Regulation of the pentose phosphate pathway by an androgen receptor-mTOR-mediated mechanism and its role in prostate cancer cell growth. *Oncogenesis.*, 3, e103.

Turk, R., Sterrenburg, E., de Meijer, E.J., van Ommen, G.J., den Dunnen, J.T., & 't Hoen, P.A. 2005. Muscle regeneration in dystrophin-deficient mdx mice studied by gene expression profiling. *BMC.Genomics*, 6, 98.

Tyynismaa, H., Carroll, C.J., Raimundo, N., Ahola-Erkkila, S., Wenz, T., Ruhanen, H., Guse, K., Hemminki, A., Peltola-Mjosund, K.E., Tulkki, V., Oresic, M., Moraes, C.T., Pietilainen, K., Hovatta, I., & Suomalainen, A. 2010. Mitochondrial myopathy induces a starvation-like response. *Hum.Mol.Genet.*, 19, (20) 3948-3958.

Uckaya, G., Karadurmus, N., Kutlu, O., Corakci, A., Kizildag, S., Ural, A.U., Gul, D., & Kutlu, M. 2008. Adipose tissue 11β-Hydroxysteroid Dehydrogenase Type 1 and Hexose-6-Phosphate Dehydrogenase gene expressions are increased in patients with type 2 diabetes mellitus. *Diabetes Res.Clin.Pract.*, 82 Suppl 2, S135-S140.

van Raalte, D.H., Ouwens, D.M., & Diamant, M. 2009. Novel insights into glucocorticoid-mediated diabetogenic effects: towards expansion of therapeutic options? *Eur.J.Clin.Invest*, 39, (2) 81-93.

Ventura-Clapier, R., Mettauer, B., & Bigard, X. 2007. Beneficial effects of endurance training on cardiac and skeletal muscle energy metabolism in heart failure. *Cardiovasc.Res.*, 73, (1) 10-18.

Waddell, D.S., Baehr, L.M., van den Brandt, J., Johnsen, S.A., Reichardt, H.M., Furlow, J.D., & Bodine, S.C. 2008. The glucocorticoid receptor and FOXO1 synergistically activate the skeletal muscle atrophy-associated MuRF1 gene. *Am.J.Physiol Endocrinol.Metab*, 295, (4) E785-E797.

Walker, B.R., Connacher, A.A., Lindsay, R.M., Webb, D.J., & Edwards, C.R. 1995. Carbenoxolone increases hepatic insulin sensitivity in man: a novel role for 11-oxosteroid reductase in enhancing glucocorticoid receptor activation. *J.Clin.Endocrinol.Metab*, 80, (11) 3155-3159.

Wallace, D.C., Brown, M.D., & Lott, M.T. 1999. Mitochondrial DNA variation in human evolution and disease. *Gene*, 238, (1) 211-230.

Walter, P. & Ron, D. 2011. The unfolded protein response: from stress pathway to homeostatic regulation. *Science*, 334, (6059) 1081-1086.

Wang, K., McCarter, R., Wright, J., Beverly, J., & Ramirez-Mitchell, R. 1991. Regulation of skeletal muscle stiffness and elasticity by titin isoforms: a test of the segmental extension model of resting tension. *Proc.Natl.Acad.Sci.U.S.A*, 88, (16) 7101-7105.

Wang, Y., Liu, L., Du, H., Nagaoka, Y., Fan, W., Lutfy, K., Friedman, T.C., Jiang, M., & Liu, Y. 2014. Transgenic overexpression of hexose-6-phosphate dehydrogenase in adipose tissue causes local glucocorticoid amplification and lipolysis in male mice. *Am.J.Physiol Endocrinol.Metab*, 306, (5) E543-E551.

Weigert, C., Brodbeck, K., Klopfer, K., Haring, H.U., & Schleicher, E.D. 2002. Angiotensin II induces human TGF-β 1 promoter activation: similarity to hyperglycaemia. *Diabetologia*, 45, (6) 890-898.

Westerblad, H., Bruton, J.D., & Katz, A. 2010. Skeletal muscle: energy metabolism, fibre types, fatigue and adaptability. *Exp.Cell Res.*, 316, (18) 3093-3099.

White, A.T., McCurdy, C.E., Philp, A., Hamilton, D.L., Johnson, C.D., & Schenk, S. 2013. Skeletal muscle-specific overexpression of SIRT1 does not enhance whole-body energy expenditure or insulin sensitivity in young mice. *Diabetologia*, 56, (7) 1629-1637.

Whitesell, R.R., Ardehali, H., Printz, R.L., Beechem, J.M., Knobel, S.M., Piston, D.W., Granner, D.K., Van Der Meer, W., Perriott, L.M., & May, J.M. 2003. Control of glucose phosphorylation in L6 myotubes by compartmentalization, hexokinase, and glucose transport. *Biochem.J.*, 370, (Pt 1) 47-56.

Whorwood, C.B., Donovan, S.J., Flanagan, D., Phillips, D.I., & Byrne, C.D. 2002. Increased glucocorticoid receptor expression in human skeletal muscle cells may contribute to the pathogenesis of the metabolic syndrome. *Diabetes*, 51, (4) 1066-1075.

Wieser, T. 1993. Carnitine Palmitoyltransferase II Deficiency. *GeneReviews.* University of Washington, Seattle (WA).

Wild, S., Roglic, G., Green, A., Sicree, R., & King, H. 2004. Global prevalence of diabetes: estimates for the year 2000 and projections for 2030. *Diabetes Care*, 27, (5) 1047-1053.

Wolfe, L., Jethva, R., Oglesbee, D., & Vockley, J. 1993. Short-Chain Acyl-CoA Dehydrogenase Deficiency. *GeneReviews.* University of Washington, Seattle (WA).

Wredenberg, A., Wibom, R., Wilhelmsson, H., Graff, C., Wiener, H.H., Burden, S.J., Oldfors, A., Westerblad, H., & Larsson, N.G. 2002. Increased mitochondrial mass in mitochondrial myopathy mice. *Proc.Natl.Acad.Sci.U.S.A*, 99, (23) 15066-15071.

Xia, R., Webb, J.A., Gnall, L.L., Cutler, K., & Abramson, J.J. 2003. Skeletal muscle sarcoplasmic reticulum contains a NADH-dependent oxidase that generates superoxide. *Am.J.Physiol Cell Physiol*, 285, (1) C215-C221.

Yaffe, D. & Saxel, O. 1977. Serial passageing and differentiation of myogenic cells isolated from dystrophic mouse muscle. *Nature*, 270, (5639) 725-727.

Yamada, T., Ivarsson, N., Hernandez, A., Fahlstrom, A., Cheng, A.J., Zhang, S.J., Bruton, J.D., Ulfhake, B., & Westerblad, H. 2012. Impaired mitochondrial respiration and decreased fatigue resistance followed by severe muscle weakness in skeletal muscle of mitochondrial DNA mutator mice. *J.Physiol*, 590, (Pt 23) 6187-6197.

Yin, H., Price, F., & Rudnicki, M.A. 2013. Satellite cells and the muscle stem cell niche. *Physiol Rev.*, 93, (1) 23-67.

Zhang, M., Lv, X.Y., Li, J., Xu, Z.G., & Chen, L. 2009. Alteration of 11β-hydroxysteroid dehydrogenase type 1 in skeletal muscle in a rat model of type 2 diabetes. *Mol.Cell Biochem.*, 324, (1-2) 147-155.

Zheng, B., Ohkawa, S., Li, H., Roberts-Wilson, T.K., & Price, S.R. 2010. FOXO3a mediates signaling crosstalk that coordinates ubiquitin and atrogin-1/MAFbx expression during glucocorticoid-induced skeletal muscle atrophy. *FASEB J.*, 24, (8) 2660-2669.

Zhu, X., Hadhazy, M., Wehling, M., Tidball, J.G., & McNally, E.M. 2000. Dominant negative myostatin produces hypertrophy without hyperplasia in muscle. *FEBS Lett.*, 474, (1) 71-75.

Zielinska, A.E., Walker, E.A., Stewart, P.M., & Lavery, G.G. 2011. Biochemistry and physiology of hexose-6-phosphate knockout mice. *Mol.Cell Endocrinol.*, 336, (1-2) 213-218.

Zima, A.V., Copello, J.A., & Blatter, L.A. 2003. Differential modulation of cardiac and skeletal muscle ryanodine receptors by NADH. *FEBS Lett.*, 547, (1-3) 32-36.